

CHIP FORMATION AND CHIP BREAKING
PROCESSES IN METAL CUTTING

A thesis submitted to the University of Sheffield for
the degree of Doctor of philosophy

ISMAIL HASSAN MAGHDI ALMANDILAWI
(M.Sc. Eng., Leningrad, U.S.S.R.)

in the

Department of mechanical Engineering
The University of Sheffield

March 1971

TO MY BROTHER

Dr. SADIQ HASSAN M. ALMANDILAWI, M.D.

CONTENTS

	Page
ACKNOWLEDGEMENT	i
SUMMARY	ii
CHAPTER 1 A Discussion of Metal Cutting Studies	1
1.1 Machinability	1
1.2 Chip Formation	5
1.3 Types of Deformed Chips	9
1.3.1 Discontinuous	9
1.3.2 Continuous without Built-up Edge	9
1.3.3 Continuous with Built-up Edge	10
1.4 Discontinuous Chip Formation	11
1.5 General Remarks on the Parameters Influencing Chip Formation Process	18
1.5.1 Influence of Rake Angle on the Chip Formation Process	18
1.5.2 Influence of a Built-up Edge on Chip Formation Process	19
1.5.3 Influence of Friction on Chip Formation Process	20
1.6 Idealisation of Materials	21
1.7 Derrivation of Strain for Single Slip-line	23
1.8 Strain for a Pair of Slip-lines	25
1.9 Strain Rate in Fan Region, Series Expression for Curvature and Numerical Integration for a Particular Example	26
1.10 Measure of Strain	30
1.11 Shape of Strained Circle	32
1.12 Direction of Texture	35
1.13 Plotting Deformed Shape	36

	Page
CHAPTER 2 Dynamometry	38
2.1 General Introduction	38
2.2 Types of Measuring Instruments	39
2.2.1 Absorption Dynamometers	39
2.2.2 Transmission Dynamometers	40
2.2.3 Force Measuring Instruments	40
2.3 Dial Gauge Dynamometers	41
2.4 Hydraulic Devices	44
2.5 Pneumatic Devices	44
2.6 Optical Devices	45
2.7 Piezoelectric Crystals	46
2.8 Electrical Devices	46
2.9 Design of Tool Dynamometer	47
2.9.1 Design, Heat-Treatment and Dimensions of the Main Parts of the Tool Dynamometer	48
2.9.2 Adjustment of the Dynamometer	53
2.9.3 Calibration of the Tool Dynamometer	53
2.10 Strain Gauge Dynamometer	54
2.10.1 Circuit Design	55
2.10.2 Dynamometer Cantilever	56
2.10.3 Determination of Several Parameters	56
2.10.4 Choice of Galvanometer	58
2.10.5 Maximum Trace Deflection	59
2.11 Instrumentation	59
2.12 Calibration of the Strain Gauge Dynamometer	60
CHAPTER 3	61
3.1 Chip Breaking	61
3.2 Cutting Operations from Chip Breaking Point of View	61

	Page
3.2.1	Turning and Boring 62
3.2.2	Drilling 62
3.2.3	Milling 63
3.2.4	Broaching 63
3.2.5	Tapping and Reaming 63
3.3	Why Use Chipbreakers? 64
3.4	Types of Chipbreakers 65
3.5	Chipbreaker Geometry 67
3.6	Breaking of the Chip 68
3.7	General Views of the Chip Breaking Methods 70
3.8	Effect of Coolant on Chip Breaking 78
3.9	The Effect of Grinding on Chip Breaking 78
3.10	Chip Breaking by means of Interrupted Feed Devices and Vibratory Methods 79
3.11	Chip Curl Radius 81
3.12	Chip Breaking Effectiveness 92
CHAPTER 4	96
4.1	Analysis of the Experimental Results 96
4.1.1	General Analysis of the Experimental Results 96
4.1.2	Summary of some of the Experimental Results 105
4.2	Deductions from the Analysis of the Experimental Results 107
4.2.1	Deductions from the Analysis of the Experimental Results obtained at Low Cutting Speeds 107
4.2.2	Deductions from the Analysis of the Experimental Results obtained at High Cutting Speeds 109

	Page
4.2.3. General Deductions from the Experimental Results	111
CHAPTER 5	113
5.1 General Discussion	113
5.2 Discussion of the Experimental Results	116
5.3 Recommendations for Future Work on Chip Breaking	119
CHAPTER 6	120
Conclusions	120
APPENDIX I	122
Theoretical Analysis of Chip Curling Mechanism for both Clamped Wedge and Ground Step Chipbreakers	
APPENDIX II	127
Forces Acting on the Chipbreaker	
BIBLIOGRAPHY	129

ACKNOWLEDGEMENTS

The author would like to express his gratitude to his father, HAJ HASSAN MAGHDI ALMANDILAWI, whose financial support made this research possible. Special thanks are due to Professor D.S. Dugdale for his supervision and guidance throughout this work. He also wishes to thank the firm of Firth Brown Tools Limited, for supplying tools and materials.

Finally the author is indebted to Mr. J. D. Trott and staff in the machine shop and photography section for their assistance.

I. H. M. A.

SUMMARY

This investigation has been carried out to analyse and discuss the chip formation and chip breaking processes in metal cutting and to demonstrate the degree of agreement between the theoretical and experimental results. Particular attention has been given to the chip breaking control.

Different materials such as steels (low, medium and high carbon steels), aluminium alloy and copper were tested under different cutting conditions using different tool geometries with ground and clamped chipbreakers, and cutting was carried out dry and with coolant. The chips obtained were measured, and the experimental results were plotted.

For the chips to be controlled at the cutting zone and effectively transported from the vicinity of the machine tool, it is essential chipbreakers are used.

Chip breaking effectiveness was found to be influenced chiefly by the ratio of chip curl radius to feed. The condition for minimum cutting force was found to be influenced chiefly by the chipbreaker proportion ratio, i.e. the width/height for ground step chipbreaker and width/angle of the inclination of the chipbreaker wedge for clamped wedge chipbreaker. Chipbreaker proportions are limited on the one hand by the need to get sufficiently broken chips and on the other hand by the need to avoid extensive increase in cutting forces, which should not increase by more than about 10 %.

During this work it was established that the use of chipbreaker having optimum dimensions will not only give broken chips with reduced cutting force, but also that there will be no increase in tool wear due to the presence of a chipbreaker. Coolant was

found to be helpful in promoting good chip breaking performance.

Charts were drawn for quickly finding chipbreaker dimensions for effective chip breaking over a wide range of cutting conditions and materials. A theoretical expression for chip breaking effectiveness in terms of chip curl radius and chipbreaker proportions was suggested.

I. H. M. A.

CHAPTER 1

A DISCUSSION OF METAL CUTTING STUDIES

1.1 MACHINABILITY

Although the term "machinability" is widely used, and from the practical point of view is readily understood as denoting a relative quality, there is no general agreement on a precise definition.

Good machinability may carry implications concerning,

- (1) Low energy absorbed in cutting.
- (2) Long tool life.
- (3) Good surface finish.
- (4) Formation of chips that can be easily disposed of.

The main factors^(1,2) related to machinability are:

(1) Workpiece Material:

grain size; chemical composition; melting and casting processes; method of fabrication, e.g. cast, forged, drawn or rolled; type of heat-treatment, e.g. annealed, hardened by quenching, tempered or aged; microstructure; distribution, type and characteristics of included non-metals; properties: tensile strength, ductility and hardness; size and shape.

(2) Cutting Tool:

e.g. form, shape, angles; heat-treatment; hardness and strength; alloy composition; accuracy of grinding.

(3) Machine Tool:

machine type; rigidity of tools and work-holding devices; specification of the operation.

(4) Cutting Conditions:

cutting speed; feed; depth of cut

(5) Cutting Fluid:

type: soluble water, mineral, lard, sulfurized oil etc.;
cooling properties.

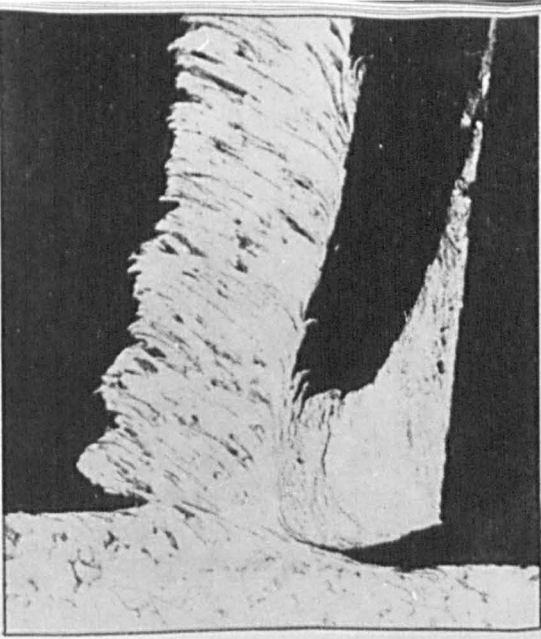
Materials having good machinability permit a high rate of metal removal with satisfactory tool life and surface finish.

Machinability assessments have been mainly based on considerations of tool wear, the chip behaviour and the energy consumption in machining.

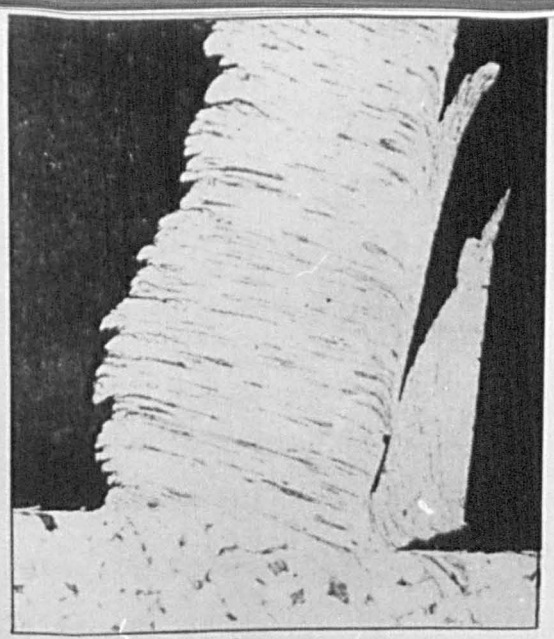
By considering in the first instance, only one criterion of machinability such as surface finish, Rubenstein⁽³⁾ considered machinability of a material as a quality that changed in an adverse way with increasing ductility, under the conditions existing during cutting. An index of ductility is shown to be a valid index of machinability as assessed by surface finish, by cutting force magnitude, or by tool wear within a limited set of cutting conditions. Metallurgical investigations into the causes of wear of cemented carbide tools have been carried out by Trent⁽⁴⁾ to provide some evidence of the conditions at the cutting edge of the tool and the factors controlling tool life and machinability.

Tool life under machine shop conditions is known to be the result of a number of different processes and factors which affect tool life in different ways and subject to different laws. Flank wear, the built-up edge (Fig.1a-e)⁽⁴⁾, deformation of the tool subjected to high temperatures and stresses, cratering wear, mechanical chipping, and thermal cracking all affect the useful length of tool life⁽⁴⁾.

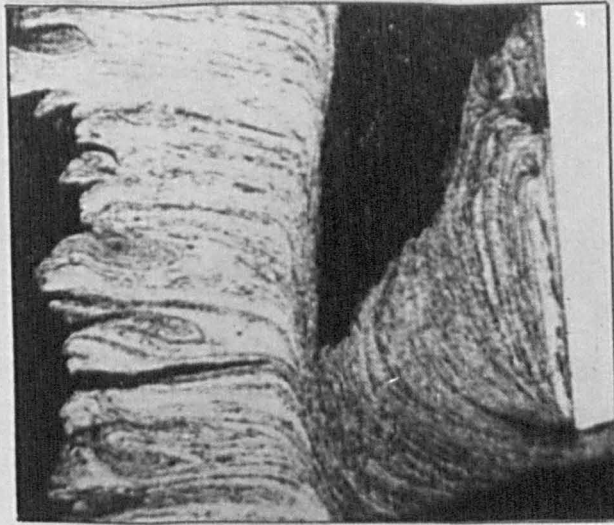
Cratering wear is a form of wear on rake (cutting) face of the tool occurring at relatively high cutting speeds. This form of wear is consequently very temperature sensitive. Oxley and Welsh⁽⁵⁾ suggested that the value of the ratio of m/k together with the value of k (where m is the slope of stress-strain curve at mean strain rate and k is the shear flow stress), which are fundamental material



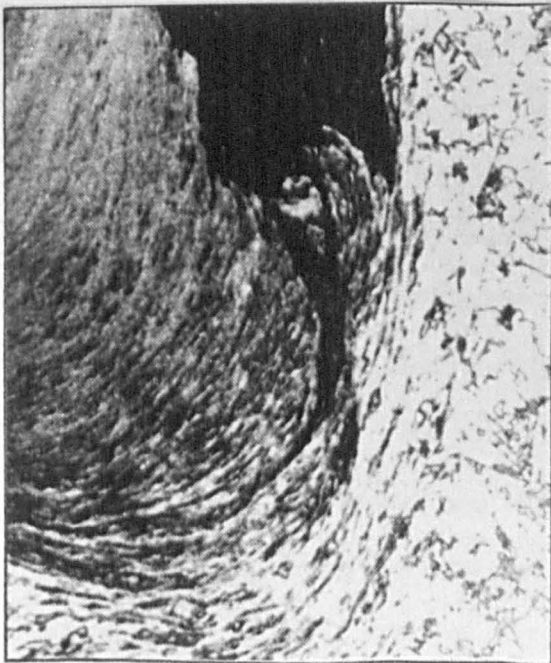
a



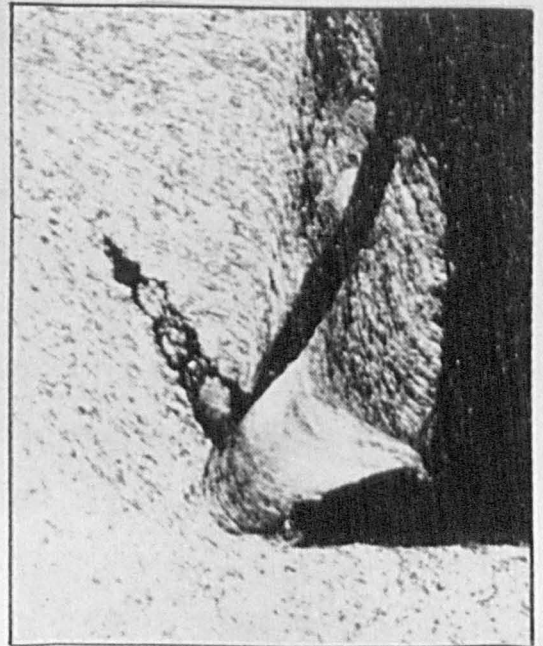
b



c



d



e

FIG 1

properties, should be taken as an indication of the way in which a material machines. Materials having high values of m/k and k are expected to machine with large cutting forces, thick chips and result in poor surface finish.

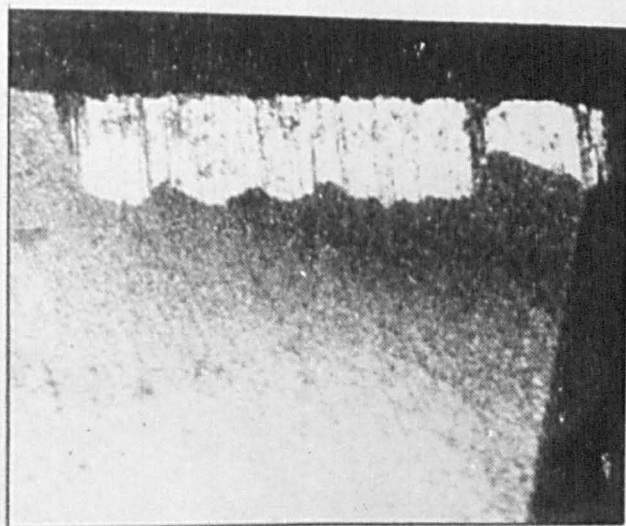
The shear angle⁽⁶⁾ has been used as a factor in estimating machinability. High values of shear angle indicate large ranges of continuous chips, low cutting forces and good surface finishes. Low shear angles are associated with small ranges of continuous chips, large cutting forces and poor surface finishes.

A basic factor in machinability is the stress required to shear the work material at high temperature and extremely high strain rate. This may explain the poor machinability of materials of high creep strength.

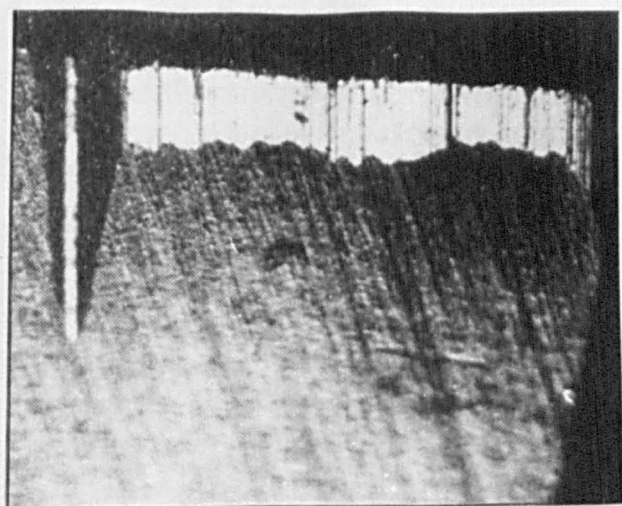
Trent⁽⁷⁾ concluded that metallurgical behaviour of the work material in extreme conditions of the flow zone, is probably the most important factor in machinability. Improvements in the machinability characteristics of steel can be made by means of inclusions such as M_nS which can act as internal lubricants, forming films on the cutting face of the tool which are easily sheared under these extreme conditions or silicates which can also act as lubricants greatly reducing stresses, temperatures, and tool wear. M_nS

The examination of worn tools⁽⁷⁾ lead to the conclusion that the main wear process on carbide tools are based on diffusion wear and attrition. Diffusion wear is mainly controlled by temperature, the flow rate of the work material very close to the tool surface, and the diffusion relations between tool and work material. Attrition is dependent mainly on irregularity in flow of material over the tool surface and is therefore greater at low speed. Neither diffusion nor attrition wear depends on high hardness of the work material (Fig. 2_{a-c})⁽⁷⁾.

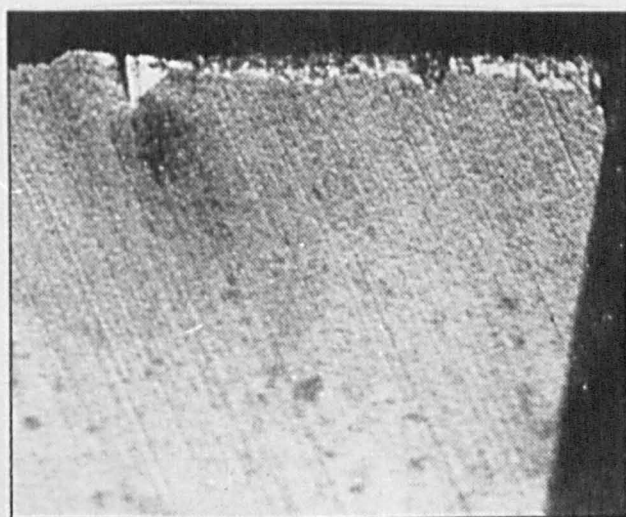
Experiments on lubrication of tools show that gases can



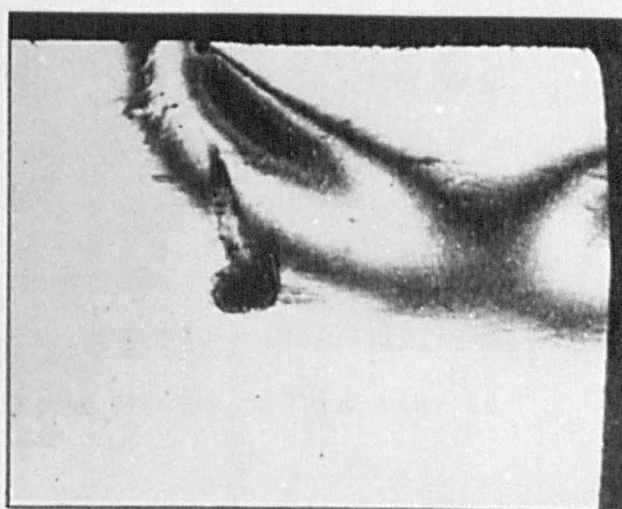
a



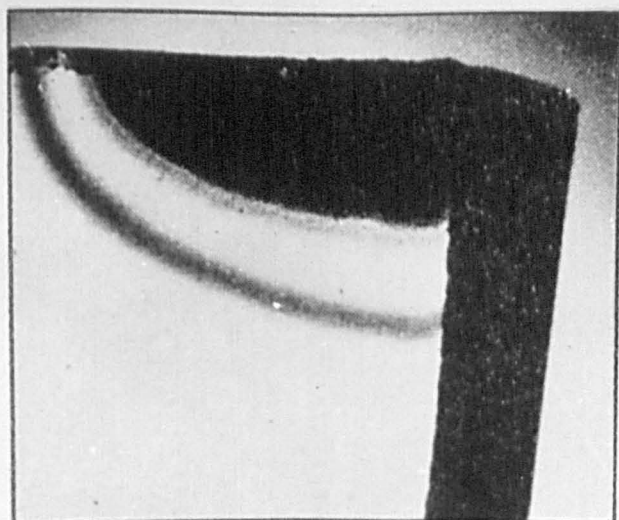
b



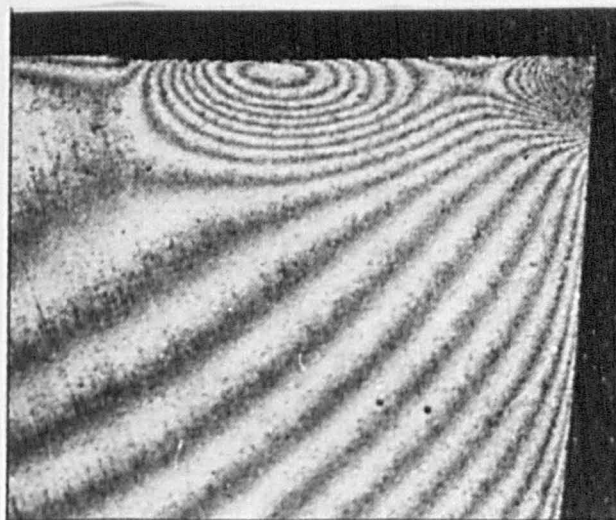
c



d



e



f

FIG. 2

penetrate to some distance between tool and work from edges of the area of contact at medium and low cutting speeds. The freshly generated metal surfaces act as an absorbent for atmospheric oxygen and protect the tool when cutting in air from a form of wear which may be very rapid when a jet of oxygen or water is directed at the tool (Fig.2_{d-f})⁽⁷⁾.

Experiments on aluminium alloys⁽⁸⁾ have shown that pure aluminium tends to weld at the tool cutting face. This tendency is reduced as the tensile properties of the aluminium are increased by alloying, heat-treatment or cold working. Built-up edge could be avoided by maintaining a keen cutting edge, polishing the tool surface over which the chips flow, allowing adequate rake and clearance angles, and providing a suitable lubricant.

Electrochemical machining (ECM) is one of the newest methods of metal removal for mass production and offers new possibilities for improving machinability. There is no problem of tool wear in ECM.

Mechanical abrasion of the tool material, micro-crumbling due to cold welding of tool material and workpiece material, diffusion between tool and workpiece materials, weakening of tool material with consequent plastic deformation, and fracture due to mechanical stress are the most effective causes of tool wear⁽⁹⁾.

One of the most successful criteria of machinability is the permissible cutting speed.

According to Kronenberg's law of cutting speed:

$$V_{60} = C_v / A^{\frac{1}{\epsilon_v}} \quad (1.1)$$

where:

V_{60} is the permissible speed- the average speed of a tool in work for 60 mins.,

C_v and ϵ_v are material constants,

A is area of cut.

For geometrically similar sections of cut the depth feed ratio C is constant

$$C = t / S$$

where:

t is depth of cut

S is feed

and the area of cut is:

$$A = t S = C S^2$$

Hence equation (1.1) reads:

$$V_{60} = C_v / (CS^2)^{\frac{1}{\epsilon_v}} \quad (1.2)$$

1.2 CHIP FORMATION

Recently, theoretical studies on metal cutting have been well developed, especially regarding the fundamental analysis of the mechanics of orthogonal cutting in which a continuous or discontinuous chip is produced. Various theories have been presented by Time⁽¹⁰⁾, Zvorykin⁽¹¹⁾, Briks⁽¹²⁾, Piispanen⁽¹³⁾, Ernst and Merchant⁽¹⁴⁾, Field and Merchant⁽¹⁵⁾, Cook, Shaw and Finnie⁽¹⁶⁾, Zorev⁽¹⁷⁾, Lee and Shaffer⁽¹⁸⁾, Hill⁽¹⁹⁾ and several others assuming a perfectly plastic solid without strain hardening or inhomogeneity of the material. In most analysis, however, it has also been assumed for the sake of simplicity, that the chip formation is a process of shear (without fracture for the continuous chip and with fracture for discontinuous chip) confined to a single plane extending from the tip of the cutting tool to the sharp intersection of free surface of workpiece and chip, i.e. the shear plane. All these theories were based on the single plane concept.

Okushima and Hitomi⁽²⁰⁾, Nakayama⁽²¹⁾, Okushima⁽²²⁾, Keceaoğlu⁽²³⁾, and Christopherson, Oxley and Palmer⁽²⁴⁾ have analysed the cutting mechanism and concluded that there is a family of shear planes within the deformation zone. Okushima⁽²²⁾ showed,

experimentally by photomicrographs, that the shear process took place over a large area instead of along a single plane.

The chip formation process during orthogonal cutting can be looked upon as a case of plane strain deformation if the width of the layer of metal being removed is considerably greater than its thickness. This method of chip formation was first suggested by Time⁽¹⁰⁾ and a further development was carried out by Zvorykin⁽¹¹⁾. According to this method the shear deformations during the transformation of the layer into a chip occur along a certain unique plane.

Deformation methods based on the single shear plane were justly criticized by Briks⁽¹²⁾. Briks suggested that the plastic shear in the working surface occurs in a family of fan wise arranged planes which pass through the cutting edge O (planes $O A_0, O A_1, \dots, O A_n$), Fig. 3. The outer surfaces of the work and the chip are separated by a certain transition surface $A_0 A_n$. This scheme of deformation has several drawbacks. Firstly, assuming that the transition surface intersects the outer surface of the chip so that the transition surface tangent at the point A_n forms a certain angle ξ (which is about half the cutting angle), with the outer surface of the chip. The particles of the machined material, thus receive infinitely great accelerations as they pass through the plane $O A_n$. Secondly, Briks considered the shear lines to be straight. As it follows from the boundary conditions on the transition surface that all the shear lines must form equal angles of $\pi/4$ with the tangents to this surface, the shear lines therefore, must be curved, Fig. 4. For example, the straight shear line OA_1 forms an angle $\delta < \pi/4$ with the tangent X_1 . In actual fact this angle must be $\pi/4$ in which case the shear line must be curved as shown in Fig. 3 by a dotted line. Since stresses σ_{x_1} and σ_{y_1} at point A_1 are principal because there are no external loads on the transition surface $A_0 A_n$, the lines of maximum tangential stress at point A_1 thus forms an angle

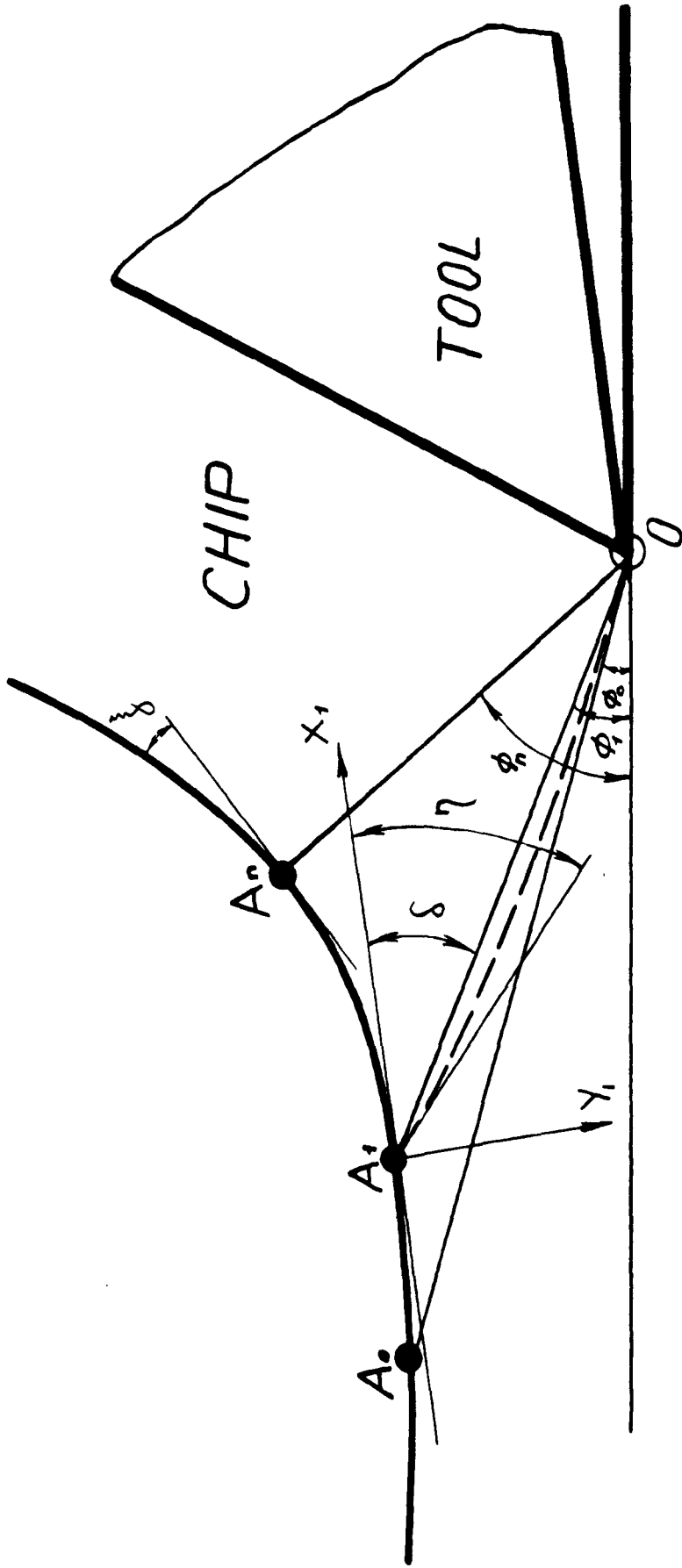


FIG. 3

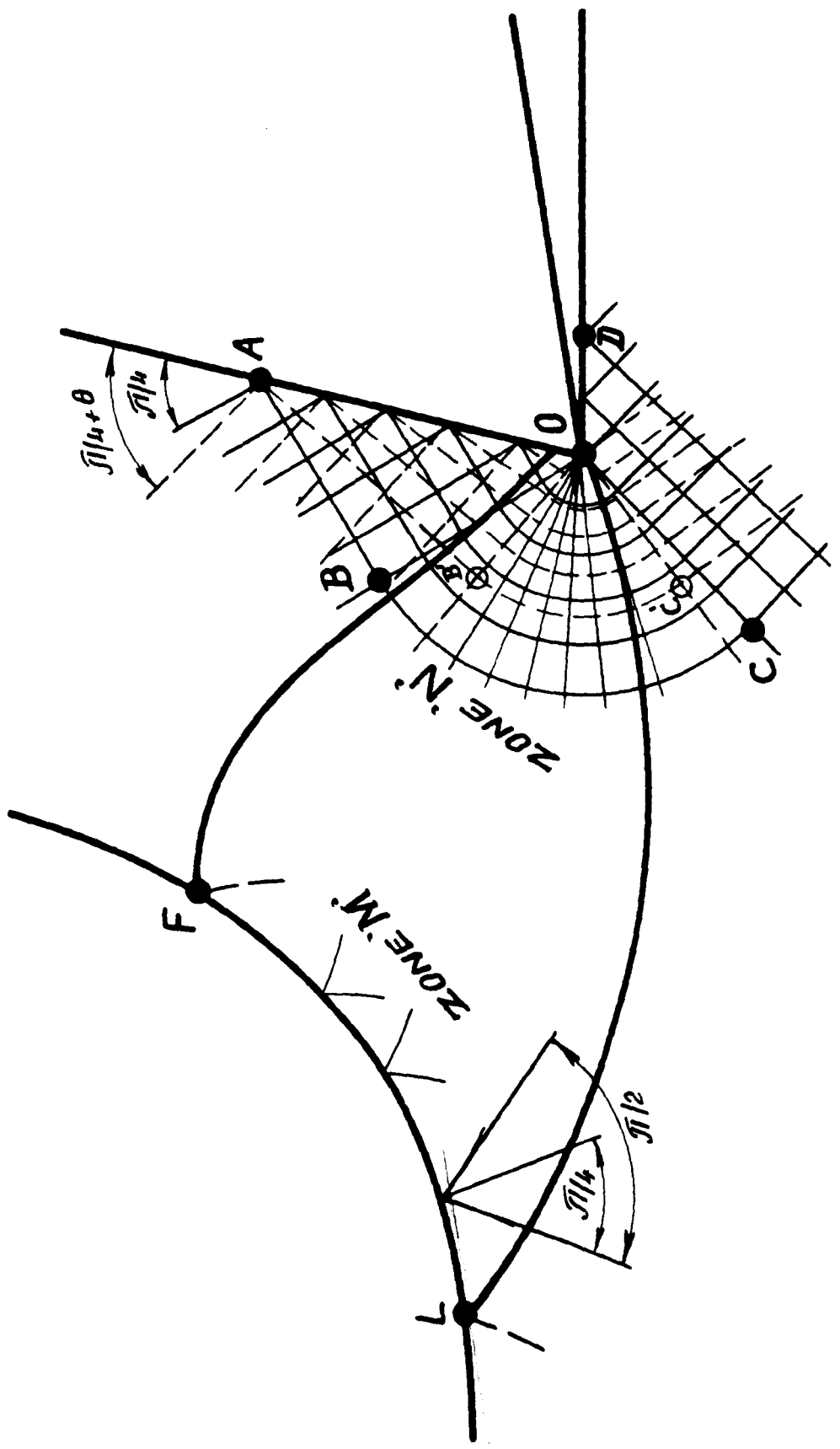


FIG. 4

$\eta = \sqrt{\pi}/4$ with tangent X_1 .

On the assumption that there is no friction on the contact surfaces, Ilyushin⁽²⁵⁾ suggested that within the deformation zone M, Fig. 4, there are two families of mutually orthogonal curves with a constant angle $\sqrt{\pi}/2$ between the tangents to a pair of neighbouring curves of one family as they move along these lines. The normal to the transition curve and the tangent to the shear line at the point of intersection, form an angle of $\sqrt{\pi}/4$. This is so, due to the fact that the normals to the transition curve coincide in direction with one of the principal stresses. Ilyushin has recognized three regions within the deformation zone N. The first region AOB is characterized by two families of mutually orthogonal straight shear lines, intersecting the cutting face of the tool at angles of $\sqrt{\pi}/4$. The second region BOC is characterized with point "O" through which pass the first family of mutually orthogonal straight shear lines in the form of a fan. The second family takes the form of concentric arcs of circles. The shear lines in the third region COD are straight and make an angle of $\sqrt{\pi}/4$ with the machined surface.

In case of the presence of friction on the contact surfaces, the families of characteristic curves will take a different form (Fig. 4 (dotted)) due to the change in the boundary conditions. For example, the friction forces between the chip and the cutting face of the tool in the region AOB will cause an anti-clockwise rotation of the shear lines. Accordingly the friction forces on the rear surface will cause a clockwise rotation of the shear lines in the region COD. The action of friction forces, thus, results in narrowing of the region BOC (region $B^1 OC^1$, Fig. 4). It is clear that this rotation of the shear lines is connected with a change in orientation of the principal stresses on the surface of contact of the chip with the front surface of the tool. By using stress circles⁽²⁶⁾ it is clear that

at a friction angle of θ the axes of the main normal stresses on the contact surface make angles of θ with front surface and with the normal to it. The shear lines thus make angles of $\pi/4 + \theta$ with the front surface and the normal to it (Fig. 4).

Taking all the foregoing into consideration Zorev⁽¹⁷⁾ suggested the following scheme of the shear lines as shown in (Fig. 4). The plastic zone LOF is limited by the starting boundary shear line OL along which the first plastic deformation in shear occurs, the ending boundary shear line OF along which the last shear deformation occurs, and line LF which is the deformed section of the outer surface of the cut. The shear deformations take place along a family of shear lines within the plastic zone LOF. As the cutting proceeds, the plastic zone LOF moves with the tool. As the particles of the work surface pass through the plastic zone, the deformation increases from zero to a certain maximum, appropriate to the final chip.

Cook and Shaw⁽²⁷⁾ established by photographic studies of the cutting process, that there is no unique shear plane and that the chip formation zone resembles a wedge, whose apex adjoins the cutting edge. Similar observation has been noticed by Albrecht⁽²⁸⁾.

Palmer and Oxley⁽²⁹⁾ have suggested that the over simplified picture of deformation represented by a single shear plane, together with the simplified stress distribution, is responsible not only for the lack of agreement between predicted and observed parameters in metal cutting, but also for the failure to explain the reason for the change from a continuous to a discontinuous chip. They observed the deformation during actual cutting and carried out an analysis using the slip-line fields theory which allowed for a variable maximum shear stress, e.g. with work-hardening. They have found that the shear zone is of a finite width and roughly triangular in shape, with the apex near the cutting edge and with stream lines of flow following smooth curves from the work into the chip (Fig. 5). The chip leaves the plastic zone

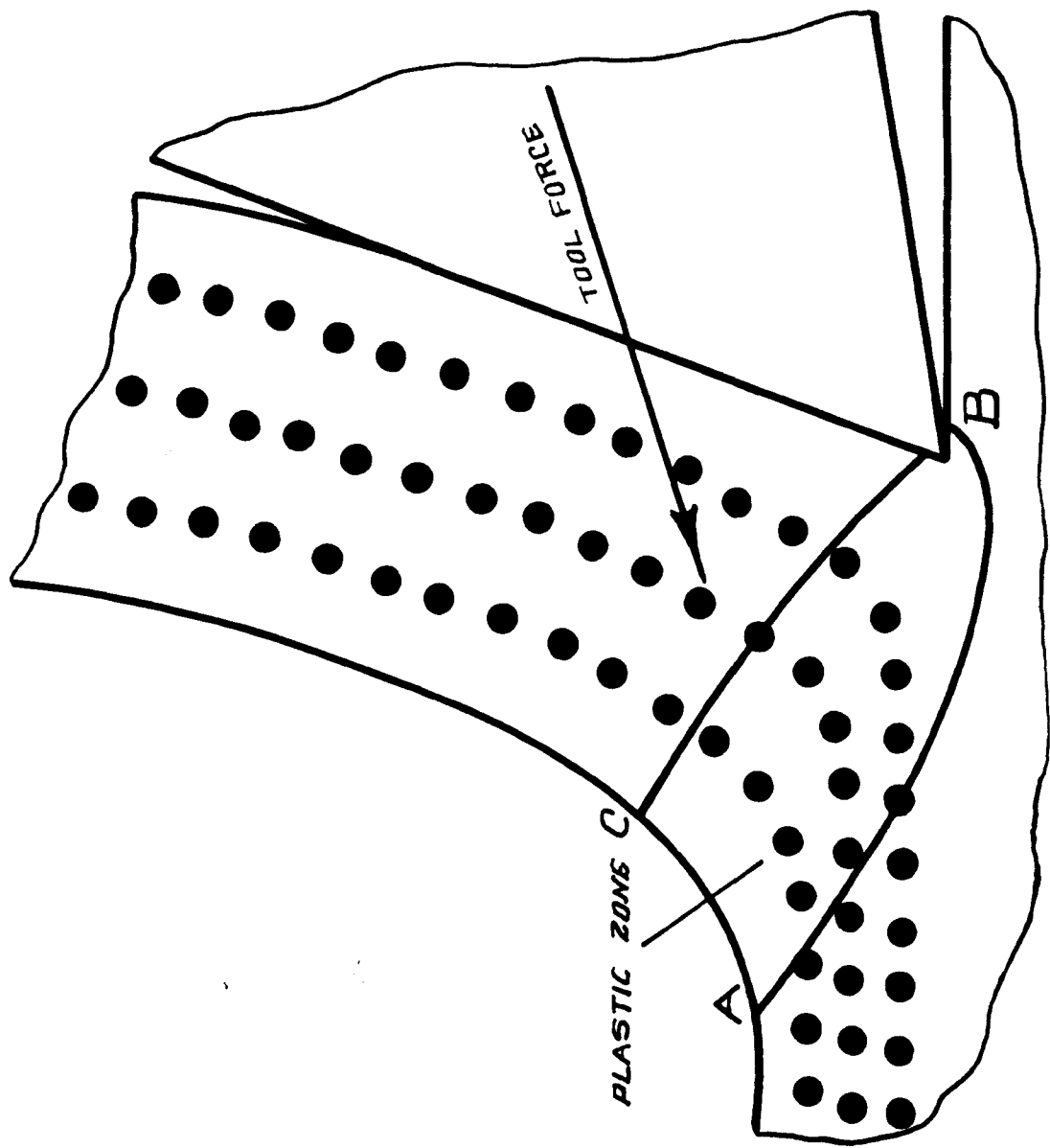


FIG. 5

curled, and only contacts the tool for a short distance above the cutting edge. The normal or hydrostatic stress varies from compression at the outer surface to tension at the cutting edge. Palmer and Oxley concluded that the presence of tensile stresses at the cutting edge of the tool could probably account for the transition from a continuous to a discontinuous chip.

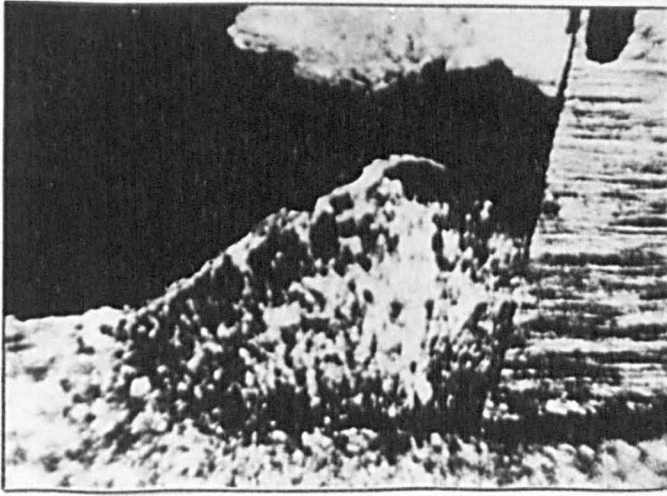
1.3 TYPES OF DEFORMED CHIPS

1.3.1 Discontinuous

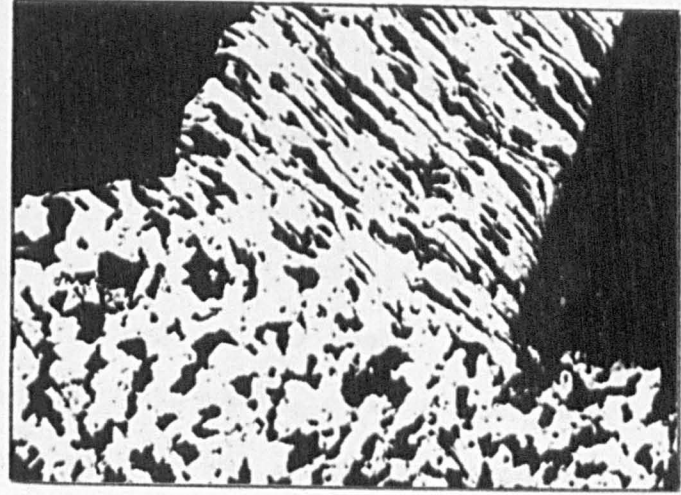
These chips are of sectional or segmented type in which an initially compressed layer passes off with each chip segment, the cycle being then repeated. Such chips are short and brittle. Discontinuous chips are made up of sections of roughly the same size (Fig. 6a)⁽¹⁷⁾ that combine to make up a long unbroken chip with a serrated surface. Frequently, however, the separate sections split off. The pitch of these segments depends upon the condition of the operation and the material being cut. When the pitch of the segments is small, a good finish is produced on the workpiece. The conditions which favour the formation of this type of chip are brittle material, large feed and depth of cut, low cutting speed and small rake angle. For such material tool life is longer, and tool failure is due to the rounding over and wearing away of the cutting edge. These segmented chips are easily disposed of.

1.3.2 Continuous Without Built-Up-Edge

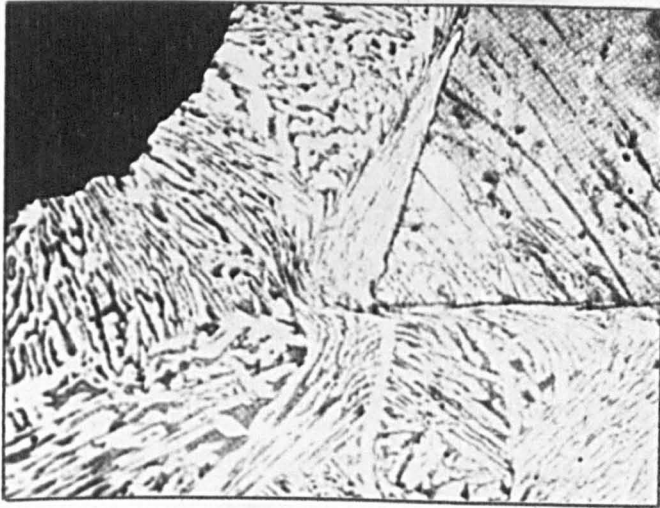
Such chips are long ribbons of uniform thickness (Fig. 6b)⁽¹⁷⁾. A continuously moving layer adjacent to the tool face in the plastic flow occurs with relatively ductile material. Conditions which are favourable for the formation of this type of chip are ductile material, small feed and depth of cut, high cutting speed, large rake angle, keen cutting edge and high polish on tool faces^(8,17). The formation of



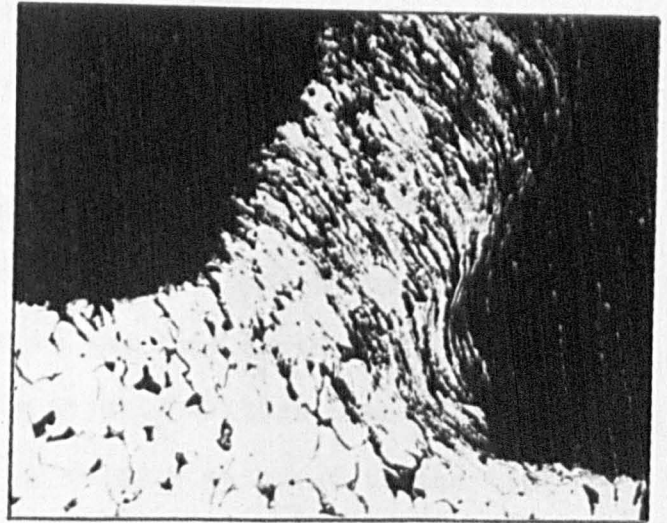
a



b



c



d

FIG. 6

this type is also favoured by the use of an effective cutting fluid in the case of high-speed cutting tools. It is characterized by the absence of the build-up edge, and therefore, a high quality of finish is produced. Tool life on such material is generally very good, and tool failure may be due partly to rounding of the cutting edge and partly to abrasion of the face close to the cutting edge.

1.3.3 Continuous With Built-Up Edge

Such chips (Fig. 6c-d)⁽¹⁷⁾ are usually long but not smooth and, generally, considerably thicker than the "feed" of the tool. Chips of this nature come from very ductile materials having medium machinability. The metal in the chip has been severely cold-worked in machining and a built-up edge has developed on the tip of the tool. The finish on the work is usually rough and has a torn appearance due to fragments of built-up edge adhering to the workpiece. The tool usually fails because of cupping or cratering of the tool face a short distance back from the cutting edge at the point of contact with the chip and by abrasion of the tool flank due to contact with the fragments of built-up edge which escapes with the workpiece. Continuous chip with built-up edge is produced when the coefficient of friction between the tool and the chip exceeds a certain minimum value depending upon the metal being cut, Under these conditions, the stress on some plane in the chip extending from the tool face down to the face of the chip becomes equal to the shear strength of the chip metal. Failure then occurs on that plane, and a section of the chip remains anchored to the tool face to form the built-up edge. As this built-up edge continues to increase in size during the cutting process, it soon reaches such proportions that it no longer can be carried by the tool, fragments of it pass off with both the chip and the workpiece.

1.4 DISCONTINUOUS CHIP FORMATION

It is generally understood that a brittle material is more liable to produce discontinuous chips than a ductile material, but some ductile materials will produce continuous, discontinuous and partially discontinuous chips depending upon the cutting conditions.

Cook, Finnie and Shaw⁽¹⁶⁾ classified the discontinuous chip into two types. They distinguished between the cracks that were just visible under the microscope in machining ductile materials and the completely discontinuous chip where the material is removed in the form of separate segments. The fracture is either of the ductile shear type or the brittle tensile type. They stated that completely segmented chip formation is entirely different from that of continuous cutting, being better described as a periodic extrusion rather than one of simple shear.

Field and Merchant⁽¹⁵⁾ noted that the discontinuous chip was formed during the machining of brittle materials like cast iron or when cutting ductile materials at low speeds and without cutting fluids. They suggested that the basic difference between the formation of continuous and discontinuous chip was that instead of shear occurring ahead of the tool continuously without fracture, rupture occurred intermittently on the shear plane thus introducing new factors into the geometry of chip formation.

Analysing the cine-films taken during the actual cutting process Field and Merchant⁽¹⁵⁾ have found that as the tool advanced with respect to the work, chip segments were produced at relatively uniform rate. Sketches corresponding to selected frames from a cine-film taken when cutting bronze are shown in fig. 7. Frame 1 shows the tool just beginning to advance into the inclined work surface produced by the previously ruptured chip segment. In Frame 16 the metal distortion indicates a high shear angle and a shear plane

CUTTING MATERIAL - BRONZE
 CUTTING SPEED 0.5 LPM
 DEPTH OF CUT 0.015 in
 WIDTH OF CUT 0.050 in
 RAKE ANGLE 14 DEG.

(ACCORDING TO FIELD AND MERCHANT (15))

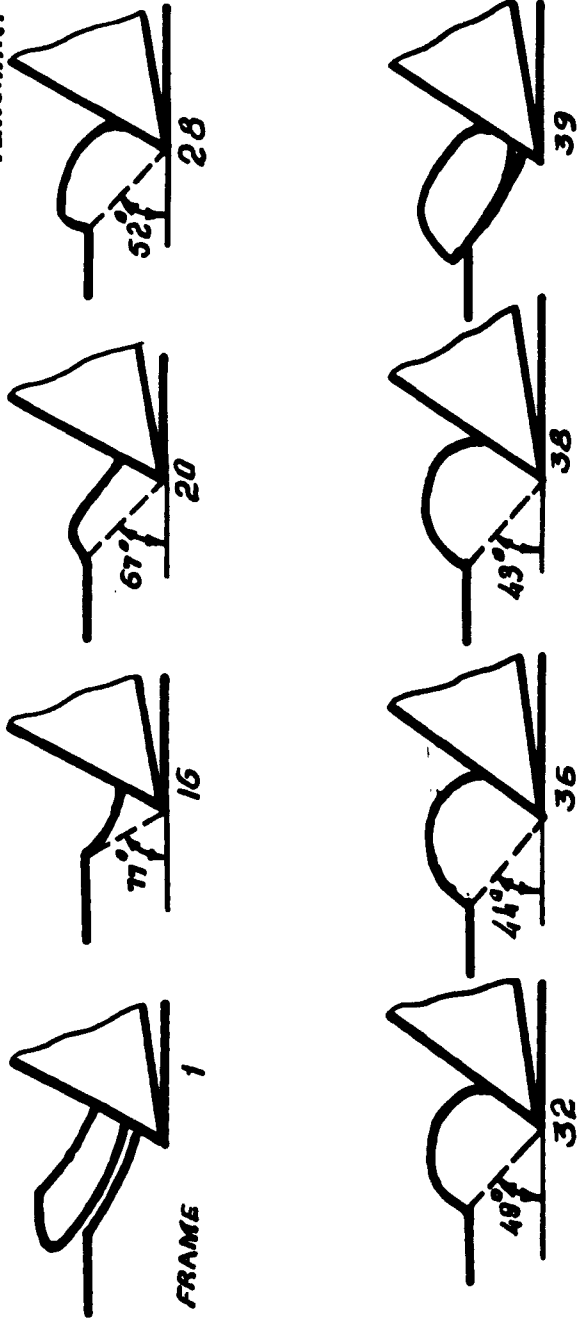


FIG. 7

extending to the inclined work surface. As the tool advances further, the shear angle decreases rapidly so that by Frame 20 the shear plane has extended to the horizontal surface. This is indicated by the start of the curvature of the surface. Still further advance of the tool results in a continuing decrease of the shear angle till rupture occurs along a shear plane thus producing a chip segment as in Frame 39. This is the end of the cycle which then repeats itself.

Investigations carried out by Bridgman⁽³⁰⁾ have shown that the amount of plastic shearing strain necessary to produce fracture increases as compressive stress is applied to the shear plane. The relationship between the shearing strain required for rupture and compressive stress is roughly of the form:

$$\epsilon_r = \epsilon_0 + K S_n \quad (1.3a)$$

where, ϵ_r is the strain required to produce rupture, ϵ_0 is the shearing strain required to produce rupture at zero compressive stress, K is the slope of the shearing strain and compressive stress curve and S_n is the compressive stress acting perpendicular to the shear plane. Fracture will thus occur on the shear plane causing a discontinuous chip whenever the shearing strain ϵ which (assuming the shear plane model of continuous chip formation) is given by

$$\epsilon = \cot\phi + \tan(\phi - \alpha) \quad (1.3b)$$

$$\begin{aligned} (\alpha &= \text{rake angle} \\ \phi &= \text{shear angle}) \end{aligned}$$

becomes equal to or greater than ϵ_r .

This rupture condition can be expressed mathematically by combining equations (1.3a) and (1.3b), bearing in mind that the shear angle at rupture is ϕ_1 ; hence:

$$\cot\phi_1 + \tan(\phi_1 - \alpha) \geq \epsilon_0 + K S_n \quad (1.4)$$

Field and Merchant⁽¹⁵⁾ claimed that to a first approximation, equation (1.4) establishes the value of the minimum shear angle ϕ_1 at which fracture will occur when cutting a given material. They argued that as the tool enters a cut and advances into the metal, the shear angle will first fall due to increasing friction between chip and tool and that if, during this process the shearing strain rises to a high enough value or the compressive stress drops to a low enough value, or both, to satisfy equation (1.4), then a discontinuous chip will result. If, on the other hand, the equilibrium value of the shear angle ϕ is arrived at before the shearing strain rises high enough or the compressive stress falls low enough then the chip will remain continuous. Field and Merchant⁽¹⁵⁾ noted that although this qualitative argument based on equation (1.4) is sound enough, the actual results given by the equation (1.4) are in poor agreement with experimental observations. This lack of agreement, appears to be due to the inadequacy of the shear plane concept.

By treating frictional conditions which varied from smooth to perfectly rough, Lee⁽³¹⁾ has found that the shear angle was almost independent of friction; this suggests that the decrease in magnitude of the shear angle, as observed by Field and Merchant⁽¹⁵⁾, is not due to the friction and may be associated with the extension of plastic flow to the initial work surface.

Piispanen⁽¹³⁾ has discussed the formation of the discontinuous chip from the standpoint of ordinary chip formation and concluded that the shear angle is initially high and decreases as the cut proceeds, finally reaching a value corresponding to a shear strain sufficient to cause fracture.

From series of experiments by Cook, Finnie and Show⁽¹⁶⁾ it was found that the normal stress on the shear plane, as influenced by rake angle or tool friction, is an important variable in determining

whether a chip will be continuous or discontinuous.

Benerjee and Palmer⁽³²⁾ concluded that the formation of discontinuous chips when cutting En9 steels has been shown to be accompanied by intermittent sticking and slipping of the chip on the rake face of the tool. During the early growth of the chip a dead-metal zone or built-up edge developed in contact with the tool.

Cook, Finnie and Shaw⁽¹⁶⁾ investigated discontinuous chip formation by analysing a cine-film taken in the cutting process of β -brass (Fig. 8). From this film (Fig. 8), the broken line indicates the lower boundary of the plastic zone, and it was reported that the whole of the chip above this line was undergoing plastic deformation with the material "rolling down" on the tool face rather than sliding up the tool.

Zener⁽³³⁾, discussing metal fracture generally, observed that the opening of a crack through the stopping of a slip band did not necessarily lead to immediate fracture. The crack would extend through the region of high stress concentration at the end of the slip band and would then stop unless its length was already above the critical value needed for self-propagation under its own stress concentration. The future history of the crack may then depend to a large extent on the hydrostatic component of the stress system, a component which has little influence on the resistance to deformation.

Okushima and Hitomi⁽²⁰⁾ remarked that previous analysis of the discontinuous chip formation had been based mainly on the single shear plane concept. They developed a method in which they applied the flow region concept. As was explained by Hitomi⁽³⁴⁾ the boundary lines of the flow region are curved. Fig. 9a shows the instant when fracture occurs on the end boundary line; once

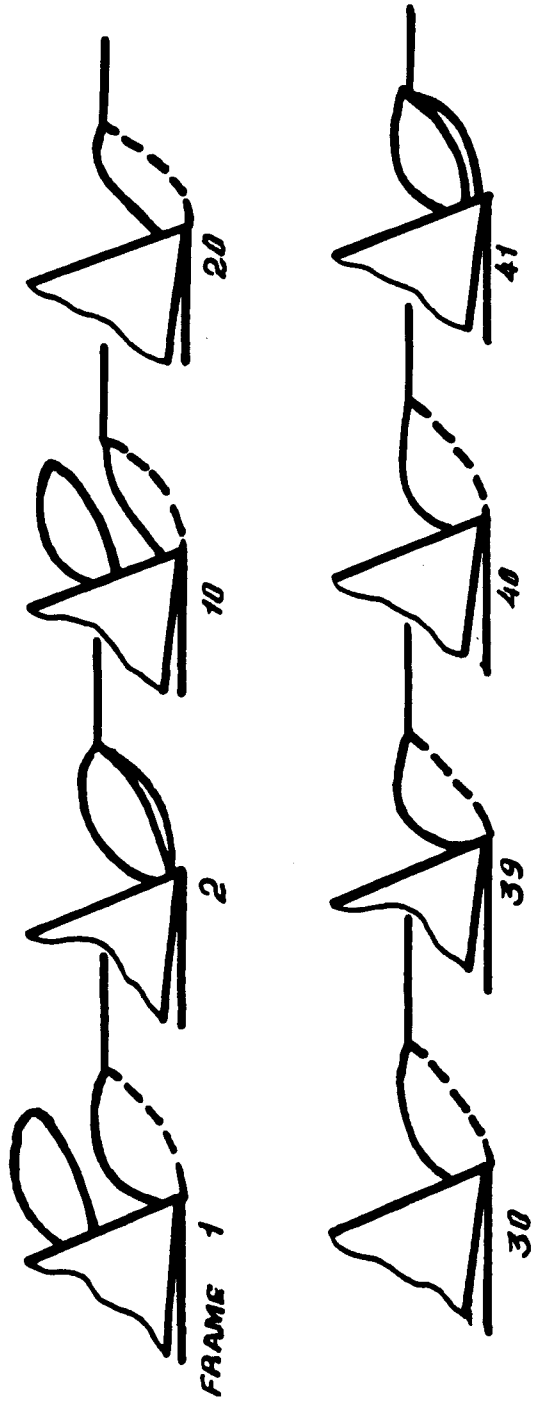


FIG. 8

CUTTING MATERIAL - β -BRASS
 CUTTING SPEED 0.5 I/PM
 DEPTH OF CUT 0.007 IN
 WIDTH OF CUT 0.160 IN
 RAKE ANGLE 75 DEG.
 (ACCORDING TO COOK, FINNIE
 AND SHAW (16))

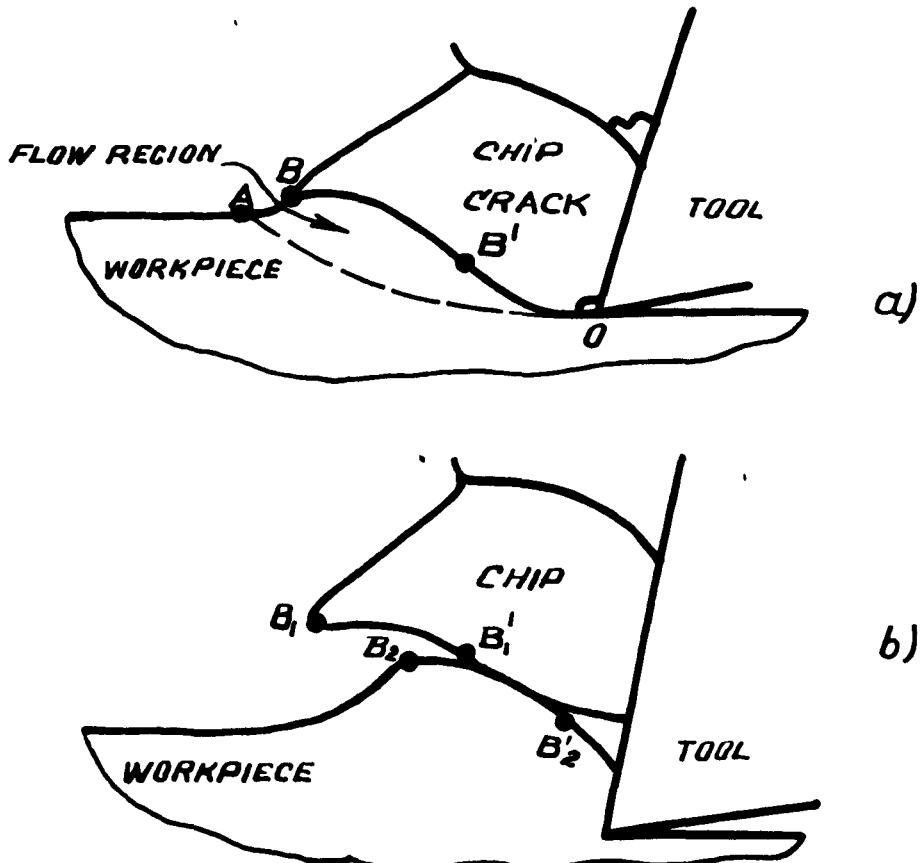


FIG. 9 EXPLANATION OF DISCONTINUOUS CHIP FORMATION

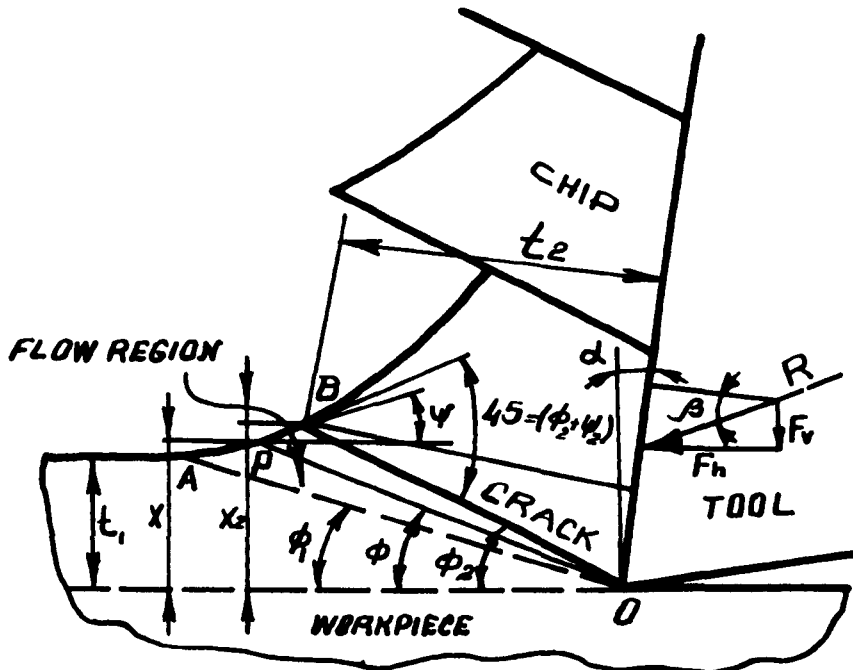


FIG. 10

ANALYSIS OF DISCONTINUOUS CHIP FORMATION BASED ON FLOW REGION CONCEPT

fracture has occurred, a fragment of the discontinuous chip flows out along the tool face without any restriction; the instant fracture occurs, the shear stress decreases below the breaking point (limit) and a new chip is to be formed.

This behaviour and the cutting process are almost the same as continuous chip formation except that fracture occurs when the shear stress on the boundary reaches the breaking point (limit) again as cutting proceeds. At the very initial stage, the workpiece which has an initial free surface at OB due to previous fracture is not cut immediately, but a portion of the workpiece near the cutting edge rises up to some degree so that some part OB' of the fracture surface OB contacts the tool face and the remaining part BB' contacts the previous fragment as shown in Fig. 9b.

The shear stress and strain are minimum at the starting boundary line OA and maximum at the end boundary line OB. The cutting force is small at the initial stage and as cutting progresses it increases. Whenever the maximum shear stress on the boundary line increases enough to exceed the breaking point (limit), fracture occurs. The process is repeated and fragments of discontinuous chip are formed one by one.

Fig. 10 shows orthogonal cutting, with depth of cut t_1 and tool rake angle α . The inclination of the starting boundary line ϕ_1 and that of the end boundary line, namely a line at which fracture occurs, ϕ_2 , are deduced theoretically in the following manner.

Since the work material should strain-harden when fracture occurs such as in the discontinuous chip formation, the relation between shear stress τ and shear strain γ may be assumed as:

$$\tau = \tau_0 + k \gamma^m \quad (1.5)$$

where τ_0 is the shear yield stress, k and m are constants showing degree of strain-hardening of the material.

The mechanism of discontinuous chip formation is described as follows: a moving particle in the undeformed work corresponds to position O (Fig. 11) and when it reaches the starting boundary line it corresponds to the position M due to the yield of the metal in shear. When a particle passes into the flow region, it changes its location from M to N continuously along the curve until it reaches the breaking point N. This corresponds to the end boundary line, i.e. the fracture line at which fracture occurs periodically, and a discontinuous chip is formed. Thus, the average shear stress must reach its maximum value at the end boundary line of the flow region.

Assuming that the shear stress distributes uniformly on the radial plane in the flow region, the shear stress on an arbitrary radial plane OP (Fig. 10) is given by:

$$\tau = \frac{R \sin \phi \cos (\phi + \alpha - \beta)}{bx} \quad (1.6)$$

where R is the maximum cutting force with which fracture is about to occur, b is the width of cut and (X) is the distance from an arbitrary point P on the free surface of the flow region to the horizontal line through the cutting edge.

This reaches a maximum when the inclination angle of an arbitrary radial plane ϕ becomes equal to the inclination of the end boundary line ϕ_2 ; i.e. from the condition

$$\left(\frac{d\tau}{d\phi}\right)_{\phi = \phi_2} = 0 \quad (1.7)$$

the following equation was obtained

$$\frac{1}{x} \frac{dx}{d\phi} = \cot \phi - \cot (\phi + \alpha - \beta) \quad (1.8)$$

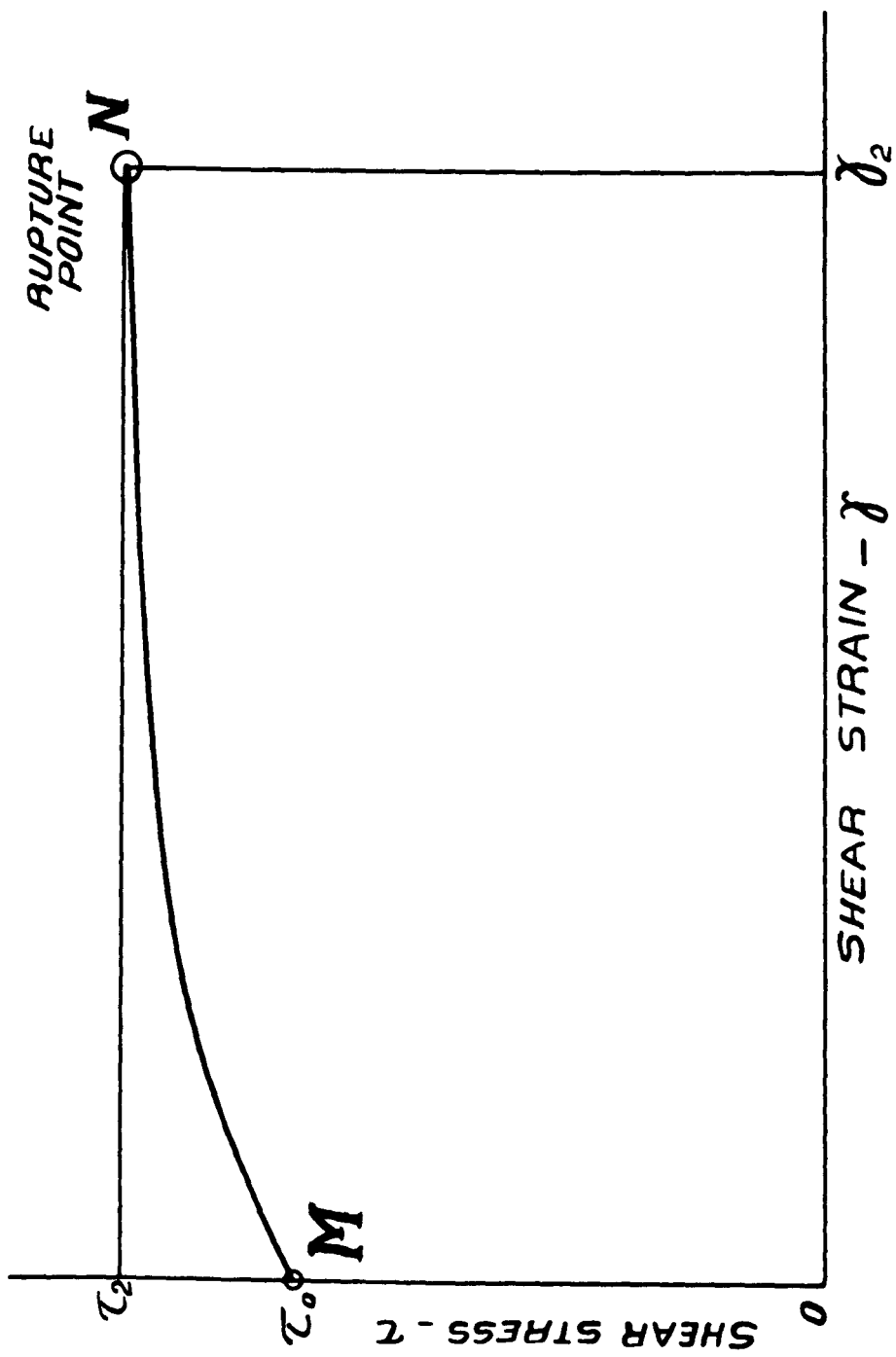


FIG. 11

Geometrically on the other hand:

$$\frac{1}{x} \frac{dx}{d\phi} = \cot \phi - \cot (\phi + \psi) \quad (1.9)$$

Hence for $\phi = \phi_2$

$$\frac{1}{x} \frac{dx}{d\phi} = \cot \phi_2 - \cot (\phi_2 + \psi_2) \quad (1.10)$$

where ψ_2 is the value of ψ at the end boundary line.

Since the end boundary line of the flow region in the case of the discontinuous chip formation is a slip-line with fracture, it makes an angle of 45° with the free surface:

$$\psi_2 + \phi_2 = \frac{\pi}{4} \quad (1.11)$$

From equation (1.8 and 1.11)

$$\phi_2 = \frac{\pi}{4} + \alpha - \beta \quad (1.12)$$

This equation shows the condition at which fracture occurs if a discontinuous chip is formed. The following expression for ϕ_1 was obtained in a similar manner:

$$\phi_1 = \frac{\alpha - \beta}{2} + \frac{1}{2} \sin^{-1} \left[\sqrt{2} \cos \left(\frac{\pi}{4} - \beta \right) - \frac{2bkt_1}{R} \left\{ \cot \left(\frac{\pi}{4} + \alpha - \beta \right) - 1 \right\}^m \sin(\beta - \alpha) \right] \quad (1.13)$$

Using the strain-hardening slip-line theory to examine discontinuous chip formation, Enahoro and Oxley⁽³⁵⁾ carried out an investigation of the hydrostatic stress distribution in the plastic zone. Various depths of cut were taken covering the range of chips from continuous to discontinuous and keeping all other conditions constant. The hydrostatic stress was found to vary from compression at the outer free surface to tension near the cutting edge; the magnitude of the tensile stress was shown to be important in determining whether or not the chip became continuous.

It is found in practice, that small changes in the cutting conditions can cause a transition from continuous chip formation to discontinuous chip formation. For example when machining a ductile material, a decrease in the rake angle, an increase in the feed or depth of cut, or a decrease in cutting speed, can cause a transition from a continuous to a discontinuous chip.

Inasmuch as the normal stress on the shear plane is inherently relatively less for small values of rake angle, the tendency to cut discontinuously increases with decreased rake angle.

An increase in cutting speed sometimes will cause a discontinuous chip to become continuous. Increase in the cutting speed will cause an increase in the shear strain required to cause fracture⁽¹⁷⁾.

It is normally found that the tendency toward discontinuous chip formation increases with the increase in the depth of cut. Shaw and Finnie⁽³⁶⁾ observed in many materials tests that when the specimen size is made very small, higher yield and flow stresses are obtained.

It is significant to mention that the use of chipbreakers can cause a continuous chip to become discontinuous (broken) without actually changing the existing cutting conditions. This process will be discussed in detail later in this work.

1.5 GENERAL REMARKS ON THE PARAMETERS INFLUENCING CHIP FORMATION PROCESS

1.5.1 Influence of Rake Angle on the Chip Formation Process

Chip formation is highly influenced by the rake angle. This influence is directly observed through the change in the direction of the chip flow and indirectly through the change in the coefficient of friction between the chip and the cutting face of the tool.

The presence of the built-up edge weakens the influence of the rake angle on chip formation. A similar effect is observed when the hardness of the machined material is increased⁽¹⁷⁾.

Figs. 12 and 13 demonstrate the effect of rake angle on the chip discontinuity and chip formation for β -brass and magnesium as observed by Cook, Finnie and Shaw⁽¹⁶⁾.

1.5.2 Influence of a Built-Up Edge on Chip Formation Process

Since the built-up edge occurs on the cutting face of the tool it therefore changes the direction of the chip flow, increasing the effective rake angle. This effect is similar at both low and high cutting speeds.

The built-up edge is significantly affected by the temperature. It was found⁽³⁷⁾ that when mild steel is cut, the built-up edge reaches the maximum size at a tool-chip contact temperature of about 300°C, then gradually decreasing and finally disappearing at a temperature of about 600°C. This could be explained by softening due to recrystallizing.

Hoshi⁽³⁸⁾ concluded from a wide range of experiments that the formation of built-up edge depends on cutting conditions and on work-piece and tool materials. He recognized three phenomena caused by the formation of built-up edge; increase in the effective rake angle, over cutting and deformation of the free surface.

Nakayama and Iguchi⁽³⁹⁾ concluded that the generation of the built-up edge is related to the cutting temperature and not to the cutting speed and the built-up edge disappears over the temperature range above the recrystallization temperature of the work material. This is true for high range of cutting speeds when the effect of the temperature is significant. Okoshi and Sata⁽⁴⁰⁾ have found, experimentally, a critical speed at which the built-up edge disappeared for different cutting conditions.

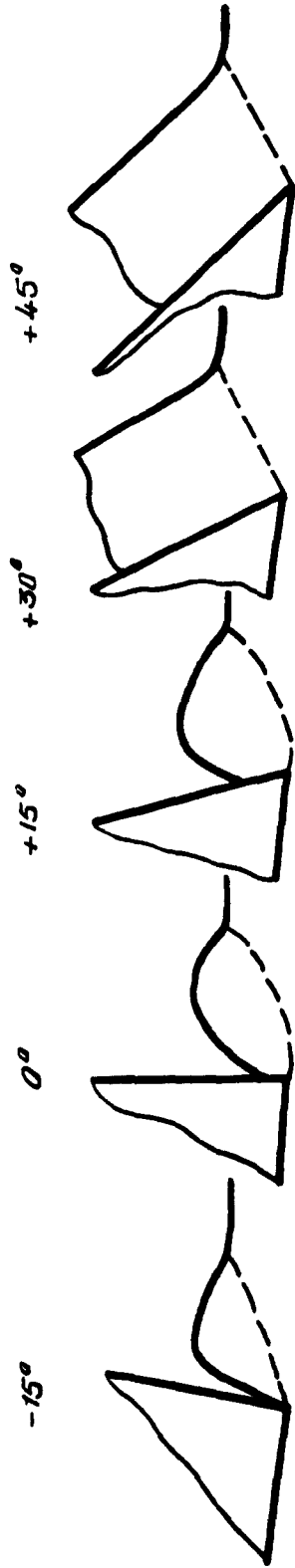


FIG. 12
 EFFECT OF RAKE ANGLE UPON CHIP DISCONTINUITY FOR β -BRASS⁽¹⁶⁾
 (DEPTH OF CUT = .007", SPEED = .5 LPM, WIDTH = .161", FLUID-NONE)

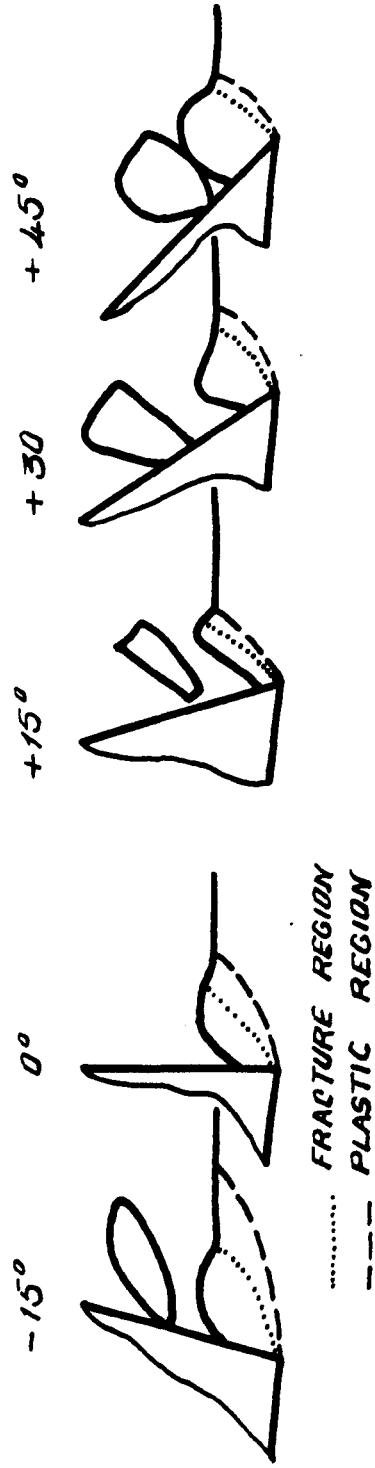


Fig. 13

EFFECT OF RAKE ANGLE UPON CHIP FORMATION FOR MAGNESIUM (16)
 (DEPTH OF CUT = .010", SPEED = .5 LPM, WIDTH OF CUT = .159", FLUID - NONE)

Mayer and Cumming⁽⁴¹⁾ showed that stable built-up edge may exist over a wide range of cutting conditions and depends strongly on cutting speed, rake angle and undeformed chip thickness.

1.5.3 Influence of Friction on Chip Formation Process

The coefficient of friction in metal cutting is often greatly different from that obtained with the same metal pair in conventional sliding friction experiments. It is shown that a coefficient of friction is inadequate to describe the friction process in cutting, being mainly an indication of the normal stress on the tool face and thus, strongly dependent on the shear process in cutting.

At the present time the most generally accepted theory of dry friction is a composite of contributions due to Holm⁽⁴²⁾, Ernst and Merchant⁽⁴³⁾ and Bowden⁽⁴⁴⁾. According to this picture of friction, sliding resistance is viewed as being composed of three factors:

- (1) A mechanical inter-locking of surface asperities.
- (2) A ploughing of the surface asperities of the harder of the two metals through the softer.
- (3) A welding of the surface asperities of one metal to the other, resulting in metallic junctions.

For relatively smooth surfaces such as we have in metal cutting, experimental evidence^(44, 45) would indicate that frictional resistance is primarily due to the shearing asperities (factor 3), while factors 1 and 2 are insignificant.

Kobayshi and Thomsen⁽⁴⁶⁾, using tools with controlled tool chip contact areas, have revealed that for SAE 112 steels and for a wide range of cutting speeds, the friction on the rake face of the tool is explainable by the junction model with possible superimposed general plastic flow above the junctions. They have revealed also that the friction mechanism at the flank-wear contact area was essentially the same as that occurring at the tool face.

The mean coefficient of tool face friction has a similar effect on the chip formation process at both high and low cutting speeds and an increase in the mean coefficient of friction causes an increase in the angle of action which results in a rise in the cutting forces.

Rozenberg and Yeremin^(47, 48) have concluded from series of experiments using different cutting conditions for different cutting materials that the tool-chip contact temperature has a great effect on the mean coefficient of friction at high speeds. They showed that the change in the coefficient of friction is related to the built-up edge process. The mean coefficient of friction reached its maximum at temperature of about 300°C, when the built-up edge reached its maximum size.

Zorev⁽³⁷⁾ and Isayev⁽⁴⁹⁾ showed that in general, at the point where the chip touches the front face of the tool, external sliding is replaced by internal shear.

Shaw, Pigott and Richardson⁽⁵⁰⁾ on the basis of experiments with various cutting fluids, established that equal mean coefficient of friction and cutting ratios do not correspond to equal temperatures.

1.6 IDEALISATION OF MATERIAL

An ideal material is the one that flows at a constant yield stress. The strain - stress diagram for such a material is shown in Fig. 14, where τ_0 is the yield shear stress flow. For such a material, there is no permanent deformation while the shear stress is less than τ_0 . Points 0; 1; 2 and 3 correspond, respectively, to the work region, the starting boundary line, the end boundary line and the chip region. In a strain hardening material whose flow curve is represented in Fig. 11, shear stress on either side of the line would not be in equilibrium, so shear along a single line is not possible. A moving metal particle in the undeformed work corresponds to the position O, Fig. 11, and when it reaches the starting boundary line, it corresponds to the position M due to the yield of the metal in shear. When a metal

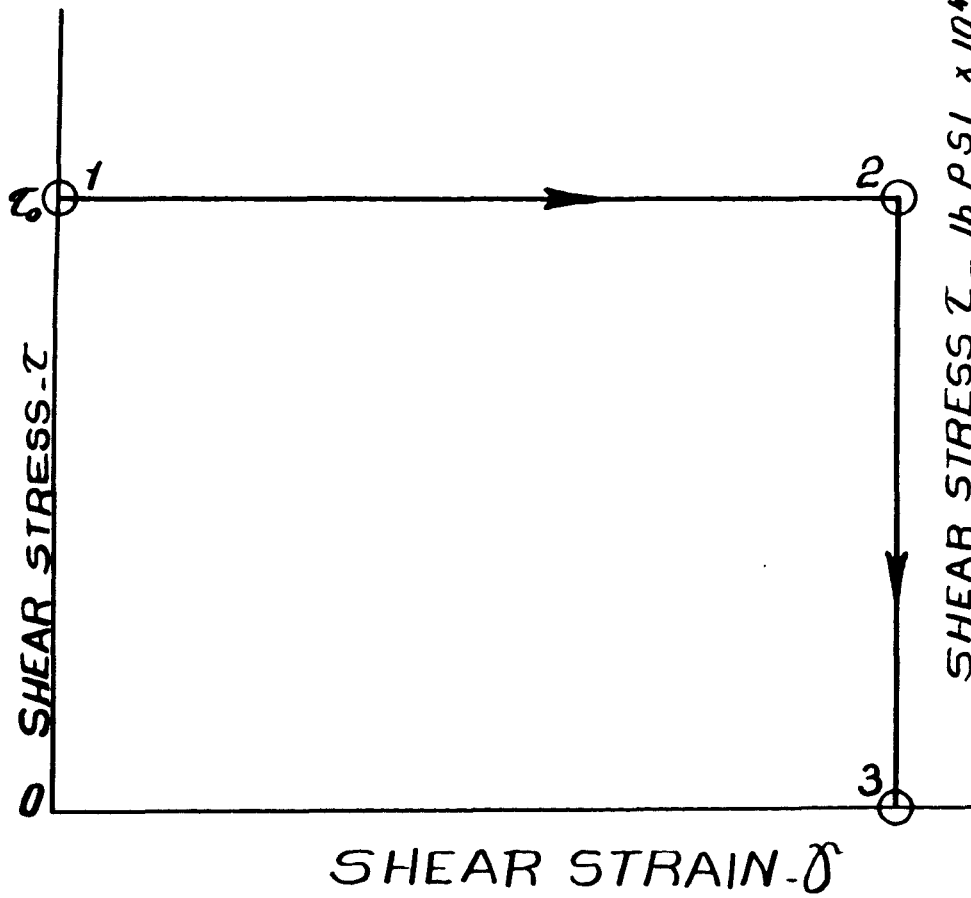


FIG. 14

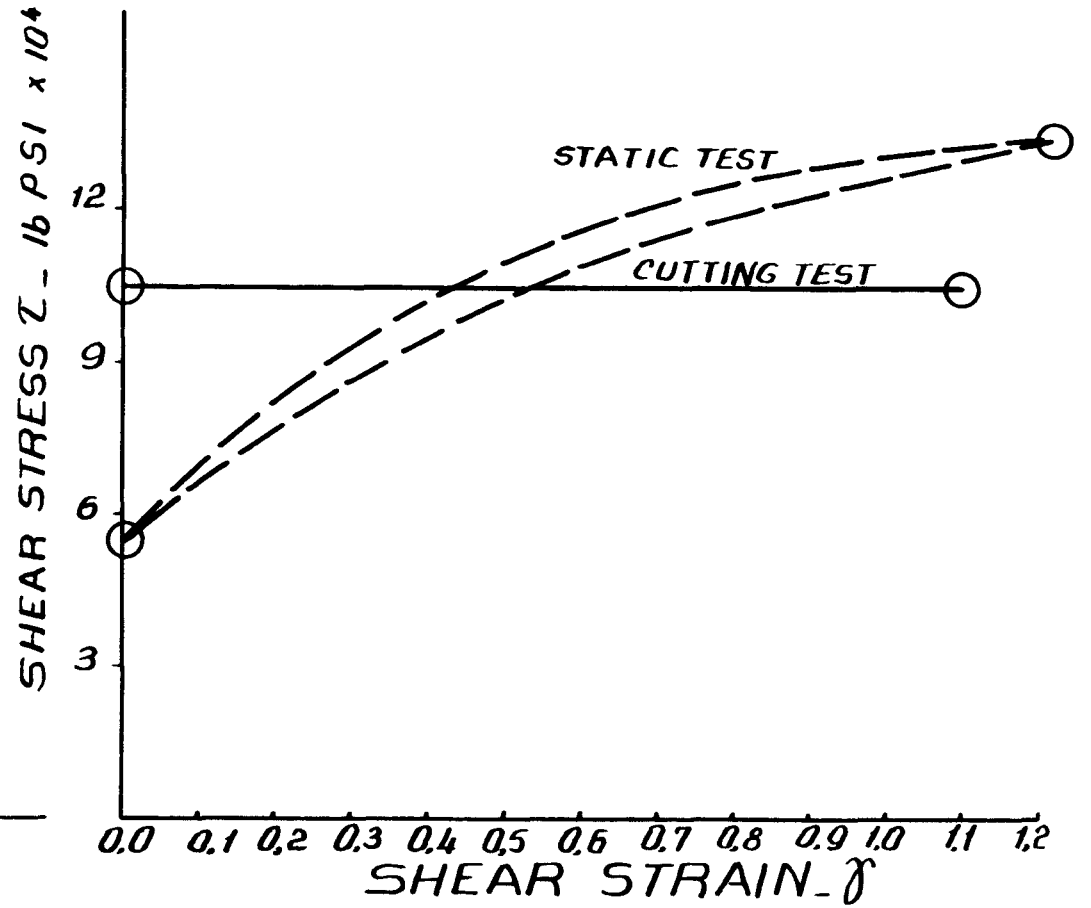


FIG. 15

particle passes into the flow region, it changes its location from the position M to position N continuously along the curve until it reaches the breaking point N. The breaking point N corresponds to the end boundary line, i.e. the fracture line, at which fracture occurs periodically. Fig. 15 shows the shear - strain diagram for carbon steel. In this figure the stress - strain diagram for the same material in a static material test is obtained from experimental results of the relation between twisting moment and specific twisting angle by Ludwik's method⁽⁵¹⁾.

1.7 DERIVATION OF STRAIN FOR SINGLE SLIP-LINE

Region (b) is uncut chip, approaching stationary tool (a) with cutting speed V , and region (c) with speed V_c is chip, as shown in Fig.16_a. Velocity is uniform through each of three regions, and can be represented on a velocity diagram Fig.16_b. The directions of these velocities are known, while relative velocity V_t is directed along slip-line OL.

Shear strain γ is defined as the change in tangential velocity as a particle crosses a slip-line divided by the velocity normal to the slip-line, so from Fig.16_b,

$$\gamma = bc/ad$$

Also,

$$ad = V \sin \phi$$

$$bd = V \cos \phi$$

NOMENCLATURE

V = cutting velocity

V_c = chip velocity

V_t = relative velocity along slip-line OL, Fig. 16

γ = shear strain

ϕ = angle defining the position of slip-line OL, or shear angle

$bc = bd + dc = V_c$, see velocity diagram Fig.16_b

$ad = V \sin \phi$, velocity normal to slip-line OL, Fig.16_b

$bd = V \cos \phi$, see velocity diagram Fig.16_b

$dc = ad \tan \phi$, see velocity diagram Fig.16_b

$\phi = \phi - \alpha$, angle between the chip velocity and the velocity normal to the SLIP-LINE OL

α = rake angle

ξ = cutting ratio

t = uncut chip thickness or depth of cut

t_c = deformed chip thickness

$(bc)^2 = (cf)^2 + (fb)^2$, see

velocity diagram Fig.16_b

$cf = V_c \cos \alpha$, velocity normal

to the direction of cutting,

see velocity diagram Fig.16_b

$fb = ba - fa = V - V_c \cos \alpha$, see

velocity diagram Fig.16_b

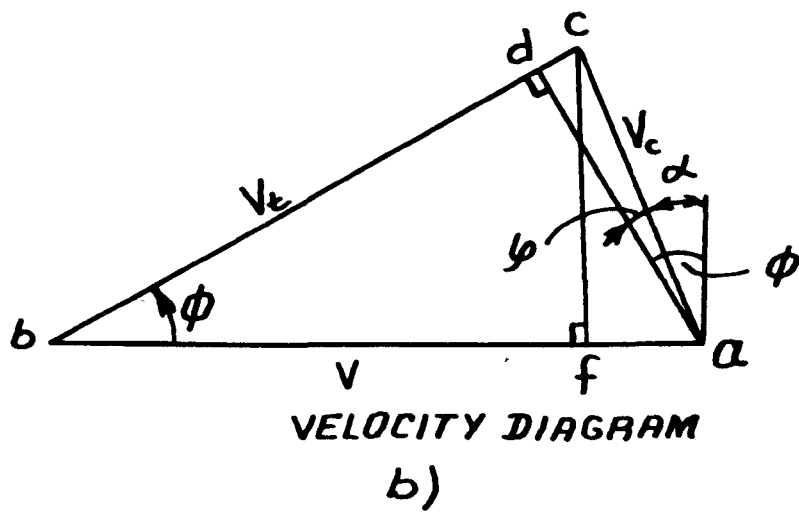
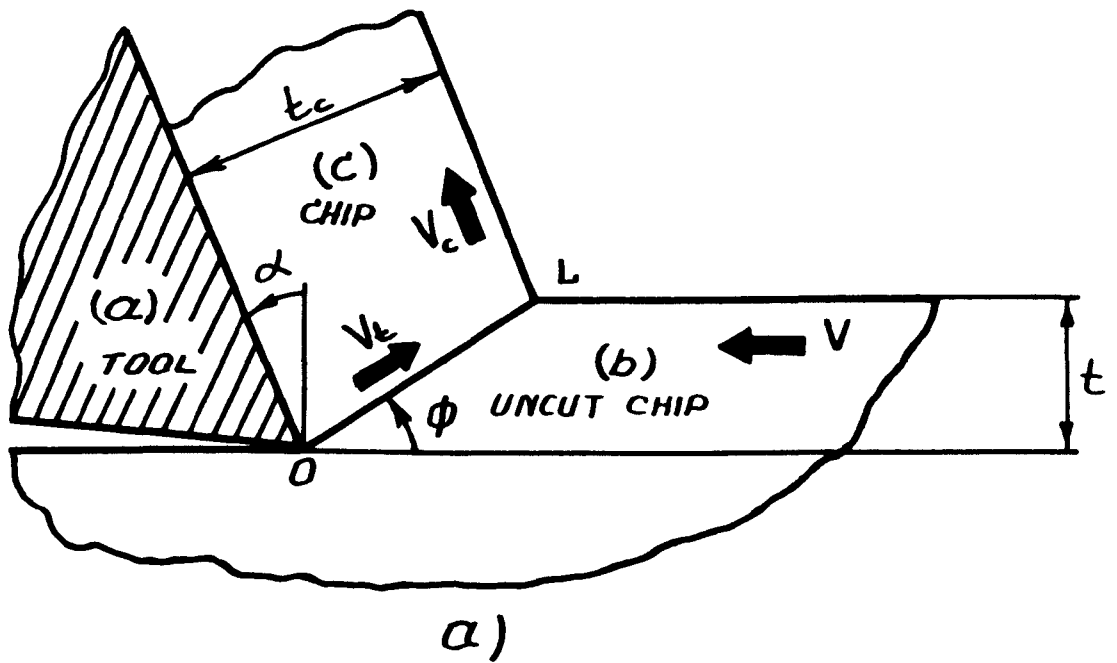


FIG. 16

$$dc = ad \tan \phi = V \sin \phi \tan \phi$$

But,

$$\phi = \phi - \alpha$$

And

$$bc = bd + dc = V \cos \phi + V \sin \phi \tan(\phi - \alpha)$$

Hence,

$$\begin{aligned} \xi &= bc / ad = \frac{V \cos \phi + V \sin \phi \tan(\phi - \alpha)}{V \sin \phi} & (1.14) \\ &= \cot \phi + \tan(\phi - \alpha) \end{aligned}$$

It is an easy matter to differentiate equation (1.14) to get the value of ϕ which gives minimum strain, $\phi = \pi/4 + \alpha/2$, which means that the shear plane bisects the angle between the tool face and direction of cutting, implying ratio $\xi = 1$, but this is not of much direct practical value. It is noted that the cutting ratio follows by expressing thicknesses t and t_c in terms of length OL,

$$\xi = t_c / t = \cos(\phi - \alpha) / \sin \phi$$

which transposes to

$$\cot \phi = \frac{1}{\xi} \sec \alpha - \tan \alpha \quad (1.15)$$

Equation (1.15) gives a practical means of finding shear plane angle.

Another derivation of strain from the velocity diagram may be of interest. Drop perpendiculars ad and cf as in Fig. 16_o (velocity diagram). By Pythagoras,

$$(bc)^2 = (cf)^2 + (fb)^2$$

But, as

$$cf = V_c \cos \alpha, \text{ and } fb = V - V_c \sin \alpha, \text{ we have}$$

$$(bc)^2 = (V_c \cos \alpha)^2 + (V - V_c \sin \alpha)^2$$

$$(bc)^2 = V^2 + V_c^2 - 2VV_c \sin \alpha$$

However, the area of the outer triangle is given by,

$$\frac{1}{2} V \times cf = \frac{1}{2} bc \times ad, \text{ giving } bc \times ad = V V_c \cos \alpha$$

Using these results, we can now find the strain in terms of

velocities and rake angle,

$$\gamma = bc/ad = (bc)^2/bc.ad = [V^2 + V_c^2 - 2VV_c \sin \alpha] / VV_c \cos \alpha$$

and as the cutting ratio is defined $\xi = V/V_c$, we get strain

$$\gamma = \left(\xi + \frac{1}{\xi} \right) \sec \alpha - 2 \tan \alpha \quad (1.16)$$

Naturally, equations (1.14), (1.15) and (1.16) are compatible as may be verified.

1.8 STRAIN FOR A PAIR OF SLIP-LINES

Suppose that chip speed represented by point c is fixed Fig.17_a. This speed is attained after slip along two lines ON and OM with an intermediate region e. As compared with the single slip-line regime, we now have tangential velocities be and ec (V_{t1} and V_{t2} Fig.17_b) slightly increased, while the normal velocities ad_1 and ad_2 are appreciably reduced. Hence the total strain in the chip, given by $\gamma = be/ad_1 + ec/ad_2$ will be increased over the value appropriate for shearing on a single plane.

NOMENCLATURE

V_{t1} = relative velocity along slip-line ON, Fig.17

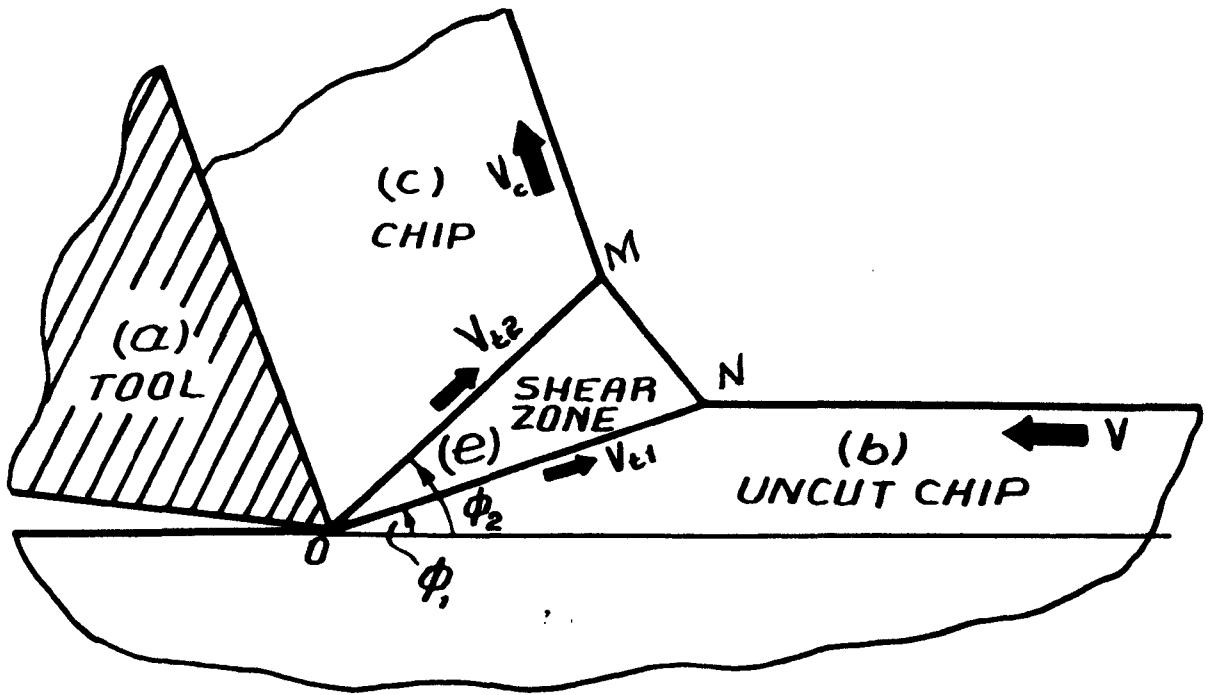
V_{t2} = relative velocity along slip-line OM, Fig.17

ϕ_1 = shear angle defining the position of slip-line ON, Fig.17

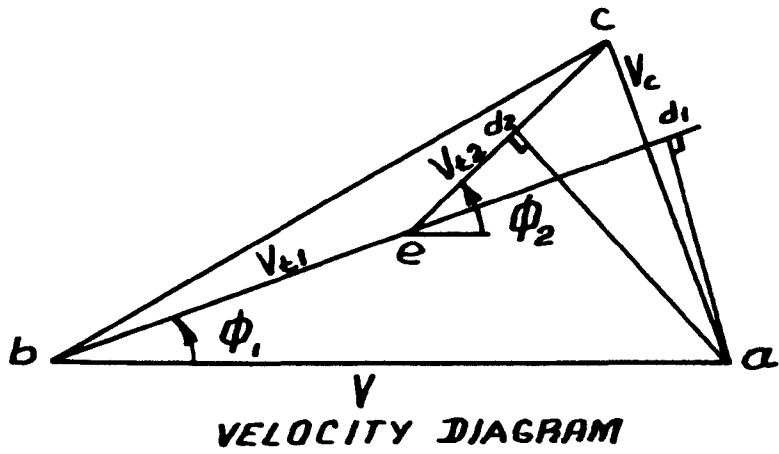
ϕ_2 = shear angle defining the position of slip-line OM, Fig.17

ad_1 = velocity normal to slip-line ON, Fig.17_b

ad_2 = velocity normal to slip-line OM, Fig.17_b



a)



VELOCITY DIAGRAM

b)

FIG. 17

1.9 STRAIN RATE IN FAN REGION, SERIES EXPRESSION FOR CURVATURE AND NUMERICAL INTEGRATION FOR A PARTI-
CULAR EXAMPLE

In any particle, strain rate in polar-coordinate is given in terms of velocities by:

$$\frac{\partial \gamma}{\partial T} = \frac{\partial V_\phi}{\partial r} + \frac{1}{r} \frac{\partial V_r}{\partial \phi} - \frac{V_\phi}{r}$$

However, velocities in the fan region ONM (Fig.18) are assumed not to vary with radius, so the first term $\partial V_\phi / \partial r$ is zero.

We can also write,

$$\frac{\partial \gamma}{\partial T} = \frac{\partial \gamma}{\partial \phi} \frac{\partial \phi}{\partial T} = \frac{\partial \gamma}{\partial \phi} \frac{V_\phi}{r}$$

Hence

$$\frac{\partial \gamma}{\partial \phi} = \frac{1}{V_\phi} \frac{\partial V_r}{\partial \phi} - 1 \quad (1.17)$$

Let perpendicular to radius R make angle θ with the tangent to the surface NM at some point M as in Fig.18. As velocity at point M must be directed along the surface, we have

$$\tan \theta = - \frac{1}{R} \frac{dR}{d\phi} = - \frac{V_r}{V_\phi}, \text{ hence}$$

NOMENCLATURE

- | | |
|--|--|
| γ = shear strain | ϕ_0 = angle of initial slip-line |
| T = time rate | ϕ_1 = angle of the final slip-line |
| V_ϕ and V_r = velocities in ϕ and r | θ = angle between the perpendicular directions to radius R and the tangent to the surface NM at point M |
| r = radius of location of any particle | V = cutting speed |
| R = radius from O to surface NM, | t = uncut chip thickness |
| Fig.18 corresponding to the | $\delta\phi$ = small variable increment of shear angle |
| R_0 = radius from O to surface NM, | $\Delta\phi$ = angle of the whole fan |
| Fig.18 corresponding to the | α = rake angle |
| initial slip-line | R_a and b = constants |
| ϕ = angle of any slip-line or general shear angle | a_2 = constant |

$$V_r = \frac{V_\phi}{R} \frac{dR}{d\phi}$$

However continuity requires that

$$R V_\phi = V t$$

We now have these velocity components:

$$V_\phi = \frac{Vt}{R} \quad \text{and} \quad V_r = \frac{Vt}{R^2} \frac{dR}{d\phi}$$

Hence equation (1.17) for strain rate becomes:

$$\frac{\partial \gamma}{\partial \phi} = R \frac{d}{d\phi} \left(\frac{1}{R^2} \frac{dR}{d\phi} \right) - 1 \quad (1.18)$$

It is very easy to see that any segment of the surface profile that happens to be straight, and is consequently expressible as $R = R_a \text{Sec}(\phi + b)$, gives zero strain rate. This is to be expected, as strain rate in both workpiece and chip is zero at all points outside the deformation fan. So it is seen that straining occurs only while the surface is curved. The total shear strain is now obtained by integrating from initial to final slip-lines,

$$\gamma = \int_{\phi_0}^{\phi_1} \frac{\partial \gamma}{\partial \phi} d\phi \quad (1.19)$$

The upper limit is obtained from Fig.18 in terms of rake angle,

$$\text{when } \phi_1 + \theta = \alpha, \text{ or } -\tan\theta = \tan(\phi_1 - \alpha) = \left[\frac{1}{R} \frac{dR}{d\phi} \right]_{\phi=\phi_1} \quad (1.20)$$

To proceed further with this theory, some particular shape of surface $R(\phi)$ must be selected. Let us take the relation:

$$R = R_0 \left[1 - (\phi - \phi_0) \text{Cot } \phi_0 + a_2 (\phi - \phi_0)^2 \right] \quad (1.21)$$

Taking the first term as unity gives $R = R_0$ when $\phi = \phi_0$. The second term is provided with coefficient $\text{Cot } \phi_0$ to ensure that there is no discontinuity in slope at the initial point of the curve (such a discontinuity would imply a sudden increase in strain across the initial slip-line, so that integral (1.19) would not be adequate). The coefficient a_2 is arbitrary, but needs to be $> (\frac{1}{2} + \text{Cot}^2 \phi_0)$ to ensure that the surface curves upwards. Higher terms in the series may be taken, but not essential. It is now straightforward to apply (1.18) and (1.20) to (1.21) to get strain rate:

$$\frac{d\gamma}{d\phi} = \frac{2(a_2 - \cot^2 \phi_0) + 6a_2 \cot \phi_0 (\phi - \phi_0) - 6a_2^2 (\phi - \phi_0)^2}{(R/R_0)^2} \quad (1.22)$$

and final slip-line ϕ_1 from

$$\tan(\phi_1 - \alpha) = \frac{-\cot \phi_0 + 2a_2 (\phi_1 - \phi_0)}{(R_1/R_0)^2} \quad (1.23)$$

As an exercise at this point, we calculate the total strain as the fan angle is reduced to zero, so that deformation becomes concentrated on a single line. To give this infinitely sharp curvature, coefficient a_2 is made very large in relation to $\cot^2 \phi_0$. Also the radius R will be virtually constant. Writing the general angle ϕ as $\phi_0 + \delta\phi$, strain rate reduces to the evidently constant value $d\gamma/d\phi = 2a_2$. Total strain from (1.19) is now $\gamma = 2a_2 \Delta\phi$. Now the upper limit given by (1.23) is

$$\tan(\phi_0 + \Delta\phi - \alpha) = -\cot \phi_0 + 2a_2 \Delta\phi$$

which expands to give

$$\tan(\phi_0 - \alpha) + \cot \phi_0 = 2a_2 \Delta\phi$$

Hence the total strain is

$$\gamma = \tan(\phi_0 - \alpha) + \cot \phi_0$$

which is precisely as given by (1.14) for shear along a single slip-line.

NUMERICAL INTEGRATION FOR A PARTICULAR EXAMPLE

Take values:

$$\alpha = 0 \quad ,$$

$$\phi_0 = 0.20 \quad ,$$

$$\cot \phi_0 = 4.93 \quad ,$$

$$\cot^2 \phi_0 = 24.3 \quad ,$$

with value $a_2 = 30$, giving an upper limit $\phi_1 = 0.286$

From (1.21) and (1.23) we get tabulated values:

ϕ	R/R_0	$d\gamma/d\phi$
0.20	1.000	11.4
0.21	.954	22.0
0.22	.913	32.5
0.23	.879	43.0
0.24	.852	53.0
0.25	.829	62.0
0.26	.812	68.0
0.27	.802	73.0
0.28	.798	75.0
0.286	.798	74.5

On integrating, the final strain is found to be $\bar{\gamma} = 4.32$. This is somewhat higher than the value obtained from (1.14) by assuming that strain occurs exclusively on the final slip-line $\phi_f = 0.286$, which is $\bar{\gamma} = 3.65$. This makes clear the insufficiency of Zorev⁽¹⁷⁾ analysis of the distribution of shear strain in the chip formation zone, which implies that the final strain is determinate from the final slip-line alone.

The width of the fan is seen to be dependent on the value taken for constant a_2 . Within this fan, alternative strain distribution could be obtained by taking higher terms in the series. For deciding which distribution is correct, some appeal would have to be made to stress equilibrium within the fan, and to the stress-strain curve for the material.

1.10 MEASURE OF STRAIN

Shear strain "Engineering definition" is defined as the reduction in angle of the outer corner of element

$$\gamma_{xy} = \pi/2 - \beta$$

Shear strain "Mathematical definition"

$$\epsilon_{xy} = \frac{1}{2}(\pi/2 - \beta)$$

So

$$\gamma_{xy} = 2 \epsilon_{xy}$$

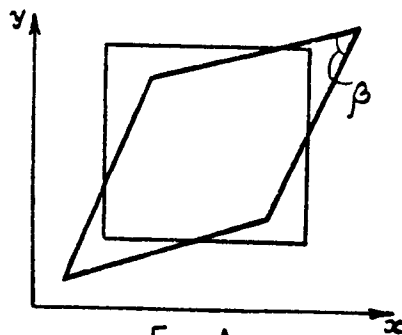


FIG. A

Equivalent shear strain $\bar{\epsilon}$ is strain which is equal to pure shear strain ϵ_{xy} when no other strain is present, and for any combination of strains "Mathematical definition"

$$\delta \bar{\epsilon} = \left[\frac{(\delta \epsilon_x - \delta \epsilon_y)^2 + (\delta \epsilon_y - \delta \epsilon_z)^2 + (\delta \epsilon_z - \delta \epsilon_x)^2}{6} + (\delta \epsilon_{xy})^2 + (\delta \epsilon_{yz})^2 + (\delta \epsilon_{zx})^2 \right]^{1/2}$$

or "Engineering" shear strain

$$\frac{1}{2} \delta \bar{\gamma} = \left[\frac{(\delta \epsilon_x - \delta \epsilon_y)^2 + (\delta \epsilon_y - \delta \epsilon_z)^2 + (\delta \epsilon_z - \delta \epsilon_x)^2}{6} + \left(\frac{1}{2} \delta \gamma_{xy}\right)^2 + \left(\frac{1}{2} \delta \gamma_{yz}\right)^2 + \left(\frac{1}{2} \delta \gamma_{zx}\right)^2 \right]^{1/2}$$

NOMENCLATURE

- | | |
|--|--|
| γ_{xy} = "Engineering" shear strain | ψ = swing angle of the side |
| ϵ_{xy} = "Mathematical" shear strain | OA of the element, Fig. 19 _a |
| $\delta \epsilon_x, \delta \epsilon_y, \delta \epsilon_z$ = direct strain increments | c = vertical movement of the element |
| $\delta \gamma_{xy}, \delta \gamma_{yz}, \delta \gamma_{zx}$ = shear strain increments | x, y = co-ordinates defining the position of the element |
| $\delta \bar{\epsilon}$ = equivalent "Engineering" shear strain component | L = current length of the element after extension |
| $\delta \bar{\epsilon}$ = equivalent "Mathematical" shear strain component | L_0 = original length of the element before extension |
| u = horizontal movement of upper side of element AB, Fig. 19 _a | δL = length increment |
| β = corner angle, Fig. A | |

or

$$(\delta\gamma)^2 = \frac{4}{6} \left[(\delta\epsilon_x - \delta\epsilon_y)^2 + (\delta\epsilon_y - \delta\epsilon_z)^2 + (\delta\epsilon_z - \delta\epsilon_x)^2 \right] + (\delta\gamma_{xy})^2 + (\delta\gamma_{yz})^2 + (\delta\gamma_{zx})^2$$

$$\delta\gamma = \left[\frac{2}{3} \left\{ (\delta\epsilon_x - \delta\epsilon_y)^2 + (\delta\epsilon_y - \delta\epsilon_z)^2 + (\delta\epsilon_z - \delta\epsilon_x)^2 \right\} + (\delta\gamma_{xy})^2 + (\delta\gamma_{yz})^2 + (\delta\gamma_{zx})^2 \right]^{\frac{1}{2}} \quad (1.24)$$

However, for plane strain deformation at constant volume

$$\delta\epsilon_z = \delta\gamma_{yz} = \delta\gamma_{zx} = 0$$

$$\delta\epsilon_y = -\delta\epsilon_x$$

Therefore, we have

$$\delta\gamma = \left[\frac{2}{3} \left\{ (\delta\epsilon_x - [-\delta\epsilon_x])^2 + (-\delta\epsilon_x - 0)^2 + (0 - \delta\epsilon_x)^2 \right\} + \delta\gamma_{xy}^2 \right]^{\frac{1}{2}}$$

$$\delta\gamma = \left[4\delta\epsilon_x^2 + \delta\gamma_{xy}^2 \right]^{\frac{1}{2}} \quad (1.25)$$

Let us examine the following cases:

a) Unidirectional shearing

The upper side of element AB moves horizontally to A'B', Fig. 19_a, through distance u while side OA swings through angle ψ . For any increments δu , the mathematical shear strain component is

$$\delta\epsilon_{xy} = \frac{1}{2} \left(\frac{\delta u}{\delta y} + \frac{\delta c}{\delta x} \right) = \frac{1}{2} \frac{\delta u}{\delta y}$$

the vertical movement c being zero. As there is no direct strain relative to the (x,y) co-ordinates, we have from (1.25)

$$\delta\gamma = \frac{\delta u}{OA}, \text{ and } \gamma = \int \delta\gamma = \frac{\dot{u}}{OA} = \tan\psi \quad (1.26)$$

b) Constant Volume Extension

At any instant, direct strain is the length increment divided by the current length, Fig. 19_b

$$\delta\epsilon_x = \frac{\delta L}{L}, \quad \delta\epsilon_{xy} = 0$$

Therefore the "Engineering" shear strain from (1.25) will be

$$\delta\gamma = 2 \frac{\delta L}{L}, \quad \gamma = 2 \ln \frac{L}{L_0} \quad (1.27)$$

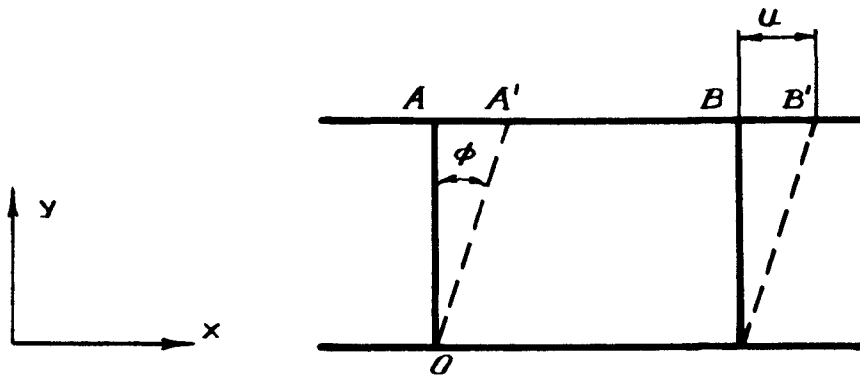


FIG. 19a

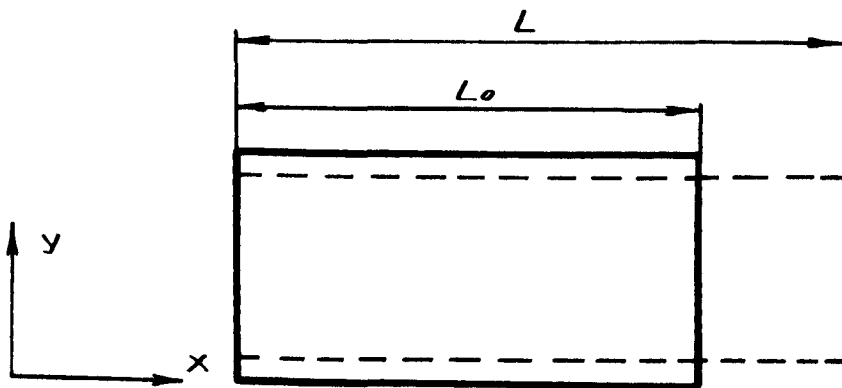


FIG. 19b

1.11 SHAPE OF STRAINED CIRCLE

a) For Unidirectional shear

Let point A be initially on a circle, Fig.20_a, so that its co-ordinate values (x,y) are related by

$$x^2 + y^2 = R^2 \tag{1.28}$$

This point moves distance Δx to A', as in Fig.20_a, while the shear strain $\tilde{\gamma}$ is imposed. From definition of shear strain for unidirectional shearing, equation (1.26), we have

$$\Delta x = \tilde{\gamma} y$$

Hence the new co-ordinates of point A' are

$$x' = x + \tilde{\gamma} y \quad , \quad y' = y \tag{1.29}$$

NOMENCLATURE

- | | |
|--|---|
| <p>x,y = co-ordinates of point A,
Fig.20_a</p> <p>R = radius of the initial circle
(unstrained), $R^2 = x^2 + y^2$</p> <p>Δx = distance which point A moves
when $\tilde{\gamma}$ shear strain is
imposed, distance AA', Fig.
20_a</p> <p>$\tilde{\gamma}$ = shear strain</p> <p>x',y' = co-ordinates of point A'
on the curve corresponding
to the shape of the strained
circle, Fig.20_a</p> <p>r, θ = polar co-ordinates of point A',
Fig.20_a</p> <p>a,b = major and minor semi-axes of
the ellipse (deformed circle)</p> | <p>β = angle of the inclination
of the major axis of the
ellipse to the line of
maximum direct strain which
is at 45°, Fig.20_a</p> <p>$\delta \epsilon_{aa}$ = direct strain increment</p> <p>$\delta \epsilon_{ab}$ = shear strain increment</p> <p>ϵ = logarithmic strain</p> <p>$\frac{t}{2}$ = half-corner angle, Fig.20_a</p> <p>ψ = angle of the inclination
of AA' to the major axis
of the ellipse</p> |
|--|---|

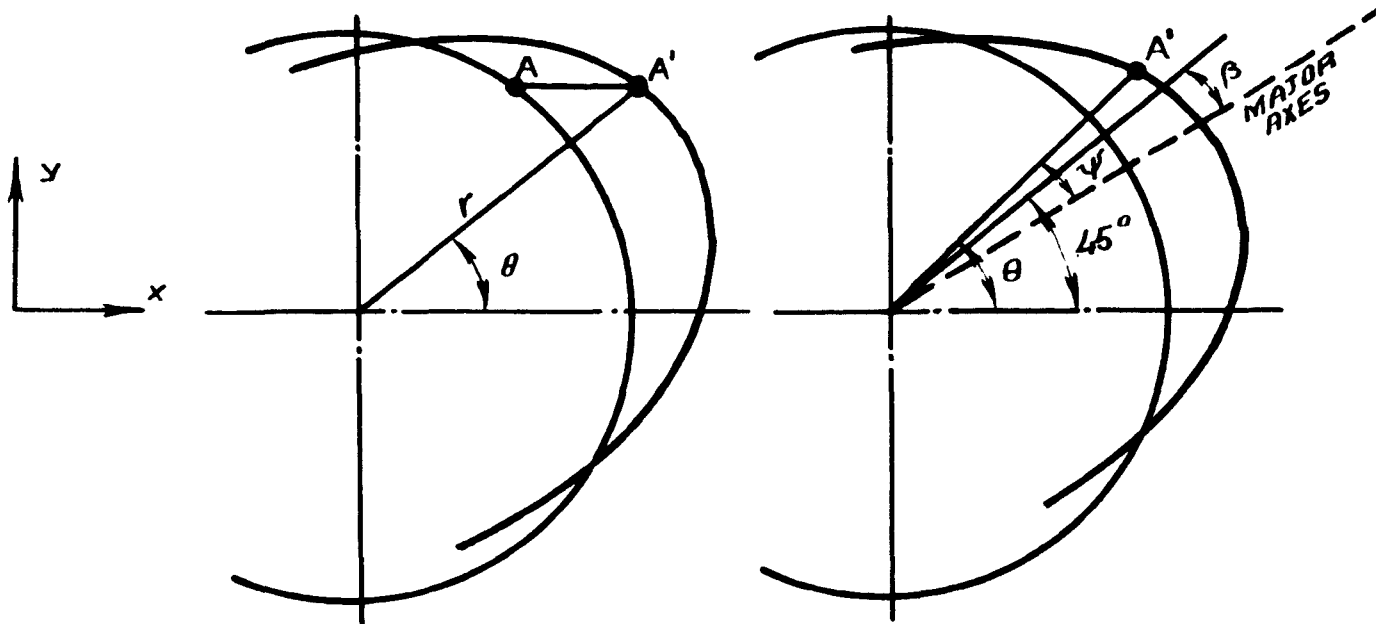


FIG. 20a

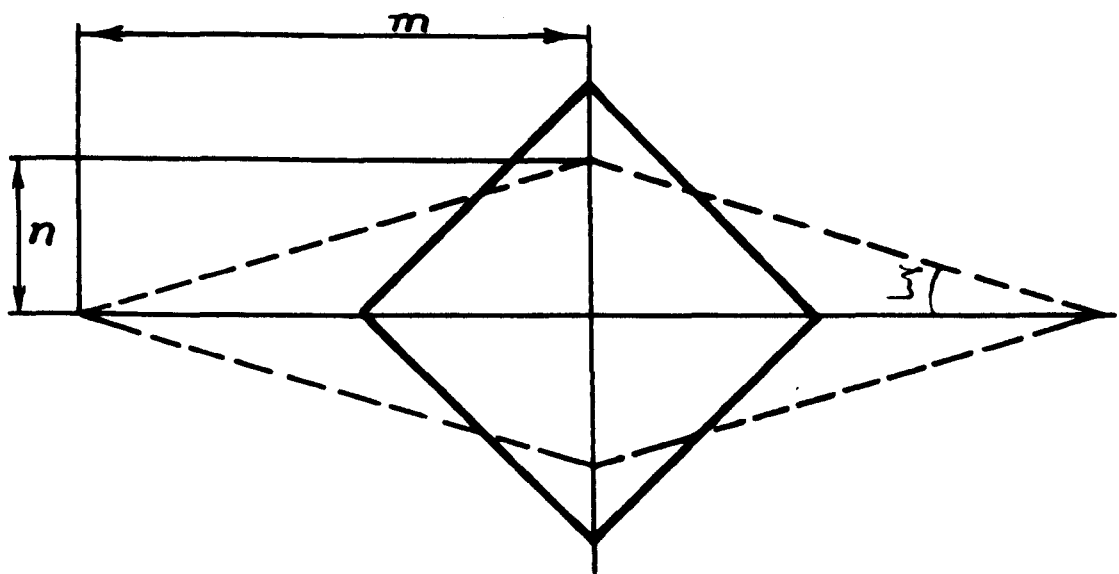


FIG. 20b

we now describe the position of A' in polar co-ordinates,

$$x' = r \cos \theta \quad , \quad y' = r \sin \theta \quad (1.30)$$

Combining (1.29) and (1.30), we get

$$x = r (\cos \theta - \gamma \sin \theta) \quad , \quad y = r \sin \theta \quad (1.31)$$

and using (1.28)

$$r^2 [(\cos \theta - \gamma \sin \theta)^2 + \sin^2 \theta] = R^2 \quad (1.32)$$

Equation (1.32) is the equation of the curve into which the circle has deformed. If we write $\theta = \psi + \pi/4 - \beta$, the equation (1.32) becomes,

$$1 + \frac{1}{2} \gamma^2 + (-\gamma \sin 2\beta + \frac{1}{2} \gamma^2 \cos 2\beta) \sin 2\psi + (-\gamma \cos 2\beta - \frac{1}{2} \gamma^2 \sin 2\beta) \cos 2\psi = R^2/r^2 \quad (1.33)$$

Equation (1.33) is recognised as the equation to an ellipse. When the $\sin 2\psi$ term vanishes, angle ψ will be taken from a datum line coinciding with the major axis, and it is seen that this is so when angle β is given value

$$\tan 2\beta = \gamma/2 \quad (1.34)$$

Putting this value in equation (1.33), we get

$$1 + \frac{1}{2} \gamma^2 - \gamma \left(1 + \frac{1}{4} \gamma^2\right)^{\frac{1}{2}} \cos 2\psi = R^2/r^2$$

The major and minor semi-axes of the ellipse a and b are given by

$$a = R \left[1 + \frac{1}{2} \gamma^2 + \gamma \sqrt{1 + \frac{1}{4} \gamma^2} \right]^{\frac{1}{2}} \quad , \quad b = R \left[1 + \frac{1}{2} \gamma^2 - \gamma \sqrt{1 + \frac{1}{4} \gamma^2} \right]^{\frac{1}{2}} \quad (1.35)$$

Some comments can now be made about these results:

Incremental direct strain referred to the ellipse axis

$$\delta \epsilon_{aa} = \epsilon_a/a$$

may be evaluated from equation (1.35) and inserted into the expression (1.25) for shear strain:

$$\delta \gamma = \delta \gamma \sqrt{1 + \frac{1}{4} \gamma^2}$$

This is obviously untrue (except at $\gamma = 0$). The reason is that a

component $\delta\epsilon_{ab}$ is also present, due to the inclination of the major axis at angle β to the line of maximum direct strain increment, which remains at 45° . When this correction is made, equation (1.25) is satisfied. It is concluded that the total strain is not determined from the final deformed shape alone, as the path by which the shape is reached must be taken into account. On these grounds, Zorev⁽¹⁷⁾ analysis of the distribution of shear strain in the chip formation zone which suggests that the final strain is determinate from the final slip-line alone can also be criticized.

b) Unidirectional Stretching

A similar exercise can be carried out for finding the final shape of a circle deformed by pure stretching, which indeed, an ellipse. Instead of a circle, we now consider a square of half-diameter initially equal to d . This is horizontally stretched to m , and vertically compressed to n , as in Fig.20_b, so that

$$m = d e^\epsilon, \quad n = d e^{-\epsilon}$$

The half-corner angle ξ is given by

$$\tan \xi = m/n = e^{-2\epsilon}$$

If we suppose that shear strain is given by the cotangent of the whole corner angle,

$$\tilde{\gamma} = \cot 2\xi = (1 - \tan^2 \xi) / 2 \tan \xi = \sinh 2\epsilon$$

This cannot be true, as we know that equivalent shear strain is given by $\tilde{\gamma} = 2\epsilon$. It appears, therefore, that shear strain is given by the cotangent of the corner angle only if (a) strain is small, or (b) shearing is unidirectional. It is again concluded that strain is not determinate from the deformed shape unless the mode of deformation is specified. Equivalent shear strain must be found by summing components correctly related to orthogonal axes at each stage of deformation. Finite strains deduced by switching axes on the deformed element (as in Nadai "theory of flow and fracture of solids") have no useful meaning.

It may not follow that strain hardening is uniquely determined by the equivalent shear strain. In many metals, unidirectional shearing is less effective in producing hardening than unidirectional stretching. However, this is not a justification for irregular definitions of large strain.

1.12 DIRECTION OF TEXTURE

In case of a single shear plane OM, Fig.21, the angle between the cutting direction and the major axis of the deformed ellipse is given by

$$\lambda = \phi + \frac{\pi}{4} - \beta \quad (1.36)$$

Angle β and shear strain are given by the equations:

$$\tan 2\beta = \gamma/2 \quad , \quad \gamma = \cot \phi + \tan(\phi - \alpha)$$

This result seems to be in agreement with results obtained by Zorev⁽¹⁷⁾ who uses an average value of shear plane angle ϕ .

Structural features of an initially isotropic workpiece material will therefore give striations in the chip at the angle λ .

When the shear plane is straight, these striation will be straight, except possibly in a very thin smeared layer of the chip under-side.

NOMENCLATURE

λ = angle between the cutting direction and the major axis of the ellipse, Fig.21.

ϕ = shear plane angle

β = angle between the major axis of the ellipse and the line of maximum direct strain which is at 45° to the shear plane, Fig.21

γ = shear strain

α = rake angle

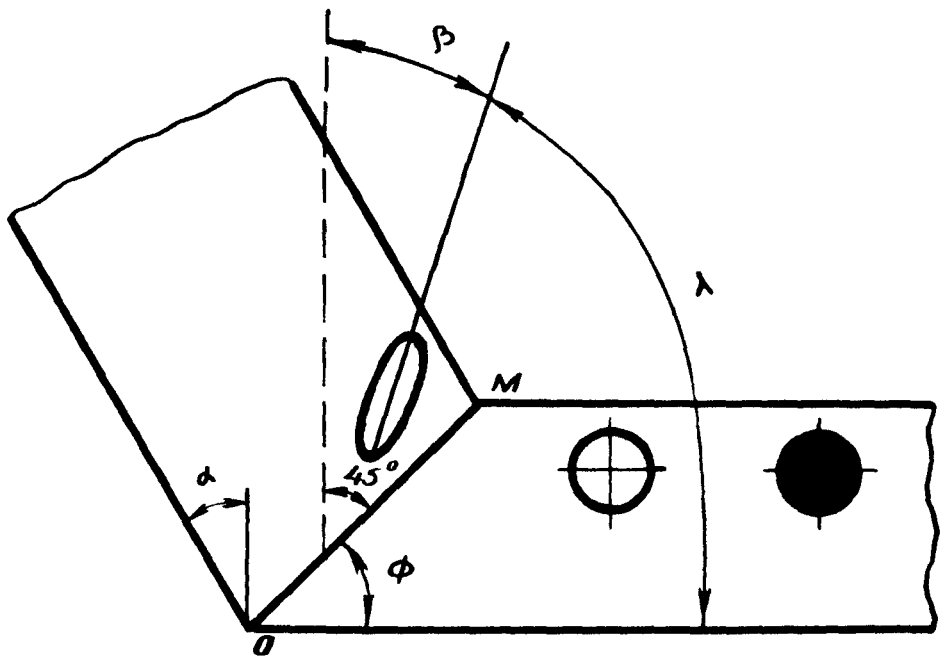


FIG. 21

1.13 PLOTTING DEFORMED SHAPE

a) For Straight Shear Plane

Take rake angle $\alpha = 15^\circ$, shear plane angle $\phi = 45^\circ$. From velocity diagram, chip thickness ratio $\xi = 1.23$ or $1/\xi = 0.82$.

Mark off convenient units along uncut chip, and intervals 0.82 along chip, drawing lines parallel to shear plane OM, Fig.21_a.

Take any line AB perpendicular to shear plane. Draw path lines through these points. Count off a certain number of spaces along path line (say six) for each point, to get points A' and B' in chip. Similarly for other points on a square or other figure drawn on uncut chip. Strain in chip is given by $\gamma = EB'/EA' = 1.58$ (because square initially aligned with shear plane deforms by unidirectional shear)

b) For Curved Shear Plane

In Fig.21_b, the deformation is analysed for a chip thickness ratio $\xi = 1.5$, rake angle $\alpha = 0^\circ$, with a pair of slip-lines of fairly large curvature. If the curvatures are equal, the tangential velocity change at each line will be the same, as the chip has no angular velocity. A hodograph (i.e. velocity diagram) must be drawn in

NOMENCLATURE

α = rake angle	S_b = distance which the same any point travels in the deformation region, Fig.21 _b
ϕ = shear angle	
ξ = chip thickness ratio	
γ = shear strain	S_c = distance from the same any point on deformed line B-B to the final slip-line, Fig.21 _b
S_a = distance from any point on line A-A to the initial slip-line, Fig.21 _b	V_c = velocity in the chip region
V_a = velocity in the undeformed region	t_a = time necessary for any point on line A-A to move a distance of S_a
V_b = velocity in the deformation region	
t_b, t_c = time necessary for any point to move a distance of S_b and S_c	

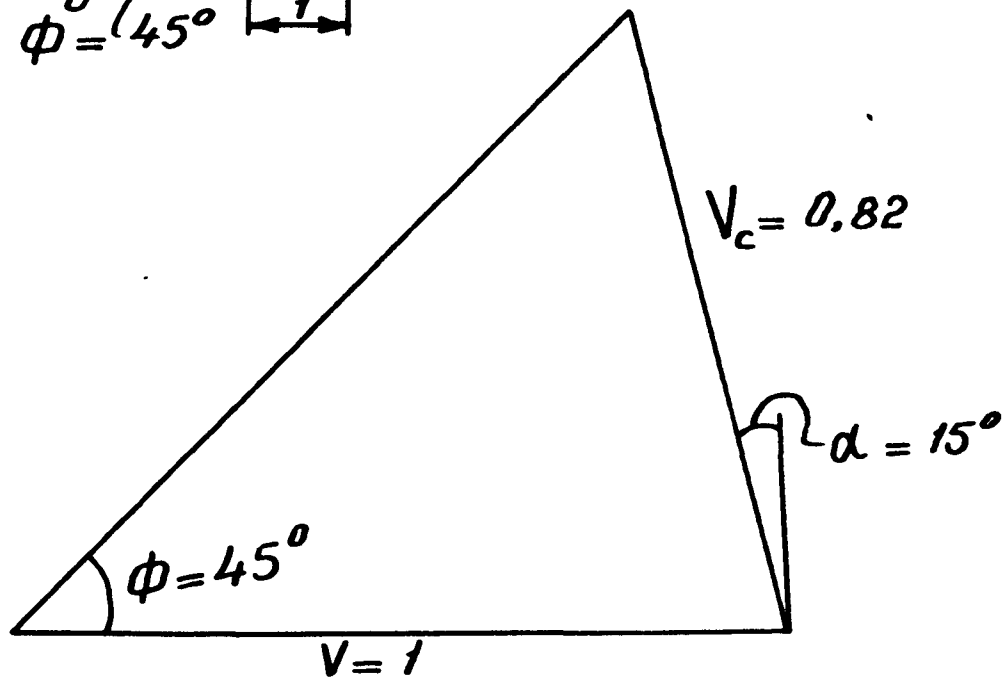
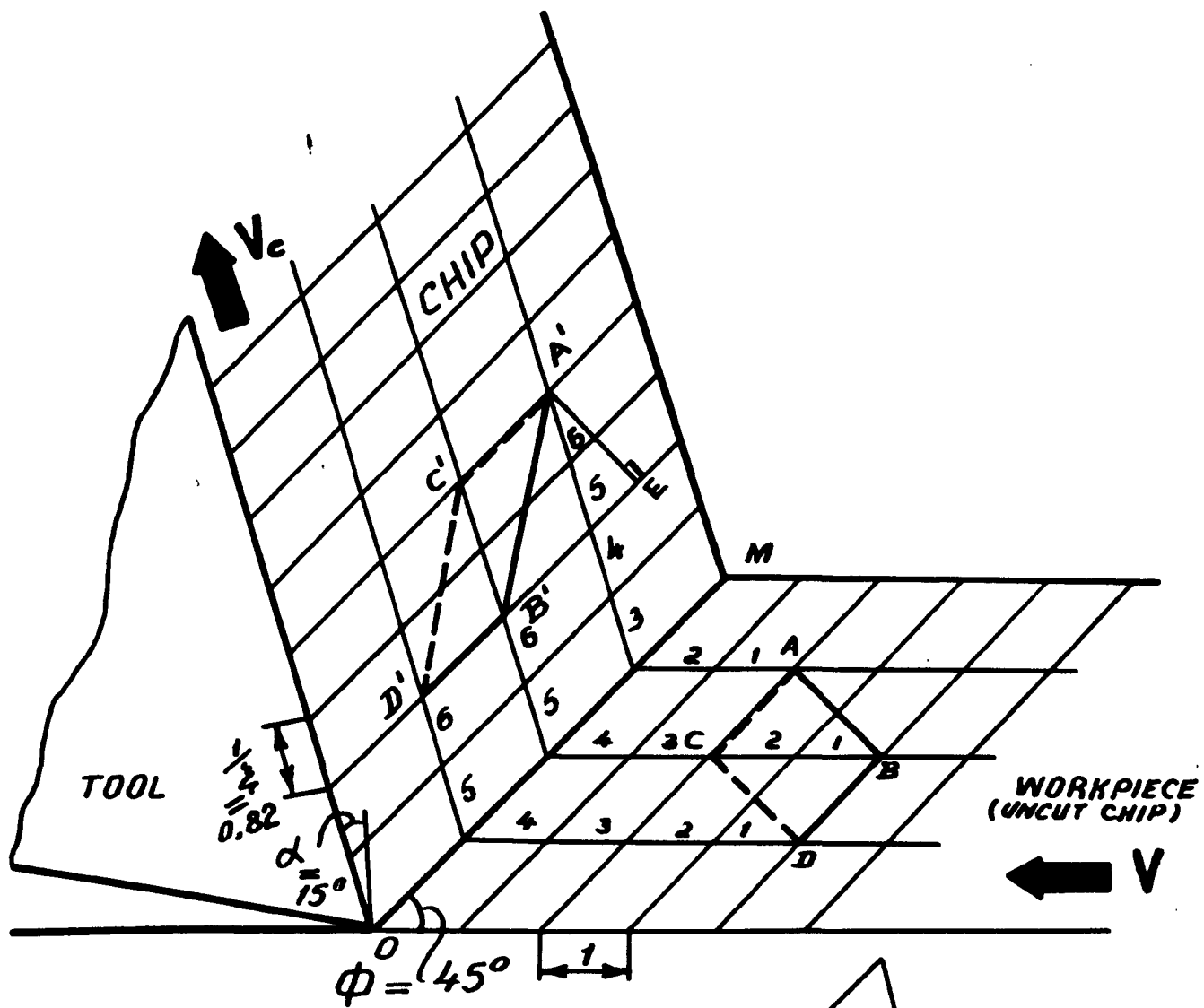


FIG. 21a

which relative velocities on either side of a slip-line are tangential to the slip-line, and absolute velocities are directed along the path lines, the path lines being indicated. Also, the three regions have uniform velocity or rotational velocity (as they do not deform internally)

Line AA deforms into line BB. This is plotted as follows: Distance S_a is measured off. This is divided by velocity V_a to get time t_a . Similarly, distance S_b is divided by velocity V_b which is measured off the hodograph, to give time t_b . Times t_a and t_b are now added, and the sum is subtracted from some convenient total time t to give time t_c available for covering distance S_c . This distance is, of course, got by multiplying time t_c by speed V_c . The distance S_c is now measured off along the path line in the chip region, to define a point on the deformed line BB. This line does not directly indicate the texture, but as it is seen to be curved, the texture is found to be curved in similar way.

Under these conditions, the strain in the lower side of the chip is extremely high (It can be easily calculated from the hodograph) and becomes infinite when the lower slip-line arc becomes tangential to the direction of cutting.

The free surface can be taken at any of the path lines.

P.S. "The discussion given on pages 23 to 37 closely follows a set of notes supplied by the supervisor".

CHAPTER 2

DYNAMOMETRY

2.1 GENERAL INTRODUCTION

One of the major objectives of the metal cutting research is the determination of the machining forces. Recently a great deal of attention has been given to force measurement, and as a result different types of dynamometers have been developed.

In designing dynamometers, two groups of requirements must be fulfilled:

Group I

1. The construction should be such that it can be made in the workshop laboratory with a minimum of cost and effort.
2. Simplicity of operation and calibration.
3. Robustness.
4. Adaptability.
5. Sufficient range of application.

Group II

1. The force components should influence the dial gauges independently.
2. Sensitivity. The sensitivity of a reliable research dynamometer should be within the range .5 - 1.0% for less than 50 kg.
3. Rigidity. The mechanical parts of the dynamometer are subjected to elastic deformation, therefore the deflections should not be so large as to affect the cutting action.
4. Stiffness. All machine tools operate with a certain amount of vibration, which may have large amplitudes in certain operations such as milling and shaping.

In order that the recorded force is not influenced by any vibrating motion of the dynamometer, its natural frequency must be large (at least four times as large) compared to the frequency of the vibration set up in the machine tool⁽⁵²⁾. For purpose of analysis, any dynamometer can be considered as a mass supported by a spring. The natural frequency of such a system is equal to:

$$W_n = \frac{1}{2\pi} \sqrt{K/m} \text{ cps} \quad (2.1a)$$

W_n - is the natural frequency of the dynamometer,

K - is the spring constant lb/in.,

m - is the mass in lb. (sec)²/in.

The natural frequency of the dynamometer in terms of the supported weight of the dynamometer (W) is given as:

$$W_n = \frac{1}{2\pi} \sqrt{Kg/W} \text{ or } W_n = \frac{1}{2\pi} \sqrt{386K/W} \text{ cps} \quad (2.1b)$$

5. There should be no cross sensitivity between the force components.
6. For the sake of convenience the calibration line should be linear.
7. The dynamometer should be stable with respect to time, temperature and humidity.
8. The friction between the moving parts of the dynamometer should be minimum.

2.2 TYPES OF MEASURING INSTRUMENTS

2.2.1 Absorption Dynamometers:

These dynamometers^(53, 54) measure the power output of some machines and then convert that mechanical energy into heat and dissipate it in an easily controlled manner.

2.2.2 Transmission Dynamometers:

These dynamometers provide an indication of the force or torque passing through. There are two main types; torsion dynamometers which measure power transmitted to or from high speed machines such as fans, turbo-compressors, centrifugal pumps, etc.⁽⁵⁵⁾ and hydraulic dynamometers^(56, 57) which measure and record the energy absorbed by slow running machines of variable load such as machine tools, plungers, etc.

2.2.3 Force Measuring Instruments:

In these instruments the cutting forces are arranged to deflect mechanical springs usually in the form of stiff diaphragms, the deflections being measured either by mechanical or electrical means. Different dynamometers were designed for different operations such as lathe dynamometer^(58, 59) (one, two and three component dynamometer), drill dynamometer^(61, 62) milling dynamometer⁽⁶³⁾ planning dynamometer⁽⁶⁴⁾, etc.

The force measurement in force measuring dynamometers involves the measurement of small deflections (10^{-3} to 10^{-4} in.) with a suitable calibration between the forces and the deflections.

Force measuring devices are classified as follows:

I Mechanical devices - Dial gauge indicators (dynamometers);

1. Single-component dynamometer.
2. Two-component dynamometer.
3. Three-component dynamometer.

II Hydraulic devices.

III Pneumatic devices.

IV Optical devices.

V Piezoelectric crystals.

VI Electrical devices.

1. Electronic transducer tube.
2. Differential transformer.

3. Strain gauges:

- (a) Magnetic tube strain gauge.
- (b) Unbonded wire resistance strain gauges.
- (c) Bonded strain gauges.
- (d) Strain rings.

2.3 DIAL GAUGE DYNAMOMETERS

Dynamometers of this type have a very limited range of use due to their poor stability at medium and high cutting speeds.

The dial gauge dynamometers are capable of reading deflections in the range of (10^{-3} - 10^{-4} in.) when functioning properly. These dynamometers are recommended for low cutting speeds up to 10 m/min.

Zorev⁽¹⁷⁾ has designed a single-component dynamometer for checking the correctness of the reading of a two-component dynamometer used for force measurement and also for use in those cases where there was need of considerable rigidity in the lathe-instrument-tool-blank system.

The dynamometer is based on a plate (1) whose bottom surface is ground to the top surface of the lathe's cross slides, Fig. (22). Into the horizontal hole of the tool-holder (2) is fitted a tool (3) which is held by two bolts screwed into the top of the tool-holder.

On the round block is secured a vertical strut (4) in the top of which is fitted a miniature gauge (5) rests on the vertical surface of hardened pin which is pressed into the hole of the tool-holder.

Under the influence of the horizontal component of the cutting force the vertical wall of the block bends and the tool-holder moves along the arc of a certain circle which by virtue of the smallness of the movement is practically a horizontal straight line. A dial gauge with a scale division of .001 mm was used for recording of these movements. It is clear that the horizontal movements of the tool-holder

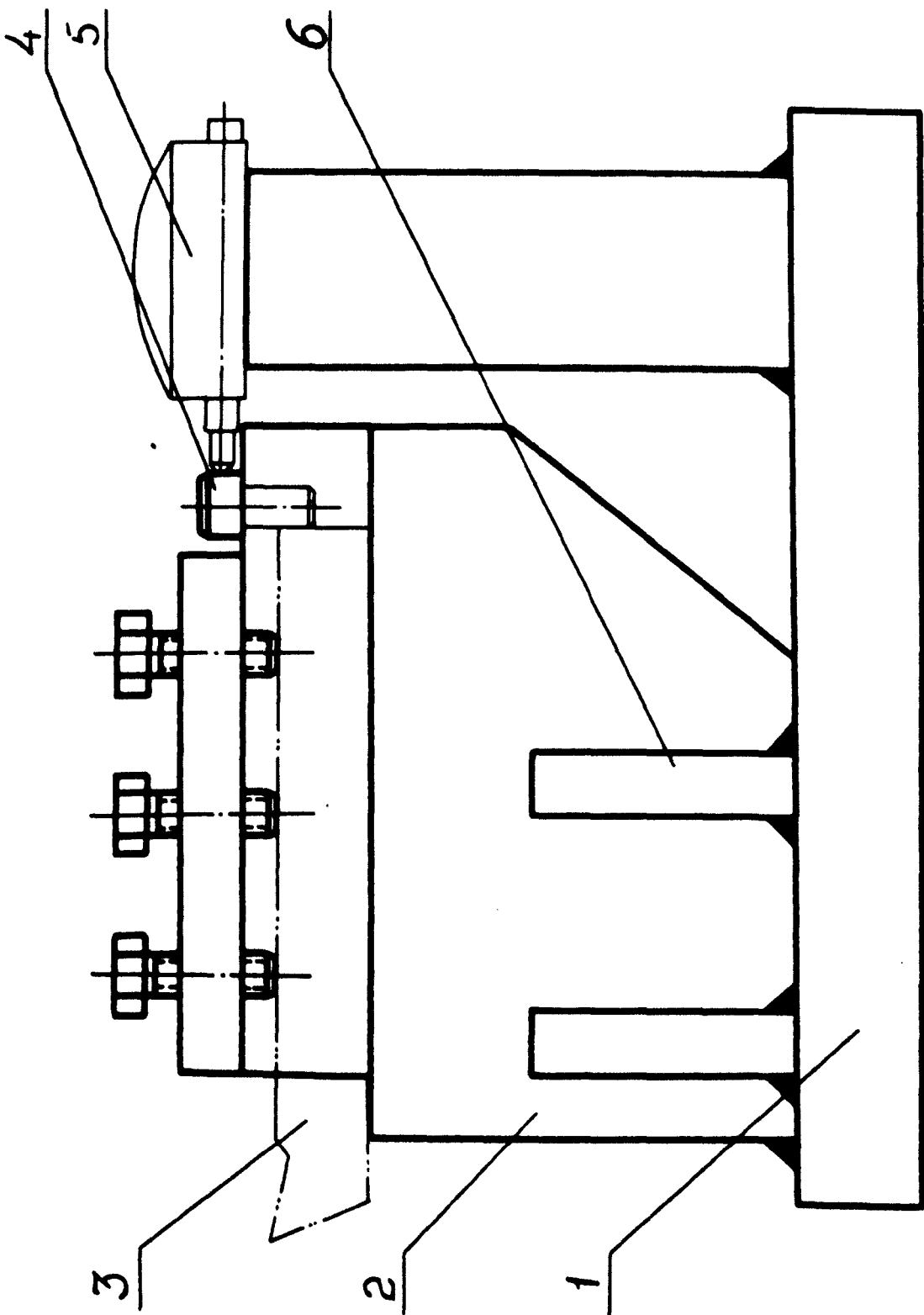


FIG. 22

are proportional to the value of the horizontal projection of the cutting force, so the readings of the dial gauge characterise the value of the horizontal projection of the cutting force. Three strengthening ribs (6) are welded to the base plate to increase the rigidity of the dynamometer and to eliminate the influence of tightening of the securing bolts on the dynamometer's characteristics. This dynamometer was used for measuring the load of up to 1000 kg.

The two-component dynamometer used by Zorev in his experiments was a combination of two single-component dynamometers. In this case the rigidity of the dynamometer is increased by welding some extra ribs.

As in the case of single component dynamometers under the action of the horizontal projection of the cutting force the vertical wall of the base plate bends and all the points of the tool-holder body move along the arc of a certain circle. These movements of the tool-holder body record through a dial gauge.

Under the action of the vertical projection of the cutting force the upper part of the tool-holder body drops. The movement of the upper part of the tool-holder are registered by dial gauge whose measuring pin rests rigidly connected with the upper part of the tool-holder body. This dial gauge reading determines the value of the vertical projection of the cutting force.

In order to eliminate the influence of the horizontal force on the readings of the vertical force measuring dial gauge it is turned in the vertical plane parallel to the tool axis. In order to eliminate the influence of the vertical force on the readings of the horizontal force measuring dial gauge the tool overhang is carefully selected.

Both single and two-component dynamometers have strictly linear calibrating characteristics which coincide during loading and unloading.

Experimental results showed exceptional stability of the calibrating characteristics and complete reliability during operations

at low cutting speeds.

A dynamometer developed by the College of Aeronautics for use with drills to measure thrust and torque was described by Town⁽⁶⁰⁾. The thrust is translated through a spindle resting on a ball bearing whose movement is resisted by a diaphragm. Deflection of the diaphragm is then measured by a dial indicator actuated by a bell crank lever. The torque is also translated by a spindle acting against another diaphragm which acts as cantilever whose deflection is measured by a dial indicator. Both indicators read to 0.001 in. and the instrument range for thrust is 500 lb. and torque 10 lb. in.

The above dynamometer can also be used for determination of power for cutting, machine efficiency, optimum tool geometry, machinability index for power, and effect of variation of drill diameter and feed and also for comparison of cutting force relationships.

Town⁽⁶¹⁾ also described a dynamometer developed by the College of Aeronautics, Cranfield to measure the cutting forces. The resultant load on the tool is resolved into three components by a rocking motion in the vertical and horizontal directions and by sliding in the backward direction. The shank of the tool-holder is an inch square in section and can hold a tool of $\frac{3}{4}$ in. diameter or $\frac{1}{2}$ in. square section. Three dial gauges with accuracy of 0.001 in. are used to record the diaphragms deflection.

This dynamometer can also be adapted to the measurement of power available for cutting and machine efficiency, the best true rake, clearance or plan approach angle, the machinability index for power, the specific cutting capacity or the effect of variation in depth of cut and feed.

Under conditions of slowly changing load at low cutting speed it should be noted that dial gauge dynamometers have considerable

advantages over electric and hydraulic dynamometers in the reproducibility of readings. In addition they have considerably greater rigidity than hydraulic dynamometers.

2.4 HYDRAULIC DEVICES

In these instruments Fig.23⁽⁵²⁾ the forces record through a diaphragm to a pressure gauge which indicates the value of the calibrated force. In comparison with dial gauge indicators, hydraulic devices have a large range of cutting speeds. They give more accurate measurements of the applied forces but less rigid than the dial gauge indicators. One of the advantages of these devices is that the force may be read at a distance from the pressure cell.

2.5 PNEUMATIC DEVICES

One of the most accurate devices of this type is the one which has been designed by "Solex" (Solex claim). Solex has designed a device called "Solex micrometer" whereby the change in back pressure that occurs when a flat surface is brought into closer contact with a sharp edged orifice are used to measure deflections in tool dynamometers. The simplicity and reliability are the main characteristics of such devices if they are carefully supplied with a clean, constant pressure air.

Lomachenko⁽⁶⁵⁾ has described a Russian designed pneumatic dynamometer.

The tool placed in a holder and clamped to it by two bolts. The holder together with the tool can move in three directions perpendicular to each other under the action of cutting force components arising in turning. The holder moves on ball bearings to minimize friction.

Force components are transmitted from the holder to the corresponding transducers, which are made in the form of rings with built-in nozzles for measuring the air pressure.

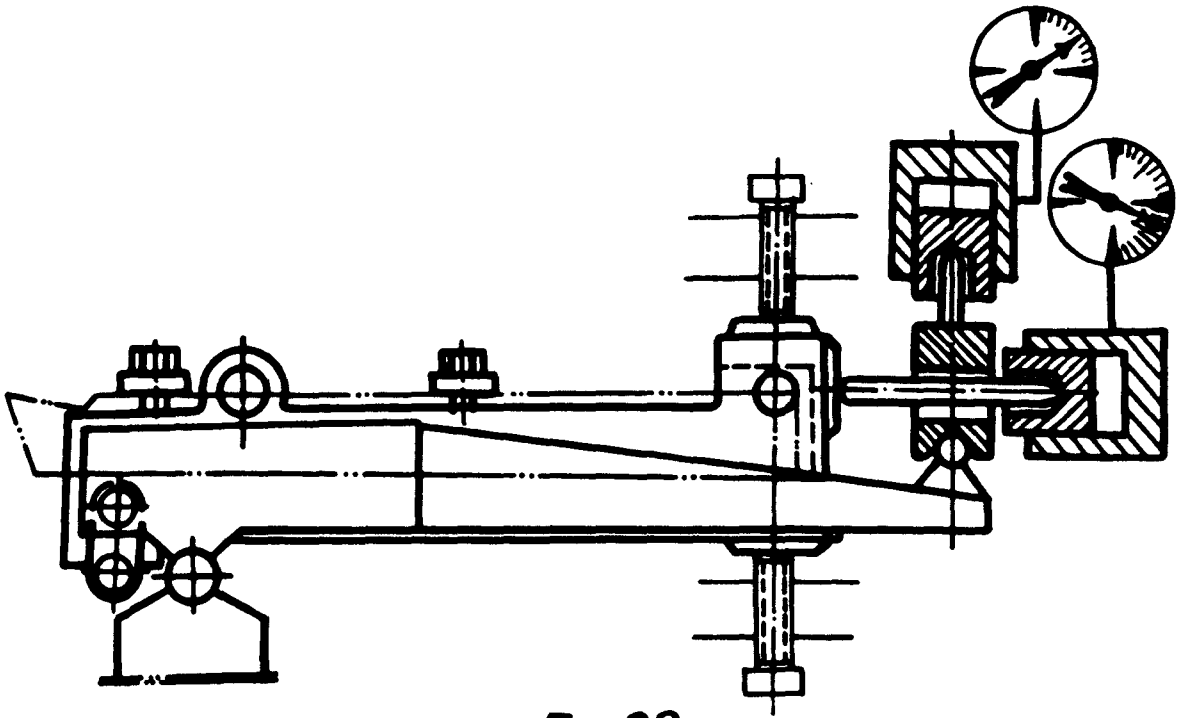


Fig. 23

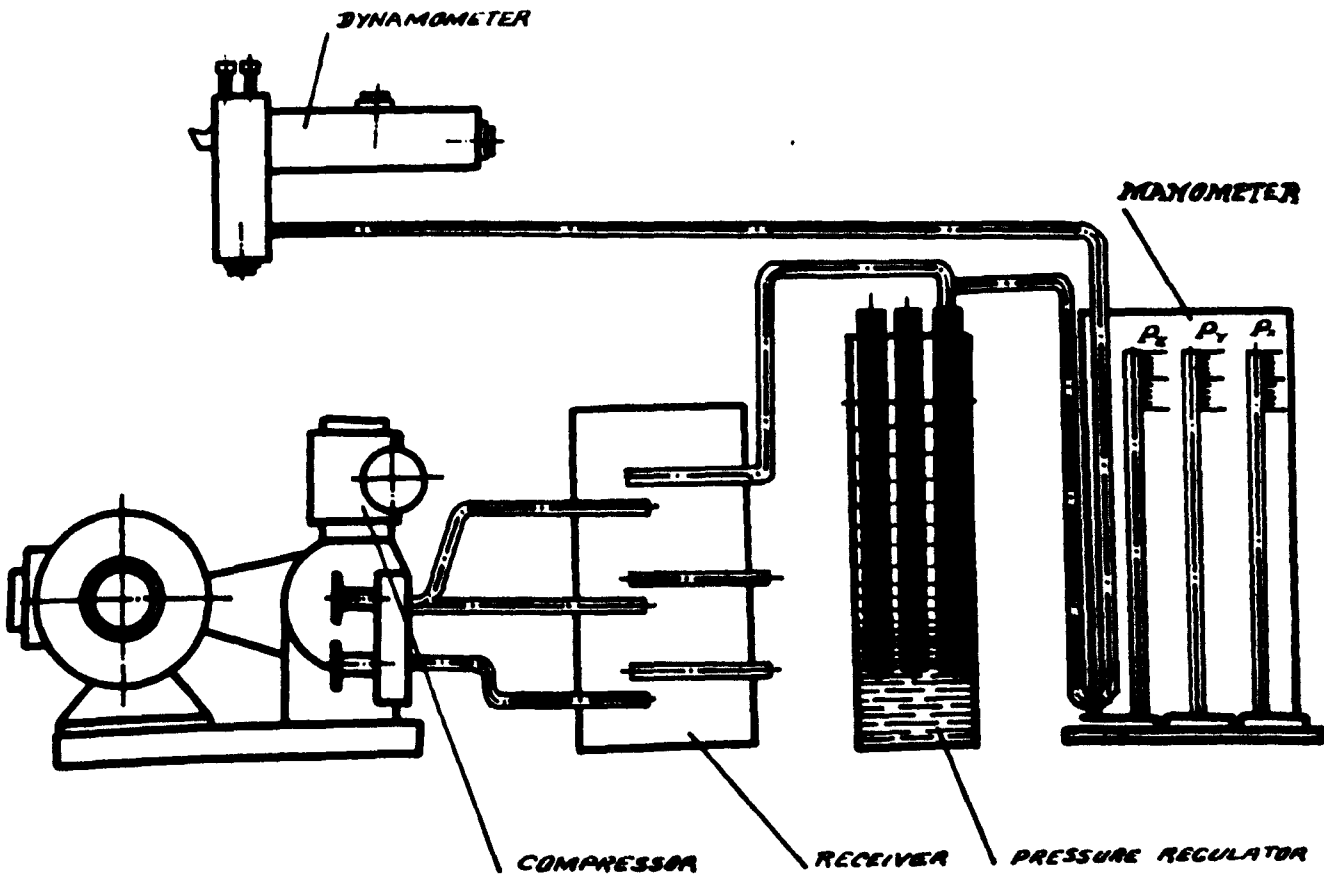


Fig. 24

Thrust seatings are provided between the holder and the transducer to reduce the interaction of one transducer on the other.

When the ring is compressed by the cutting forces, then the orifice of the nozzle opens by means of a ball which is under the action of a spring. The amount of orifice opening is proportional to the applied force. Various opening of the orifice produce various air flow, which is immediately reflected by the indications of the manometer. Such a design of the transducer allows control of the initial air gap and thus of the sensitivity of the dynamometer.

The arrangement of the pneumatic installation for measuring cutting forces is shown in Fig. (24). The compressed air from the compressor is fed to a special receiver through throttling valves. The receiver function is to smooth out the pulsation in the air pressure, which would effect indications of the manometer. The air is fed from the receiver via a regulator to the dynamometer.

The calibrations of the dynamometer transducers are carried out firstly one after the other and secondly by means of a special device, all the three transducers are calibrated together. The results obtained have shown a high reliability of the device. ⁽⁶⁵⁾

2.6 OPTICAL DEVICES

The use of the optical devices in the engineering field has a very wide application because of their high accuracy and simplicity. These devices provide very precise measurements using the wave length of light as a yardstick. For the purpose of force measurements, optical principles could be used for measurement of the dynamic deflections caused by the action of the cutting forces. Very small angular deflections can be readily measured by reflecting a beam of light from the moving surface.

2.7 PIEZOELECTRIC CRYSTALS

These crystals have been used in metal cutting dynamometers as force measuring units. The use of these crystals for the force measuring purposes is narrowly used because piezoelectric crystals produce an electric charge rather than a current, therefore the equipment can become quite unwieldy and leakage effects can be troublesome.

2.8 ELECTRICAL DEVICES

Electrical devices are the most sensitive instruments at high cutting speeds. They can measure very small deflections of 10^{-7} - 10^{-8} in. They are characterized by their simplicity and high sensitivity. The most preferred types of electrical force measuring devices are:

Electronic Transducer Tube

The electronic transducer tube is a very sensitive instrument which measures a deflection of the order of 10^{-6} in.

Electronic transducer tube has been used in metal cutting dynamometers⁽⁵²⁾ for their simplicity and high sensitivity. Experimental results with dynamometers of this type have proved their reliability.

The electronic transducer tube is essentially a small triode vacuum tube with a moveable plate, the tube characteristics being changed as the plate moves. A pin connected to the moveable plate rotates at approximately $\pm \frac{1}{2}$ degree and the minimum motion of the end of the pin can be accurately measured to the order of 10^{-6} in. The electrical system associated with this tube is relatively simple.

Differential Transformer

The differential transformer consists essentially of three transformer coils on a common axis with a moveable core. AC current is supplied to the centre primary coil which induces an EMF in the two secondary coils. The outputs of the two secondary coils are wired to oppose each other so that when the core is displaced, an output is obtained which is proportional to the displacement, with a phase depending upon the direction of motion. The electrical system associated with this instrument is rather complex because of the necessary high amplification and phase sensitivity. The sensitivity of the differential transformer is in the order of 10^{-6} in.

Strain Gauges

In the recent time the use of strain gauges in stress analysis have got a very wide application because of their simplicity and high sensitivity.

Measurement of small deflections of about 10^{-7} in. can be successfully obtained from strain gauges of different types.

The magnetic tube strain gauge is very simple and has a sensitivity of about 10^{-5} in. The electrical system connected with the magnetic tube strain gauge is very simple.

The wire resistance strain gauges have been widely used in force measuring devices. When this type of strain gauge is connected in the form of wheatstone bridge, it can measure deflections of the order of 10^{-5} in.

The strain rings have been used to measure an arbitrarily placed three dimensional force or torque such as the cutting force components.

2.9 DESIGN OF THE TOOL DYNAMOMETER

The dynamometer shown in Fig. 25 was designed to measure the vertical and horizontal components of the cutting force within 1000 kg

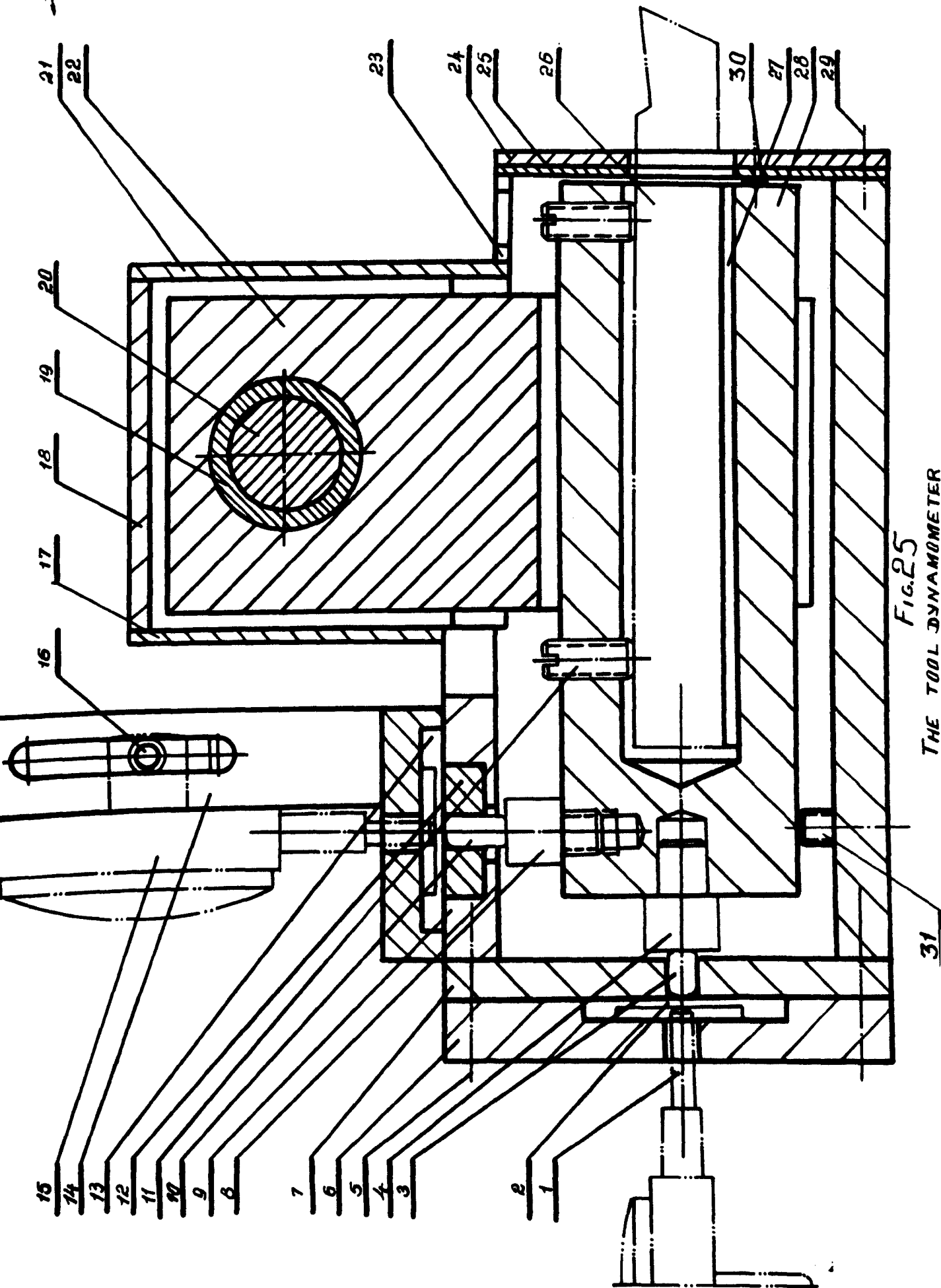


Fig. 25
THE TOOL DYNAMOMETER

31

for a cutting

The

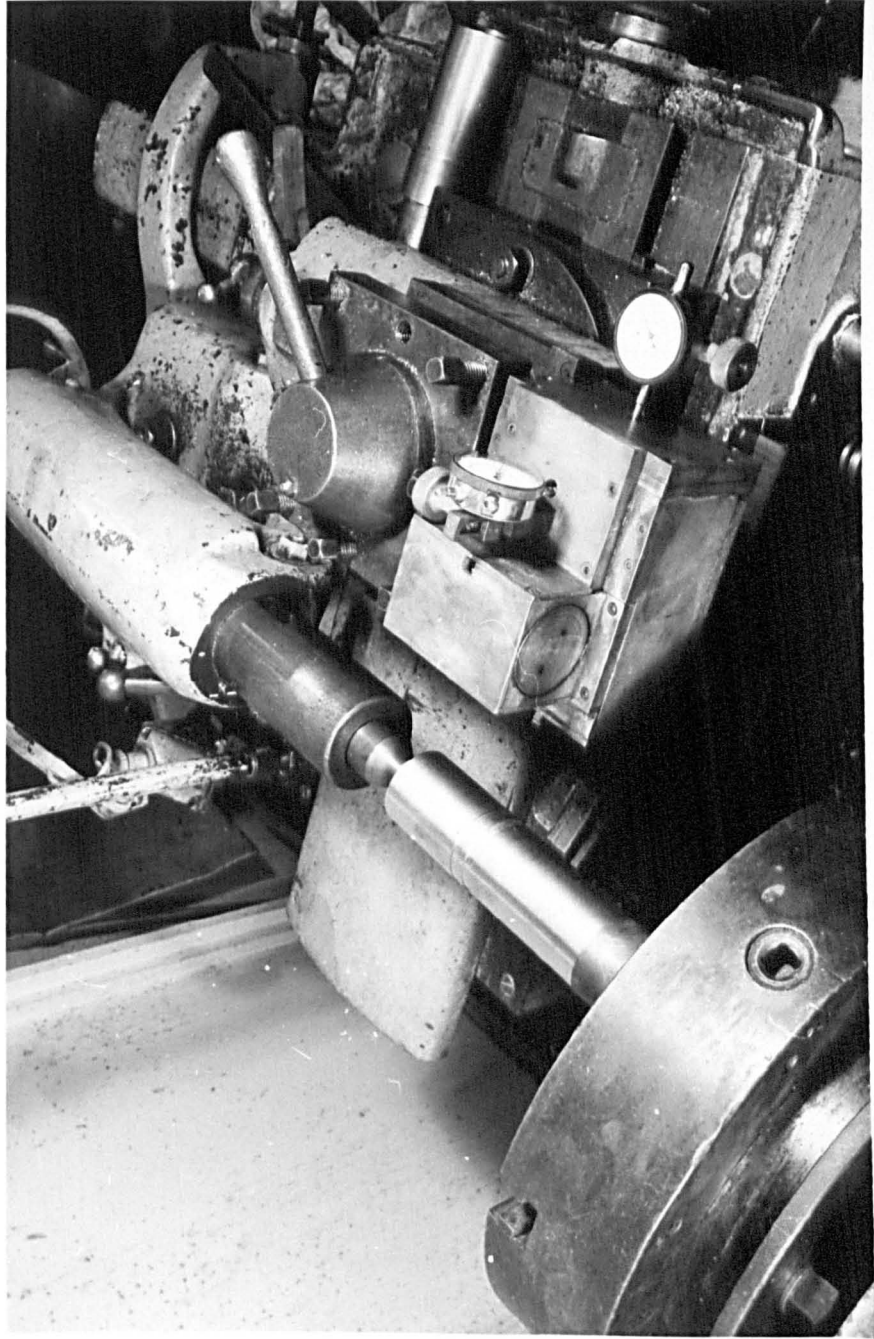


FIG. 25

2.9.1 Des

of

Diaphragm

designed

Hoar (8)

deflection

considering

circular

maximum

the following

for a cutting speed up to 10 m/min, used during this work.

The dynamometer consisted of the following parts:

- | | |
|--|---|
| 1. Horizontal dial gauge. | 9. Bottom part of the dynamometer body. |
| 2. Horizontal diaphragm. | 10. Vertical diaphragm pin. |
| 3. Horizontal diaphragm pin. | 11. Screw. |
| 4. Horizontal pin. | 12. Ring. |
| 5. Bolts | 13. Vertical diaphragm plate. |
| 6. Horizontal flanged cover plate. | 14. Vertical flanged cover plate. |
| 7. Horizontal base plate. | 15. Dial gauge. |
| 8. Vertical pin. | 16. Handle. |
| 17. Cover plate. | 23. Cover plate. |
| 18. Upper part of the dynamometer body | 24. Cover plate. |
| 19. Stopper. | 25. Rubber pad. |
| 20. Roller. | 26. Cutting tool. |
| 21. Cover plate. | 27. Base plate. |
| 22. Link. | 28. Tool holder. |
| | 29. Screws. |

2.9.1 Design, Heat Treatment and Dimensions of the Main Parts of the Dynamometer.

Diaphragm Plates:

Circular diaphragm plates of spring steel ASE-8660 were designed according to Vallance and Doughtie⁽⁶⁶⁾ with reference to Roark⁽⁶⁷⁾ and Den Hartog^(67*), so that to give a sufficient deflection that could be accurately recorded by a dial gauge. By considering the diaphragm as a freely supported (edge supported) circular plate with central concentrated load W , Fig. 26, the maximum stress at the centre of the diaphragm was determined from the following relationship:

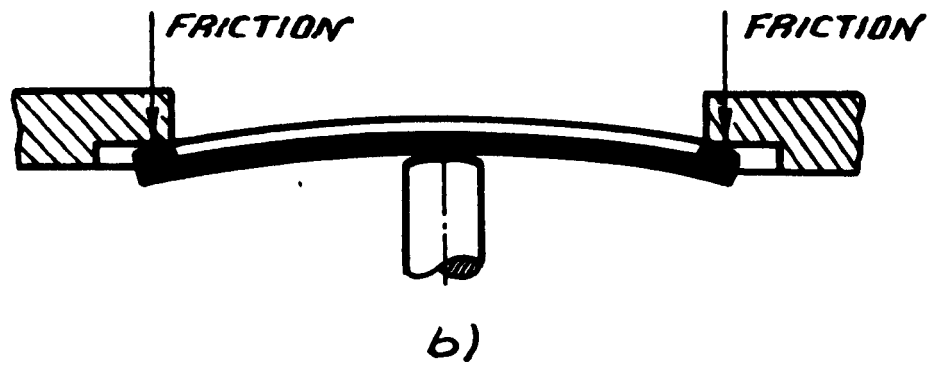
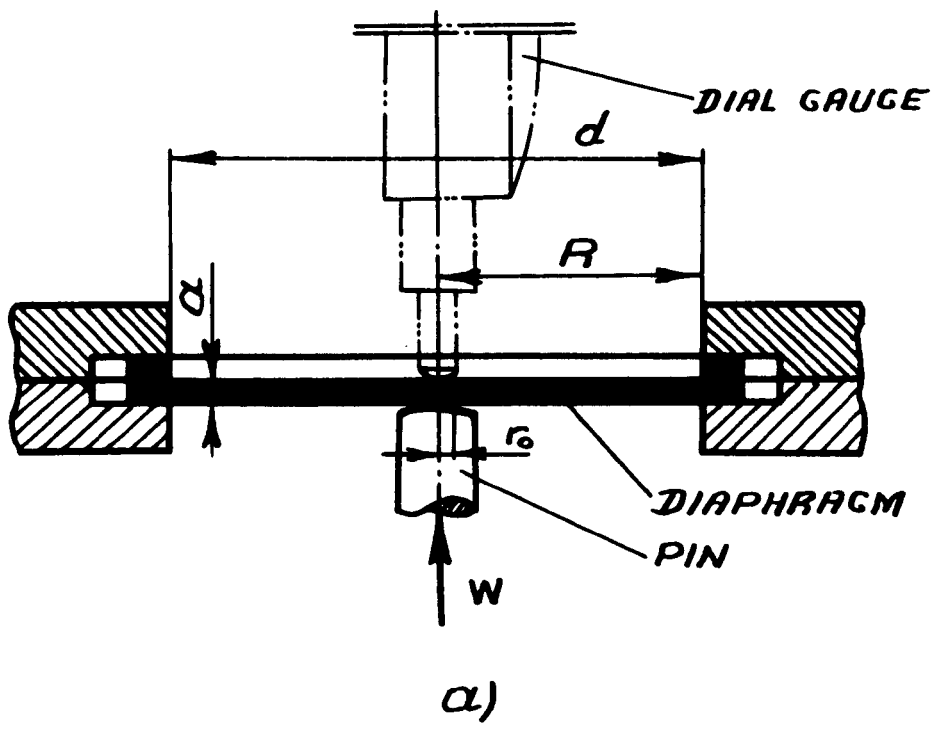


FIG. 26

$$\sigma_{\max} = \frac{3(1 + \nu)}{8} \frac{W}{h^2} \ln \frac{1}{\alpha} = \frac{3(1 + \nu)}{4} \alpha^2 \ln \frac{1}{\alpha} W \frac{d^2}{a^2} = k_s \left(\frac{d}{a}\right)^2 W \quad (2.2)$$

where,

σ_{\max} = maximum stress at the centre of the diaphragm plate,
lb/in²

ν = Poisson's ratio, $\nu = 0.3$

W = maximum applied load, lb

h = $a/2$

a = thickness of the diaphragm plate, in

α = r_o/R

r_o = radius of the circular area through which the
load W is transmitted on to the diaphragm plate,
in, Fig. 26.

R = effective radius of the diaphragm plate, in,
Fig. 26.

d = effective diameter of the diaphragm plate, in,
Fig. 26

k_s = design factor depending on the construction. For
diaphragm plate with edges supported, Fig. 26

$$k_s = \frac{3(1 + \nu)}{4} \alpha^2 \ln \frac{1}{\alpha}, \text{ For } \nu = 0.3, \alpha = 0.1$$

k_s is = 0.023

As suggested by Den Hartog^(67*), the diaphragm was considered as a circular plate with central concentrated load W , Fig. 26 (i.e. r_o is very small compared with d). The maximum deflection of the diaphragm plate was calculated from the following relationship^(67*):

$$\delta = \frac{1}{16\pi} \frac{WR^2}{D} = 0.0199 \frac{WR^2}{D}, \text{ in} \quad (2.3a)$$

or

$$\delta = 0.217 WR^2/E a^3, \text{ in} \quad (2.3b)$$

where,

δ = maximum deflection of the diaphragm plate at the centre, in

D = stiffness of the diaphragm plate, lb. in

$$D = \frac{1}{12} \frac{a^3 E}{(1 - \nu^2)} = 0.0916 E a^3, \text{ lb. in}$$

E = Young's modulus of elasticity, lb/in², E = 30 x 10⁶ lb/in²

For maximum vertical (or horizontal) load of 2000 lb, diaphragm plate thickness of 0.125 in., and effective diaphragm plate radius of 1.5 in, the maximum deflection was 0.017 in. The maximum stress at the centre of the diaphragm was 26.5 x 10³ lb/in² which is much less than the maximum permissible stress for spring steel ASE-8660 which is 120 x 10³ lb/in².

These spring steel diaphragm plates were hardened in oil at 880°C, tempered at 200°C and cooled in oil. The Vickers hardness was H_v = 700. The diaphragm plates were reground to give a smooth contact surface:

It is significant to mention that different diaphragm plates (i.e. diaphragm plates with different thickness and effective diameter) were used, so that to obtain a satisfactory calibration between the applied load and the deflection. The diaphragm plate dimensions shown above were considered quite satisfactory for the above purpose. However the effect of friction between the diaphragm and cover plates as shown in Fig. 26b reduces the sensitivity of the dynamometer. Therefore, any improvement in the construction of the diaphragm plates leading to a reduction in the friction (between the diaphragm and cover plates) will be welcomed.

Diaphragm Flanged Cover Plates:

The flanged cover plate dimensions were calculated according to Faires⁽⁶⁸⁾ by taking into consideration the shear stress area and the permissible stress, using the relationship

$$\pi d h s = w F \quad (2.4)$$

where,

- d = diaphragm diameter
- h = height for effective shear stress
- s = permissible shear stress
- w = maximum load
- F = safety factor

Each cover plate was clamped to the dynamometer body by six bolts. By using a safety factor of 3 and a design stress of 60,000 lb/in², the bolt diameter was $\frac{1}{4}$ in.

Diaphragm Pins:

Diaphragm pins were made of silver steel. The diameter of the pin was calculated from equation (2.4) by taking into consideration the area under shear stress $\pi d_1 h$ Fig. 27, and the annular bearing area $\frac{\pi}{4} (d_2^2 - d_1^2)$,

$$d_1 = \frac{w}{\pi h s_a} \quad (2.5)$$

where, s_a = maximum allowable shear stress.

For $h = 0.4$ in. the pin diameter was $= \frac{1}{4}$ in.

The diaphragm pins were hardened in oil at 820°C and tempered at 170°C. The Vicker's hardness $H_v = 500$. The contact surface of the pins were polished to reduce the friction.

Tool Holder:

The tool holder was made of gauge steel and designed to hold tools up to 1 sq. in. shank. A tool adapter was fitted into the tool holder to prevent it from rotating while the tool was under the action

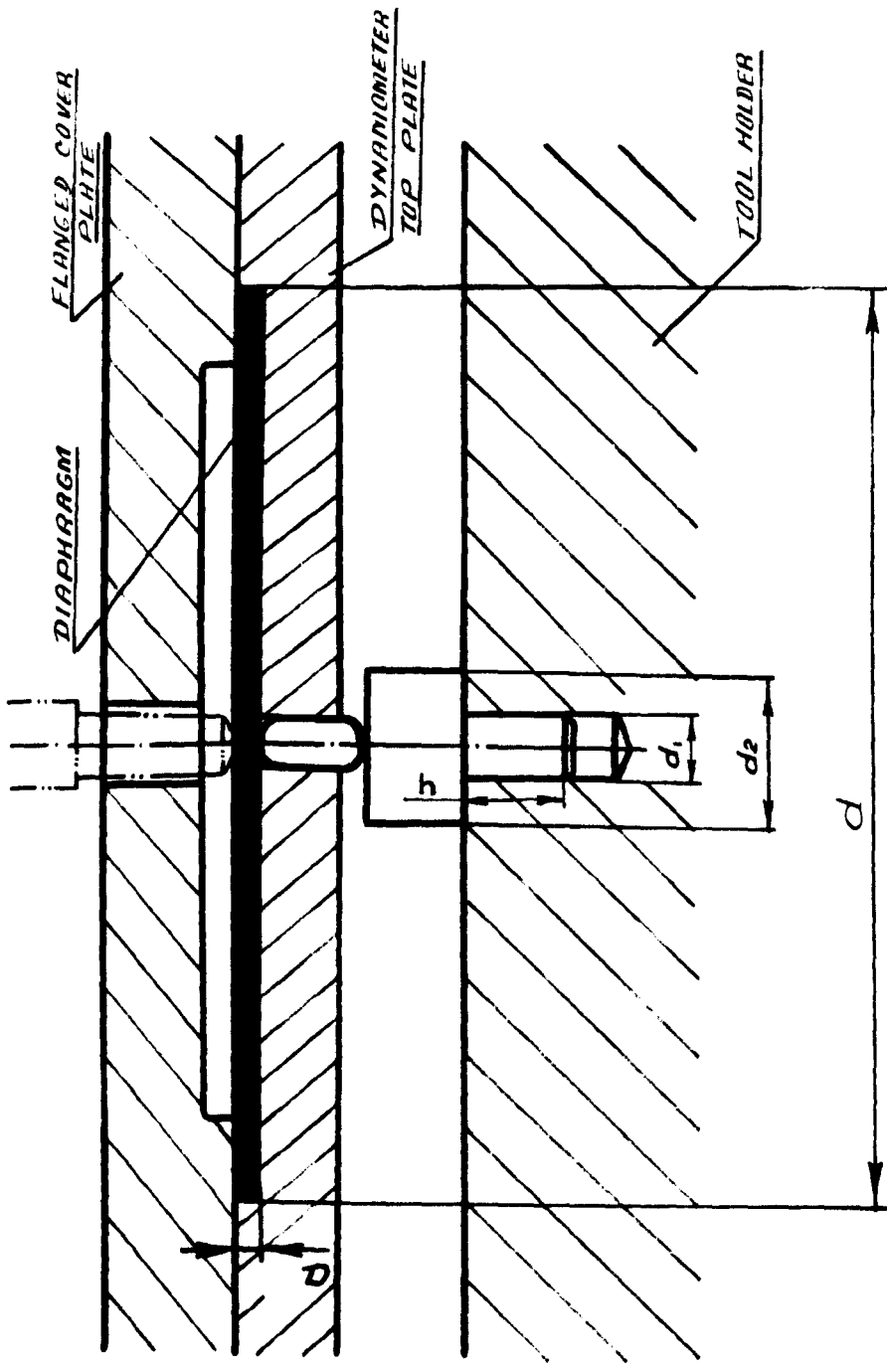


FIG. 27

of the vertical and horizontal components of the cutting force.

The tool holder was hardened in oil at 800°C, tempered at 150°C, and cooled in oil. The Vickers hardness was $H_v = 400$.

Roller:

The roller was made of soft steel. The diameter of the roller was determined from the following relationship⁽⁶⁹⁾, taking into consideration that the load was applied to the middle of the roller,

$$M_{\max} = P \frac{l}{4}$$
$$d_o = \sqrt[3]{\frac{32}{\pi s_t} k_m M_{\max}} \quad (2.6)$$

where,

- P = maximum load applied to the roller
- l = distance between the ball bearings
- s_t = maximum tensile stress
- k_m = safety factor

For $P = 2000$ lb., $s_t = 12,000 - 16,000$ lb/in², $l = 1.5$ in., and $k_m = 1.0 - 1.5$, the roller diameter was $d_o = 0.8 - 1.0$ in.

The roller was hardened at 800°C, tempered at 150°C, and cooled in oil.

Dynamometer Body Plates:

The thickness of the dynamometer body plates was determined by taking into consideration the diameter of the connecting bolts. The thickness of the dynamometer body plates was taken 2.5 times larger than the diameter of the connecting bolts. The plate thickness was therefore = 5/8 in. This thickness ensured a safe drilling of the connecting holes of 1/4 in. diameter.

2.9.2. Adjustment of the Dynamometer

Before the start of the tests during this work the tool holder was positioned in both vertical and horizontal directions. The tool holder was moved in the vertical direction by means of the adjustable screw (31), Fig. 25, until the dial gauge (15) had just begun to read, the screw was then covered with plasticine to fix its position. The dial gauge reading was made zero. Similarly the tool holder was positioned in the horizontal direction by means of screw (30).

During cutting the vertical component of the cutting force was transmitted onto the diaphragm (13) through the pin (8) as the tool holder (28) moved vertically. The vertical movement of the tool holder was achieved through its vertical rotation around the link (22). The deflection of the diaphragm caused by the action of the vertical component of the cutting force was then recorded by the dial gauge (15). Similarly the dial gauge (1) recorded the deflection caused by the action of the horizontal component of the cutting force.

The use of ball bearings and effective lubrication have reduced considerably the friction between the contact surfaces of the dynamometer.

It is important to mention that the use of the above dynamometer was limited due to the poor stability of readings at medium and high cutting speeds when chattering existed. The results obtained from the dynamometer at low cutting speeds up to 10 m/min. were quite accurate for the purpose of this work.

2.9.3 Calibration of the Tool Dynamometer

The calibration of the tool dynamometer for both vertical and horizontal loads was carried out by static loading on a special lever device. The dynamometer was bolted to a specially constructed holder, Fig. 28, which was rigidly clamped to the base plate (1) by means of five bolts. The load was applied to a high speed steel tool (similar to those used in the cutting tests) fitted into the tool holder through

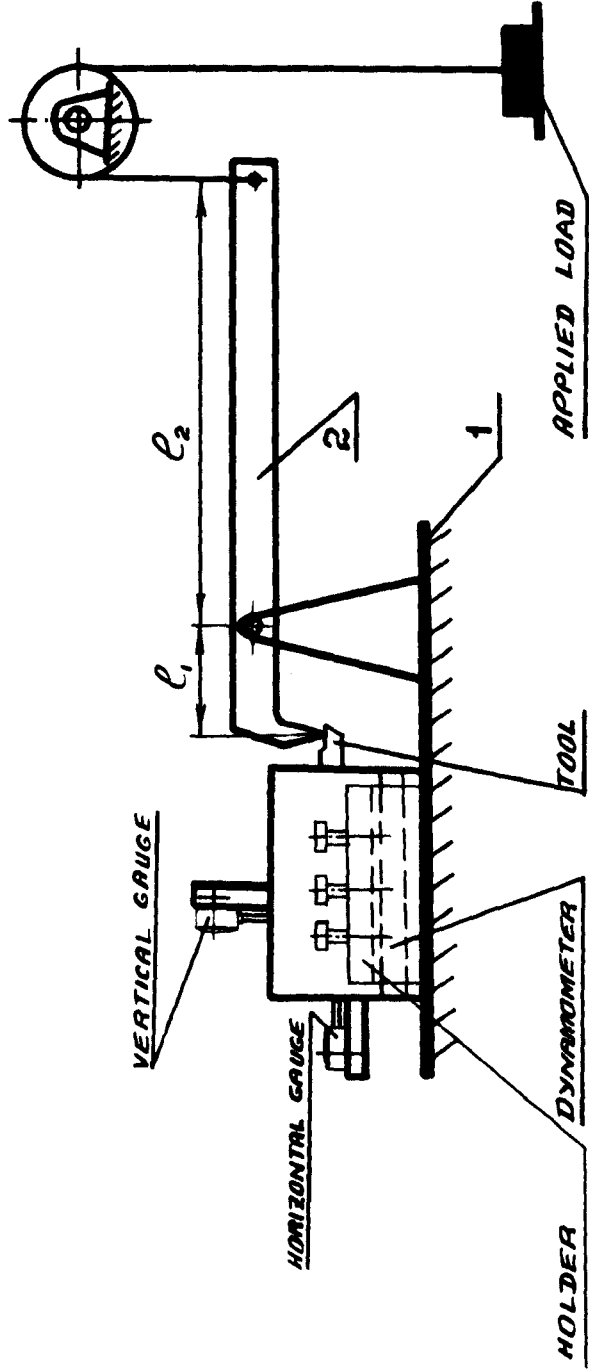


FIG. 28

the pin of the lever (2). The pin was made of silver steel, hardened and tempered to 500 V.P.H. with a rounded Vee shape. The pin was fitted to the end of the lever so that to apply the load at the same distance from the tool holder, just as the cutting tool would have done during the actual cutting operation. The vertical and horizontal calibrations were made in the same manner. At the beginning a small load was applied to the tool till the dial gauge indicator had just begun to move. This position of the tool holder was then fixed and the dial gauge readings were made zero. After that the load was applied in increments of 50 kg and the dial gauge readings were recorded. After a maximum load of 500 kg was applied, the unloading calibration was carried out by reducing the load in the same increment of 50 kg, and the dial gauge readings were also recorded.

The cross-sensitivity of the dynamometer was checked for both vertical and horizontal loads, and it was found that the vertical and horizontal calibrations were independent of each other.

The first calibration curves for both vertical and horizontal loads were not satisfactory. By examining the contact surface of the diaphragms under the microscope, several cracks were found. Then it was decided to change the heat treatment of the diaphragm. But the results were still unsatisfactory, now due to the poor sensitivity of the diaphragms. Finally by reducing the diaphragm thickness, polishing the contact surfaces of the diaphragms and diaphragm pins and by applying an effective lubricant (Mobilgrease AA1) to all moving parts of the dynamometer, a satisfactory linear calibration for both vertical and horizontal loads was obtained, Figs. 29 and 30.

2.10 STRAIN GAUGE DYNAMOMETER

The strain gauge dynamometer was designed to measure the strain produced in the cantilever tool holder shank by the action of the vertical and horizontal components of the cutting force at high and medium cutting speeds.

FIG. 29 CALIBRATION CURVE OF THE
DIAL GAUGE DYNAMOMETER
FOR THE VERTICAL LOAD.

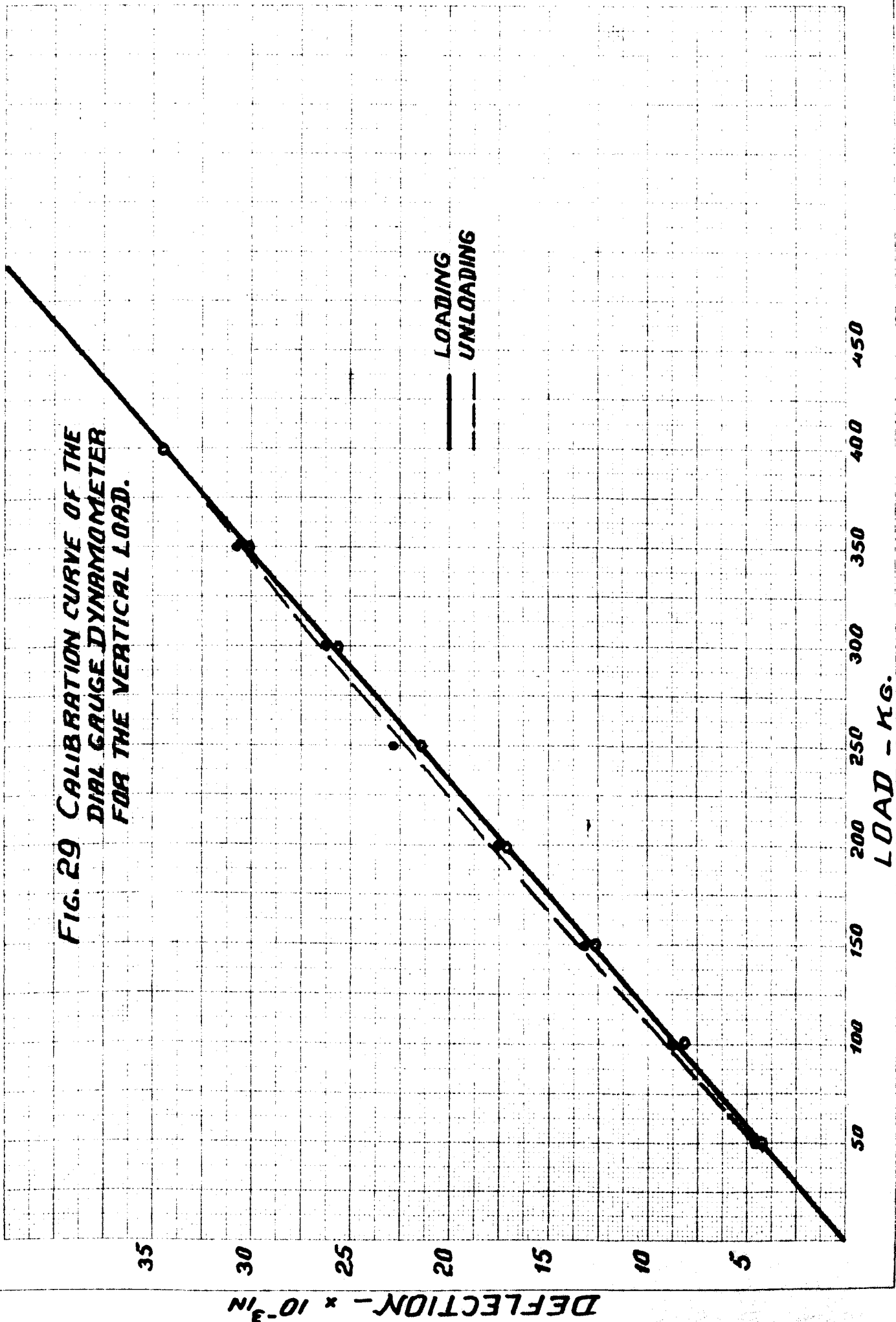
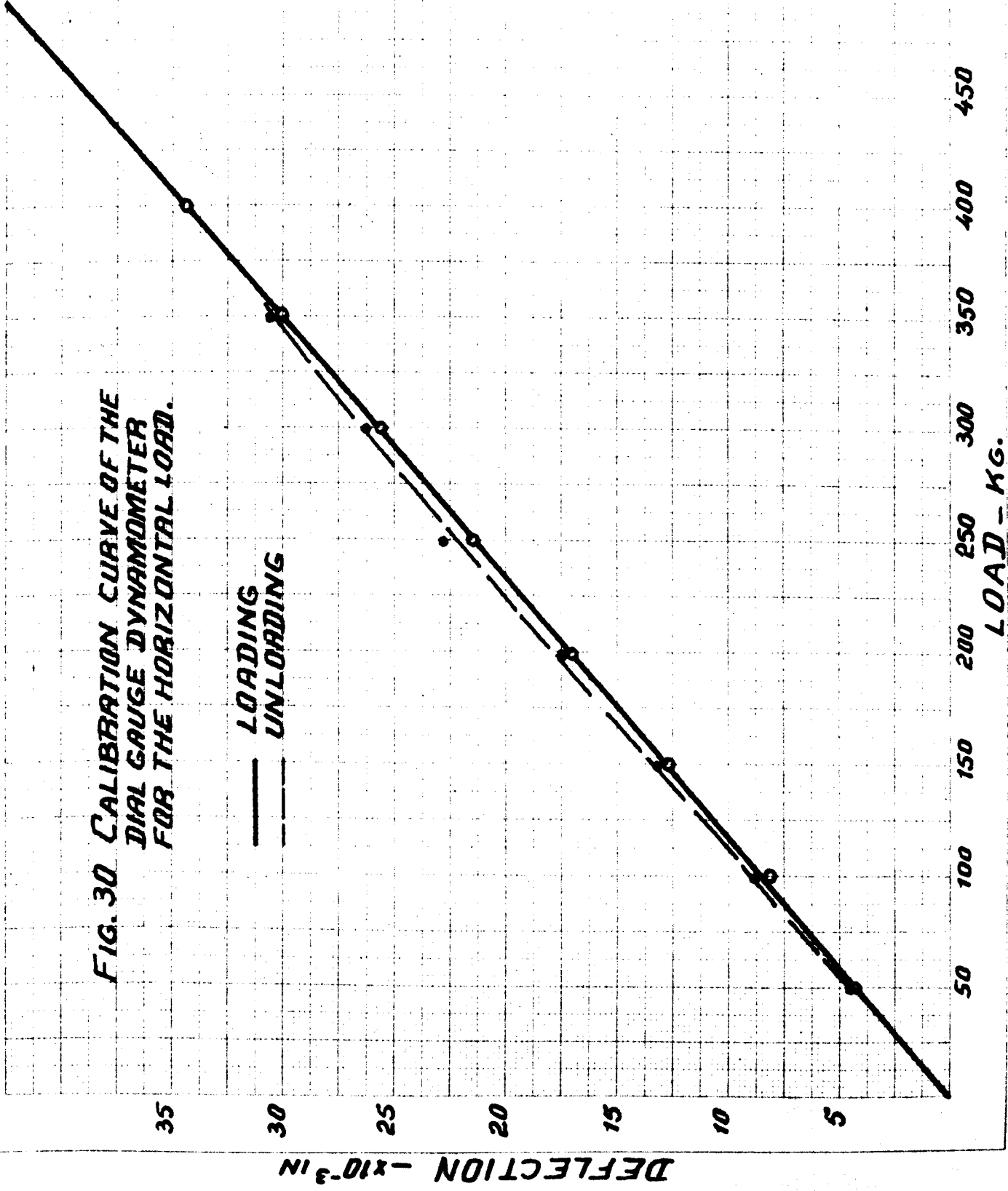


FIG. 30 CALIBRATION CURVE OF THE
DIAL GAUGE DYNAMOMETER
FOR THE HORIZONTAL LOAD.

— LOADING
- - - UNLOADING



Inaccuracies in the readings of this dynamometer caused by either a movement in the point of the application of the force, or temperature effect, or interaction between the vertical and horizontal components of the cutting force were minimized by a careful calibration of the dynamometer and by using a correct electrical circuit.

2.10.1 Circuit Design

In designing the dynamometer, the Wheatstone Bridge circuit was found to be the most suitable for measuring the strains produced by the action of the cutting forces. The position of the strain gauges on the cantilever and in the circuit was chosen as shown in Fig. 31a to be the best from the following points:

1. Increased output voltage from the bridge. The positioning of the four active strain gauges V_1 , V_2 , V_3 , V_4 as shown in Fig. 31b, will increase the output voltage. This could be explained by the fact that the strain gauges which are on the same side of the cantilever, are on the opposite side of the bridge, which means that the electrical strains experienced by them will be additive. Under the action of the vertical component of the cutting force strain gauges V_1 and V_3 , Fig. 31b, experience tensile strain, while strain gauges, V_2 and V_4 , compressive strain of equal magnitude.
2. No cross-sensitivity. The effect of the cross-sensitivity between the vertical and horizontal components of the cutting force was eliminated by the symmetrical positioning of the strain gauges on the cantilever and by using the bridge circuit shown in Fig. 31b.
3. Low temperature sensitivity. Using the circuit shown in Fig. 31b, the cantilever experienced a uniform change in the temperature. Consequently there was no change in the bridge output.

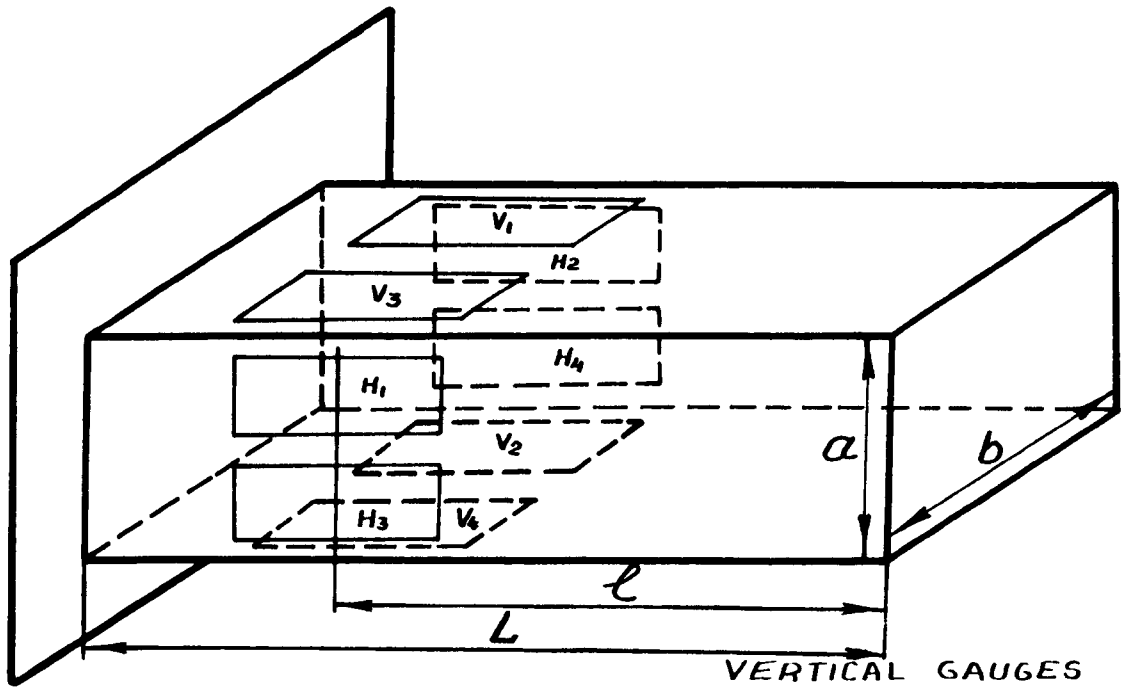


FIG 31a

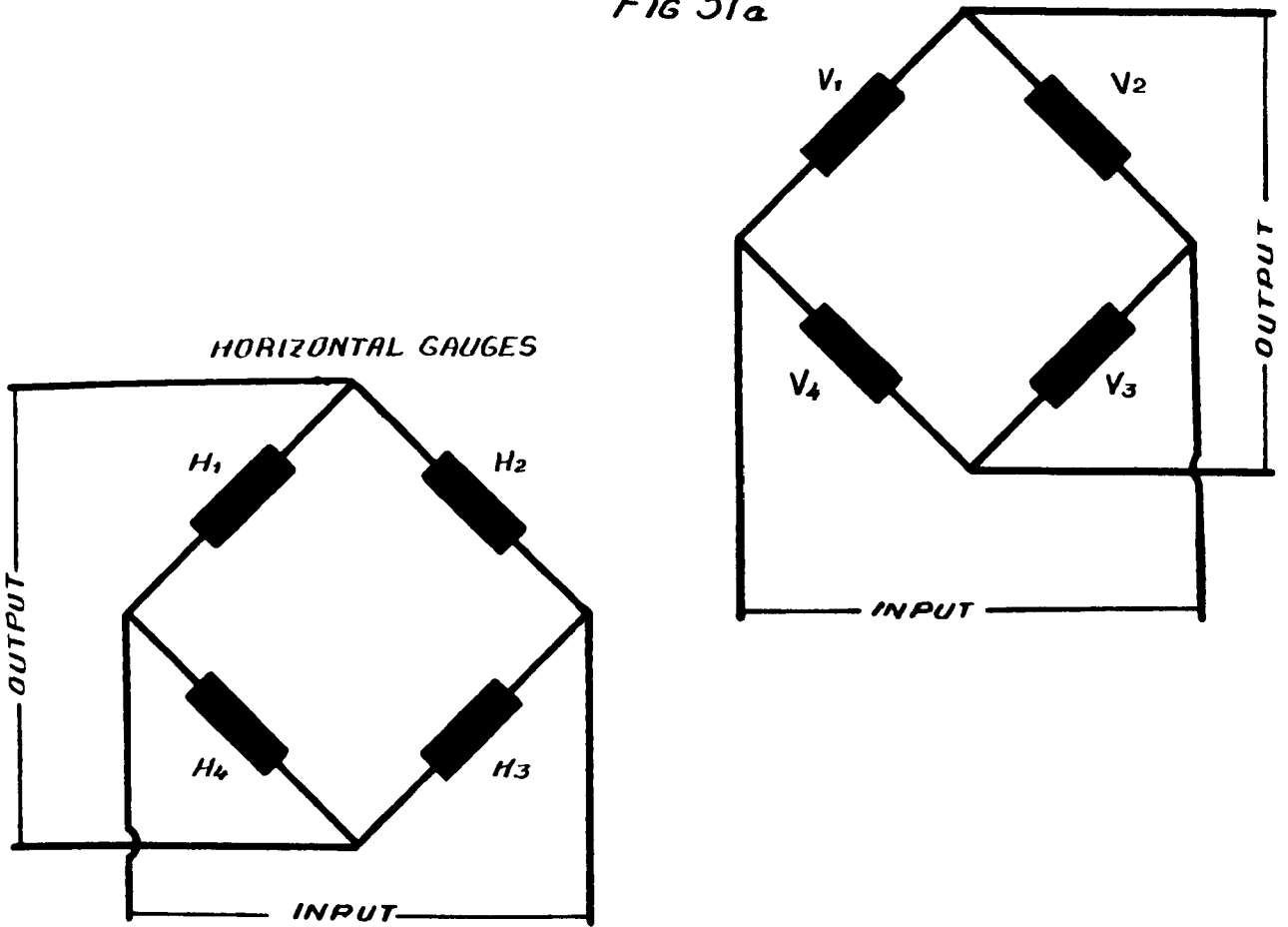


FIG. 31b

4. Effect of radial or thrust forces. Since the cutting forces were applied a distance from the axis of the cantilever, a twisting moment was produced. The magnitude of this twisting moment was small compared with the bending moments, therefore its effect was considered to be negligible.

The full electrical circuit is shown in Fig. 32. Power was supplied to the circuit from a Farnell type M.S.U. power supply unit. Saunders-Roe foil type strain gauges were chosen to be the most suitable for the above purpose. Each circuit was balanced so that it would give a zero output in the unstrained condition. This was done by changing the resistance in each arm of the bridge through a Beckman precision potentiometer. A clamp galvanometer was connected to the circuit with a switching device to find the balance point of each circuit. After balancing, the circuits remained undisturbed for a short time before checking the balance conditions so that to eliminate any drift caused by the heating of the strain gauges. All circuit system components were earthed. The circuit was protected from the coolant and flying chips by a plastic cover.

2.10.2 Dynamometer Cantilever

A special tool, Fig. 33, with a cross section of $1\frac{1}{2}$ " x 1" was chosen as being rigid enough for this investigation. The tool type "A" with carbide tips were obtained from Firth Brown Tools Limited. The overhang of the tool was taken so that to give a high rigidity and sufficient space for the mounting of the strain gauges.

2.10.3 Determination of Several Parameters

Using Saunders foil strain gauges of 1 " x $\frac{1}{4}$ " x 75Ω and gauge factor of 2.17, the maximum voltage for safe operation of any of the gauges is given by ⁽⁵²⁾.

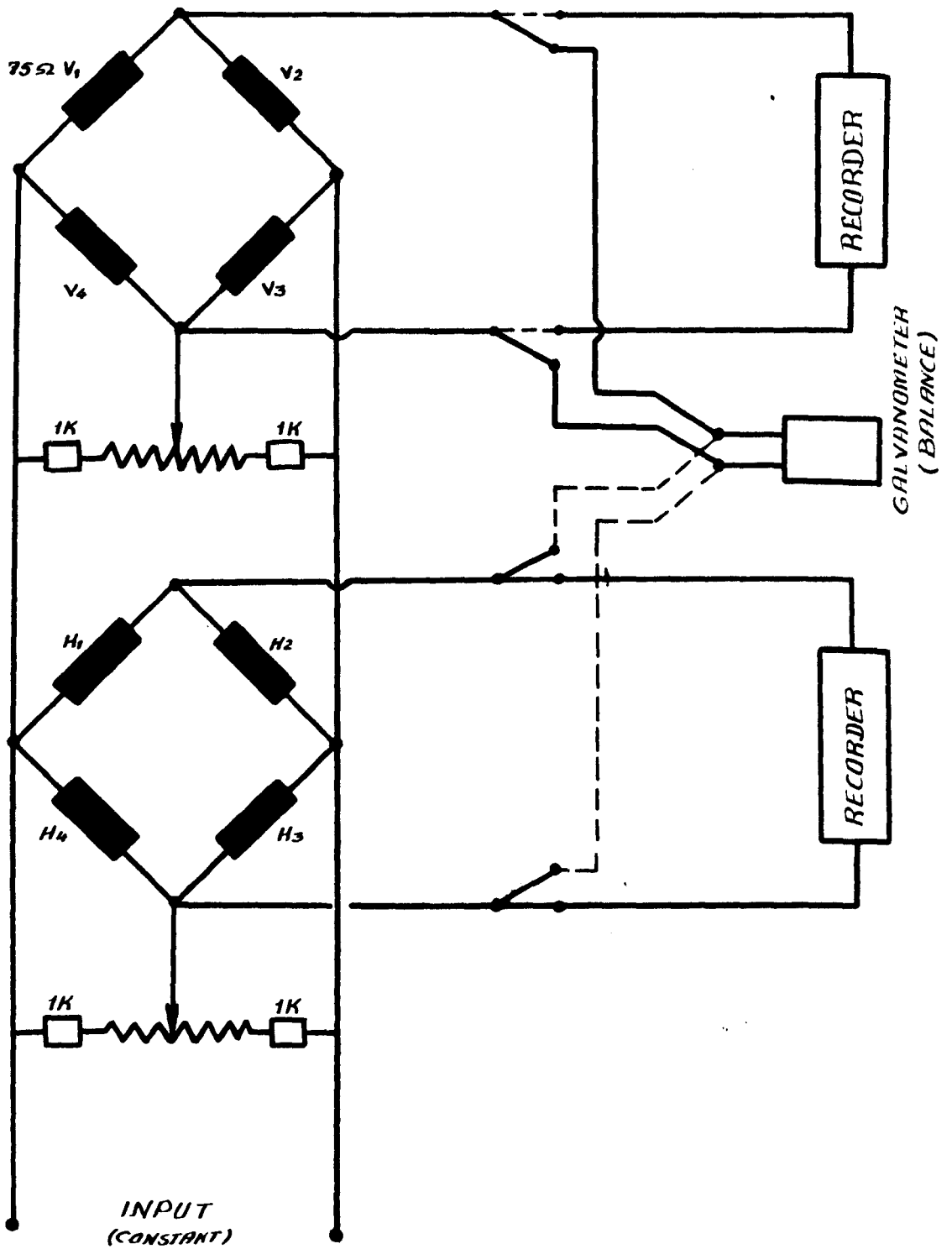


FIG. 32

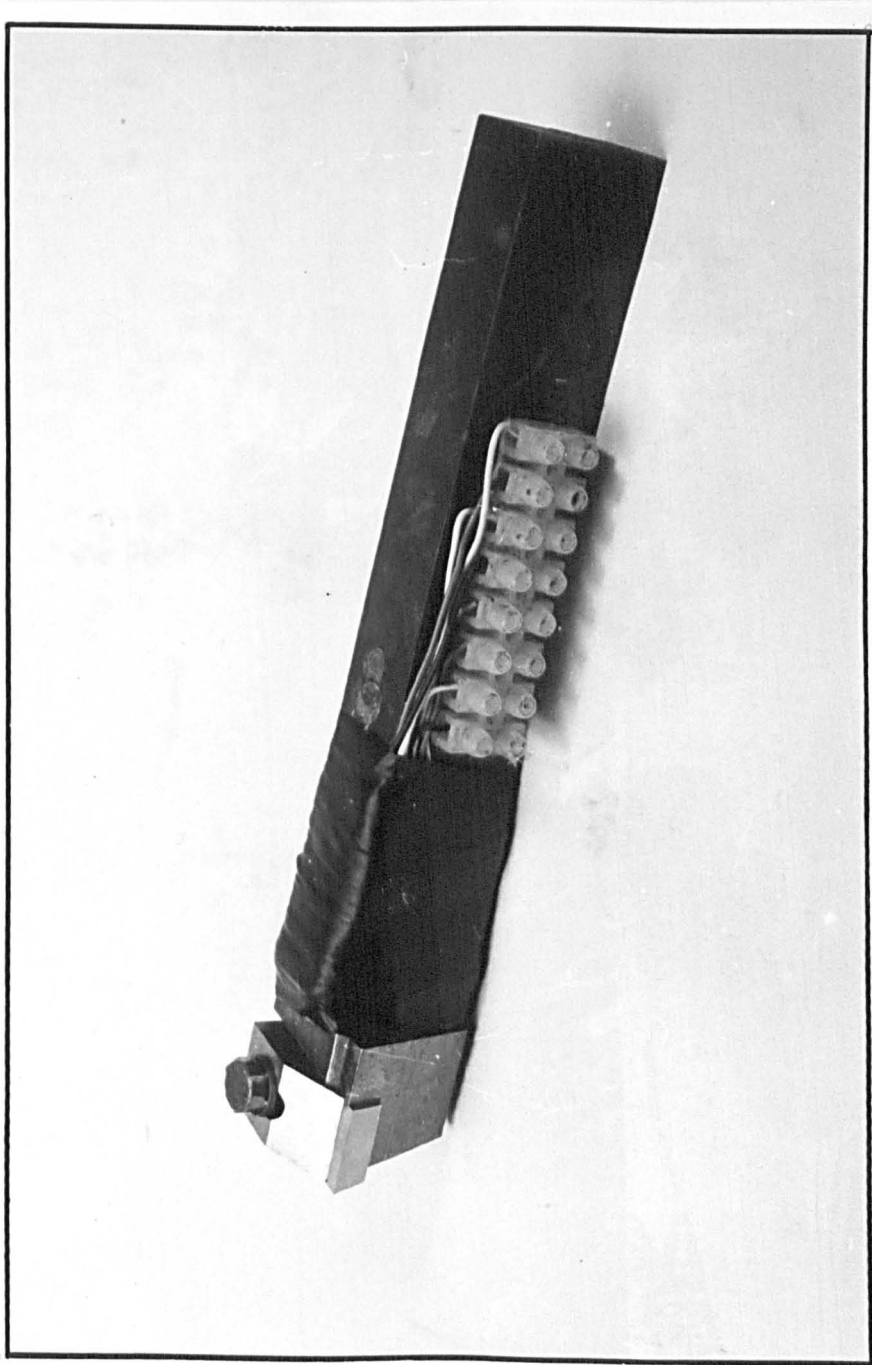


FIG. 33

Hence for the above

For the above

is given by

where,

using values

and,

relationship

for $H = 732$

$\Delta R = .0722\%$

$R_1 = R_2 = R_3$

For the above

Hence,

$$\text{Output voltage} = 13.7 \times 0.000964 = 0.0132 \text{ V.}$$

So a 1" strain gauge in the above case gives 13.2 mV.

$$V_{\max}^2 = \text{Resistance} \times 10 \times \text{gauge area} \quad (2.7)$$

Hence for the above gauge,

$$V_{\max} = 13.7 \text{ volts}$$

For the cantilever shown in Fig. 31a, the strain at the gauge centre is determined as follows:

$$e_H(1.2) = \frac{1}{2} b M_H / E I_H \quad (2.8)$$

where,

$$I_H = a b^3 / 12$$

using values $a = 1 \text{ in.}$ and $b = 1\frac{1}{2} \text{ in.}$, we have.,

$$I_H = 0.27 \text{ in}^4$$

and,

$$e_H(1.2) = 444 \times 10^{-6} \text{ in/in}$$

The change in the resistance is determined from the following relationships:

$$\Delta R = R \times F \times e \quad (2.9)$$

for $R = 75 \Omega$, $F = 2.17$ and $e = 444 \times 10^{-6}$, the change in the resistance $\Delta R = .0722 \Omega$.

For any bridge circuit, having strain gauges of resistance $R_1 = R_2 = R_3 = R_4$, wired as used in the dynamometer:

$$\frac{\text{Output voltage}}{\text{Input voltage}} = \frac{R_2 R_4 - R_1 R_3}{(R_1 + R_2) (R_3 + R_4)} \quad (2.10)$$

For the above case,

$$\frac{\text{O.V.}}{\text{I.V.}} = \frac{0.0722}{75} = 0.000964$$

Hence,

$$\text{Output voltage} = 13.7 \times 0.000964 = 0.0132 \text{ V.}$$

So a 1" strain gauge in the above case gives 13.2 mV.

The deflection of the cantilever Fig. 31a is:

$$\delta = PL^3/3 EI \quad (2.11)$$

For $P = 2000 \text{ lb.}$, $L = 4''$, $E = 30 \cdot 10^6 \text{ lb/in}^2$ and $I = 0.27 \text{ in}^4$, the maximum deflection of the cantilever $\delta_{\text{max}} = 0.005''$.

The natural frequency of the dynamometer is determined according to Ferberg and Kemler⁽⁷⁰⁾:

$$f_n = c \sqrt{\frac{g \cdot E \cdot I}{w L^4}} \quad (2.12)$$

where,

$c =$ constant depending on the mode of vibration. For the fundamental mode $c = 0.560$.

$w =$ the weight of the beam/unit length = 0.354 lb/in.

$g =$ acceleration due to gravity = 386 in/sec^2

$E = 30 \cdot 10^6 \text{ lb/in}^2$ and $I = 0.27 \text{ in}^4$.

then,

$$f_n = 3540 \text{ cycles/sec.}$$

2.10.4 Choice of Galvanometer

By using galvanometers type SMI/S with ($f_n = 160$, $R_g = 75 \Omega$, $R_d = 250 \Omega$, $S_v = 0.375 \text{ mV/cm}$)

$$I_g = \frac{\Delta R \cdot E}{R(R + R_g)} \quad (2.13)$$

where,

$\Delta R =$ Change of resistance in each gauge Ω ,

$E =$ E.M.F. of the input V ,

$R =$ Resistance of one gauge Ω ,

$R_g =$ Galvanometer resistance Ω .

$$I_g = \frac{.0722 \times 12}{75(75 + 75)} = 77 \text{ mA.}$$

2.10.5 Maximum Trace Deflection

The maximum trace deflection was determined from the following relationships:

$$R_1 = R_d - R_g = 250 - 75 = 175$$
$$D = \frac{I_o}{S_i} = \frac{V_o}{S_i(R_1 + R_g)} \quad (2.14)$$

where,

R_1 = balancing resistance Ω ,

R_d = damping resistance of the galvanometer Ω ,

S_i = galvanometer sensitivity mA/cm,

V_o = maximum safe voltage V.

For $V_o = 13.2$ mV; $S_i = 0.005$, $R_1 = 175 \Omega$ and $R_g = 75 \Omega$ the maximum trace deflection $D = 10.6$ cm. which is large enough to record low values of cutting forces.

2.11 INSTRUMENTATION

An ultra-violet recorder series M.1250 was chosen as the best instrument to provide a continuous record of the forces. Galvanometers were selected by taking into consideration the maximum output voltage expected from each bridge and the frequency of the force variation.

Galvanometers type SM1/S with a natural frequency of 160 c/s were found to be accurate enough to record the change in the cutting forces.

For optimum frequency response and damping the galvanometer must see a resistance of 250Ω . That was done by adding a resistance of 150Ω to the circuit between the bridge and the recorder. The strain gauge dynamometer and its attachments are shown in Fig. 34.

3.12 CALIBRATION

on the scale
of the dial
specially dev

taken as clo
lent. The
was carried
increments o
maximum load
increment of
recorded and
obtained.

dynamometer
as possible
and for

this cantile
affected by
Calibrating
actual error
The
reliable.

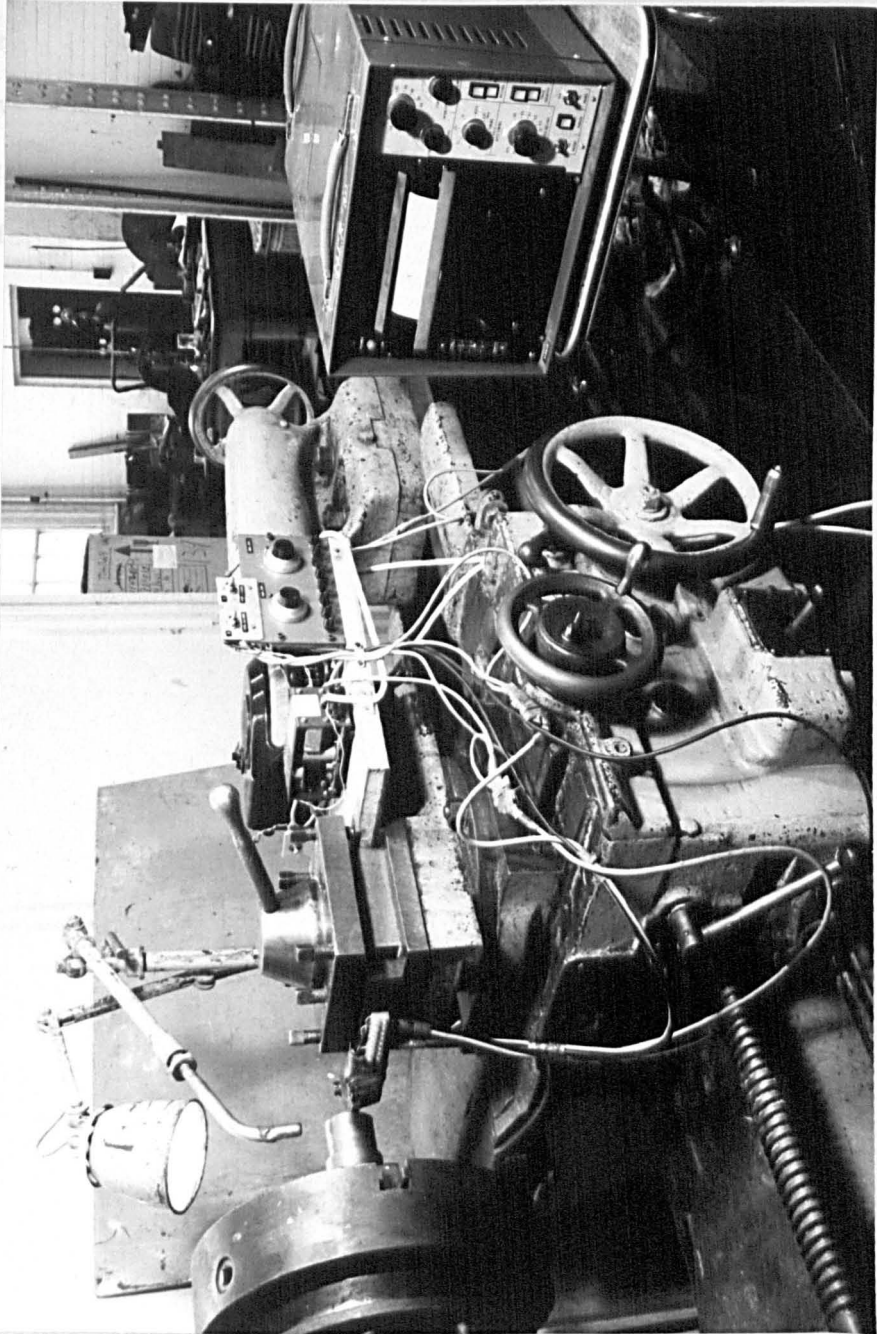


FIG. 34

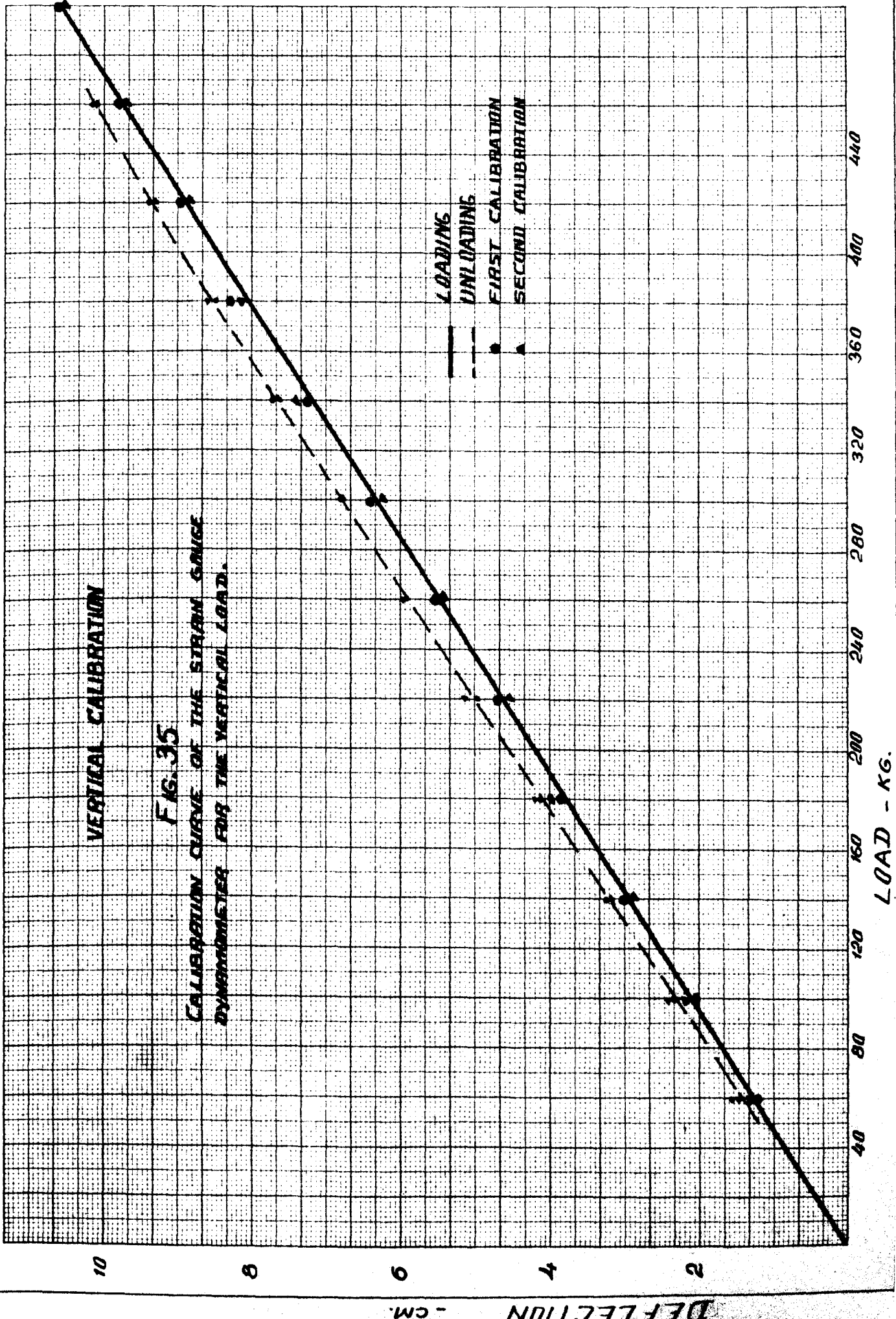
2.12 CALIBRATION OF THE STRAIN GAUGE DYNAMOMETER

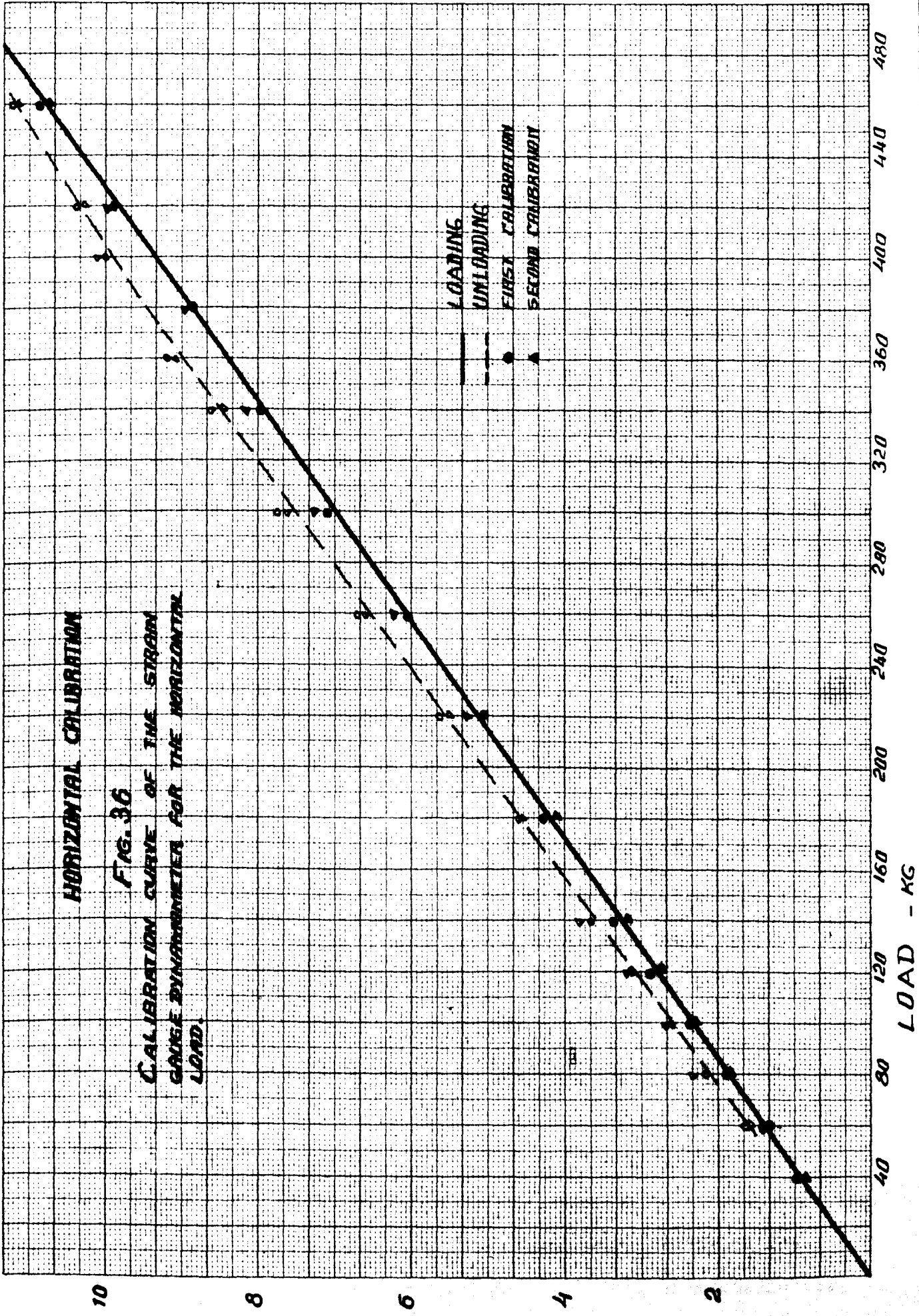
The calibration of the strain gauge dynamometer was carried out on the same lever device, Fig. 28, which is used for the calibration of the dial gauge dynamometer. The dynamometer was mounted in a specially designed toolpost. The overhang of the dynamometer was taken as close as possible to the actual overhang used during cutting tests. The vertical and horizontal calibration of the dynamometer was carried out in the same manner by applying a static load in increments of 50 kg through the pin of the lever Fig. 28. After a maximum load of 600 kg, the unloading was carried out in the same increment of 50 kg. All these points for loading and unloading were recorded and the calibration curves shown in Fig. 35 and 36 were obtained.

Although the strain gauges were mounted symmetrically on the dynamometer's shank and the calibration was carried out as carefully as possible, there was still a cross-sensitivity between the vertical and horizontal loads, but it was very small.

It is important to mention that one of the main drawbacks of this cantilever type of dynamometer was that its reading was highly affected by any change in the position of the applied forces. Calibrating the dynamometer at conditions similar to those of the actual cutting has reduced this effect.

The results obtained from the above dynamometers were quite reliable.





DEFLECTION ON THE TRACING PAPER.C.M.

CHAPTER 3

3.1 CHIP BREAKING

Swarf disposal has been a problem since machine tools were developed and up to the present time the metal cutting industry is in need of sufficient and reliable methods of chip breaking. Due to the appearance of new tool materials such as sintered carbide, ceramics and cast alloys which allow a high rate of metal removal, the chip breaking and chip disposal problems have stimulated extensive investigation. To obtain maximum efficiency from these high-speed tool materials a suitable means has to be provided, such as chip-breakers, for curling and breaking the chips into small pieces so as to remove them from the vicinity of the tool point, and to facilitate mechanized systems of chip disposal.

To obtain the desired degree of chip breaking for a particular cutting condition, two facts must be remembered:

1. Chip breaking depends upon the control of chip flow.
2. Chip flow control is accomplished by bending the chip.

Although the Sheffield area accommodates a fair proportion of the tool making industry in the United Kingdom, questions of chip breaking and chip disposal have not commanded the attention they deserve until recently, when certain of the tool-making firms have started to develop tools with reliable chipbreakers.

3.2 CUTTING OPERATIONS FROM CHIP BREAKING POINT OF VIEW

The production of continuous chips during turning, boring, milling, drilling, facing, thread cutting, broaching, tapping and reaming operations require a solution to the problem of chip breaking.

Chip breaking in all cutting operations depends on the duration and continuity of the cutting cycle, tool characteristics, cutting conditions, and the work-piece material.

From the chip breaking point of view the cutting operations are classified in the following order:

3.2.1 Turning and Boring

Both turning and boring are processes of metal removal by means of single pointed tools. A great deal of investigation has been carried out by Henriksen⁽⁷¹⁾, Muller⁽⁷²⁾, Bickel⁽⁷³⁾, Okushima⁽⁷⁴⁾, Zorev⁽¹⁷⁾, and several others to establish the effect of different cutting conditions, tool geometries and work-piece materials on the shape, the size, and the direction of the flow of the chip. As a result of these investigations they concluded that the depth of cut and feed are the main factors determining the shape and the size of the chips.

Eugene⁽⁷⁵⁾ has noticed an increase in the roughness and irregularity of the chip as the cutting speed or the rake angle is reduced.

3.2.2 Drilling

In drilling operations the metal removal is achieved by means of multi-pointed cutting tools (drills). Drilling requires not only the breakage of the chips during cutting but also its removal from the vicinity of the drill. Crowding of the chips within the drill flutes may result in breakage of the drill. Unsatisfactory removal of chips may lead to a wrapping of the chips around the drill, thus obstructing the flow of the swarf.

The main factors affecting the shape and the size of the chips are the drill design, cutting conditions and work-piece material.

It is essential that the feed and speed should be selected so that to ensure a satisfactory chip removal and tool life.

3.2.3 Milling

Although milling is a discontinuous cutting process, chip breaking is necessary for some types of cutters.

The milling cutter must be designed so that the space between the cutter teeth will avoid overcrowding of the chips which might result in the breakage of individual teeth.

The angle of the inclination of a single cutting edge is found⁽⁷⁶⁾ to have a significant effect on the chip flow. Positive angle⁽⁷⁶⁾ will tend to spiral the chip away from the work, whilst a negative angle will force the chip to move towards the work.

3.2.4 Broaching

In broaching operations it is essential that the broach should be designed with sufficient space for the chips. Otherwise the chips will tend to pack between the teeth, resulting eventually in failure of the broach.

Correct cutting fluid will alleviate the forming of a built-up edge on the cutter teeth.

Carter⁽⁷⁷⁾ has found that the chip's shape and dimensions depends on the hook angle (angle of the inclination of a single cutting edge) of the broach (decrease in hook angle tightens the chip coil), cutting speed and work-piece material.

The use of chip-breakers, increased chip thickness, and decreased chip width will considerably reduce the cutting forces⁽⁷⁸⁾.

3.2.5 Tapping and Reaming

The main problem in tapping is to ensure a sufficient space for the chips. If chip space is increased by reducing the number of flutes, decreasing the width of the land or by increasing the hook of the cutting edges, this may reduce the life of the tap. Spiral-pointed taps⁽⁷⁶⁾ will push the chips ahead of the tap. Helical fluted taps⁽⁷⁶⁾ will tend to direct the chips toward the shank of the tap.

In reaming although the amount of material to be removed is very small, reaming is a finishing operation and therefore there must be no overcrowding of the chips in the vicinity of the reamer teeth which might reduce the quality of the surface finish.

The use of lubricant increases the life of the tap and decreases the build-up of material in reaming which improves the quality of the surface finish.

Operations like shaping and planing do not require chip breaking, because of discontinuity of the cutting cycle.

3.3 WHY USE CHIP - BREAKERS?

In large-batch production when high-output machine tools such as automatic and semi-automatic lathes are used, reliable methods of chip breaking are essential so as to eliminate the stoppage time required for clearing away the swarf from the vicinity of the machines. Reliable control of the chip breaking and chip flow processes ensures a sufficient protection to the operator from the dangers caused by the flying chips, especially at high cutting speeds. It is also desirable to have the chip broken into small pieces as it leaves the cutting face of the tool, so as to avoid any possible damage to the surface finish.

Another reason why chip breaking is used is based on consideration of the chip disposal process. The efficiency of swarf removing devices such as conveyors is highly dependent on the type and size of the chips produced. The smaller the size of the chips produced, the more effective the chip disposal system can be. Chips up to two inches long are quite satisfactory. However, a further consideration is that if the swarf is in long ribbons, it may need crushing before it is dispatched from the works, but this would be unnecessary if small chips are produced by the machine tools.

3.4 TYPES OF CHIP-BREAKERS

1. Ground Chip-Breakers:

- (a) Ground Step Type Chip-Breaker: This consists of a step or platform ground into the cutting (rake) face of the tool at some distance from the cutting edge (Fig. 37). The cutting edge and rake angle remain unchanged.
- (b) Groove Type Chip-Breaker: A groove of some profile is ground into the cutting face of the tool at a short distance from the cutting edge. This distance must be related to the feed. The chip-tool contact area and consequently the chip curvature is controlled by this distance.

Ground chip-breakers are the most commonly used in the machine tool industry. The main function of the ground chip-breakers is to curl the chip. The chip will break either as a result of its contact with the work-piece, the tool box or any other obstacle or as a result of an increase of stress in the chip as its radius of curvature is increased. The step type chip-breaker is characterized by its width and height.

If, in an angular step type chip-breaker, the width of the chip-breaker is not constant, the chip flow is controlled by the minimum width of the chip-breaker. If such a chip-breaker has a negative opening angle (angle between the chip-breaker and the direction parallel to the cutting edge fig. 39) with the minimum width at the rear of the cut, as in Fig. 39, the chip-breaker has a great tendency to direct the chip against the uncut surface of the workpiece. To avoid the danger of over-breaking of the chip, Henriksen⁽⁷¹⁾ suggested that the opening angle should be within minus 5 to minus 8 degrees for deep cut and minus 8 to minus 15 degrees for shallow cut.

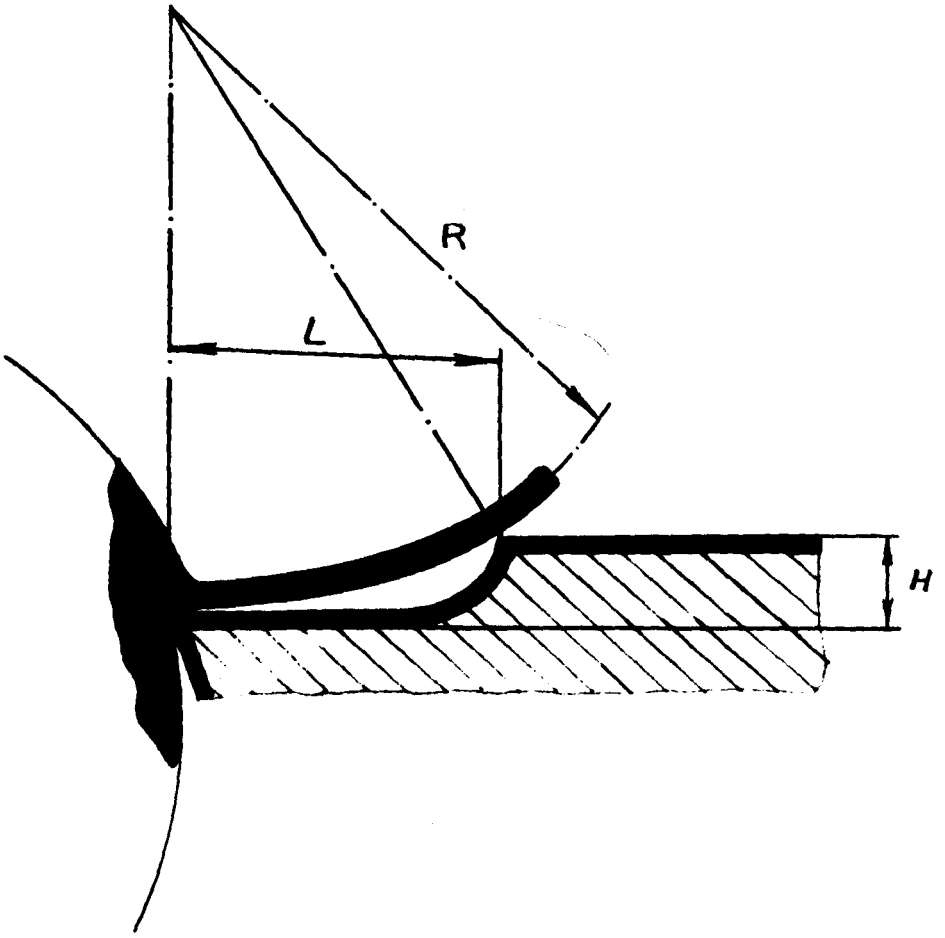


FIG. 37

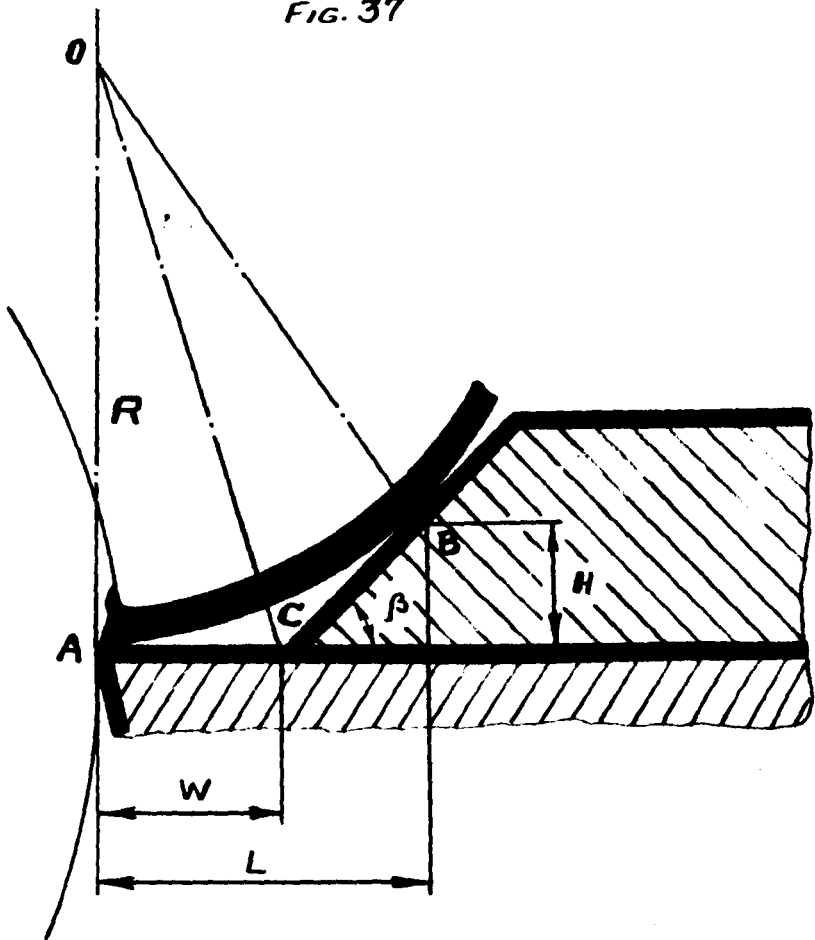


FIG. 38

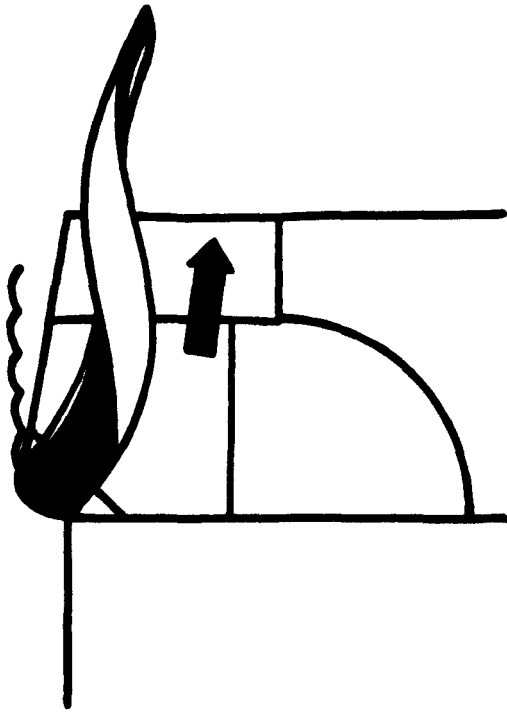
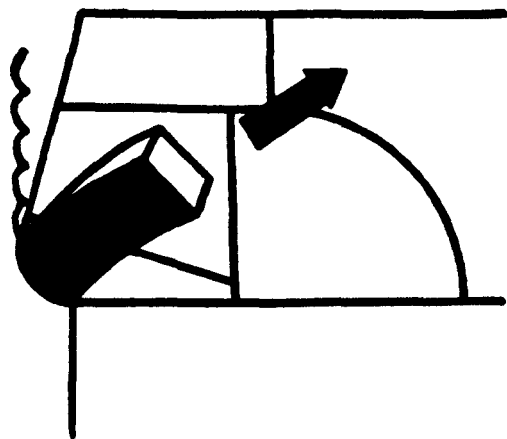


Fig. 39



2. Clamped Chip-Breaker:

The clamped chip-breaker is a block of hard material with an inclined wedge, firmly clamped to the cutting face of the tool and set at some distance from the cutting edge, Fig. 38. Clamped chip-breakers differ significantly from ground chip-breakers in that they can be taken apart. The position of the chip-breaker can be adjusted and the height of the chip-breaker is considerably larger than those of the ground chip-breakers.

The main advantages of the clamped chip-breaker as listed by Henriksen are:

1. It consumes no carbide material out of the tool blank.
2. It does not require diamond wheel grinding.
3. Lower tool wear, longer tool life.
4. Simplicity, speed and cheapness of grinding.
5. Adjustability.

The most important factors in controlling the clamped chip-breaker's performance are the angle of the inclination β and the face width of the chip-breaker w , Fig. (37). However, with small inclination angles the chip breaking action becomes soft and increasingly erratic, while for large angles it becomes sharp and violent. This can be explained by the change in the chip-tool contact pressure, friction and temperature. During this work, best results were obtained when $\beta = 40$ to 50 degrees.

It is essential that the chip-breaker wedge does rest firmly on the cutting face of the tool. Otherwise the sharp edge of the chip might get caught in between the tool face and the chip-breaker which could lead to overcrowding of the chips which will eventually lead to the breakage of the chip-breaker (Fig. 40). (74)

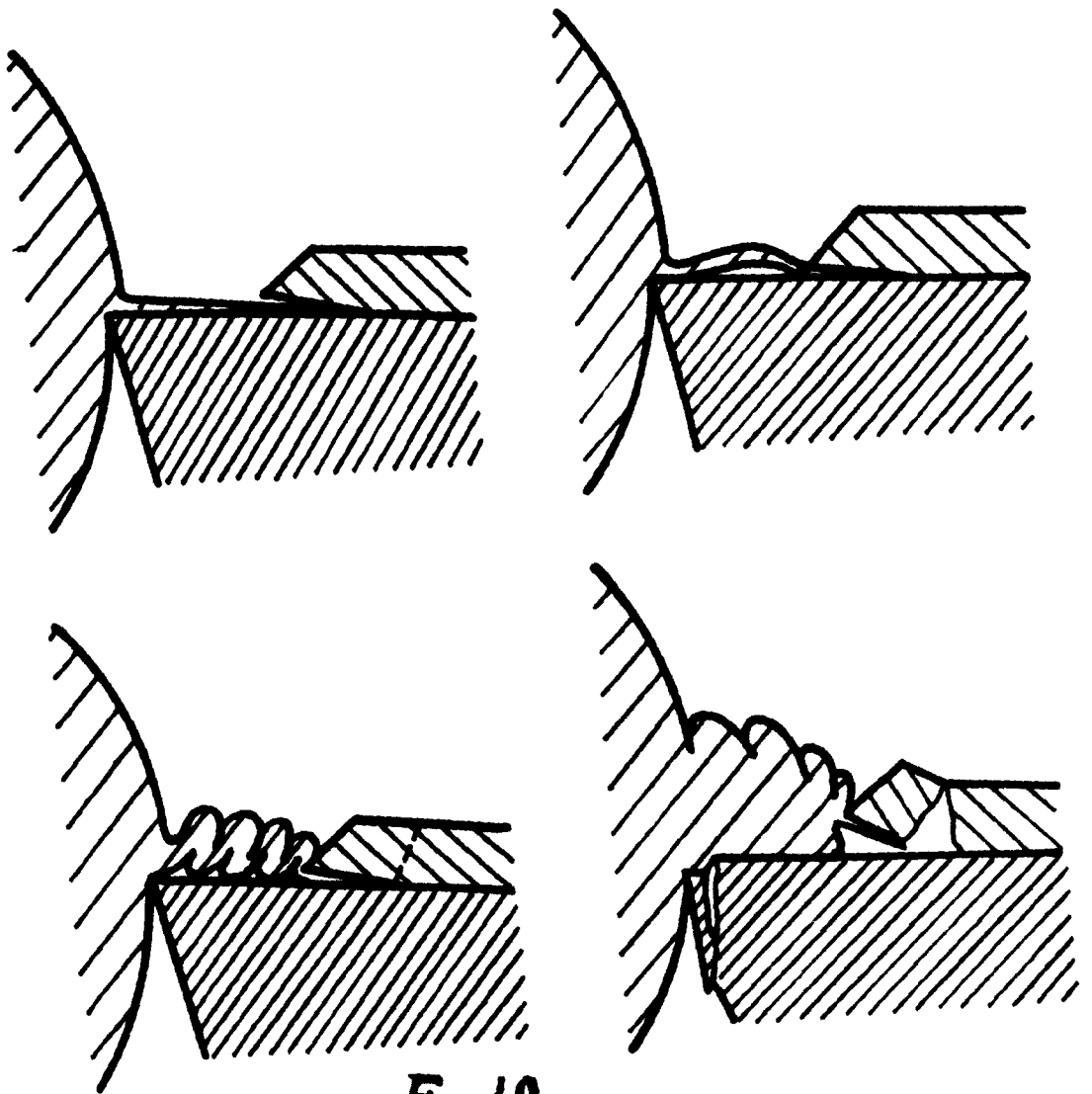


FIG. 40

3. Special Chip-Breakers:

Chip-breakers of special geometries are used in those cases where the conventional chip-breakers are not effective. Chip-breakers shown in Fig. 41a gives a satisfactory chip breaking with hard steels. A negative land of 0.2 to 0.3 mm on the cutting edge of the tool is used to break the chip. For ductile materials chip-breakers shown in Fig. 41 b-c produce a reliable chip breaking for a fairly wide range of cutting conditions. Special deflectors such as shown in Fig. 41d provide a satisfactory chip control. (69)

3.5 CHIP-BREAKER GEOMETRY

Here attention is restricted to chip breaking devices consisting of an obstruction located on the cutting face of the tool so that to produce plastic deflection of the chip into a coil of the desired radius. Theoretically this radius is found as follows:

(a) For step chip-breaker: From the geometrical relationship

$(R - H)^2 + L^2 = R^2$ Fig. 37, it is seen that:

$$R = \frac{1}{2} \left(\frac{L^2}{H} + H \right) \quad (3.1)$$

where

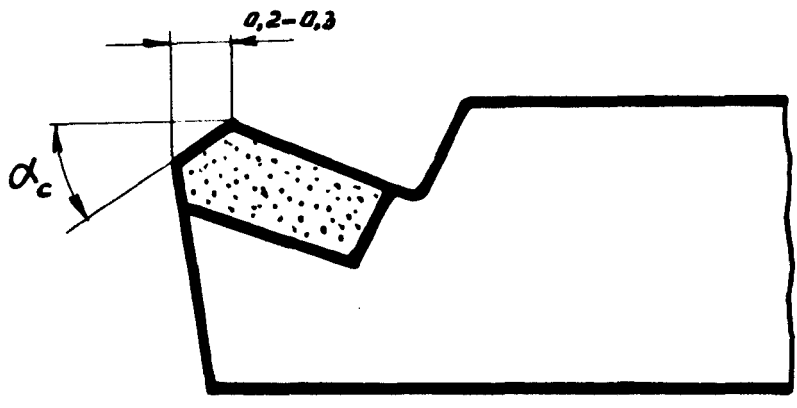
R = theoretical bending radius of the chip

L = chip-breaker width

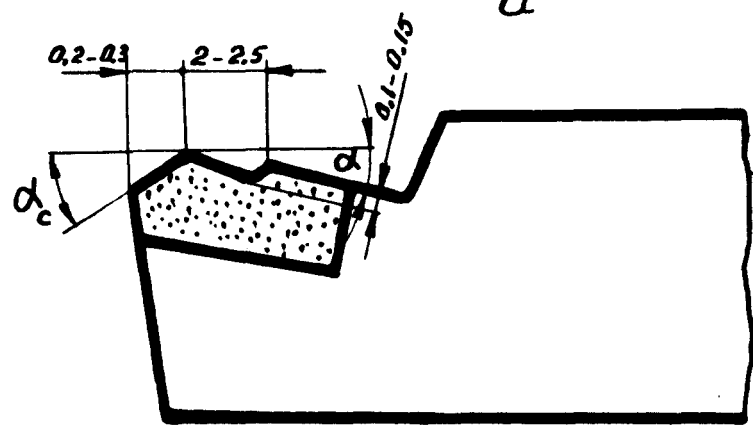
H = chip-breaker height

This formula has previously been obtained by Henriksen (71) from purely mathematical considerations. The actual bending radius of the chip is affected not only by the tool geometry but also by the cutting condition (mainly the feed) and the cutting material. The bending radius of the chip will be thoroughly investigated later in this chapter.

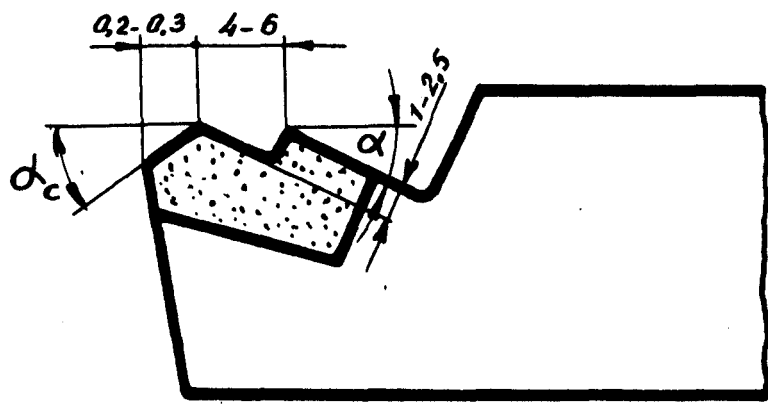
(b) For clamped chip-breaker: By assuming that the inclined face of the chip-breaker wedge is long enough to ensure that the chip becomes tangential to it at some point B .



a

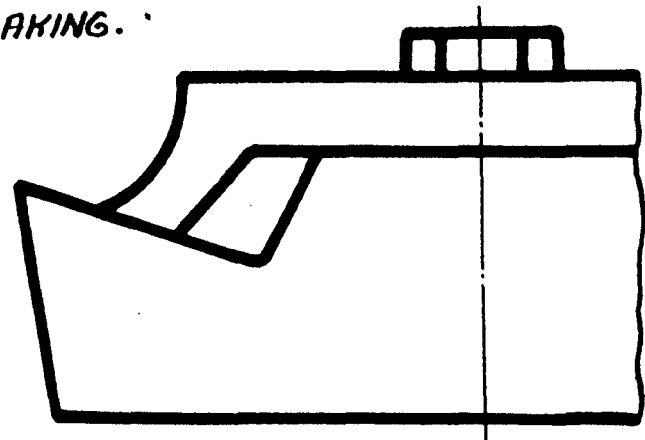


b



c

ALL DIMENSIONS IN MM
 α_c - EFFECTIVE RAKE
 ANGLE FOR CHIP
 BREAKING.



d

FIG.41

Fig. 38, and as angles AOC and BAC are equal to $\frac{1}{2}\beta$, we have

$$\frac{R}{W} = \frac{L}{H} = \cot \frac{1}{2}\beta \quad (3.2)$$

where,

R = bending radius of the chip

W = width of the chip-breaker wedge

L = distance from the contact point of the chip with the chip-breaker to the cutting edge

H = Height of the point of the contact of the chip with the chip-breaker

β = angle of the inclination of the chip-breaker wedge

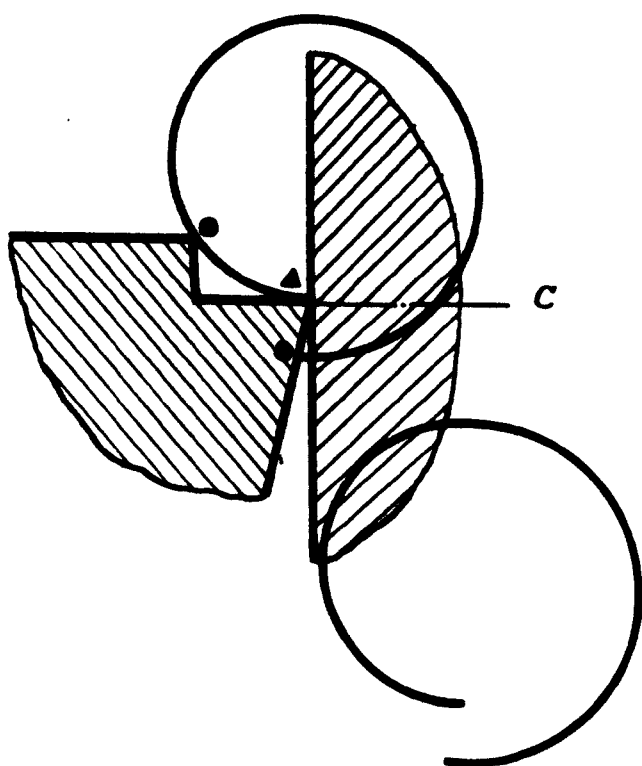
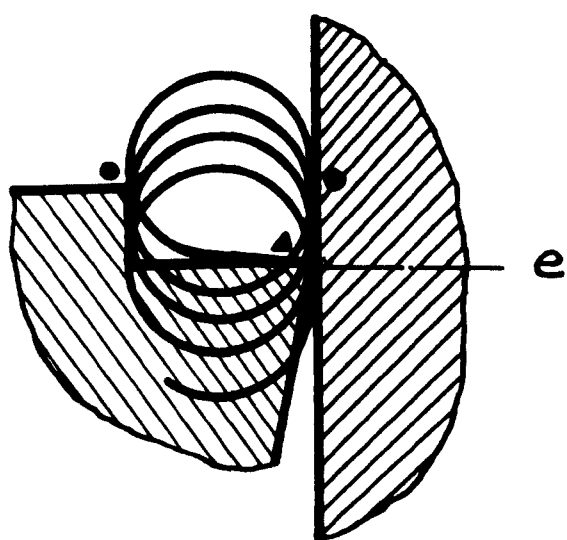
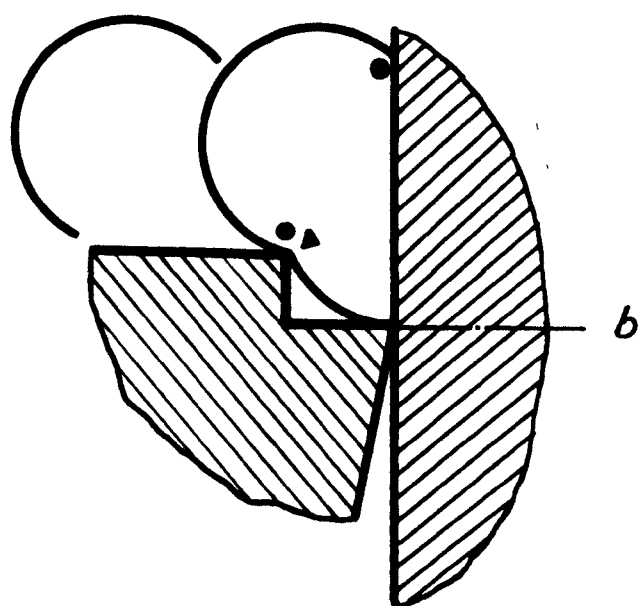
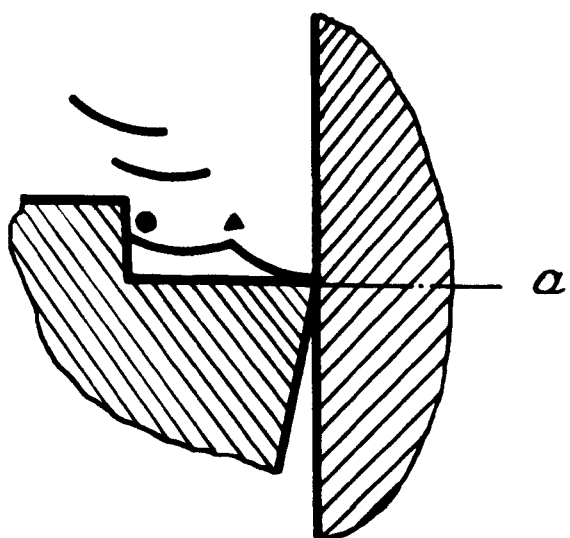
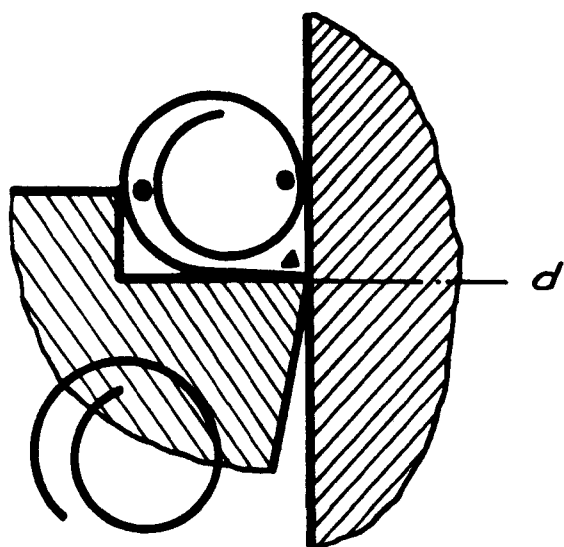
3.6 BREAKING OF THE CHIP

One of the simplest and reliable methods of chip breaking are those based on changes in the cutting conditions. Although reliable chip breaking can be obtained by simply changing the cutting conditions, such as increasing the feed, depth of cut, or reducing the rake angle, the tool life will be reduced considerably by these extreme cutting conditions (17, 71, 72, 95).

The methods of widest practical interest are those based on the use of chip-breakers to accentuate the curl of the chip as it is formed. The principal types of these chip-breakers have been already discussed earlier in this chapter. By suggesting that the chip breaking effectiveness, depends on the chip curl radius, it is found that under any given operating conditions, a certain radius of the chip curl is needed for effective chip breaking. The curled chip has a rough outer surface containing many cracks. The underside of the chip is smooth and strong under tension. Curling of the chip merely puts the rough outer side under compression, and unless the

curling is very severe, the chip will not break at this stage. To break the chip it has to be bent so as to put the rough side of the chip under tension. This is done by straightening the chip, so as to give a fracture starting from the rough surface of the chip coil. Particular ways of straightening the curled chip are:

1. The chip coil tends to straighten as its end comes in contact with the chip-breaker wedge. Fracture occurs at some point not far from the chip-breaker wedge, Fig. 42a. The chips may consist of small straight pieces or chips with a slight curvature.
2. The chip coil tends to open as its end strikes some obstacle such as the work-piece or the tool box, giving a bending action at the end still in contact with the tool, resulting in fracture at this point (Fig. 42 c - d). The chips may consist of half-turns or possibly one or more turns.
3. The chip coil opens as its end strikes the work-piece giving a bending action in the direction of easy chip breaking at the contact point of the chip with the chip-breaker wedge, Fig. 42b. As a result fracture occurs at that point. The chips consist of half-turns or full-turns.
4. The chip is coiled on itself, as, for example, in the chip formed by a parting tool. As the outer layers of the chip coil are forced open by the inner layers, breakage occurs, after a certain number of turns have been coiled.



● POINT OF CHIP CONTACT
 ▲ POINT OF CHIP BREAKING

FIG. 42

5. When the free end of a helical chip is restrained from rotating as it comes in contact with an obstacle, bending is induced near the cutting edge in the direction of easy breaking. For example, in a chip-breaker drill, a close coiled helix is formed, which then impinges on the side of the hole.
6. In turning, a close-coiled helix may be formed, which has a fairly high weight per unit length compared with the straight chip, Fig. 42e. Whirling of the free end due to rotation of the helix gives the bending action near the tool necessary for breaking the chip.

Interrupted feed devices and vibratory cutting methods have proved effective and reliable to give broken chips for a wide range of cutting conditions. Various types of chip-breakers such as deflectors, rollers and other special devices will be described later in this chapter. The use of the coolant is often found to promote effective chip breaking.

3.7 GENERAL VIEWS OF THE CHIP BREAKING METHODS

Progress in machine design has accentuated the need for co-operation and mutual understanding between tool makers and machine designers. It is essential that the cutting tools should be designed so that to give a satisfactory chip breaking with a comparatively high tool life.

Although chip breaking has several advantages (as mentioned before), their use is strictly limited due to the increased tool wear caused by the incorrect method of chip breaking. As mentioned earlier, chip breaking based on changes in the cutting conditions reduce the tool life, and their use is strictly limited to rough cutting operations. The chip breaking process is significantly

affected by the feed. For tools without chip-breakers a fine feed produces a thin stringy chip (called snarling chip) with no tendency to break. This type of chip is so flexible that it can wrap itself around the work-piece, the tool, or any other obstacle on its way. As the feed is increased the chip becomes more rigid and travels in almost straight lines. At very high feeds the chip may sometimes show a tendency to break in roughly regular manner, thereby imposing a violent variation in the pressure on the tool which leads to an increased tool wear. The effect of variation in the rake angle is so small that it can be ignored as long as the rake angle remains within the conventional limits, as was noticed during this work.

It is observed^(71, 95) during cutting that a chip passing over a straight cutting edge has a natural tendency to flow in a direction perpendicular to the cutting edge. With a large depth of cut the effect of the side cutting edge is significant⁽⁷¹⁾, and the chip flows almost perpendicular to the side cutting edge, Fig. 43a. With a small depth of cut the effect of the side cutting edge is considerably reduced and the effect of the nose and the end cutting edge is strong enough to swing the chip away from the surface of the work⁽⁷¹⁾, Fig. 43b. Sinapalnikov and Eikhmans⁽⁷⁹⁾ have found that the cutting edge radius has a considerable effect on the chip breaking process (through its effect on the cutting forces) when the chip thickness is small. (This is equivalent to bluntness of the tool). Albright⁽²⁸⁾ has found a similar effect of the cutting edge radius on the cutting process.

Tests⁽¹⁷⁾ on carbon steel 45 (0.45% C) using carbide tipped tools (T5K12) having a 10° rake angle, 8° clearance, 10° plan approach

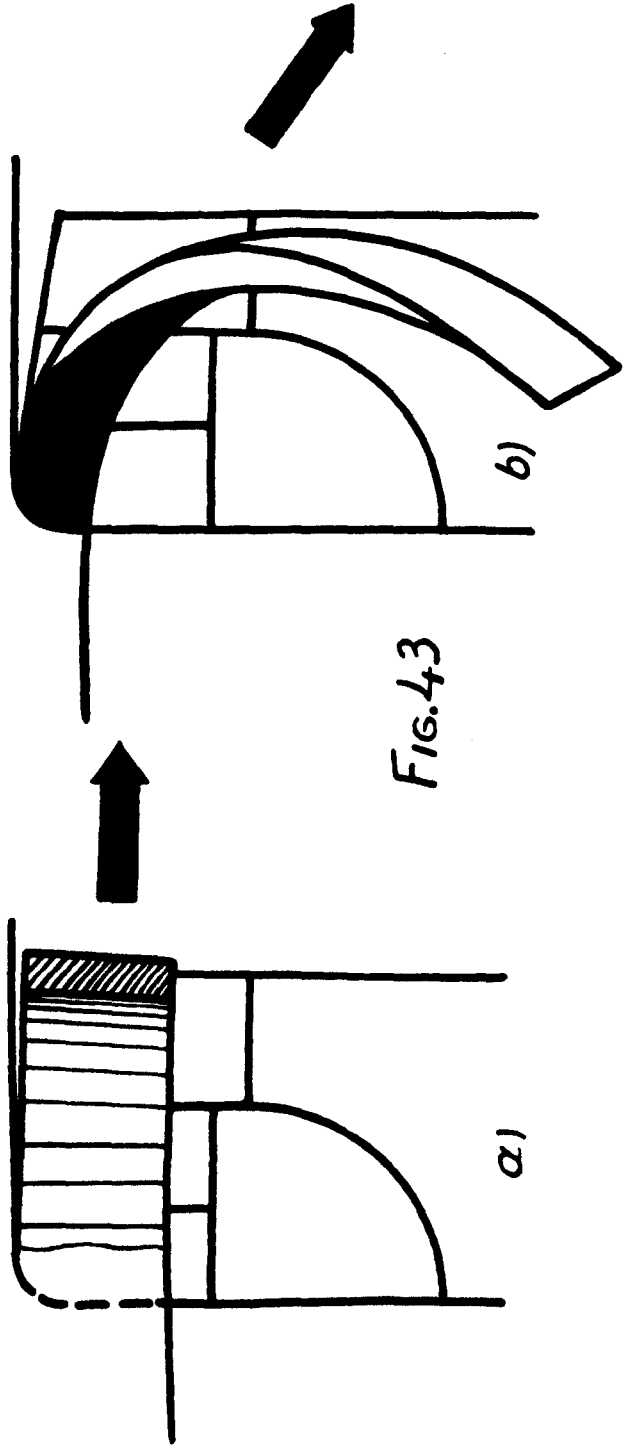


FIG. 43

at a speed of 43-45 m/min. and a feed rate of 0.07 mm/rev. have shown an increase of 20 to 40% in the cutting forces as the tool nose radius was increased from 12 to 22 mm.

Recently a great deal of research has gone into establishing the performance of the mechanical chip-breakers. Henriksen⁽⁷¹⁾ has found that for each cutting material there is a limited range of feed at which the chip-breaker gives a reliable chip breaking effect. For feeds below this range the chip-breaker is not effective, while for feeds above this range the chips are over-broken and extremely small in size. Although the over-broken chips are preferred from swarf-removal point of view, the tool wear at high feeds is considerably increased⁽⁷¹⁾. Free machining steels have been found to permit a wide range of feeds⁽⁷¹⁾.

Chip-breaker performance is also affected by the depth of cut, the side cutting edge angle and the cutting speed⁽⁸⁰⁾. An increase in the side cutting edge angle or the cutting speed will decrease the chip thickness. Decrease in the depth of cut influences the direction of the chip flow, thus changing the angle of the chip contact with the chip-breaker which leads to an increase in the effective radius of the chip curl.

Nakayama⁽⁸⁰⁾ has found that effective chip breaking performance of the step type chip-breakers depends on the chip curl radius, the work-piece material and the chip thickness. The effect of the depth of cut was found to be significant at low cutting speeds.

To ensure a reliable chip breaking Lutov⁽⁸¹⁾ has found that the main dimensions of the chip-breaker groove should be as follows:

1. The land width (distance "a" Fig. 44) \leq (0.5 to 0.7) times the chip thickness or \leq (0.25 to 0.35) times the contact length.

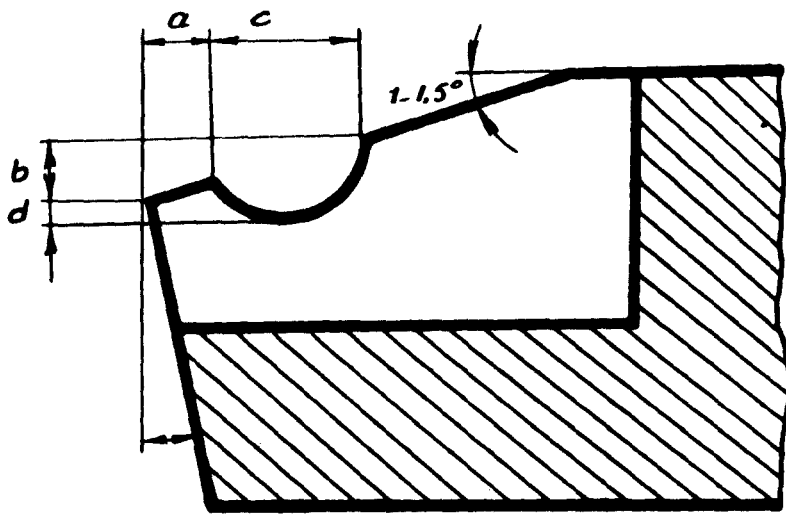


FIG. 44

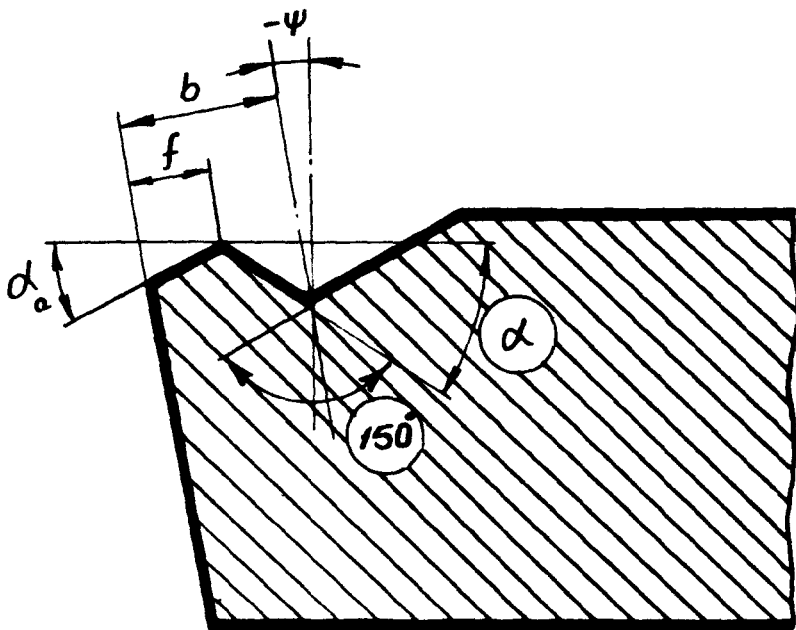


FIG. 45_a

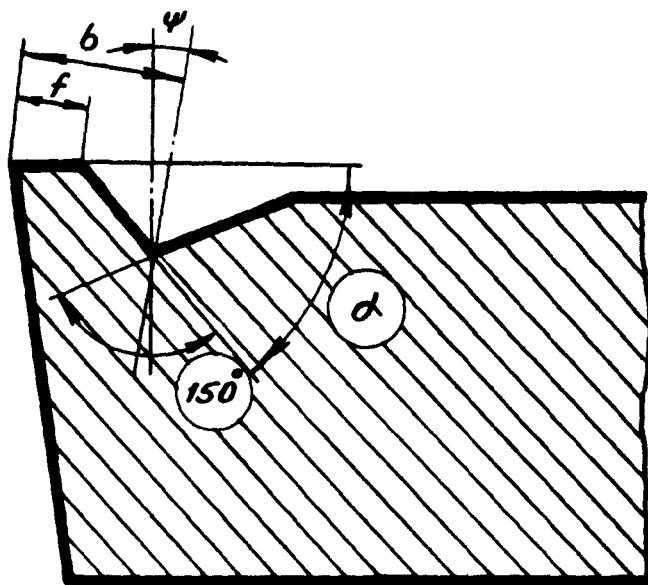


FIG. 45_b

2. The groove radius within 0.5 to 4.0 mm when the land width is within (0.05 - 0.10 to 0.5 - 0.8)mm.
3. The groove depth within 0.1 to 0.2 mm.

As a result of investigation Kabanov⁽⁸²⁾ has recommended the following dimensions of the chip-breaker groove to be the best from the chip breaking point of view, Fig. 44.

Cutting Material		Groove Dimensions			
Steel		a	b	c	d
Tensile Strength	Hardness				
kg/mm ²	HB	mm	mm	mm	mm
34 and 38	137 and 143	0.1 - 0.15	1.0	7	1.5
42 and 54	170 and 787	0.2 - 0.3	0.8	6	1.0
58 and 61	187 and 197	0.4 - 0.5	0.4	5	0.8
63	207	0.5 - 0.6	0.2	3-4	0.5

Using tools with a shallow chip-breaker groove Igoshim⁽⁸³⁾ has established conditions at which effective control of the chip breaking process was obtained. Experimental tests⁽⁸³⁾ on soft steels using a shallow chip-breaker groove-type tool (at a cutting speed of 70 to 150 m/min., depth of cut of 0.35 to 1.2 mm and feed rate of 0.5 to 1.1 mm/rev.) have shown that the best chip breaking result is obtained when:

1. The chip-breaker land width = (feed + 0.2) mm for feed range within 0.13 to 0.9 mm/rev.
2. The depth of the groove = 0.2 to 0.3 mm.
3. The width of the groove = 1.2 to 2.0 mm and the groove radius = 1.5 to 2.0 mm.

It was observed⁽⁸³⁾ during cutting with tools having a shallow chip breaking groove that the chip deforms immediately and starts to fracture in the groove, finally breaking as soon as it contacts an obstacle.

Vee type⁽⁸⁴⁾ chip-breakers, Fig. 45, were satisfactorily used to curl the chip. Using tools with Vee type chip-breaker Proskuryakov⁽⁸⁴⁾ has found that best chip control is achieved with tools having the following dimensions:

1. The Vee angle = 150° .
2. The angle of the groove centre axis should be for tensile strength,

$$\sigma_t \leq 60 \frac{\text{KG}}{\text{mm}^2}, \psi = \alpha_a = 0^\circ$$

$$\sigma_t \geq 60 \frac{\text{KG}}{\text{mm}^2}, \psi = \alpha_a = 5^\circ$$

3. For tools cutting at constant feeds and speeds, dimensions (f) and (b) should preferably be proportional to the actual chip thickness (t_1)

$$b = (2 \text{ to } 3) t_1 \text{ and } f = 0.5 t_1$$

It is essential to mention that determination of the tool dimensions in terms of chip thickness is not desirable due to the difficulties in finding the correct chip thickness.

Bazhenov⁽⁸⁵⁾ has found an increase of about 35 to 60% in the cutting forces as the depth of the groove is increased. The following relations were established:

$$\frac{h}{R} \left(\frac{\text{groove depth}}{\text{groove radius}} \right) = \frac{1}{2} \text{ to } 2; \quad \frac{R}{S} \left(\frac{\text{feed}}{\text{depth of cut}} \right) = 10 \text{ and } \frac{R}{t} \left(\frac{\text{depth of cut}}{\text{depth of cut}} \right) = \frac{1}{3}$$

Good chip control was obtained by means of carb-o-lock inserts (inserts with a negative rake land backed up by a high positive rake), within the feed range of about 0.007 in. per rev. up to 0.020 in. per rev. Crowding and corrugating which were resulting in excess heating of the insert, reducing therefore the cutting edge hardness which leads to a reduction in the tool life, were observed at feeds above 0.02 in. per rev.

It has been established⁽⁸⁶⁾ that the chip breaking methods based on the use of fine chip breaking grooves is one of the most effective and economical means of chip control.

A step on the cutting face of tool has the same effect on the chip breaking control as the groove. Special geometry⁽⁸⁷⁾ of the step has shown an increase of about 20 to 30% in the tool life with a satisfactory chip control. During this work best chip breaking was obtained when the height of the chip-breaker was within 0.15 up to 2 mm and the chip-breaker distance (distance from the cutting edge to the step) was within 0.2 up to 3 mm.

The significance of a clamped chip-breaker is that the position of the chip-breaker block can be adjusted so that it will give a satisfactory chip breaking over a wide range of cutting conditions.

The angle of the inclination of the chip-breaker face (wedge angle) is found to be one of the main parameters controlling the chip breaking process. Best chip breaking results were obtained with a wedge angle within 40° to 50°⁽⁹⁵⁾.

A special deflector⁽⁸⁶⁾ type of clamped chipbreaker (Fig. 46) with a groove-type tool was successfully used by Proskuryakov to control the chip breaking process when large steel pipes (up to 1 m in diameter) were machined. Best chip breaking results were obtained when $B = 5$ to 6 mm and $H = 10$ mm for machining steel pipes with a diameter of 700 to 820 mm at a cutting speed of 132.5 to 151.5 m/min., a feed rate of 0.8 to 1.1 mm/rev. and depth of cut of 8 to 12 mm using the following dimensions of the groove:

The groove radius = 3.5 to 4.0 mm

The groove depth = 0.9 to 1.2 mm

The chipbreaker distance = 0.9 to 1.2 mm

Although this device is claimed to work satisfactorily for a wide range of cutting conditions, the hand feeding used with this device suggests that the chip breaking might be affected by the variability of the feed.

Ioffe⁽⁸⁹⁾ has designed a special device for breaking the chip. It consists of a roller clamped to the cutting face of the tool tip. Under the action of the chip pressure, the roller rotates and forces the chip to bend. Finally the chip breaks as it comes in contact with the unmachined part of the work-piece. Although this device is very simple and gives a satisfactory chip breaking for a wide range of cutting conditions, the roller must be mounted on the tool tip with a considerable care to obtain efficient performance. This device has been modified by Kondratov⁽⁹⁰⁾ and Kiseler⁽⁹¹⁾ so that to ensure a good reliability and to eliminate the possibility of the chip passing between the roller and the work-piece. This was done by using a highly polished roller with a close setting to the cutting edge.

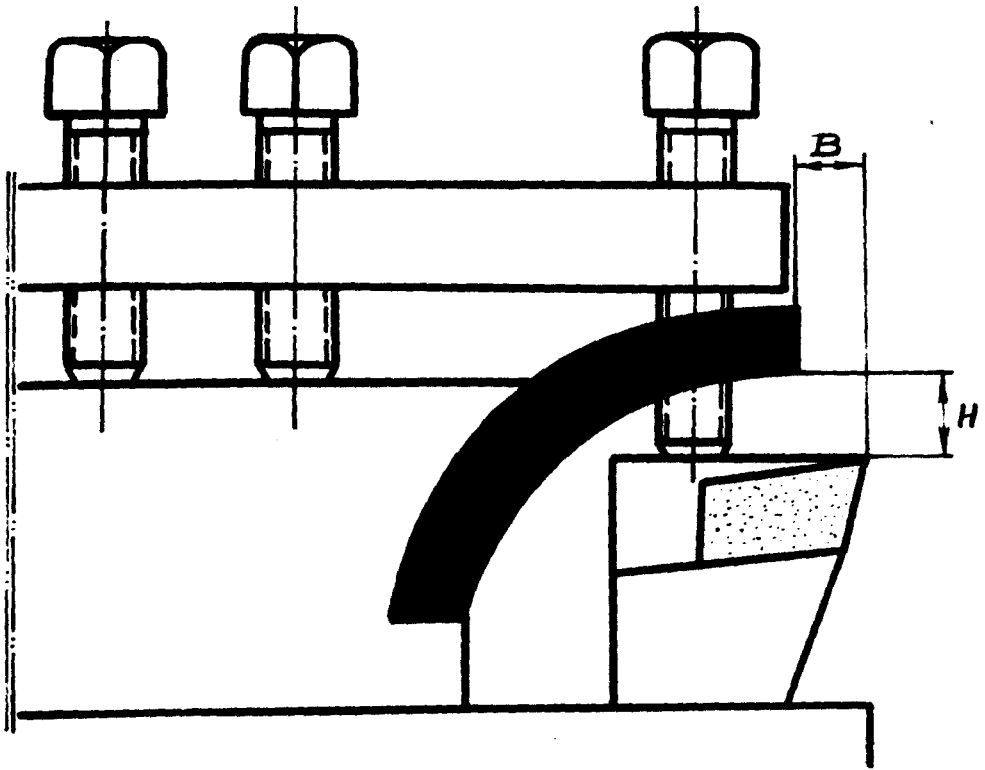


FIG. 46

Pologov⁽⁹²⁾ has designed a universal clamped chip-breaker with automatic self adjustable step working on the principle of balancing between the chip breaking force and the applied spring force (Fig. 47).

Tests have shown that the chip-breaker with automatic setting of the chip-breaker step operates successfully within the range of cutting conditions commonly used for carbide and ceramic tools.⁽⁹²⁾ It has been established that the distance between the step and the cutting edge changes in direct proportion to the depth of cut (similarly the feed) and in inverse proportion to the cutting speed. The main danger with this design is that the sharp edge of the chip can get caught between the tool face and the chip-breaker which will lead to the breakage of the chip-breaker.

Interrupted feed devices and vibratory methods were claimed^(93, 94, 97, 98) to provide a reliable chip breaking within a wide range of cutting conditions. (Interrupted feed devices and vibratory methods will be discussed in detail later in this chapter).

Tests⁽⁹⁵⁾ at high cutting speeds within 200 to 400 f/min. as well as at low cutting speeds have shown that the distance from the cutting edge to the chip-breaker wall and the angle of the inclination of the chip-breaker wall for clamped chip-breaker, the height of the step and the distance of it from the cutting edge for step type chip-breaker and the radius of the groove, the depth of it and the width of the chip-breaker land are the most significant parameters controlling the chip breaking process.

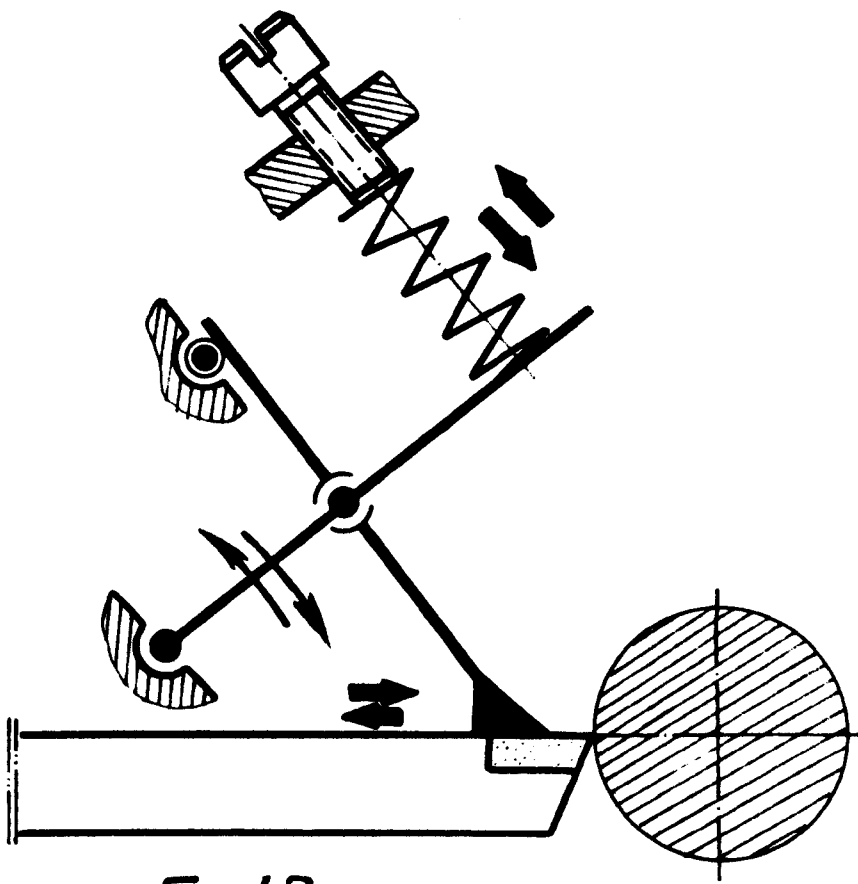


FIG. 47

3.8 EFFECT OF COOLANT ON CHIP BREAKING

The use of coolant in cutting operations is considered to be significant in promoting effective chip breaking.

It is important to mention that lubrication is essential to avoid over crowding and corrugation of the chips at the chip-breaker when the chip-breaker width is small⁽⁹⁵⁾.

The effect of the coolant on the chip-breaker performance has been widely investigated by Bazhenov⁽⁸⁵⁾. Coolant was found to have a slight effect on the chip size. However, effective lubricant reduces the chip size⁽⁸⁵⁾. The significance of the coolant in promoting good chip breaking can be explained by the fact that quenching of the chip will help in developing fracture.

It is also significant to mention that using a strong jet of coolant will prevent the chips from flying, therefore reducing hazards to the operator. Coolant is also used to direct the chips towards the swarf removal units.

3.9 THE EFFECT OF THE GRINDING ON CHIP BREAKING

The chip breaking effectiveness is significantly affected by the grinding finish of the contact surfaces of the tool and chip-breaker. For accurately polished tool and chip-breaker faces the chip flow is conditioned by the chip-breakers geometry. As the tool starts to wear off the chip flow control becomes mainly dependent on the roughness of the cutting face of the tool. Opitz⁽⁹⁾ has shown that as the depth of the crater formed on the cutting face of the tool is increased, the radius of the chip curl drops, and the tendency towards producing small chips increases. However, excessively small radius of the chip curl will obstruct the chip flow and lead to a considerable increase in the cutting forces^(9, 17, 71, 95, 101).

Kozacka⁽⁹⁶⁾ has found that the chip breaking process is affected by the direction of the grinding marks on the chip-breaker's face, which leads to a change in the cutting forces. If the grinding marks are parallel to the side cutting edge (i.e. if the chip slides perpendicular to the marks), then the cutting forces produced are less than if the marks are at right angles to the cutting edge (i.e. if the chip slides along the grooves left by the grinding wheel). However, this effect disappears if the marks are shallow. For best chip-breaker performance Kozacka⁽⁹⁶⁾ suggests the lapping of the carbide tool tips.

3.10 CHIP BREAKING BY MEANS OF INTERRUPTED FEED DEVICES AND VIBRATORY METHODS

Recently the use of interrupted feed devices for different cutting operations have shown a satisfactory chip breaking performance. In these devices the breakage of the chip is achieved by a periodical change in the chip thickness, due to the discontinuity of the cutting cycle. Interrupted feed is applied either by electrical or mechanical vibration of the cutting tools. The chip breaking effectiveness of these devices depends mainly on the direction, amplitude and frequency of the applied vibration. For effective chip breaking the following requirements must be satisfied.

1. The direction of the vibration should coincide with the direction of the feed.
2. The amplitude of the vibration must be made as high as possible.
3. The frequency of the vibration should be between 5 and 120 cycles per second.

The reasons why interrupted feed devices are widely used in metal cutting operations are based on the following advantages:

1. Interrupted feed devices can be applied to different cutting operations such as turning, boring, milling, etc.
2. The tool life obtained from these devices is longer than those obtained from a conventional chip-breaker.
3. Interrupted feed devices ensure a reliable chip breaking for a wide range of materials (including hard materials) and cutting conditions.
4. Tool vibration enables the coolant to distribute and penetrate more effectively.

Reduced efficiency of the machine tool as a result of increased machining time caused by interrupting the feed, is the main drawback of interrupted feed devices. However, this could be improved by using high cutting speeds and feeds. It is also significant to mention that interrupted feed devices are complex and expensive to install, and that some of these devices produce a poor quality of the surface finish.

The vibratory turning⁽⁹³⁾ of the highly ductile metals with tool vibration of low frequency up to 5 cycles per second and high amplitude of about 1.5 mm ensure reliable chip breaking within a wide range of cutting conditions. Chip breaking based on this method⁽⁹³⁾ has shown an increase of 50% in the tool life, a reduction of up to 65% in the consumed power and a satisfactory surface finish.

Chip breaking methods based on self-exciting vibrations⁽⁹⁴⁾ induced by the cutting process is highly reliable. It is suitable for use in mass-production conditions when machining components with a uniform machining allowance and with metals which ensure the possibility of inducing self-excited vibrations.

Zakharov⁽⁹⁷⁾ describes a hydraulic interrupted feed device, whereby the tool is given an interrupted movement by means of an auxiliary hydraulic system. He found that the chip length can be accurately predicted and depends mainly on the diameter of the work-piece. Zakharov suggests a combination of interrupted feed device and conventional chipbreaker, for effective chip breaking when work-piece of large diameters (50 mm) are machined.

Several interrupted feed devices are also described by Koponov⁽⁹⁸⁾; Baranov⁽⁹³⁾, Schnellmann⁽⁹⁹⁾, Podugaev⁽⁹⁴⁾, Weill⁽¹⁰⁰⁾, and others.

3.11 CHIP CURL RADIUS

Chip curl radius is one of the most significant parameters determining good machinability characteristics, due to the fact that the chip-tool contact is controlled by the chip curl radius. It is also significant as it was suggested earlier in this chapter that the chip curl radius represents the effectiveness of the chip breaking process.

The chip curling mechanism has been investigated in detail by Ernst and Merchant⁽¹⁴⁾, Albricht⁽²⁸⁾, Okoshima, Hoshi and Fujinawa⁽¹⁰¹⁾, Henriksen⁽⁷¹⁾, Nakayama⁽⁸⁰⁾, Ponkeshe⁽¹⁰²⁾, Lamm⁽¹⁰³⁾, Cook, Jhaveri and Nayak⁽¹⁰⁴⁾, Dawe and Rubenstein⁽¹⁰⁵⁾ and many others. As a result of these investigations, different suggestions were made to explain why the chip curls. Ernst and Merchant⁽¹⁴⁾ were first to suggest that the chip curling is a result of greater extension in the underside of the chip compared with the upper side as a result of variation in the rate of deformation across the shear plane. Henriksen⁽¹⁷⁾ by considering the chip as a cantilever beam under the action of the chip-tool contact pressure, suggests that the chip bends as a result

of non-uniformity of the chip-tool contact pressure. Albricht⁽²⁸⁾ suggested that the chip curls as a result of non-collinearity between the lines of action of the resultant cutting force acting on the work-piece and the cutting tool, which leads to the appearance of a bending moment which forces the chip to curl. Similar suggestion was made⁽¹⁰³⁾ by taking into consideration the thermal strains produced in the chip during cooling. Ponkshe⁽¹⁰²⁾ suggests that non-uniformity of the shear zone width, leads to a different degree of strain hardening across the chip width. Since the chip is unstressed after it leaves the cutting face of the tool, there must be a stress-relieving zone adjacent to the shear zone, resulting in non-uniform residual shear strain across the width of the chip and hence rotation. Cook, Jhaveri and Nayak⁽¹⁰⁴⁾ have found that when materials which do not strain-harden (such as lead) were cut at low cutting speeds and at room temperature the chips do not curl, while the chips curl when strain-hardening materials (such as steel, aluminium, copper) were cut under the same identical conditions. From this they concluded that the chip curls due mainly to the strain-hardening. They also concluded that the chip breakage is strongly dependent upon the natural curling tendencies of a material, which vary from one material to another. Conclusions similar to those of Albricht were arrived at by Dawe and Rubestein⁽¹⁰⁵⁾. They suggested that the phenomenon of chip curl can be attributed, basically to non-collinearity of the resultant cutting force acting on the work-piece and the resultant cutting force acting on the chip. All these suggestions are based on experimental evidence and therefore they are equally plausible. However, some of these suggestions are in better agreement with theoretical explanations of the nature of the chip curvature than the others.

All these suggestions which were made are to explain the chip curling mechanism without the use of a chipbreaker. However, the situation is changed when chipbreakers are used and the chip curl radius will mainly depend on the geometry of the chipbreaker. It is significant to mention that these effects which were suggested earlier still exist and will have a secondary effect.

The theoretical chip curl radius was first determined by Henriksen from purely geometrical considerations. From the geometrical relationships between the chipbreaker's width and height and the chip curl radius, Henriksen has developed the formula described earlier in this chapter for determining the theoretical chip curl radius. However, this formula does not take into consideration the effect of the cutting conditions on the chip curl radius. By taking into consideration the effect of cutting conditions, tool characteristics and cutting material, Okushima⁽¹⁰¹⁾ has analysed the mechanism of chip curling and found a theoretical expression for the chip curl radius in terms of the above mentioned factors. The writer considers that the theoretical analysis of chip curling mechanism suggested by Okushima is fairly representative if the effect of the chip-tool contact on the chip curl radius has also been taken into consideration. Therefore, it was decided to show in detail the theoretical analysis of chip curling mechanism originated by Okushima by taking into consideration the fact that the chip starts curling away from the face of the tool as soon as it reaches the end of the chip-tool contact region. This means that the effective chipbreaker width must be taken as the distance from the end point of the chip-tool contact to the chipbreaker heel (i.e. distance L-f, Fig. 48), instead of the whole chipbreaker width (i.e. the distance from the cutting edge to the chipbreaker heel, L, Fig. 48).

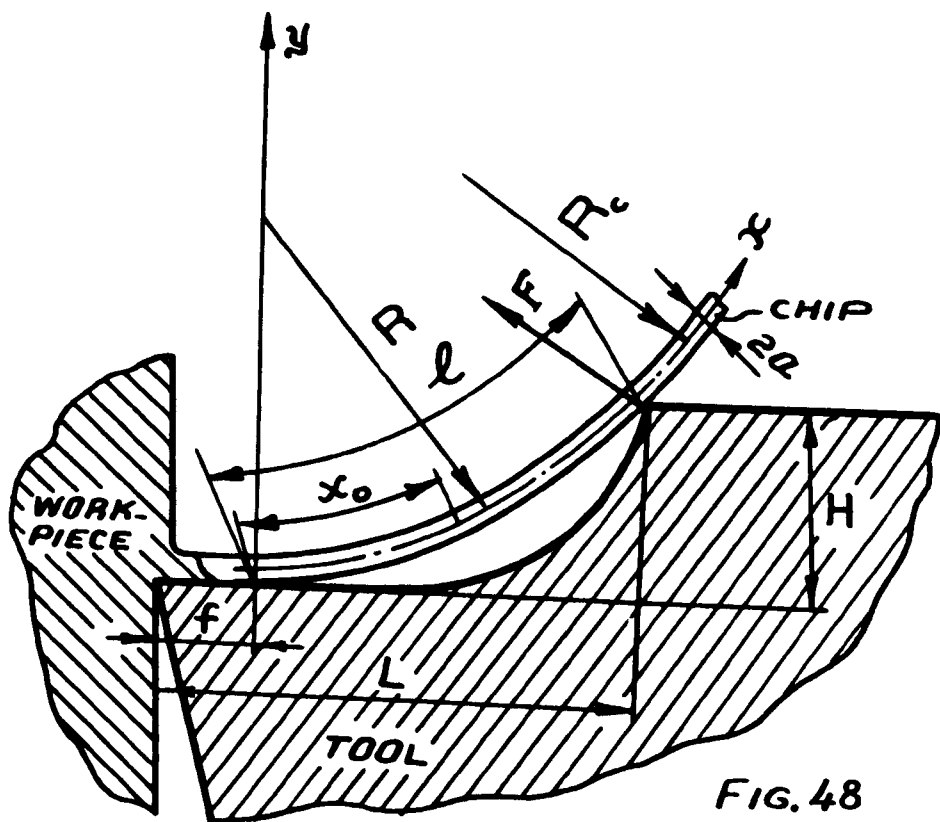


FIG. 48

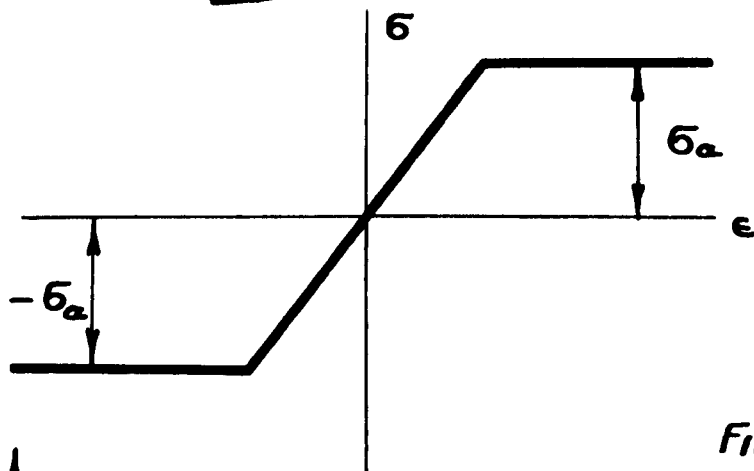


FIG. 49

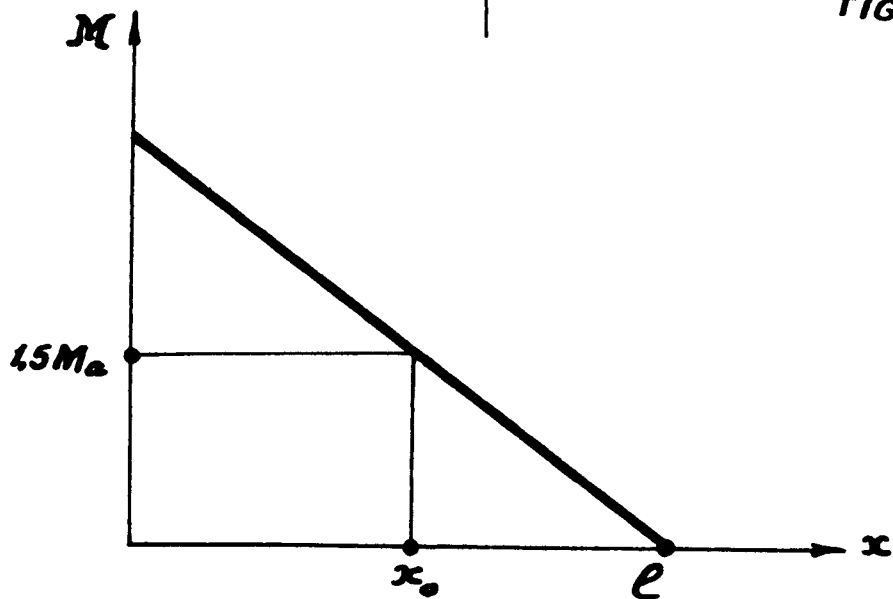


FIG. 50

NOMENCLATURE

- L = chipbreaker width, Fig. 48
distance from the cutting edge
to the heel of the chipbreaker
measured parallel to tool rake
face
- f = chip-tool contact length,
Fig. 48
- F = bending force exerted by the heel
of the chipbreaker on the chip
- M = bending moment
- σ = normal stress
- a & $-a$ = upper and lower half of the
chip thickness
- b = width of the chip
- y' = height of an element above the
centre-line of the chip
- σ_a = yield stress of the chip
- I = moment of inertia of chip cross
section
- M_a = bending moment caused by the
bending force exerted by the
chipbreaker when the stress on
the chip surface reaches yielding
point.
- V_c = chip velocity
- x = chip direction co-ordinate
- y = Vertical co-ordinate
- t_c = chip thickness
- K = constants for a given
material
- x_o = the length over which the
final plastic deformation
of the chip is obtained.
- $M_p = 1.5 M_a$
- R = radius of the centre-line
of the chip.
- t = time
- c = constant
- l = chip length from the end
point of the chip-tool
contact to the chipbreaker
heel.
- E = modulus of elasticity of
the chip
- A_1 & B_1 = constants, see
equation (3.14)
- A_2 & B_2 = constants, see
equations (3.15)
- H = chipbreaker height
- R_c = natural radius of the chip
curvature bent by the chip-
breaker
- ϕ = shear angle
- α = rake angle
- s = feed
- C_1 & C_2 = constants depending on
the cutting material, tool,
geometry, chip thickness, and
cutting speed

The chip curl radius is calculated by applying the theory of plasticity under the following assumptions:

1. The material being cut has no work hardening, Fig. 49.
2. The chip flows straight along the cutting face of the tool for a tool without a chipbreaker.
3. The cross section of the chip which was plane before bending remains plane after bending, and the neutral layer is always at the middle of the chip thickness.
4. The heel of the chipbreaker exerts a bending force F on the chip, Fig. 48. The bending moment produced by this bending force is assumed to be linearly distributed along the chip length, Fig. 50.
5. By taking into consideration the time rate, and by considering the chip as a beam of rectangular section, the normal stress at any arbitrary point in a cross section and the bending moment at the same section can be represented by the following equation:

$$M = b \int_{-a}^a \sigma y' dy' \quad (3.3)$$

At yielding point, the bending moment is calculated from equation (3.3) by taking

$$\sigma = \sigma_a (y'/a) \quad (3.4)$$

$$M_a = b \int_{-a}^a \frac{\sigma_a}{a} y'^2 dy' = \frac{2}{3} \sigma_a b a^2 = \sigma_a I/a \quad (3.5)$$

When the whole cross section is under plastic deformation, the bending moment is:

$$M = \sigma_a \int_{-a}^a y' dy' = b \sigma_a a^2 = \frac{3}{2} \sigma_a I/a = 1.5 M_a \quad (3.6)$$

When the bending moment M is more than $1,5 M_a$, it is assumed that the bending deformation increases with the time. However, the duration of the time for the chip flowing at a constant velocity V_c under such a bending action is short. Therefore, the rate of the deformation is significant in this case. Since the bending moment along the chip length (l) is maximum at the end point of the chip-tool contact which is at a distance f from the cutting edge, the time rate of deformation will be maximum at the same point. As the chip leaves the end point of the chip-tool contact, the bending moment decreases, and therefore decreasing the rate of the deformation. The point $1,5 M_a$ corresponds to the end of plastic deformation. It means that the chip has had sufficient plastic deformation within $x = x_0$ and as the bending moment value drops below $1,5 M_a$ the chip will undergo no further plastic deformation. Therefore, as long as $M < 1,5 M_a$, i.e. $x > x_0$, the deformation of the chip conforms to the theory of elasticity.

Assuming that the time rate of the deformation is proportional to $M - 1,5 M_a$ as long as $M > 1,5 M_a$, and writing $1,5 M_a = M_p$, we have

$$\frac{d(1/R)}{dt} = C(M - M_p), \quad (0 < x < x_0) \quad (3.7)$$

From assumption (4)

$$M = \frac{l - x}{l - x_0} M_p \quad (3.8)$$

Hence,

$$\frac{d(1/R)}{dt} = C \left(\frac{l - x}{l - x_0} - 1 \right) M_p = C M_p \frac{x_0 - x}{l - x_0}, \quad (0 < x < x_0) \quad (3.9)$$

Since the chip flows perpendicular to the cutting edge,

$$V_c = dx/dt \quad (3.10)$$

Hence equation (3.9) becomes,

$$\frac{d(1/R)}{dx} = \frac{C M_p}{V_c} \left(\frac{x_0 - x}{1 - x_0} \right), \quad (0 < x < x_0) \quad (3.11)$$

Integrating equation (3.11) with $1/R = 0$ at $x = 0$,

$$\frac{1}{R} = \frac{C M_p}{V_c (1 - x_0)} \left(x_0 x - \frac{x^2}{2} \right), \quad (0 < x < x_0) \quad (3.12)$$

According to assumption (5) when $x > x_0$, the chip conforms to the theory of elasticity. As the bending moment decreases, the chip curvature reduces by an amount which at any distance x is equal to

$$\frac{M_p}{EI} \frac{x - x_0}{1 - x_0}$$

So curvature at points ($x > x_0$) is

$$\frac{1}{R} = \frac{C}{V_c} \frac{M_p}{1 - x_0} \frac{x_0^2}{2} - \frac{M_p}{EI} \frac{x - x_0}{1 - x_0}, \quad (x_0 < x < 1) \quad (3.13)$$

Now we have two equations (3.12) and (3.13) giving curvature $\frac{1}{R} = \frac{d^2y}{dx^2}$

By integrating equation (3.12) we have:

$$\frac{dy}{dx} = \frac{C M_p}{V_c (1 - x_0)} \left(x_0 \frac{x^2}{2} - \frac{x^3}{6} + A_1 \right) \quad)$$

$$y = \frac{C M_p}{V_c (1 - x_0)} \left(x_0 \frac{x^3}{6} - \frac{x^4}{24} + A_1 x + B_1 \right) \quad) \quad (0 < x < x_0) \quad (3.14)$$

By integrating equation (3.13) we have:

$$\frac{dy}{dx} = M_p \left[\frac{C}{V_c} \frac{x}{1-x_0} \frac{x_0^2}{2} - \frac{\frac{x^2}{2} - x_0 x}{EI(1-x_0)} + A_2 \right]$$

$$y = M_p \left[\frac{C}{V_c} \frac{x^2}{2} \frac{1}{1-x_0} \frac{x_0^2}{2} - \frac{\frac{x^3}{6} - x_0 \frac{x^2}{2}}{EI(1-x_0)} + A_2 x + B_2 \right] \quad (x_0 \leq x \leq 1) \quad (3.15)$$

From initial conditions $dy/dx = 0$ at $x = 0$, we get,

$$A_1 = B_1 = 0$$

Hence,

$$\left. \frac{dy}{dx} \right|_{x=x_0} = \frac{C M_p x_0^3}{3V_c(1-x_0)} \quad (3.16)$$

and

$$y \Big|_{x=x_0} = \frac{C M_p x_0^4}{8V_c(1-x_0)} \quad (3.17)$$

These expressions are used in (3.15) to determine constants A_2 and B_2

$$A_2 = -\frac{1}{6} \frac{C x_0^3}{V_c(1-x_0)} - \frac{x_0^2}{2EI(1-x_0)} \quad (3.18)$$

$$B_2 = \frac{1}{24} \frac{C x_0^4}{V_c(1-x_0)} + \frac{1}{6} \frac{x_0^3}{EI(1-x_0)} \quad (3.19)$$

Hence equation (3.15) becomes in general terms

$$y = M_p \left[\frac{C}{V_c(1-x_0)} \left\{ \frac{x_0^2 x^2}{4} - \frac{x_0^3 x}{6} + \frac{x_0^4}{24} \right\} + \frac{1}{EI(1-x_0)} \left\{ \frac{-x^3}{6} + \frac{x_0 x^2}{2} - \frac{x_0^2 x}{2} + \frac{x_0^3}{6} \right\} \right] \quad (3.20)$$

As the conditions for chip contact with the chipbreaker is $y = H$ at $x = 1$, we have

$$H = \frac{M_p C x_o^2}{V_c (1-x_o)} l^2 \left[\frac{1}{4} - \frac{1}{6} \left(\frac{x_o}{l}\right) + \frac{1}{24} \left(\frac{x_o}{l}\right)^2 \right] - \frac{M_p l^3}{EI(1-x_o)} \left[\frac{1}{6} - \frac{1}{2} \left(\frac{x_o}{l}\right) + \frac{1}{2} \left(\frac{x_o}{l}\right)^2 - \frac{1}{6} \left(\frac{x_o}{l}\right)^3 \right] \quad (3.21)$$

or

$$\frac{M_p C x_o^2}{V_c (1-x_o)} = \frac{24}{6 - 4\left(\frac{x_o}{l}\right) + \left(\frac{x_o}{l}\right)^2} \left[\frac{H}{l^2} - \frac{M_p}{6EI} \left(1 - \frac{x_o}{l}\right)^2 \right] \quad (3.22)$$

But as $M_p = 1,5 M_a$, hence equation (3.22) becomes:

$$\frac{M_p C x_o^2}{V_c (1-x_o)} = \frac{24}{6 - 4\left(\frac{x_o}{l}\right) + \left(\frac{x_o}{l}\right)^2} \left[\frac{H}{l^2} - \frac{M_a}{4EI} \left\{ \left(1 - 2\left(\frac{x_o}{l}\right) + \left(\frac{x_o}{l}\right)^2\right) \right\} \right] \quad (3.23)$$

From equation (3.23), (3.20), (3.13) and (3.5) when $x=1$ or $l = L-f$, the natural radius of the chip curvature R_c bent by the chipbreaker is,

$$\begin{aligned} \frac{1}{R_c} &= \frac{M_p C}{V_c} \frac{x_o^2}{2(1-x_o)} - \frac{M_p}{EI} \frac{1-x_o}{1-x_o} = \\ &= \frac{1}{6-4\left(\frac{x_o}{L-f}\right) + \left(\frac{x_o}{L-f}\right)^2} \left[12 \frac{H}{(L-f)^2} - \left\{ 12 - 12\left(\frac{x_o}{L-f}\right) + 4,5\left(\frac{x_o}{L-f}\right)^2 \right\} \frac{\sigma_a}{E} \frac{1}{a} \right] \quad (3.24) \end{aligned}$$

Now it is assumed that the ratio $\frac{x_o}{L-f}$ is determined by the chip velocity, chip-tool contact length, work material and tool geometry. Therefore, the expressions

$$6 - 4\left(\frac{x_o}{L-f}\right) + \left(\frac{x_o}{L-f}\right)^2 \quad \text{and} \quad 12 - 12\left(\frac{x_o}{L-f}\right) + 4,5\left(\frac{x_o}{L-f}\right)^2$$

are considered to be determined by the same factors. σ_a and E are properties of the material, and they vary with the temperature of the chip. Consequently (σ_a/E) is a function of cutting velocity as this affects the temperature of the chip.

Since a is half of the chip thickness and is given in terms of shear plane angle by

$$a = \frac{\text{Cos}(\phi - \alpha)}{2\text{Sin}\phi}$$

the expression (3.25) reduces to:

$$\frac{1}{R_c} = C_1 \frac{H}{(L - f)^2} - C_2 \frac{1}{S} \quad (3.25)$$

But according to Creveling, Jordan and Thomsen⁽¹⁰⁶⁾, the chip tool contact length is represented in terms of chip thickness as follows:

$$f = K t_c$$

They⁽¹⁰⁶⁾ also found that for steel, $K = 1$ and although this is probably not true for all conditions and materials it seems unlikely that the value of K will vary considerably and that for the present purpose it would seem reasonable to assume that

$$f/t_c = 1$$

Hence equation (3.25) becomes,

$$\frac{1}{R_c} = C_1 \frac{H}{(L - t_c)^2} - C_2 \frac{1}{S} \quad (3.26)$$

Equation (3.26) will now allow the natural radius of curvature of chips to be estimated for a chipbreaker of given dimensions and will take into consideration the effect of the chip-tool contact length.

However, there seem to be severe limitations in the significance of this analytical result. It indicates that at a particular tool and cutting conditions, radius R_c should vary with L and H as predicted

by expression (3.26). However, any change in tool geometry or cutting conditions will give different C_1 and C_2 .

During this work a series of tests were carried out so that to establish the values of the constants C_1 and C_2 in equation (3.26). The values of C_1 and C_2 were determined, by measuring the chip curl radius and chip thickness for a large number of chips. As a result of these measurements the values of C_1 and C_2 were established for each particular tool and cutting conditions. For steel EN1A and aluminium alloy HE30WP using carbide tipped and high speed tools of 15° rake angle at a cutting speed of 50 to 100 m/min, a feed range of 0.05 to 0.50 mm/rev. and with 3 and 6 mm depth of cut and with coolant, the values of C_1 and C_2 were found to be 1.8; 1.52 and 2.2×10^{-2} ; 3.0×10^{-2} respectively. The values of C_1 and C_2 obtained for steel EN1A differ noticeably from those obtained by Okushima⁽¹⁰¹⁾ for carbon steel (0.4%C) cut at conditions similar to those mentioned above for steel EN1A (according to Okushima $C_1 = 4.4$ and $C_2 = 1.2 \times 10^{-2}$). This is expected to be so due to the fact that the values of C_1 and C_2 obtained from the experimental tests carried out during this work, do take into account the effect of the chip-tool contact length as well as the effect of the parameters mentioned by Okushima.

In appendix I the author suggests a different theoretical approach to the mechanism of chip curling for both ground step and clamped chipbreakers.

Trim and Boothroyd⁽¹⁰⁷⁾ have developed a theoretical expression for the chip curl radius based on the Henriksen formula for chip curl radius, by taking into consideration the effect of the chip-tool contact length.

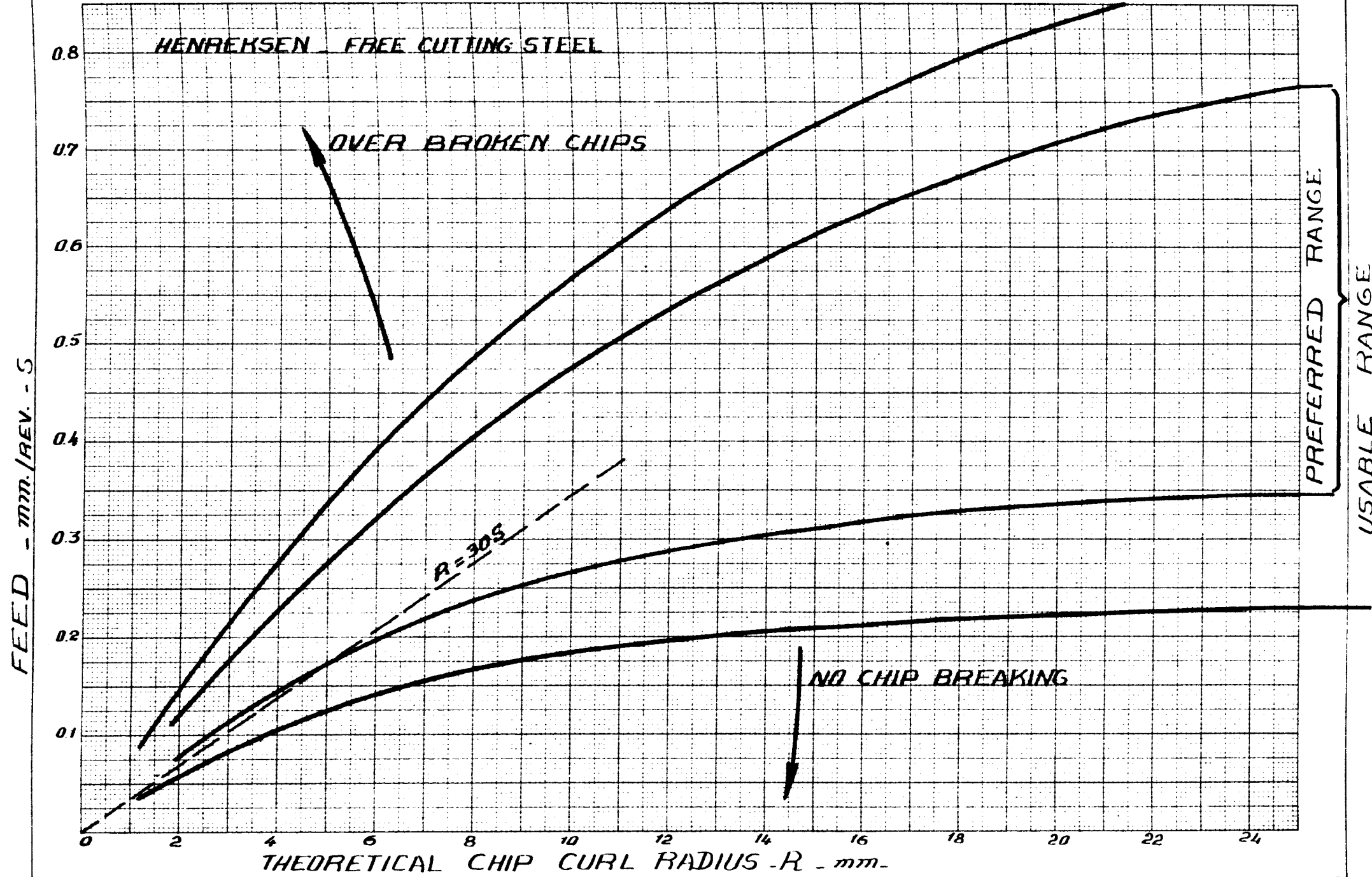
$$R = \frac{(L - t_c)^2}{2H} + \frac{H}{2}$$

This equation allows to determine the radius of the curvature of chips obtained from a chipbreaker of given dimensions and will take into account the effects of any changes in feed rate or undeformed chip thickness.

3.12 CHIPBREAKING EFFECTIVENESS

In this investigation, the chipbreaking process is analysed on the basis that the experimentally measured chip curl radius agrees with the theoretical and that for a given material and feed, the theoretical radius of the chip curl expresses the effectiveness of chipbreaking. For the sake of simplicity, it is also suggested that the chip curl radius should be some multiple of chip thickness. Since it is difficult to have an accurate measurement of the chip thickness and for a convenient plotting of the results it was decided to represent the chip curl radius in terms of feed(S) per revolution, that is the uncut chip thickness. Figs. 51, 52, 53, 54 show some of the experimental results obtained by Henriksen⁽⁷¹⁾, Okushima⁽¹⁰¹⁾ and this recent work. Figs. 53 and 54 were plotted as follows: The chip curl radius was measured for many chips obtained with different chipbreaker proportions and feed at the conditions mentioned on each of Figs. 53 and 54. The chips state unbroken, broken (half turn, one turn or more with chip length over 5 mm), over broken (half turn or less with chip length less than 5 mm) was registered. All these results were plotted. After plotting a fair amount of measurements, three lines were drawn. The first line (A) Figs. 53-54 was drawn so that to separate the points corresponding to unbroken chips from those corresponding to broken chips. The second line (C) separates the over broken and built-up chips from those of effectively broken ones. Chips were considered effectively broken when their length

FIG. 51 CHIP BREAKING DEGREE IN RELATION TO CHIP CURL RADIUS AND FEED ACCORDING TO HENREKSEN



OKUSHIMA
 0.4 %C STEEL
 FIG. 52 DEGREE OF CHIP BREAKING IN RELATION TO THE
 CHIP CURL RADIUS AND THE FEED FOR 0.4% C STEEL
 ACCORDING TO OKUSHIMA.

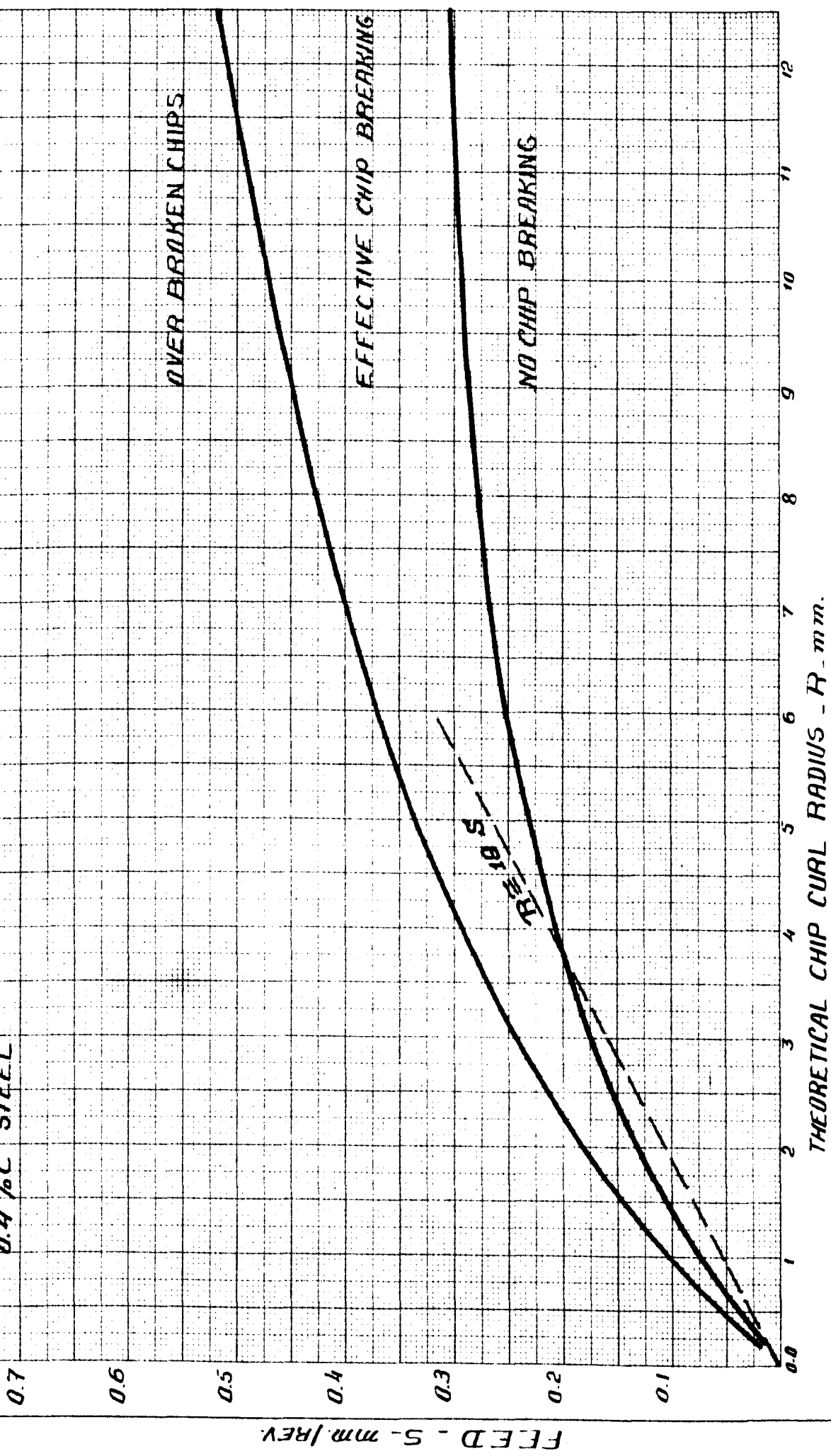


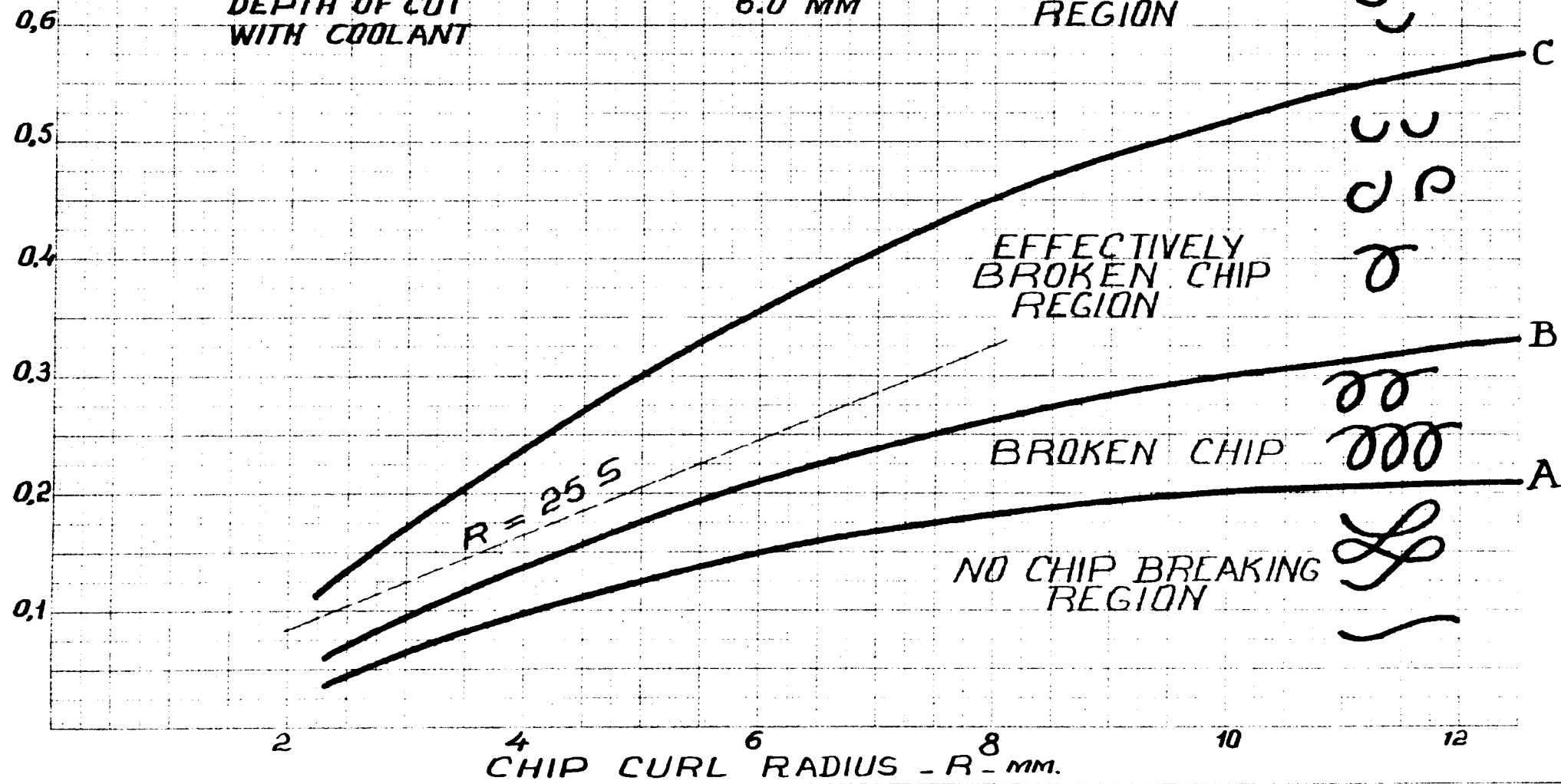
FIG. 53 CHIP BREAKING EFFECTIVENESS FOR ALUMINIUM ALLOY HE30WP USING A GROUND STEP CHIP BREAKER.

ALUMINIUM ALLOY HE30WP

CUTTING SPEED UP TO 100 M/MIN.
 RAKE ANGLE 15°
 DEPTH OF CUT 6.0 MM
 WITH COOLANT

OVER BROKEN
 AND BUILT-UP CHIP
 REGION

FEED - S - MM/REV.



EFFECTIVELY
 BROKEN CHIP
 REGION

BROKEN CHIP

NO CHIP BREAKING
 REGION

R = 25 S

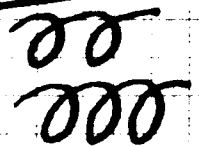
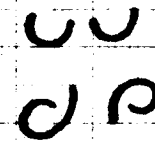
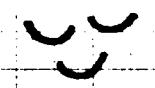


FIG. 54 CHIP BREAKING EFFECTIVENESS FOR GROUND STEP CHIPBREAKER

STEEL ENIA

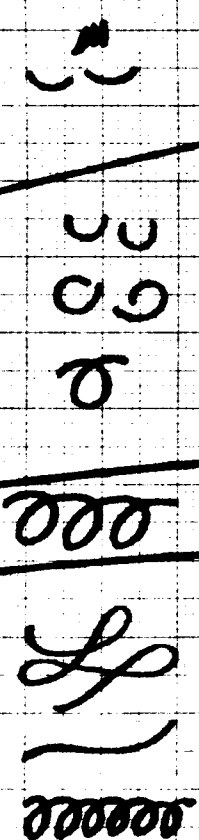
CUTTING SPEED 100 M/MIN
 RAKE ANGLE 15°
 DEPTH OF CUT 3 MM
 WITH COOLANT

OVER BROKEN
 AND BUILT UP CHIP
 REGION

EFFECTIVELY
 BROKEN CHIP
 REGION

NO CHIP BREAK
 ING REGION

R = 205



FEED - S - MM/REV.

0.6
0.5
0.4
0.3
0.2
0.1

2 4 6 8 10 12

CHIP CURL RADIUS - R - MM

C
B
A

was not more than 50 mm. In order to separate the effectively broken chips from those half broken a third line (B) was drawn. The relationship between the chip curl radius and the feed defining a line of equal chipbreaking effectiveness appears to be parabolic rather than linear. This could be explained by taking into consideration the fact that the strength of the chip does not increase with the thickness in the manner of a homogeneous beam, because a thicker chip will contain deeper cracks on its top surface, with a relatively thinner zone of secondary shear on its underside. It is also significant that the tool vibration increases with an increase in the feed. This will tend to deepen the fissures in the chip and the chip will tend to break due to chattering of the tool. However, it is difficult to explain in a completely satisfactory way the causes leading to the parabolic shape of these chipbreaking boundary curves.

In each of the Figs. (51, 52, 53, 54) a linear dotted curve is shown for a particular cutting material and a limited range of feeds. All the points on these lines correspond to effectively broken chips. The dotted lines represent a linear relationship between the chip curl radius R_c and the feed S . On the basis that the chips obtained at the chipbreaker geometries corresponding to the points on the line $\frac{R_c}{S}$ were effectively broken, the factor $\frac{R_c}{S}$ was, therefore, considered to represent the chipbreaking effectiveness. However, the factor $\frac{R_c}{S}$ will vary with a variation in the cutting conditions, and in particular for high cutting speeds the factor $\frac{R_c}{S}$ will be smaller than those for low cutting speeds. That is because the chipbreaking becomes more difficult at high cutting speeds⁽⁹⁵⁾.

According to Henriksen, Fig. 51, two zones of chipbreaking are recognised. The first zone covers a usable range of feed at which a reliable chipbreaking is obtained and called the usable range. Best

chipbreaking results are obtained within the preferred range. The second zone covers the feeds below and above this range. For feeds below this range the chip is not broken and for feeds above this range the chips are overbroken and extremely small in size. Both the unbroken and overbroken chips are not recommended due to the chip disposal problem and reduced tool life respectively. For best chipbreaking effectiveness the factor $\frac{R}{S} \frac{C}{S}$ for free cutting steels at cutting speeds of 50 to 150 m/min. and a depth of cut of 2 to 6 mm, was found to be equal to $\frac{R}{S} \frac{C}{S} = 30$.

Okushima has carried out a similar experiment and found that best chipbreaking results for carbon steel (0.4%C) at a depth of cut of 3 mm and cutting speed of 50 to 200 m/min., was obtained when $\frac{R}{S} \frac{C}{S} = 18$, Fig. 52.

In this investigation the chipbreaking effectiveness was fully studied. Different materials such as aluminium alloys, copper, high, medium and low carbon steels and stainless steel were tested under different cutting conditions using different shapes of the cutting tools and chipbreakers, dry and with coolant. Some of the experimental results is shown in Fig. 53 and 54. It was the aim of this investigation to find a reliable parameter for controlling the chipbreaking process. Experimental evidence suggests that the factor $\frac{R}{S} \frac{C}{S}$ more or less represents the chipbreaking effectiveness.

According to the experimental results shown in Fig. 53, the factor $\frac{R}{S} \frac{C}{S} = 25$ was found to characterise an effective chipbreaking when cutting aluminium alloys HE30WP at a speed of up to 10 m/min. using a ground chipbreaker with 15° rake angle and coolant. At high cutting speeds up to 120 m/min. the factor $\frac{R}{S} \frac{C}{S}$ was found to be within 18 to 20. Accordingly the experimental results obtained when machining aluminium alloys at cutting speeds up to 120 m/min., suggest

that best chipbreaking results is obtained when $\frac{R_c}{S} = 18$ to 25. In Fig. 53 four regions are recognised. The first region covers the no chipbreaking range, where a continuous chip is produced at very low feed. It is not recommended to work within this range of feed due to the disadvantages accompanied with the appearance of continuous chips. The second region is the broken chips range. This range of feeds produce chips half broken and half unbroken, and for good chip disposal performance, it is preferred not to work within this range of feeds. The third region covers the effectively broken chips. The chips are of small size and very convenient for disposal. The tool life and surface finish are satisfactory. The fourth region covers the overbroken chips. It is not recommended to work with this range of feed due to the increased tool wear at high feeds.

Similar results were obtained for steel EN1A. Fig. 54 shows the experimental results obtained when machining steel EN1A at cutting speed up to 120 m/min., and rake angle of 15° using coolant. These results show that effective chipbreaking is obtained when $\frac{R_c}{S} = 20$. Covering a wide range of steels and some other materials it was found that best chipbreaking is obtained when factor $\frac{R_c}{S} = 15$ to 20.

CHAPTER 4

4.1 ANALYSIS OF THE EXPERIMENTAL RESULTS

4.1.1 General Analysis of the Experimental Results

The aim of this work was to find a suitable solution to the chip breaking problem and to provide reliable information concerning the efficiency of chipbreakers. To analyse this process, different materials (aluminium alloys, steels) were tested under different cutting conditions using different geometries of the chipbreaker.

The tests attempted during this investigation can be classified in the following way:

- (1) Tests on ground step chipbreakers and on clamped wedge chipbreakers.
- (2) Tests at low cutting speeds up to 10 m/min and at high cutting speeds up to 100 m/min using a feed range of 0.05 to 0.5 mm/rev.
- (3) Tests on aluminium alloys and soft steels.
- (4) Force measurement.
- (5) Chip curl radius and chip thickness measurements.

The effect of rake angle, depth of cut and coolant were also taken into account. A dial gauge dynamometer has been used for measuring cutting forces in the low speed range. A strain gauged and calibrated tool shank was used to measure the cutting forces in the high speed range. Both the dial gauge and the strain gauge dynamometers were described earlier in Chapter 2. A micrometer was used to measure the chip thickness and chip curl radius.

As far as the chipbreaker effectiveness was concerned, this work considered it important to confirm that the measured radius of the chip curl, should not only agree with theoretical (suggested in Chapter 3) but also for a given material and feed, the theoretical

chip curl radius should express the chipbreaker effectiveness in breaking up the chip.

This work has been carried out in two stages:

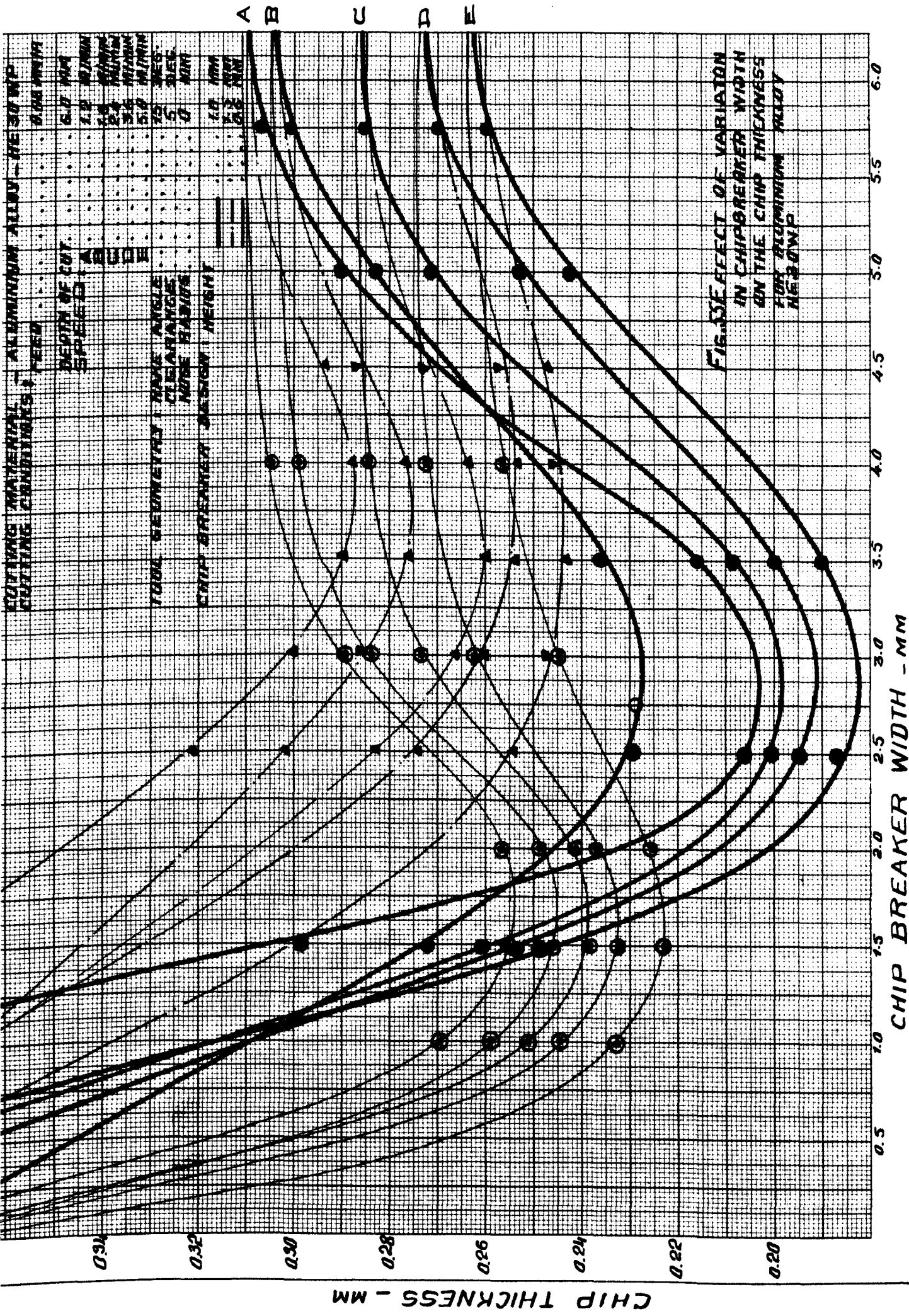
First Stage

This part of the investigation included experimental tests in the low range of cutting speeds up to 10 m/min. These tests were performed on a lathe equipped with a 12.5 H.P. main motor, using high-speed tools with ground step chipbreakers of different dimensions, A set of results given by slow speed tests on aluminium alloy HE30WP in the shape of bars of 80 mm in diameter using a sharp tool of 15° rake angle with a ground step chipbreaker are shown in Fig.55 .

CHEMICAL COMPOSITION AND MECHANICAL PROPERTIES OF ALUMINIUM ALLOY HE30WP

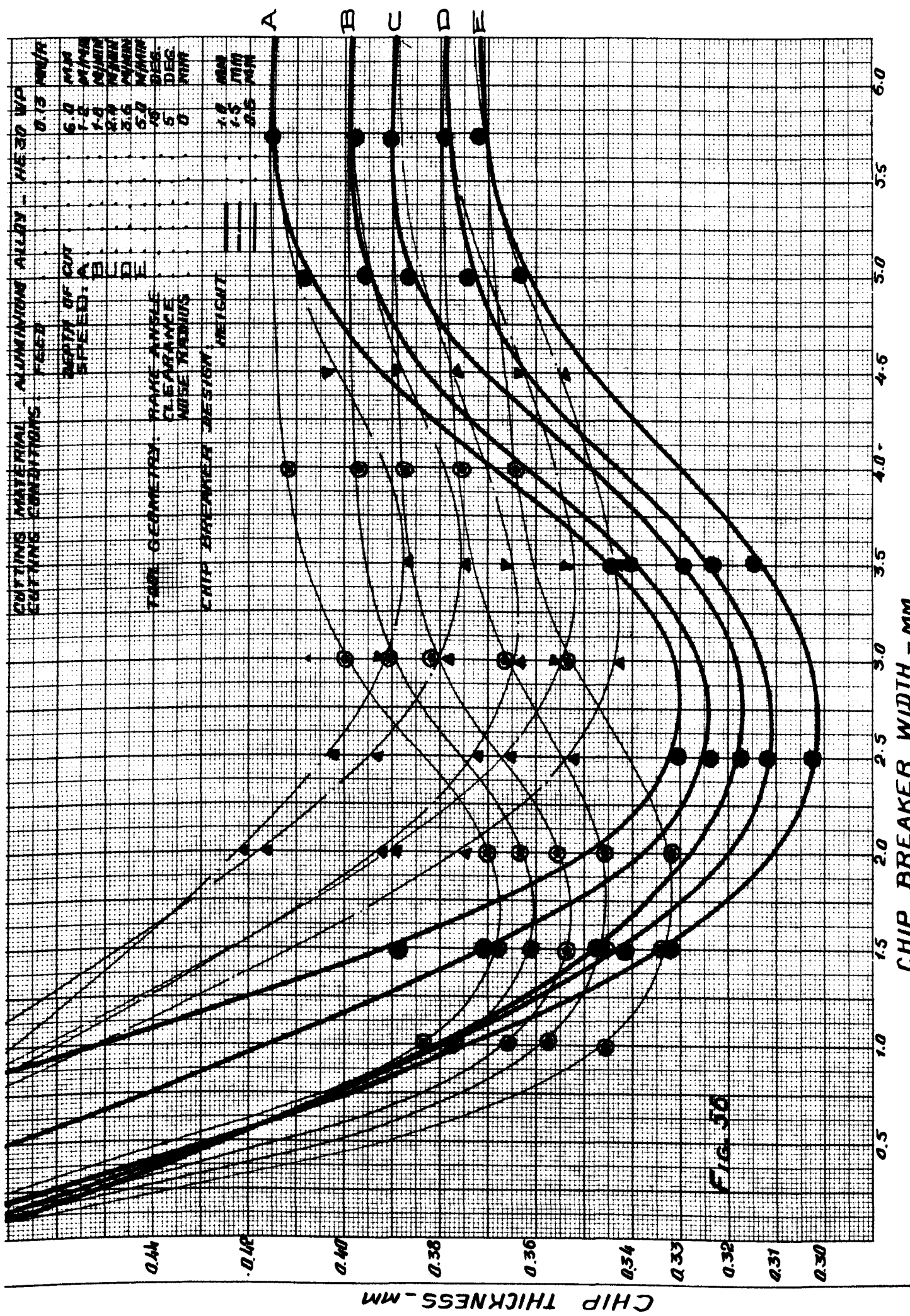
COMPOSITION (PER CENT)									MINIMUM MECHANICAL PROPERTIES			
Al	Cu	Mg	Si	Fe	Mn	Zn	Cr	Ti	Size (Dia-meter mm)	1.0% Proof Stress kg/mm ²	Tensile Strength kg/mm ²	Elongation on 50mm %
rem.	0.1	0.4-1.5	0.6-1.3	0.6	0.4-1.0	0.1	0.5	0.2	up to 150	25.2	29.9	10

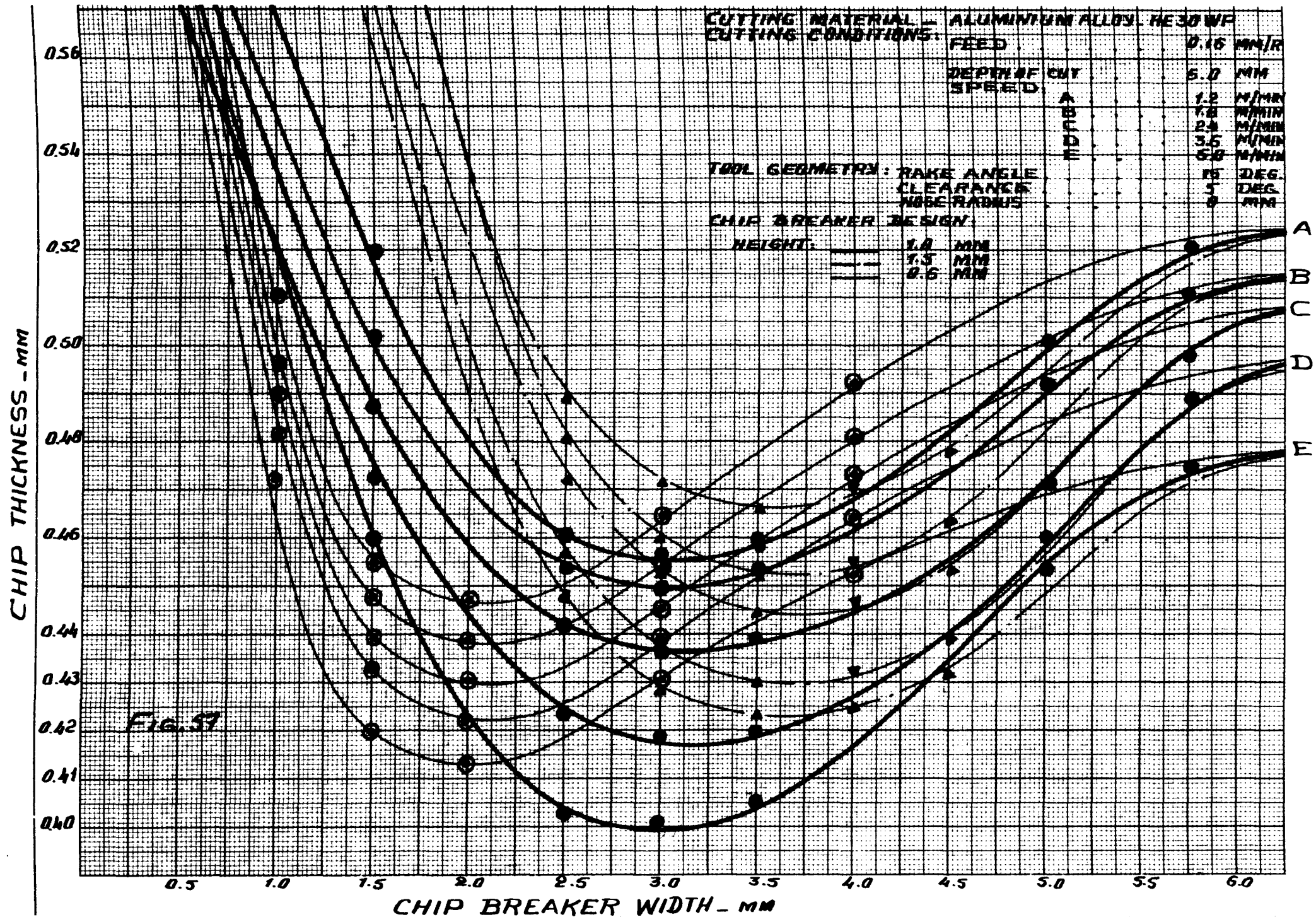
These tests were carried out in dry conditions with a speed range of 1.2 to 5.0 m/min. and a feed rate of 0.08 mm/rev. using different chipbreakers heights (1.5; 1.0; 0.6; ...). Fig.55 demonstrates that as the chipbreaker width (L) Fig.37 was increased from 0.5 to 6.0 mm, the chip thickness reached a certain minimum value (at L = 3.6 mm for chipbreaker height H = 1.5 mm; L = 2.7 mm for H = 1.0 mm, and L = 1.5 mm for H = 0.6 mm) and then increased to the value obtained with a large width, that is, for the conditions when the chipbreaker was virtually absent. The width of the chipbreaker at which the chip



thickness was minimum depended mainly on the height of the chipbreaker. The higher the chipbreaker step the larger the optimum width of the chipbreaker. It can also be seen from Fig. 55 that the change in the cutting speed in the range of 1.2 to 5.0 m/min has no significant effect on the optimum width of the chipbreaker at which chip thickness was minimum. From Fig. 55 it is clear that the use of chipbreakers will not lead to an increase in the chip thickness but actually gives a reduced chip thickness compared to those obtained without chipbreakers. Similar results were obtained for feeds 0.13; 0.16; and 0.25 mm/rev. (Figs. 56, 57 and 58 respectively). From Figs. 55-58 it can be seen that the optimum chipbreaker width is slightly affected by the feed. However, the larger the feed the larger the optimum chipbreaker width should be. It may be concluded from Figs. 55-58 that in order to obtain minimum cutting ratio the chipbreaker dimensions must be chosen by taking into consideration the effect of the feed.

It was considered important to analyse the effect of the rake angle on the chip thickness, so that to be able to judge the chip breaking process from this aspect. A set of experimental results obtained at the same conditions mentioned earlier but with a 30° rake angle are shown in Figs. 59-62. From Figs. 55-62 it was pointed out that positive rake angles within 15° to 30° had a small effect on the chip thickness. However, this effect was significant for rake angles within $+8^\circ$ to -15° , where large chip thickness values were obtained at negative rake angles. Negative rake angles will lead to a discontinuous cutting, and can be useful in obtaining broken chips. However, use of negative rake angles will lead to a considerable reduction in the tool life caused by extreme conditions of high force and temperature at the cutting zone.





CUTTING MATERIAL ALUMINIUM ALLOY-HE30 WP
 CUTTING CONDITIONS

FEED 0.25 MM/R
 DEPTH OF CUT 6.0 MM
 SPEED: A 1.2 M/MIN
 B 1.4 M/MIN
 C 2.4 M/MIN
 D 3.4 M/MIN
 E 5.0 M/MIN

TOOL GEOMETRY
 TAKE ANGLE 15 DEG.
 CLEARANCE 5 DEG.
 NOSE RADIUS 0 MM

CHIP BREAKER DESIGN
 HEIGHT: 1.0 MM (solid line), 1.5 MM (dashed line), 2.0 MM (dotted line)

CHIP THICKNESS - MM

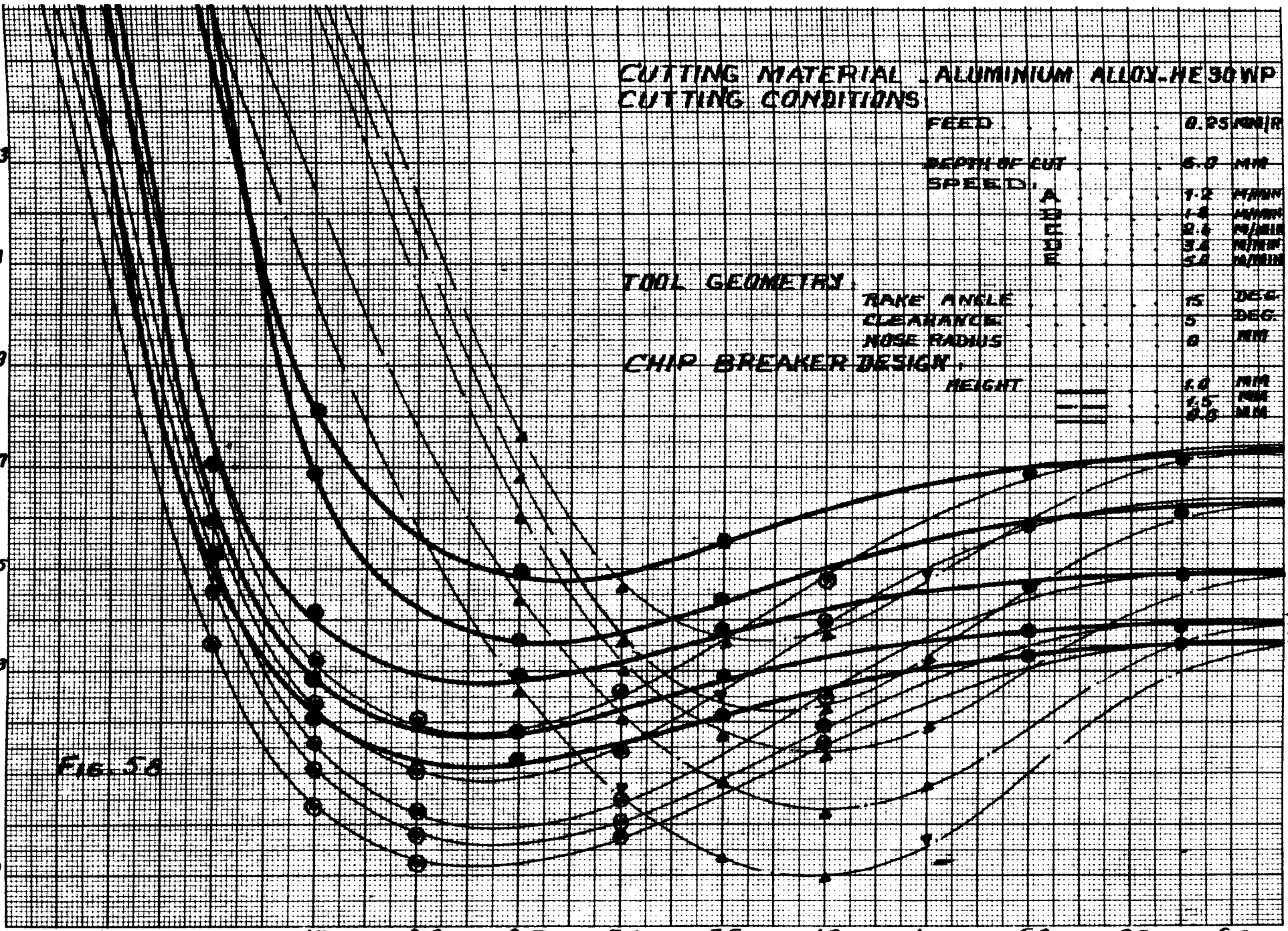
0.73
0.71
0.69
0.67
0.65
0.63
0.61
0.59

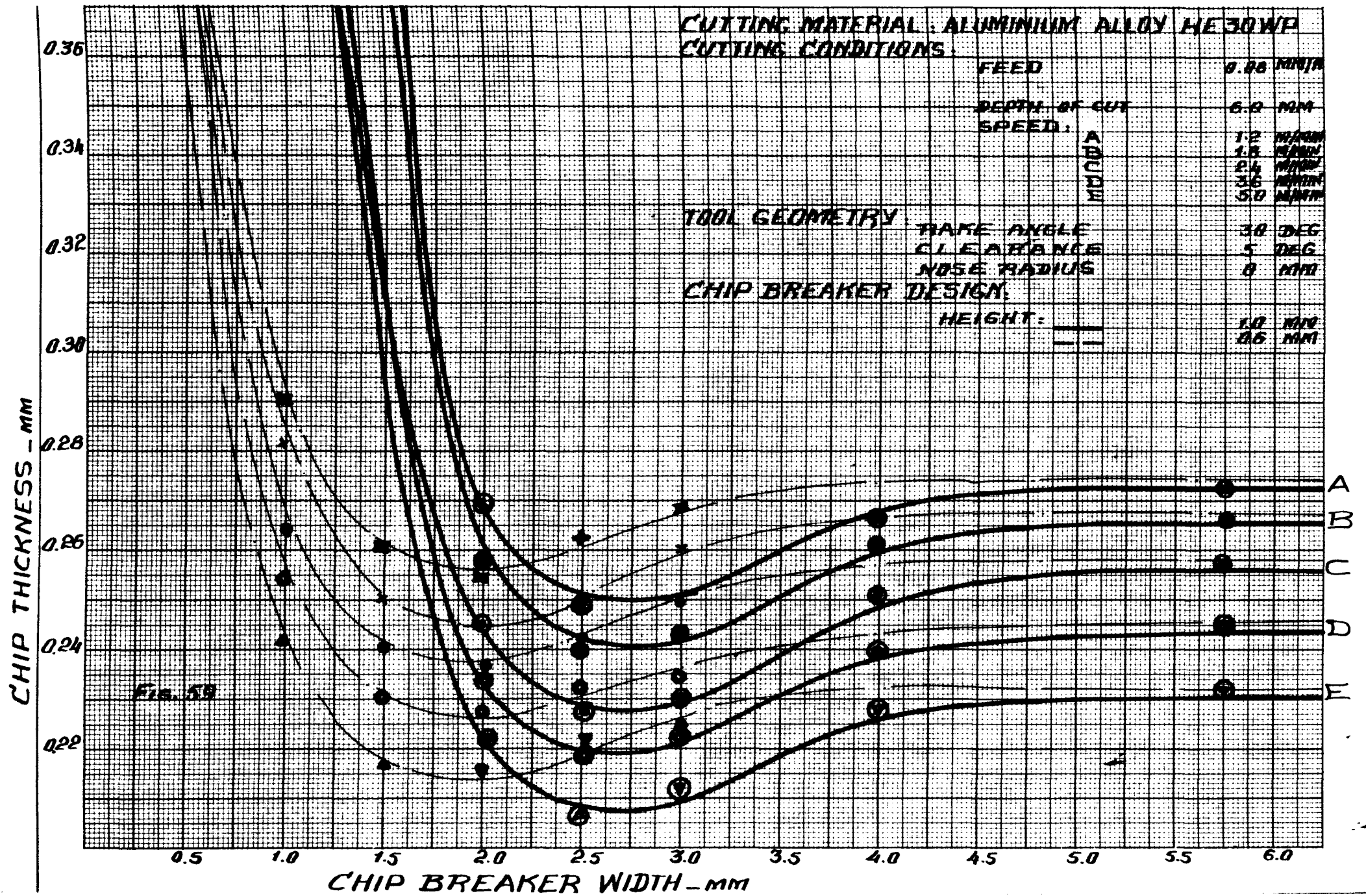
A
B
C
D
E

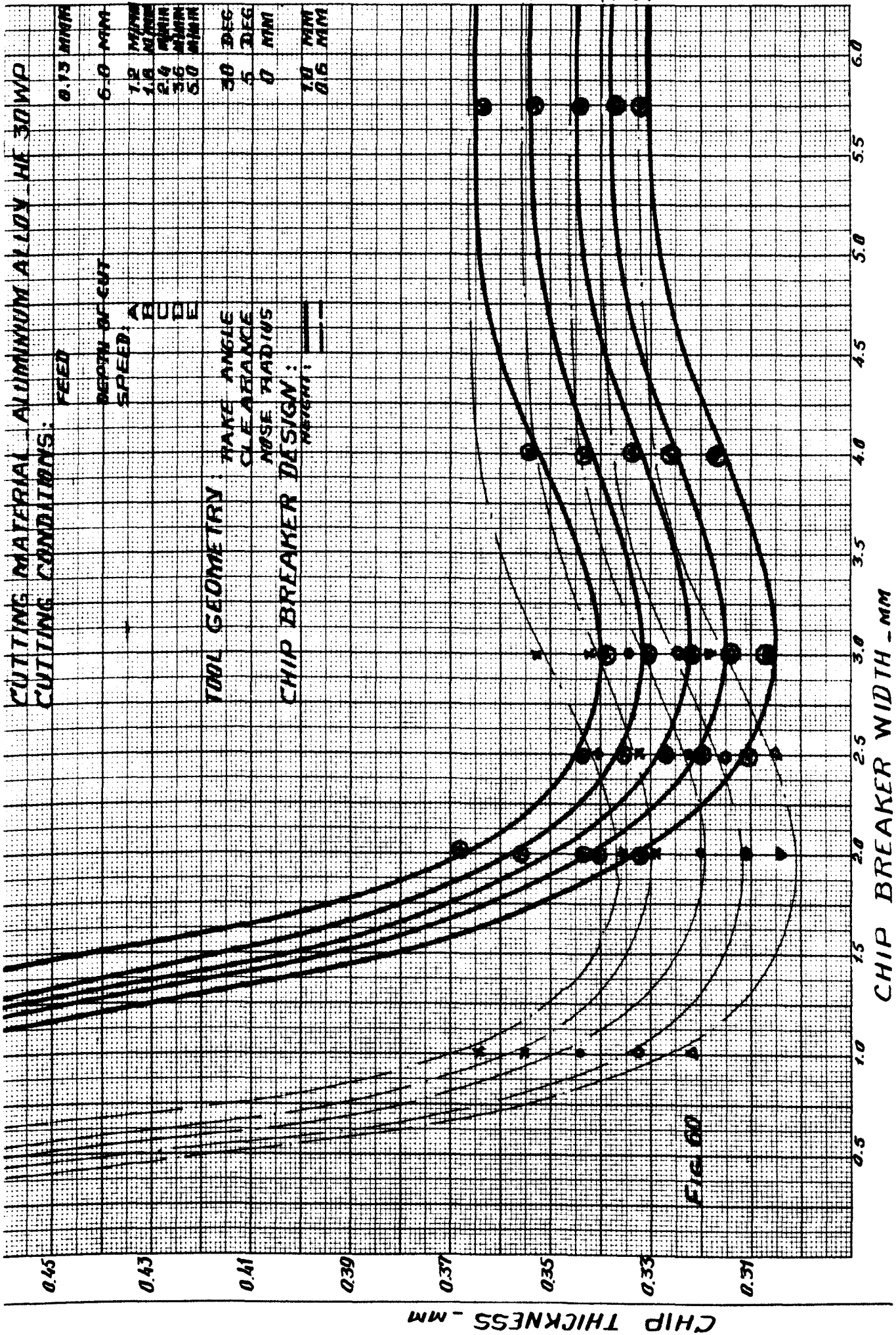
FIG. 58

CHIP BREAKER WIDTH - MM

0.5 1.0 1.5 2.0 2.5 3.0 3.5 4.0 4.5 5.0 5.5 6.0







CHIP THICKNESS - MM

CHIP BREAKER WIDTH - MM

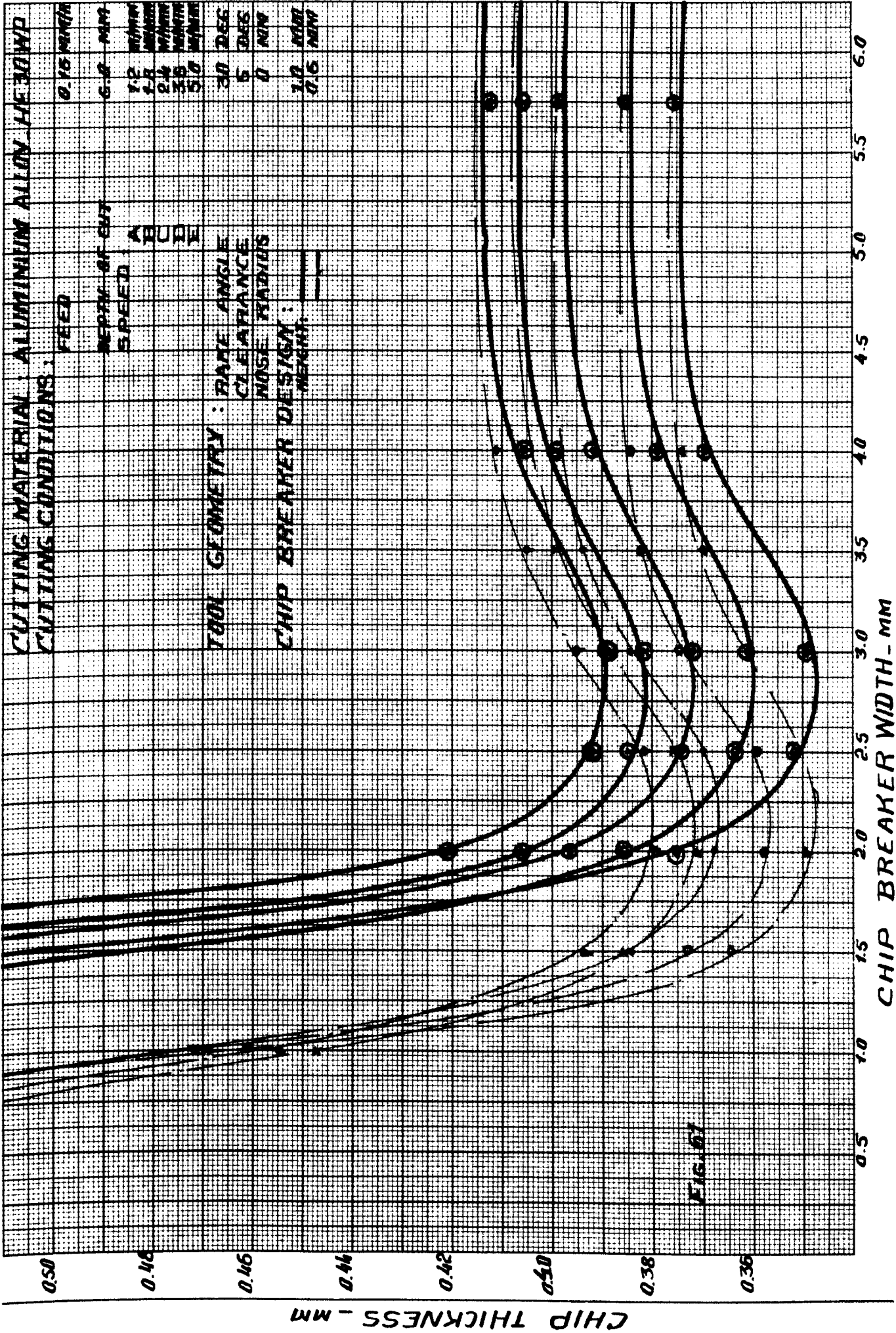
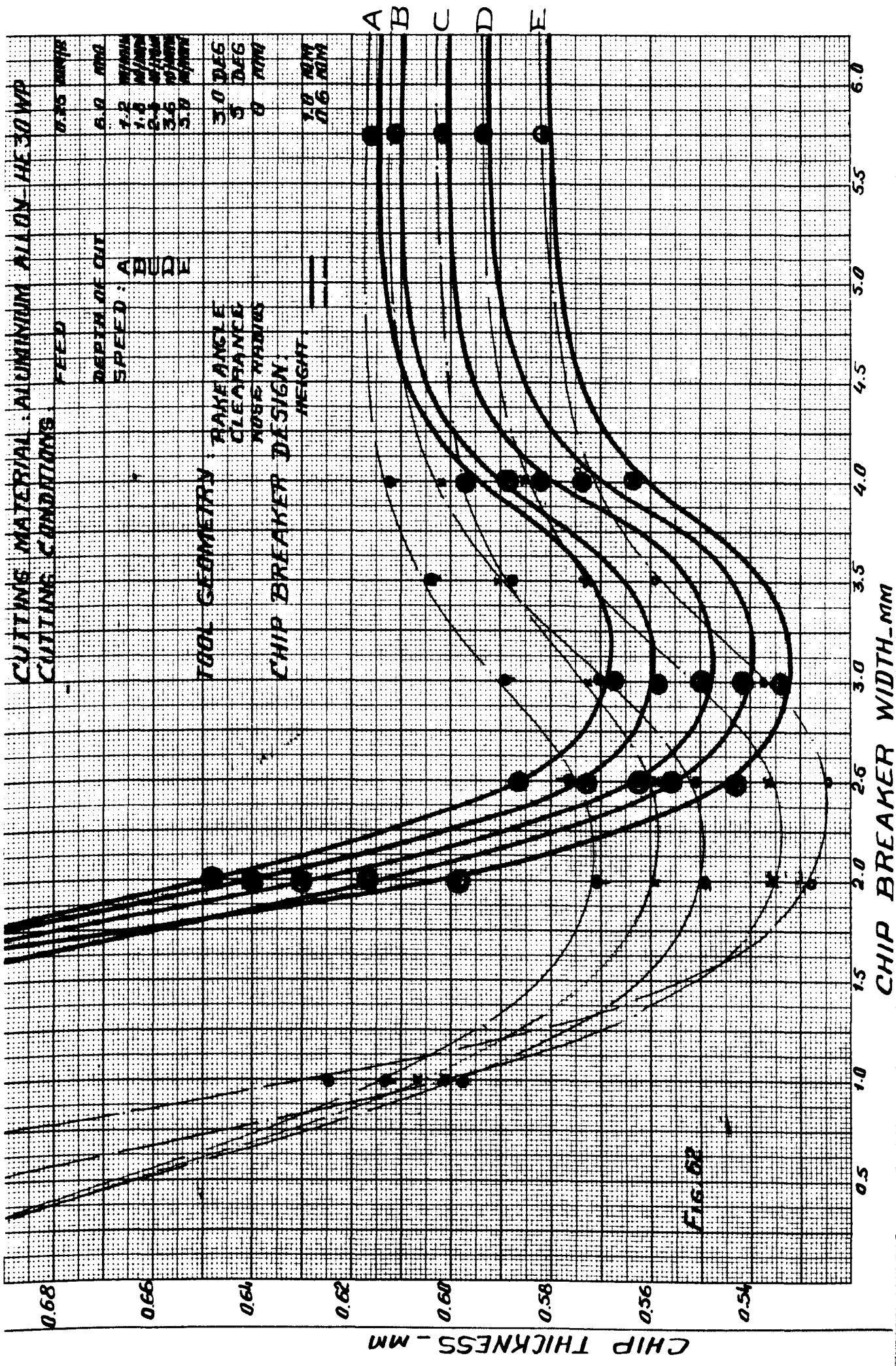


FIG. 67



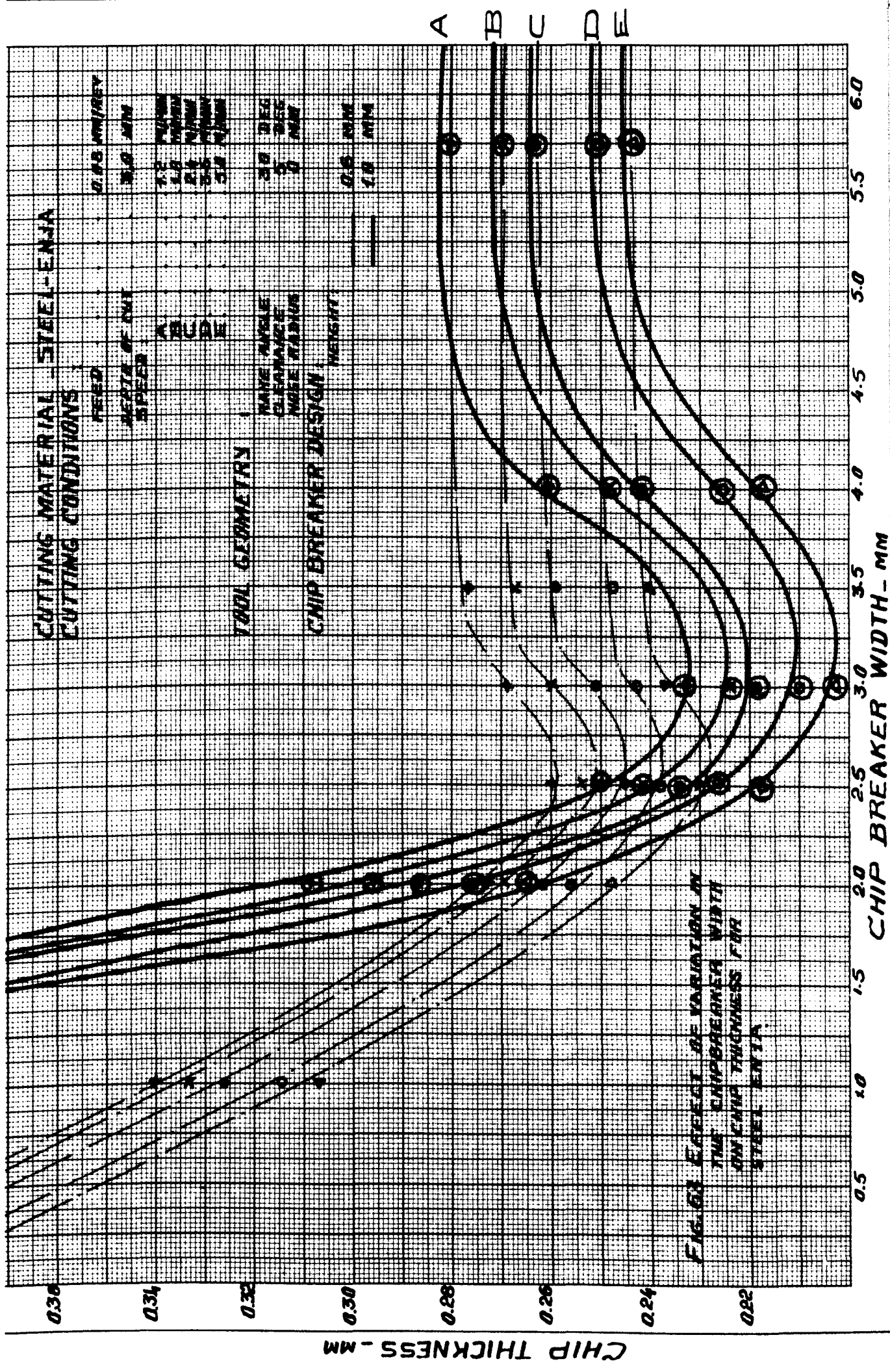
Similar relations between the chip thickness and chipbreaker width Figs. 63-66 have been obtained from tests on steel (EN 1A) bars of 80 mm in diameter.

CHEMICAL COMPOSITION AND MECHANICAL PROPERTIES OF STEEL EN1A

CHEMICAL COMPOSITION (PER CENT)					Size Diameter (mm)	MECHANICAL PROPERTIES
C	Si	Mn	S	P		Tensile Strength kg/mm ²
0.07-0.15	0.10 max.	0.80-1.20	0.20-0.30	0.07 max.	Over 65	36

The chip thickness curves shown in figs. 63-66 have similar points of minimum chip thickness which correspond to particular values of chipbreaker width.

The significance of this variation in chip thickness for both aluminium alloy HE30WP and steel EN1A is that cutting forces (Figs. 67-69) follow a similar pattern. Figs. 67-69 show the variation in the vertical component of the cutting force in relation to the change in the chipbreaker width for those two materials when a ground step chipbreaker with 15° rake angle was used. Figs. 67-68 show the effect of the feed upon the vertical component of the cutting force obtained for aluminium alloy HE30WP. From Figs. 67-68 it was clear that the optimum chipbreaker width at which the cutting force was minimum is noticeably effected by the feed. Here from the cutting force curves it can be concluded that the use of chipbreakers may give lower cutting forces. Similar results were obtained for the horizontal component of the cutting force. By analysing the experimental results shown in figs. 67-68 it was suggested that the manner in which the cutting force and the chip thickness were changed might be connected to the change in the mean coefficient of friction of the chip-tool contact which resulted in change in the specific normal



CHIP THICKNESS - MM

CHIP BREAKER WIDTH - MM

A B C D E

CHIP THICKNESS - MM

0.42
0.40
0.38
0.36
0.34
0.32
0.30
0.28

Fig. 64

0.5 1.0 1.5 2.0 2.5 3.0 3.5 4.0 4.5 5.0 5.5 6.0

CUTTING MATERIAL: STEEL EN-1A
CUTTING CONDITIONS:

FEED

0.13 mm/A

DEPTH OF CUT SPEED

3.0 m/m

A B C D E

1.2 m/min
1.8 m/min
2.4 m/min
3.0 m/min
3.6 m/min

TOOL GEOMETRY
CHIP BREAKER DESIGN
HEIGHT: 0.5 mm
RADIUS: 1.0 mm

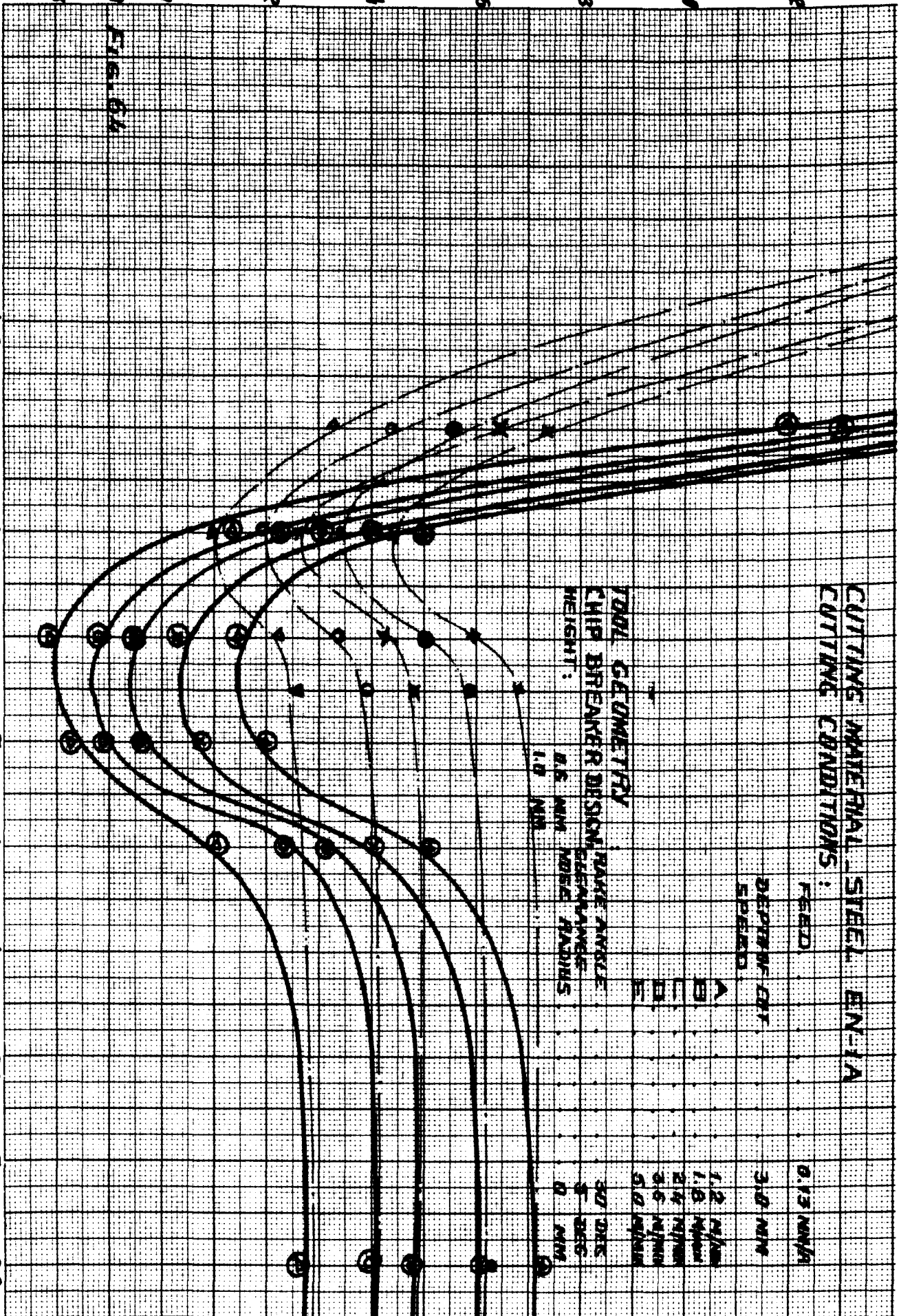
30 DEG
5 DEG
R mm

RAKE ANGLE

CLEARANCE

ANGLE

A
B
C
D
E



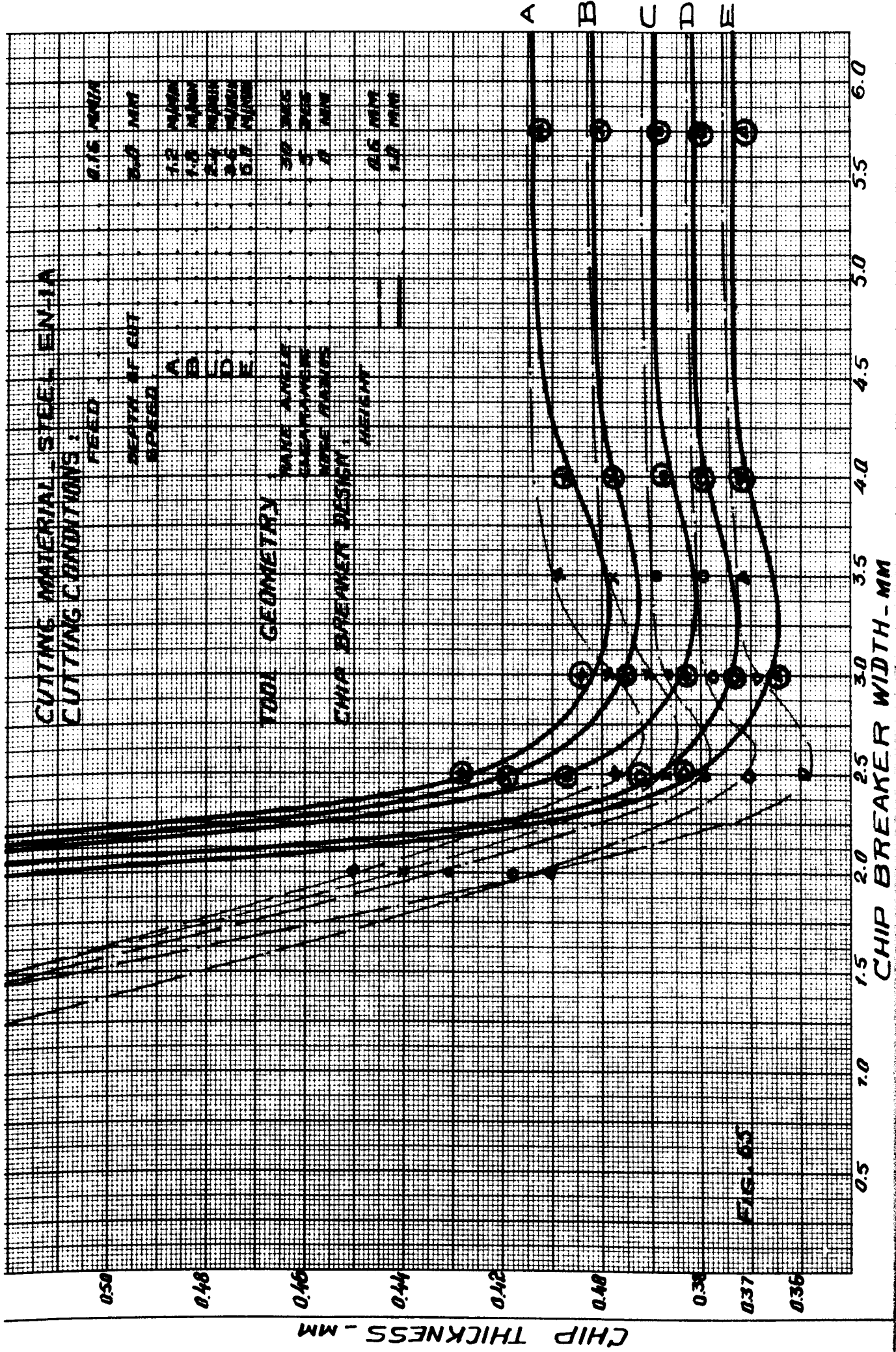
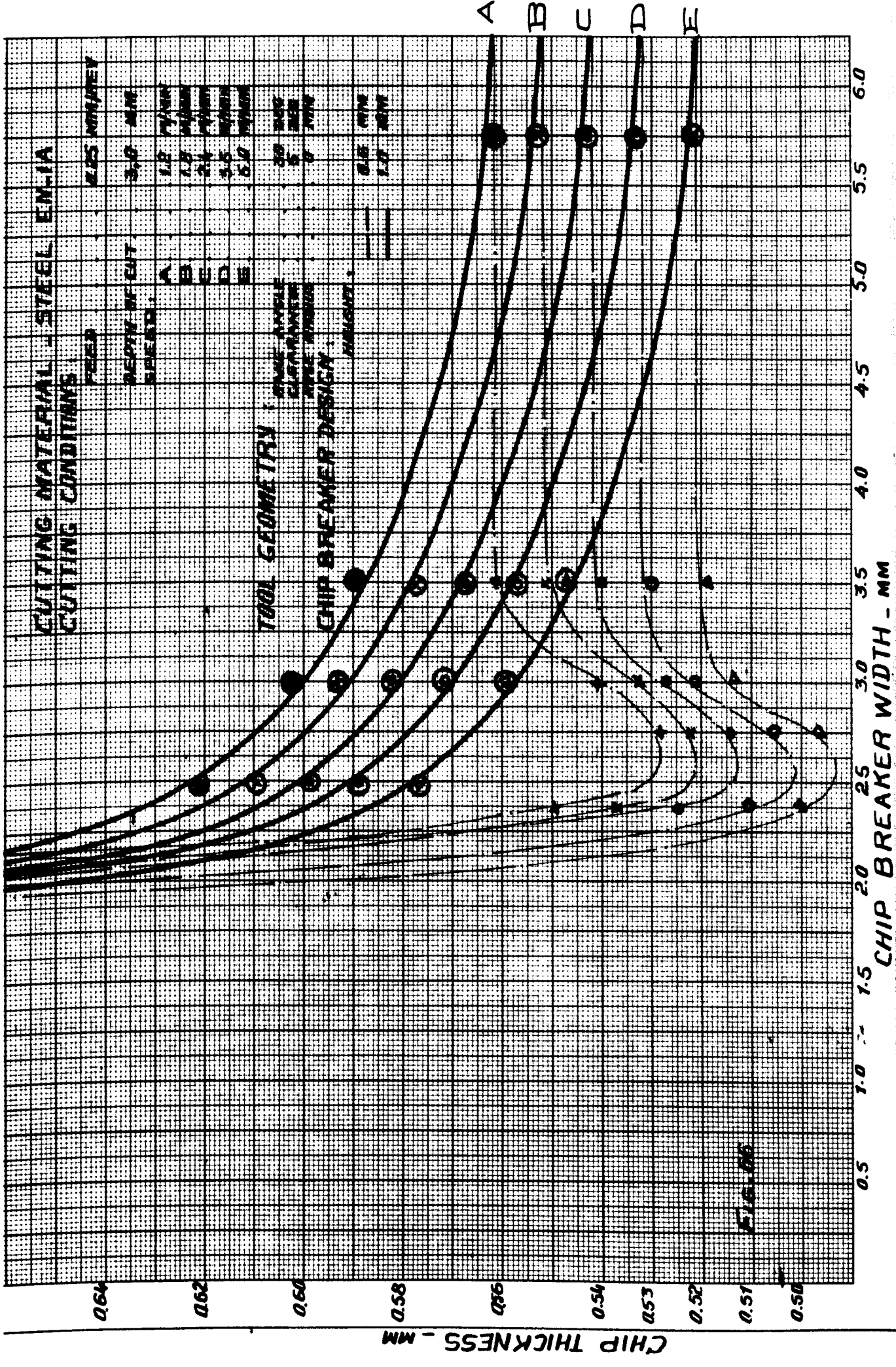


FIG. 65

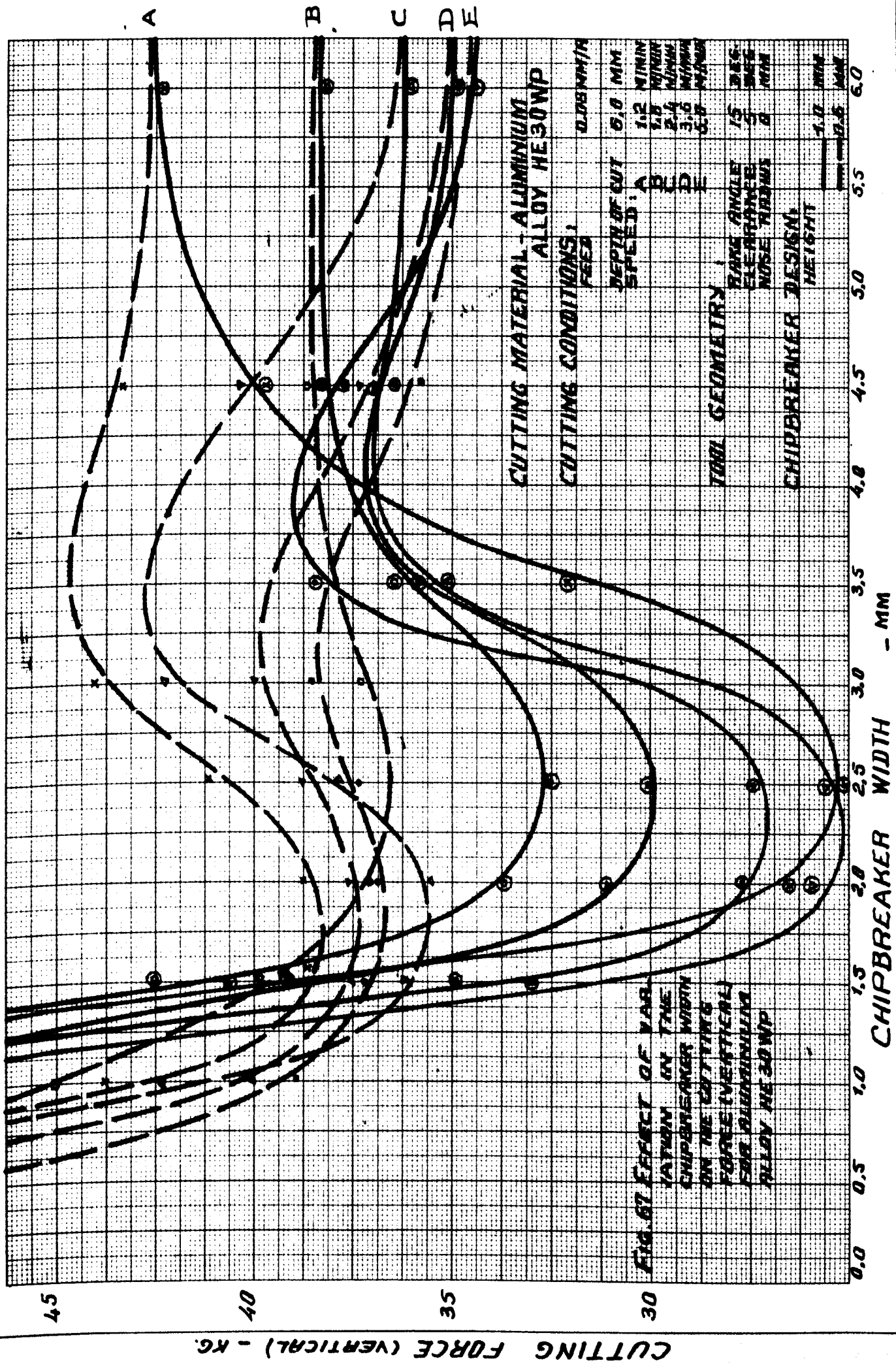
CHIP THICKNESS - MM

CHIP BREAKER WIDTH - MM



CHIP THICKNESS - MM

CHIP BREAKER WIDTH - MM



CUTTING FORCE (VERTICAL) - KG.

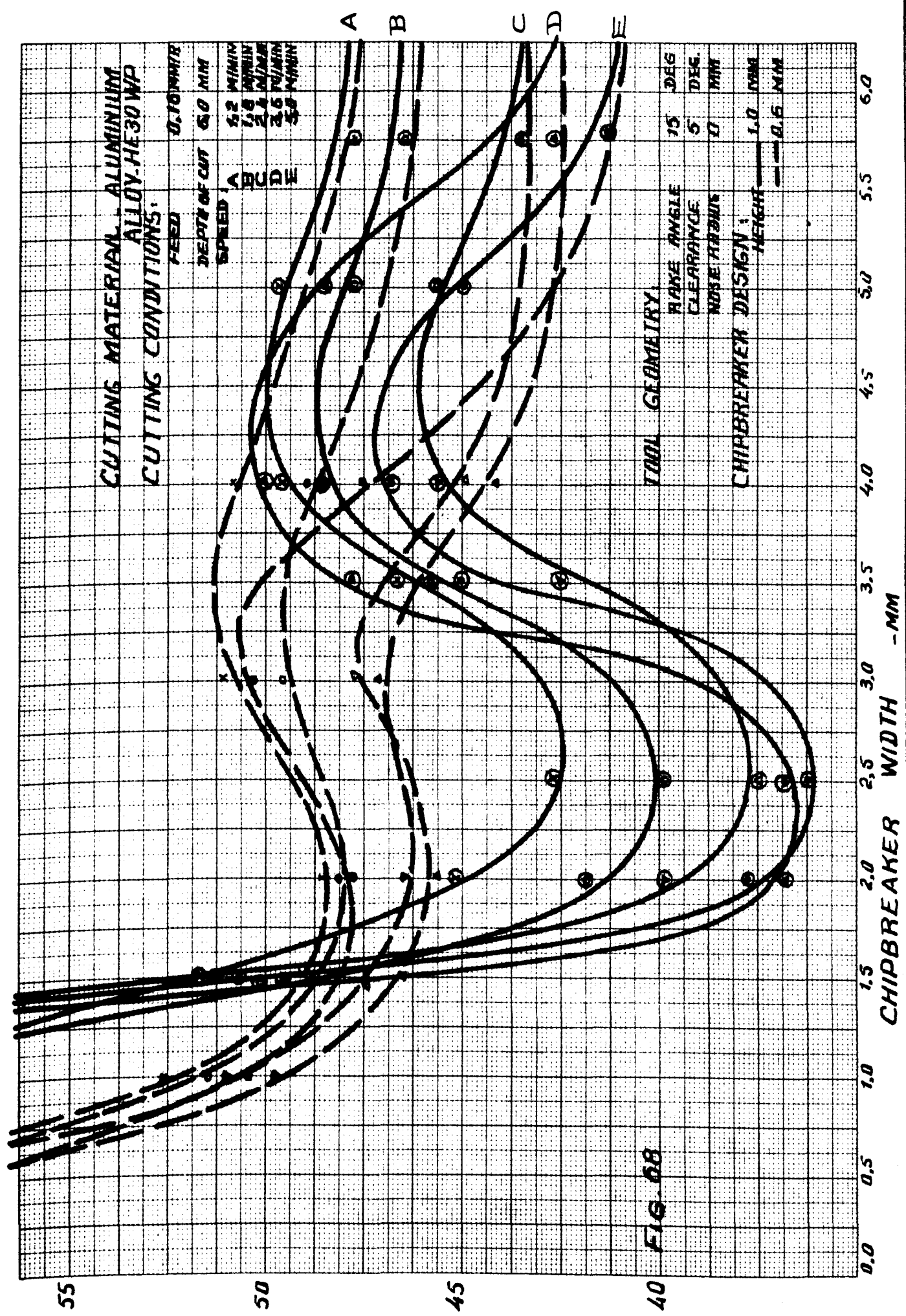


FIG. 68

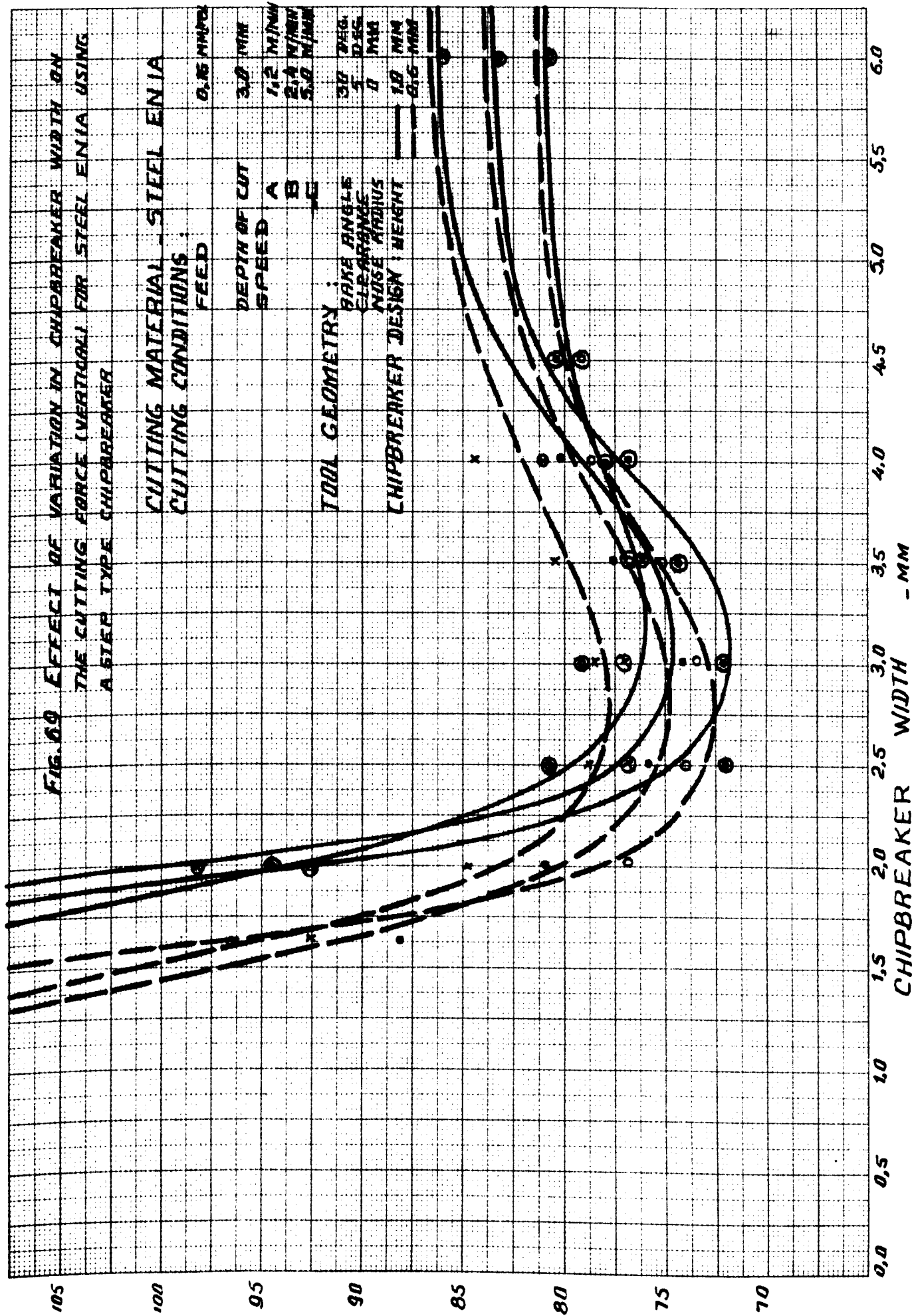
FIG. 69 EFFECT OF VARIATION IN CHIPBREAKER WIDTH ON THE CUTTING FORCE (VERTICAL) FOR STEEL ENIA USING A STEP TYPE CHIPBREAKER

**CUTTING MATERIAL - STEEL ENIA
CUTTING CONDITIONS:**

FEED 0.15 MM/REV
DEPTH OF CUT 3.0 MM
SPEED A 1.2 MIN/REV
B 2.4 MIN/REV
C 5.0 MIN/REV

TOOL GEOMETRY:

RAKE ANGLE 30 DEG.
CLEARANCE 5 DEG.
NOSE RADIUS 0 MM
CHIPBREAKER DESIGN HEIGHT 1.0 MM
0.6 MM



CUTTING FORCE (VERTICAL) - KG.

CHIPBREAKER WIDTH - MM

A B C

pressure on the cutting face of the tool, however, no theoretical support to the above explanation has been obtained. The characteristic change in the cutting force shown in figs. 67-68 was explained as follows: When the chipbreaker width was reduced, the chip was forced away from the tool face and the extent of the tool-chip contact was reduced. Due to this there was an increase in the specific normal pressure and a drop in the mean coefficient of friction which led to a reduction in the cutting force and chip thickness. That was so up to the characteristic points of minimum cutting force and chip thickness. Further reduction in the chipbreaker width led to the condition that the chip was bent so tight so that it gave an extra frictional force. Very small chipbreaker width will lead to over-breaking or building-up the chips in the vicinity of the chipbreaker which lead to an extensive increase in the cutting force and chip thickness and finally breaking the tool. The additional cutting force and change in chip thickness are to some extent affected by the amount of bending of the chip. Although chip breaking at low cutting speeds can be satisfactorily obtained by using ground step chipbreakers in dry conditions, coolant was found to be very helpful in providing good chipbreaking results when small chipbreaker width was used.

From each curve in Fig. 55 and similarly 56-69, two characteristic values of chipbreaker width may be selected. One of these was taken to be the value at which chip thickness or cutting force reached the highest allowable, beyond which built-up and over-broken chips occurred. This condition corresponded to the lowest permissible chipbreaker ratio (width/height). The other value of the chipbreaker width was that giving minimum chip thickness or cutting force.

Figs. 70-74 summarize these values, and show that optimum proportions of the chipbreaker are almost independent of feed. Figs. 70, 71 and 73 show the chipbreaker proportion for two conditions for aluminium alloy HE30WP and steel EN1A respectively. The first condition corresponds to the minimum chip thickness, and the other condition corresponds to the lowest permissible chipbreaker ratio, below which built-up and over-broken chips occur. By classifying the chips obtained during these tests (when using chipbreaker proportion ratios varying from those giving minimum cutting force and chip thickness, to those beyond which built-up chips were obtained) to effectively broken, partially broken and unbroken chips, low values of chipbreaker ratio were found to give more effectively broken chips. Similarly Figs. 72 and 74 show the conditions for minimum cutting force and lowest permissible chipbreaker ratio to avoid built-up and over-broken chips. The lowest permissible chipbreaker ratios for steel EN1A are distinctly higher than those for aluminium alloy HE30WP. The interpretation of Fig. 70 is that for the conditions mentioned, the chipbreaker might have a preferred shape $WIDTH/HEIGHT = 2.5$, or any other value not less than 1.5. From Figs. 70-74 it can be concluded that in order to obtain broken chips with lower cutting force on the tool face, the chipbreaker ratio must be taken equal to the largest chipbreaker ratio within the conditions of lowest permissible chipbreaker ratio which avoids the built-up chips, and minimum cutting force which gives broken chips. It is significant to mention that during these experiments, some of the dial gauge readings were affected by the chatter of the tool dynamometer and machine tool system. However, this did not change the manner in which the cutting forces changed in relation to the change in the chipbreaker width.

FIG 70 CONDITIONS FOR MINIMUM CHIP THICKNESS
WHEN CUTTING ALUMINUM ALLOY HF 30 WP
USING 30° RAKE ANGLE.

ALUMINUM ALLOY HF 30 WP

RAKE ANGLE 30°

CUTTING SPEED 10 M/MIN

EMPIREXER HEIGHT

○ 0.5 mm

× 1.0 mm

CHIPBREAKER RATIO - W/H

1.0
2.0
3.0
4.0

0.1 0.2 0.3

FEED - S - mm/REV.

CONDITIONS FOR MINIMUM
CHIP THICKNESS

LOWEST PERMISSIBLE TO
AVOID BUILT-UP CHIPS

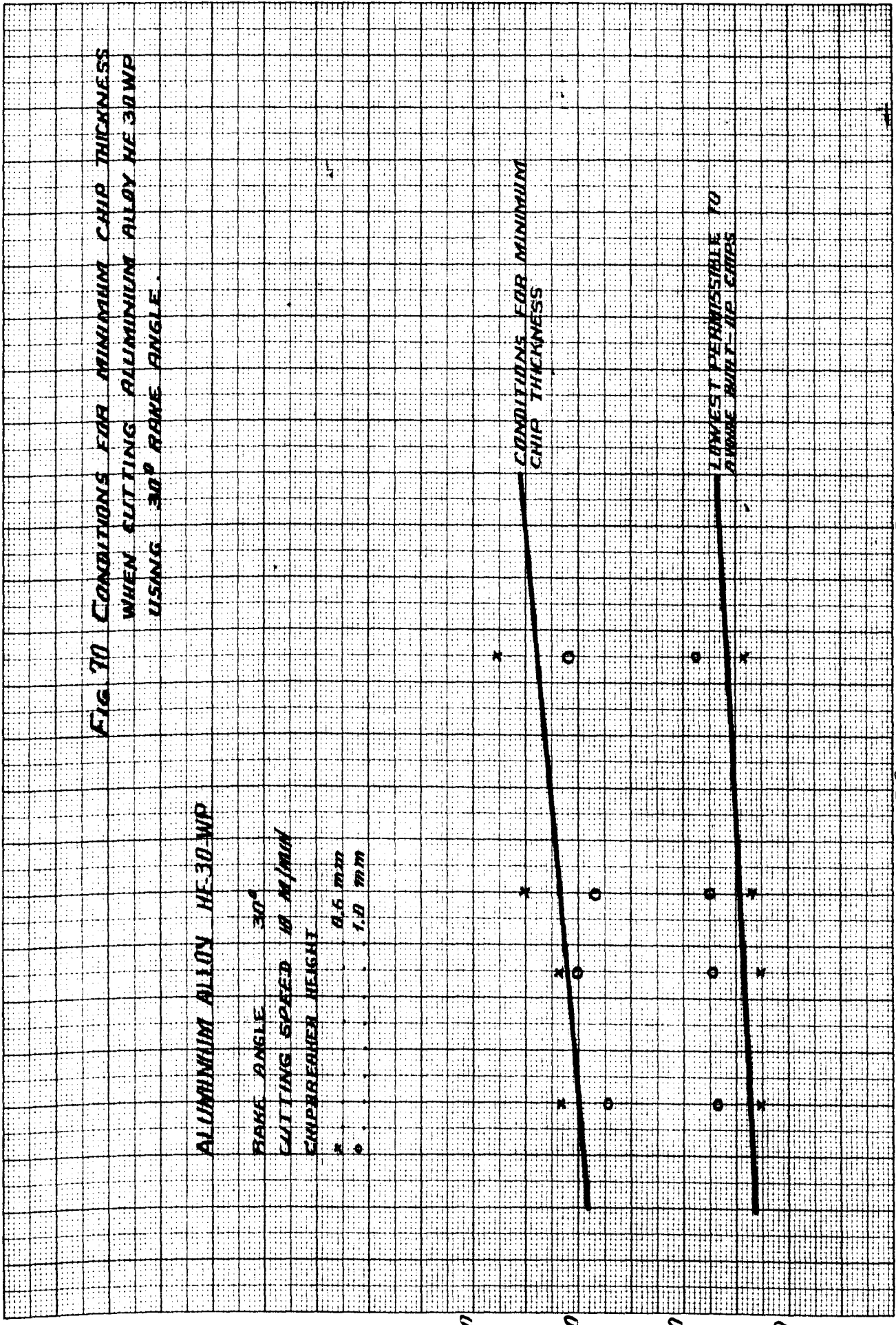


FIG. 71 CONDITIONS FOR MINIMUM CHIP THICKNESS WHEN CUTTING ALUMINUM ALLOY USING A 15° RAKE ANGLE

ALUMINUM ALLOY HE-30-WP

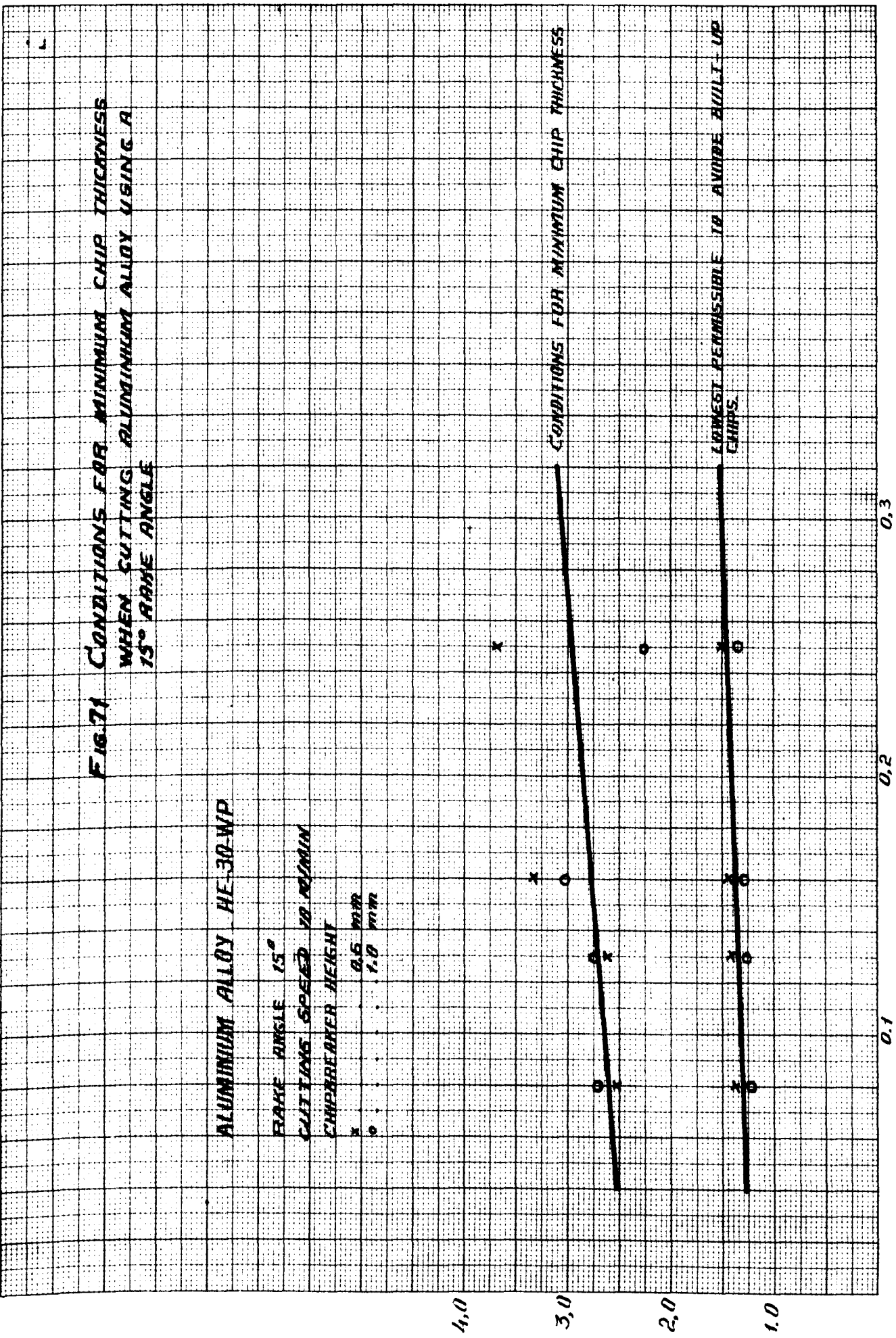
RAKE ANGLE 15°

CUTTING SPEED 10 M/S

CHIPBREAKER HEIGHT

x 0.5 mm

o 1.0 mm



FEED - S - mm/REV

CHIPBREAKER RATIO - w/h

**FIG 72 CONDITIONS FOR MINIMUM CUTTING FORCE
WHEN CUTTING ALUMINIUM ALLOY HE30 WP
USING 15° RAKE ANGLE**

ALUMINIUM ALLOY HE-30-WP

RAKE ANGLE 15°

CUTTING SPEED 1000 MIN

CHIPBREAKER HEIGHT

X 0.6 MM

o 1.0 MM

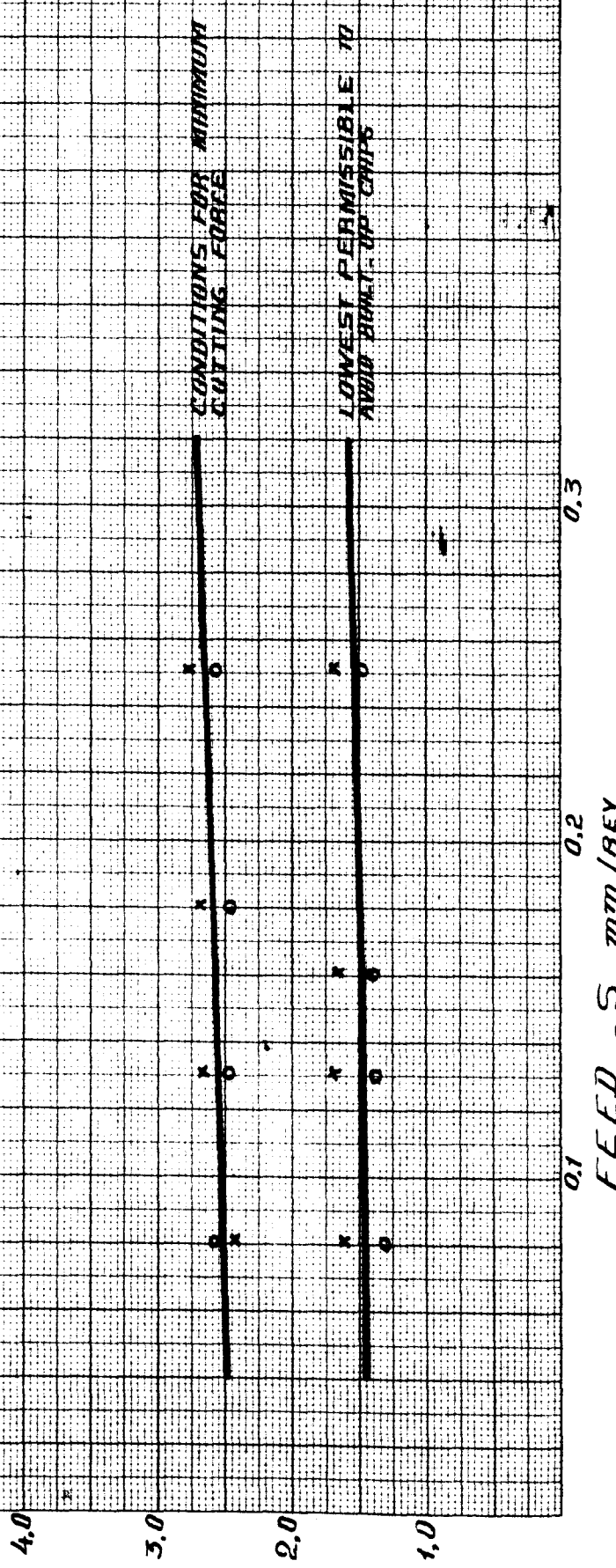


FIG. 73 CONDITIONS FOR MINIMUM CHIP THICKNESS WHEN CUTTING STEEL EN 1A USING 30° RAKE ANGLE.

STEEL EN-1A

RAKE ANGLE 30°

CUTTING SPEED 10 M/MIN

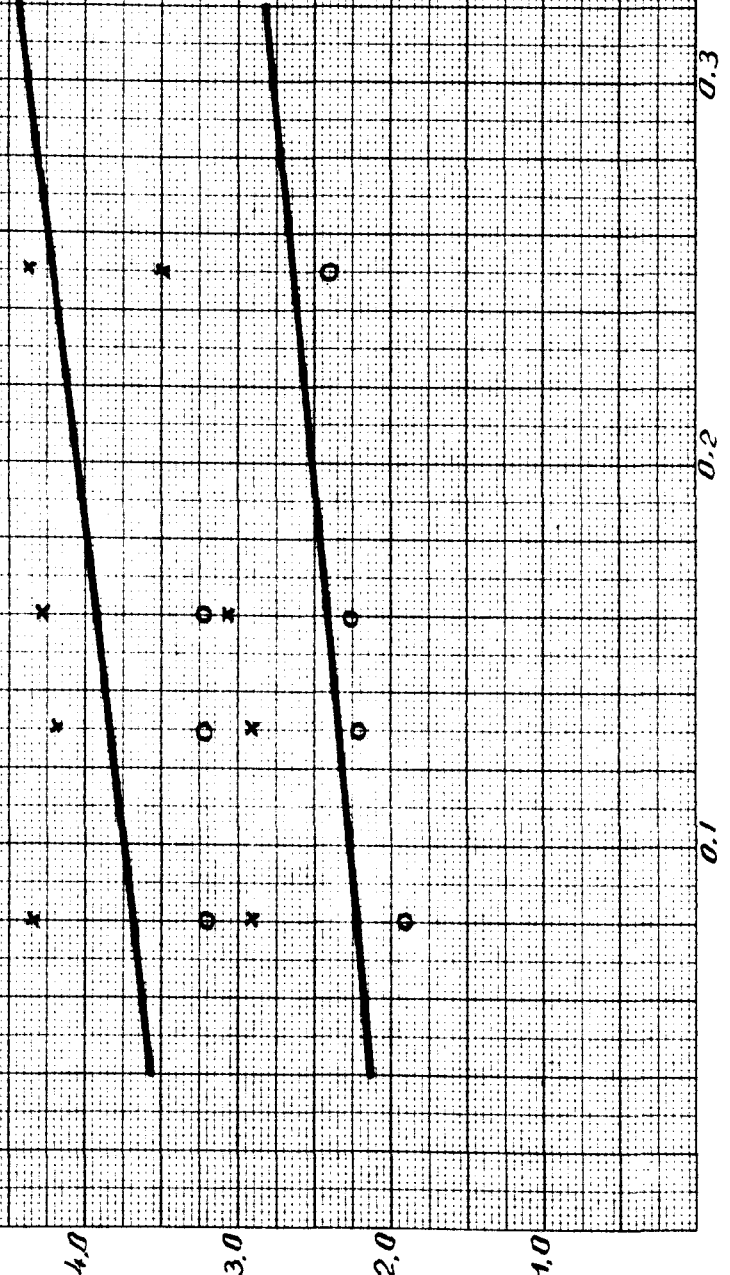
CHIPBREAKER HEIGHT

x 0.6 mm

o 1.0 mm

CONDITIONS FOR MINIMUM CHIP THICKNESS

LOWEST PERMISSIBLE TO AVOID BUILT UP CHIPS



CHIPBREAKER RATIO - W/H

FEED - S - mm/REV.

FIG. 74 CONDITIONS FOR MINIMUM CUTTING FORCE FOR STEEL EN 1A USING 30° RAKE ANGLE

STEEL EN1A

RAKE ANGLE 30

CUTTING SPEED 10 M/MIN

CHIPBREAKER HEIGHT

x 0.6 MM

o 1.0 MM

CHIPBREAKER RATIO-W/H

CONDITIONS FOR MINIMUM CUTTING FORCE

LOWEST PERMISSIBLE

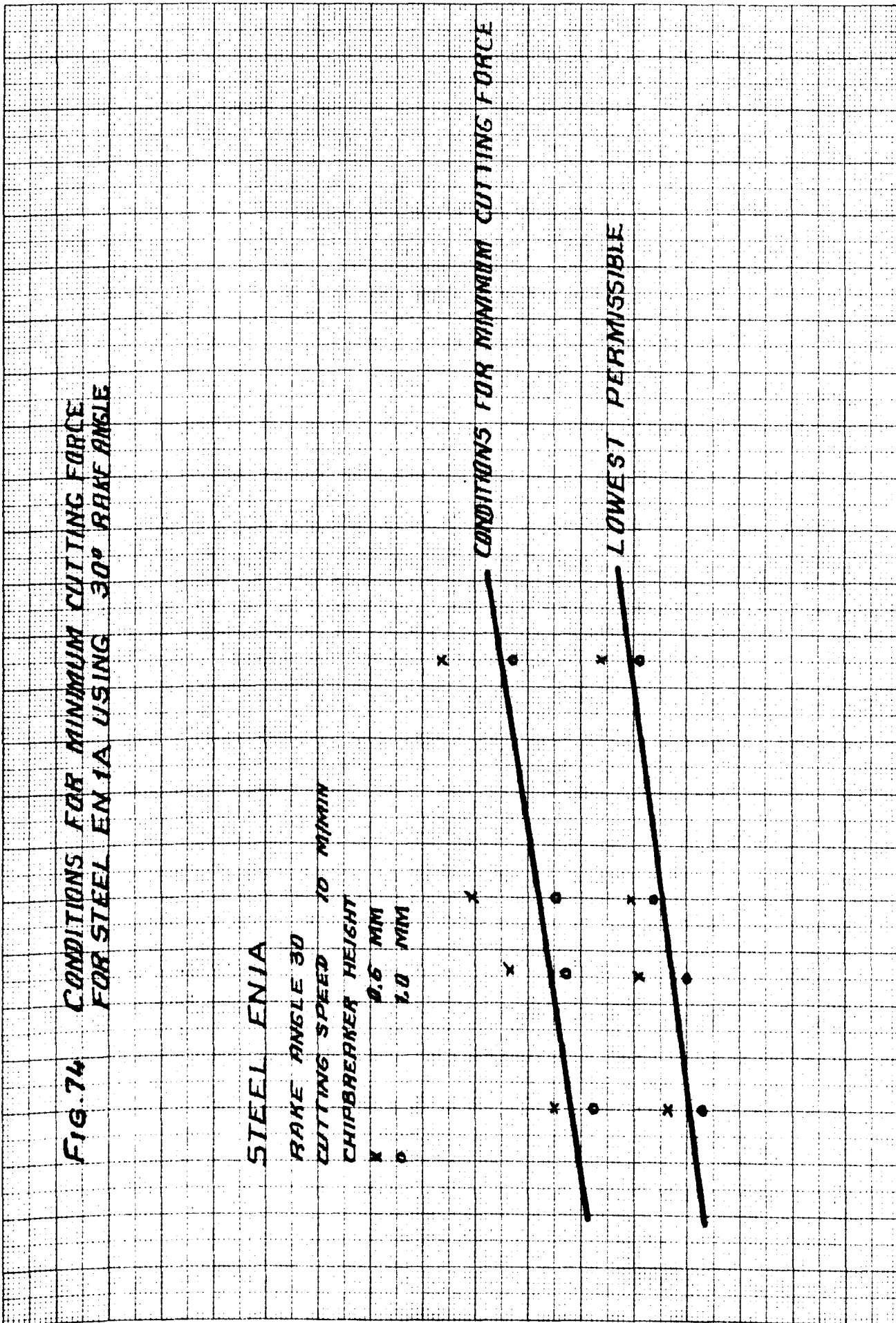
0.3

0.2

0.1

FEED - S - MM/REV.

5
4
3
2
1



Second Stage

This part of the investigation included the analysis of the experimental results obtained at high cutting speeds up to 100 m/min. Tests were performed on a lathe equipped with 12.5 HP main motor using a special tool holder fitted with highly polished sintered carbide tip (Fig. 33). Strain gauges were mounted on the shank of the tool holder to provide an accurate measurement of the vertical and horizontal components of the cutting force. Curves were plotted of cutting force and chip thickness versus distance of the chipbreaker wedge from the cutting edge (distance w Fig. 38). A set of results for aluminium alloy HE30WP cut at a speed up to 70 m/min using a tool of zero rake angle and a chipbreaker of 55° wedge angle (angle of the inclination of the chipbreaker face from the cutting face of the tool) are shown in Fig. 75. Similar to cutting at low cutting speeds the cutting forces (both the vertical and horizontal) as well as the chip thickness passed through a certain minimum value as the chipbreaker width was increased. From each curve in Figs. 75-77 two particular values of chipbreaker width may be selected. First value of chipbreaker width was taken to be the value at which cutting force and chip thickness reached minimum. The other value of the chipbreaker width was taken to be the value at which cutting force and chip thickness reached a level 10% higher than those obtained at very large width (virtually without chipbreaker). This value was taken first by assuming that if the cutting force (or chip thickness) is not increased by more than 10% the tool wear will not be significantly increased. During these tests, it was found that the number of regrinds required by the tool tip at those two conditions of cutting force were nearly the same. Therefore, the assumption made earlier was considered to be valid. The significance of the chipbreaker width at which the cutting force was 10% higher than those for large

74

FIG. 75 EFFECT OF VARIATION IN CHIPBREAKER WIDTH ON THE VERTICAL AND HORIZONTAL COMPONENTS OF THE CUTTING FORCE FOR ALUMINIUM ALLOY HE 30 WP USING A WEDGE ANGLE OF 55°.

66

10%
58

50

42

10%
34

34

VERTICAL

CUTTING MATERIAL - ALUMINIUM ALLOY - HE 30 WP

CUTTING CONDITIONS:

FEED	0.15 MM/R
DEPTH	5.0 MM
SPEED	
— (solid line)	70 M/MIN
— (dashed line)	35 M/MIN
— (dash-dot line)	20 M/MIN

TOOL GEOMETRY:

RAKE ANGLE	0 DEG.
CLEARANCE	8 DEG.
NOSE RADIUS	0 MM

CHIPBREAKER DESIGN:

CHIPBREAKER WEDGE ANGLE 55° WITH COOLANT

CONDITIONS FOR MINIMUM CUTTING FORCE

HORIZONTAL

CHIPBREAKER WIDTH - MM

CUTTING FORCE - KG.

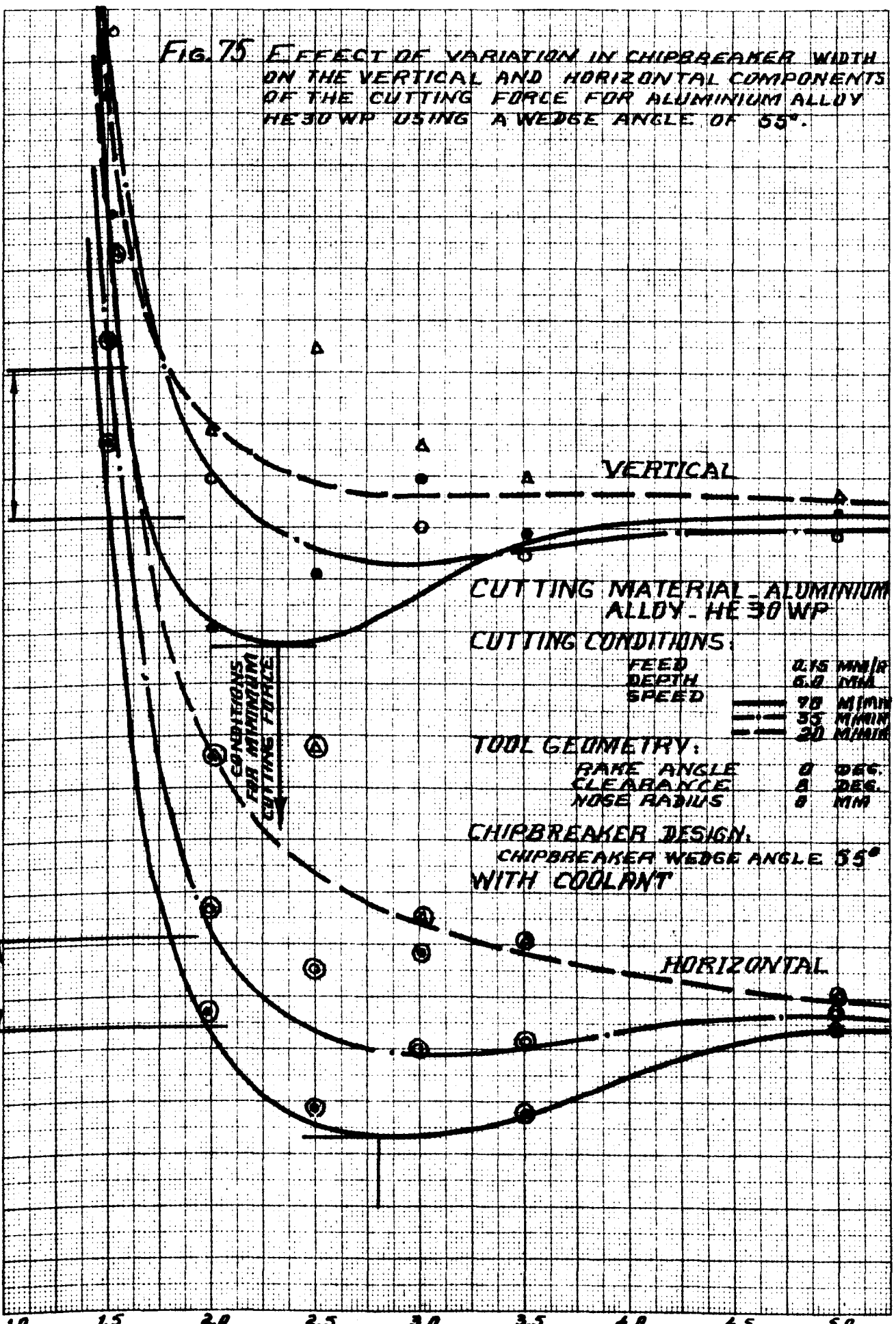
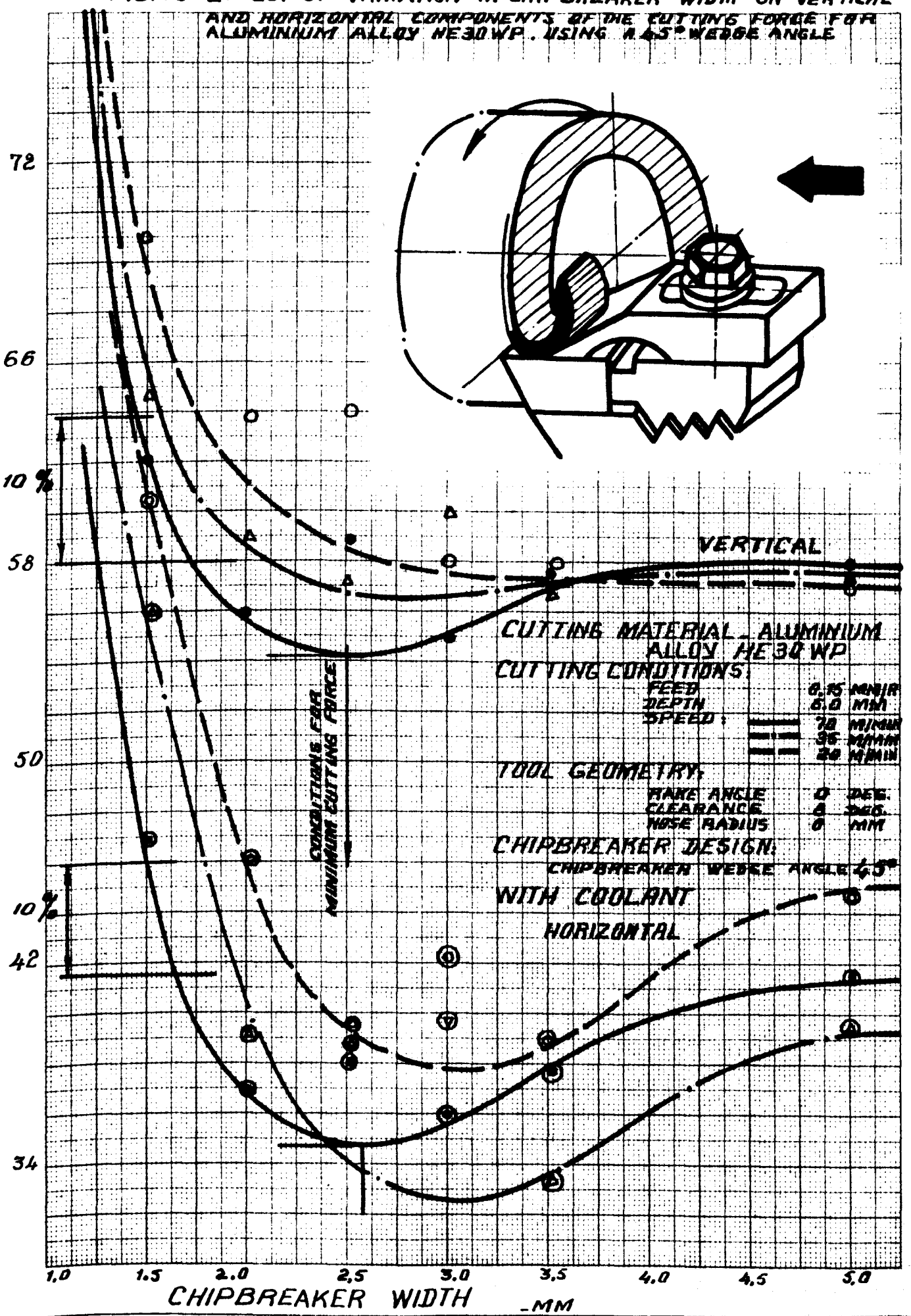


FIG. 76 EFFECT OF VARIATION IN CHIPBREAKER WIDTH ON VERTICAL AND HORIZONTAL COMPONENTS OF THE CUTTING FORCE FOR ALUMINIUM ALLOY HE30 WP. USING A 45° WEDGE ANGLE

CUTTING FORCE - KG.



CUTTING MATERIAL - ALUMINIUM ALLOY HE30 WP
CUTTING CONDITIONS:
 FEED 0.15 MM/R
 DEPTH 6.0 MM
 SPEED: ——— 70 M/MIN
 - - - - 35 M/MIN
 - · - · 20 M/MIN

TOOL GEOMETRY:
 RAKE ANGLE 0 DEG.
 CLEARANCE 0 DEG.
 NOSE RADIUS 0 MM

CHIPBREAKER DESIGN:
 CHIPBREAKER WEDGE ANGLE 45°
WITH COOLANT

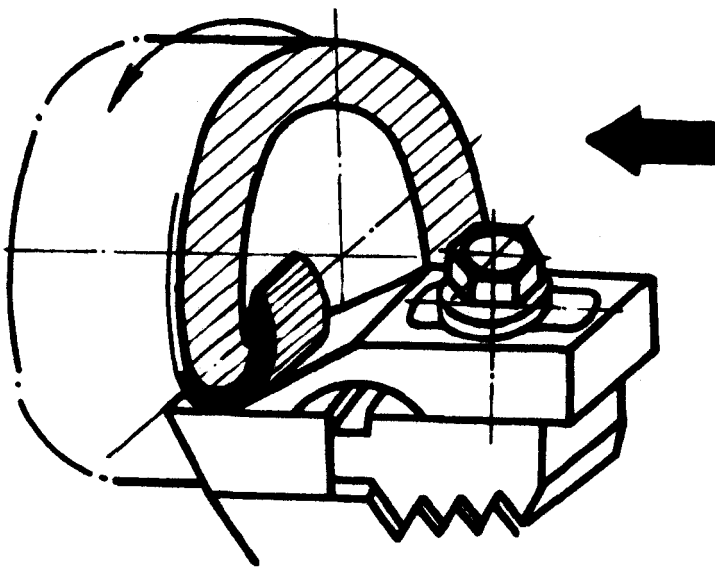
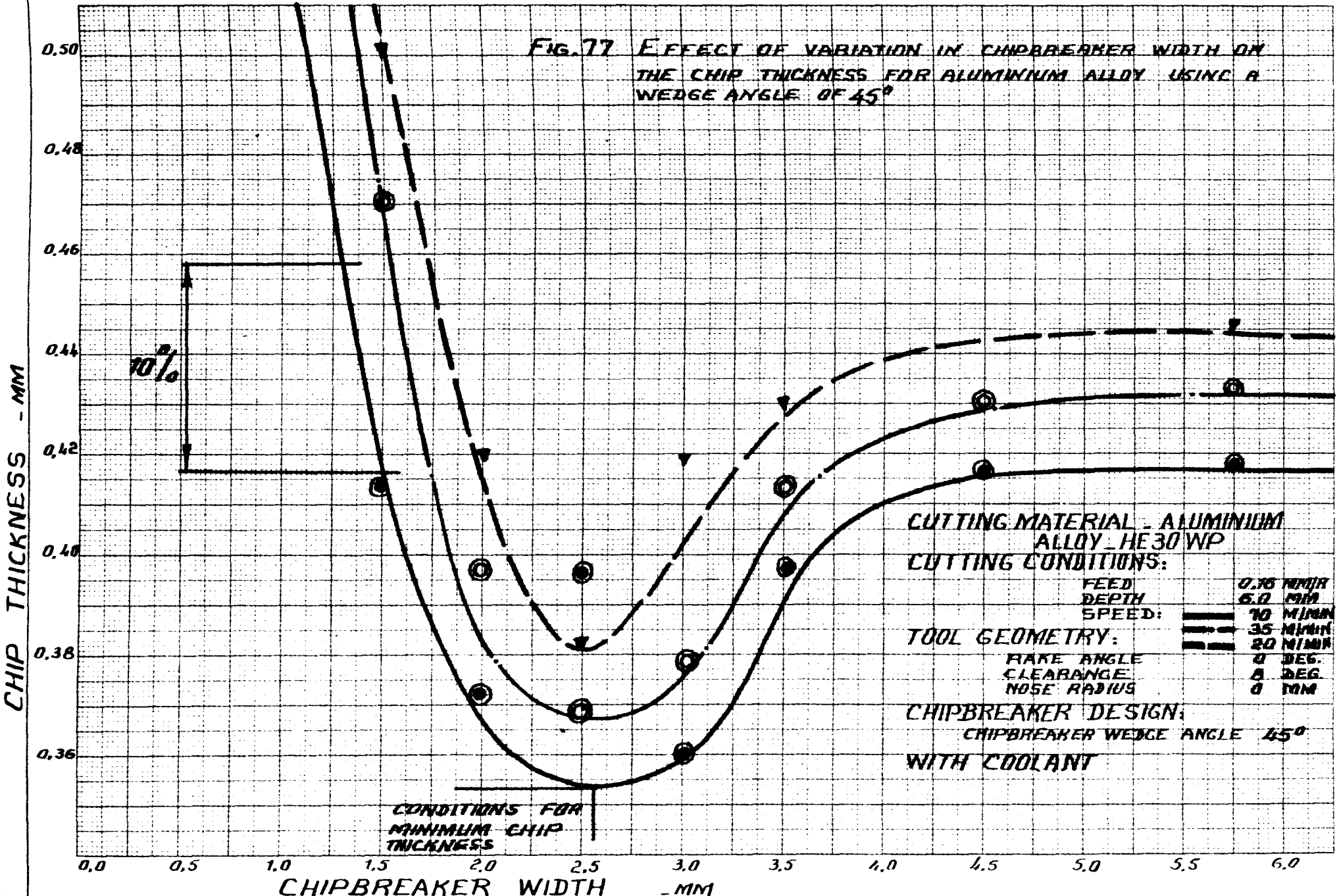


FIG. 77 EFFECT OF VARIATION IN CHIPBREAKER WIDTH ON THE CHIP THICKNESS FOR ALUMINIUM ALLOY USING A WEDGE ANGLE OF 45°



width was in producing good chipbreaking performance provided coolant was used to eliminate the appearance of the built-up edge and to reduce the danger of built-up chips. By examining the chips produced during these tests it was found that the tendency toward producing effectively broken chips was increased as the chipbreaker width approached the value corresponding to 10% increase in the cutting force. However, sometimes built-up and over-broken chips were produced at that value of the chipbreaker width. From Fig. 75 it can be seen that the conditions for both minimum cutting force and cutting force not exceeding 10% for the vertical component of the cutting force were obtained at a chipbreaker width slightly smaller than those for the horizontal component of the cutting force. Figs. 76 and 77 show the effect of the chipbreaker width on cutting forces and chip thickness for aluminium alloy using a 45° wedge angle. Curves shown in Figs. 76 and 77 are similar to those shown in Fig. 75. From Figs. 75 and 76 it can be pointed out that the ratio of chipbreaker width to feed for 55° wedge angle is slightly larger than that for 45° wedge angle. That means, in order to obtain good chipbreaking results, the chipbreaker wedge should be set closer to the cutting edge when using small wedge angles. From Fig. 75, for 55° wedge angle, the conditions for an increase in the cutting force not exceeding 10% was found to be $w/s \geq 10.5$ for the vertical force and $w/s \geq 12$ for the horizontal force. Similarly from Fig. 76 for 45° wedge angle, the conditions for an increase in the cutting force not exceeding 10% was found to be $w/s \geq 9.2$ for the vertical force and $w/s \geq 10.0$ for horizontal force. However, the numerical values for lower speeds were slightly higher. From Figs. 75 and 76 it is clear that the cutting forces increase with a decrease in the wedge angle. That is explained by

the fact that the length of the chipbreaker contact increases with the reduction in the wedge angle. However, extremely large wedge angles may obstruct the chip flow. Experimental results obtained when cutting steel EN1A using a chipbreaker wedge angle of 45° , Figs. 78-79, show that conditions for cutting force not exceeding 10%, was obtained at a slightly larger ratio w/s for both vertical and horizontal force ($w/s \geq 10.5$ for vertical force and $w/s \geq 12$ for horizontal force) than those obtained for aluminium alloy HE30WP. The coolant was found to be very effective in promoting good chip-breaking and at some small chipbreaker width it was not possible to work without coolant. Such an effect of coolant was explained by the fact that it was responsible for the elimination of the built-up edge, and reduction in the friction and temperature effects. On the basis of these experimental results it may be concluded for this type of clamped wedge chipbreaker that, in order to obtain satisfactory chipbreaking, the chipbreaker wedge need not only to be set at a certain distance w , which can be expressed as some multiple of the feed s , depending on the material being cut, but also to have a certain angle of the inclination of the chipbreaker face (wedge angle) taken in accordance with (w) .

To establish the performance of the ground step chipbreakers, different chipbreaker dimensions were tested with different materials at cutting speeds up to 100 m/min. Figs. 80-83 show some results of the experimental tests for aluminium alloy HE30WP and steel EN1A obtained at the conditions mentioned using coolant. Similar to those results obtained at low cutting speed, the chipbreaker width was found to be the most important parameter in controlling the chipbreaking process. The chipbreaker height, feed and cutting speeds were found to have a similar effect to those at low cutting speeds.

FIG. 78 EFFECT OF VARIATION IN CHIPBREAKER WIDTH ON THE VERTICAL AND HORIZONTAL COMPONENTS OF THE CUTTING FORCE FOR STEEL ENIA USING A WEDGE ANGLE OF 45°.

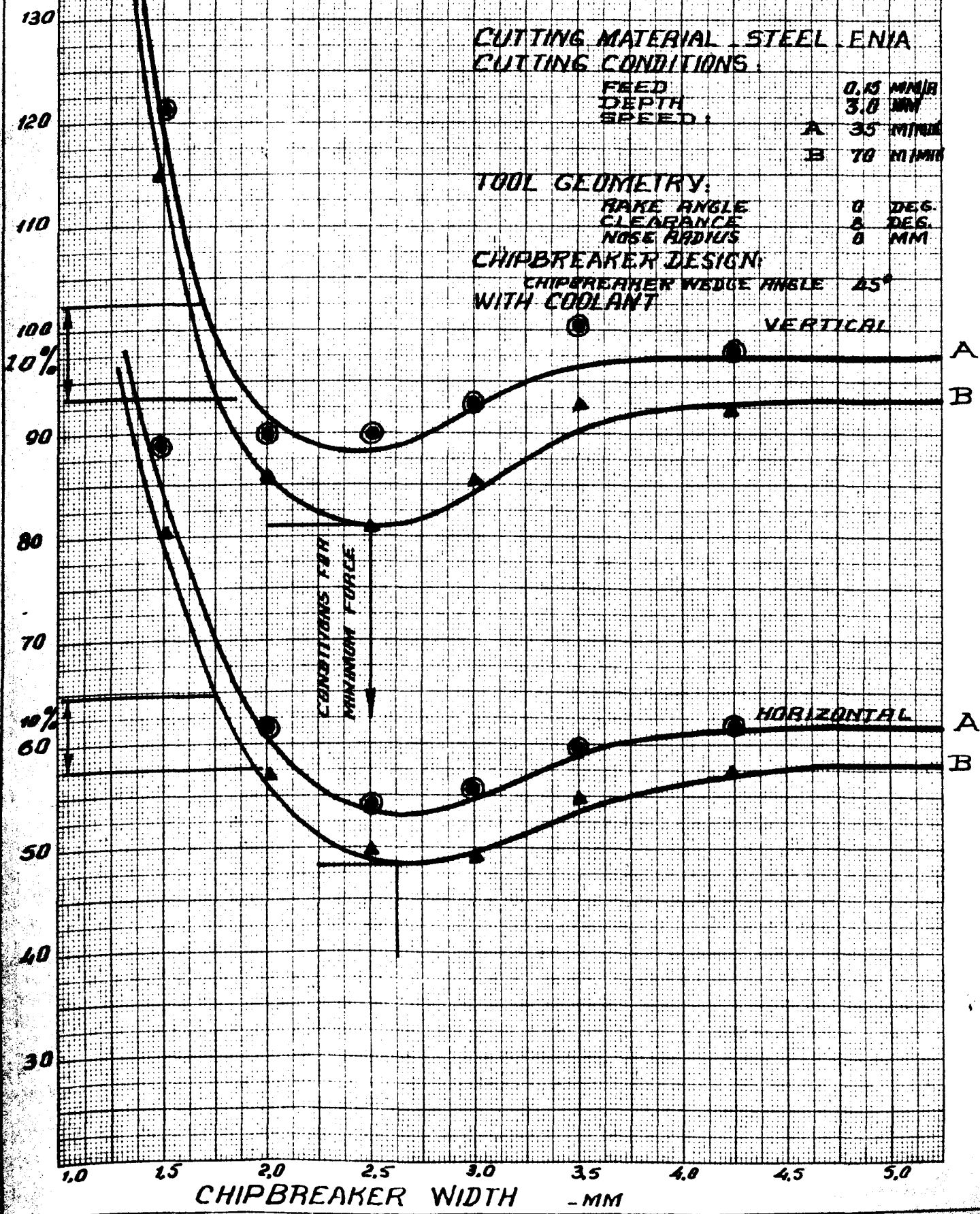


FIG. 79. EFFECT OF VARIATION IN CHIPBREAKER WIDTH ON THE CHIP THICKNESS FOR STEEL ENIA USING A WEDGE ANGLE OF 45°.

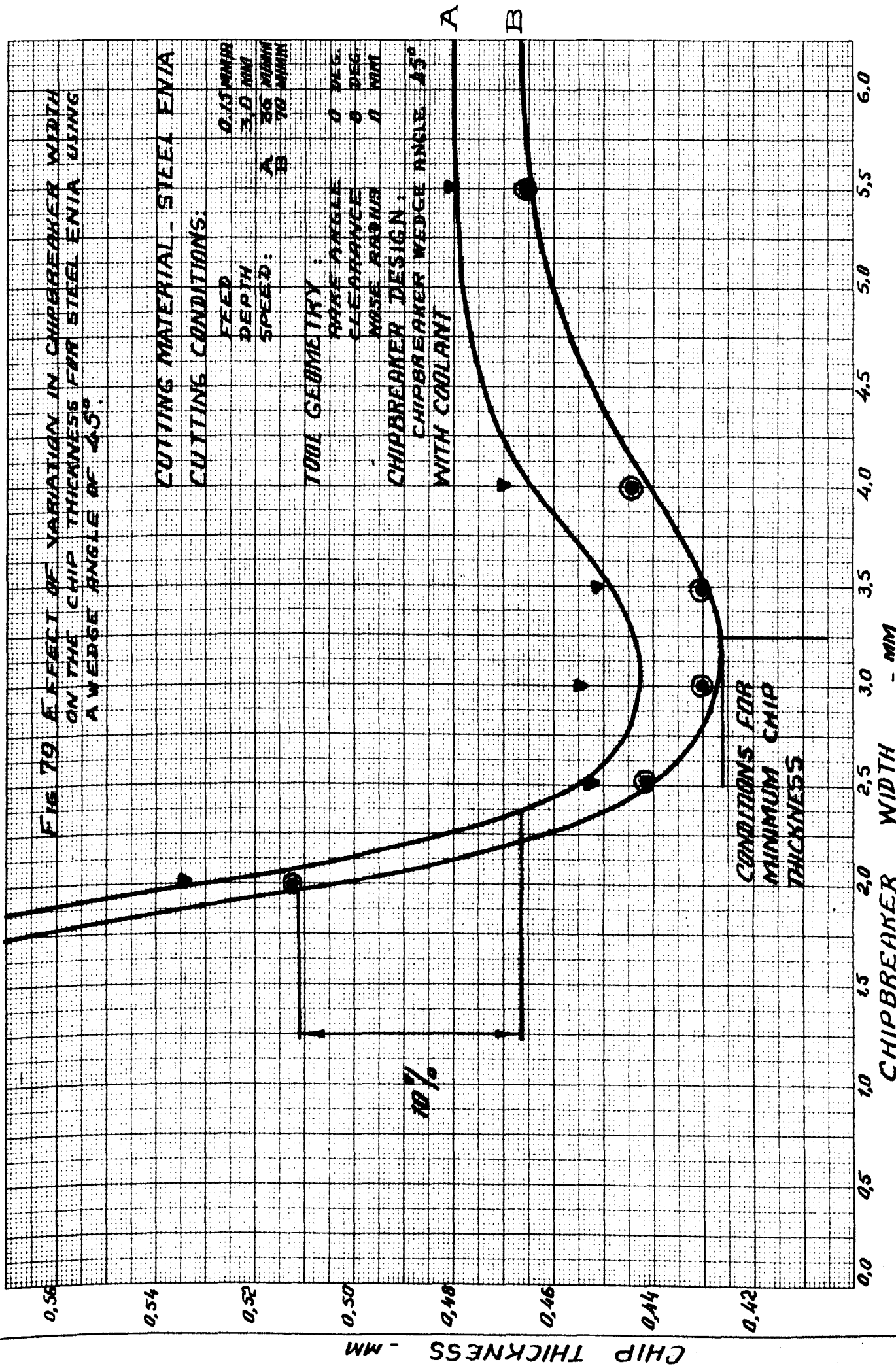


FIG. 80 EFFECT OF VARIATION IN CHIPBREAKER WIDTH ON CUTTING FORCE (VERTICAL) FOR ALUMINIUM ALLOY HE30 WP USING A STEP TYPE CHIPBREAKER AND A RAKE ANGLE OF 30°

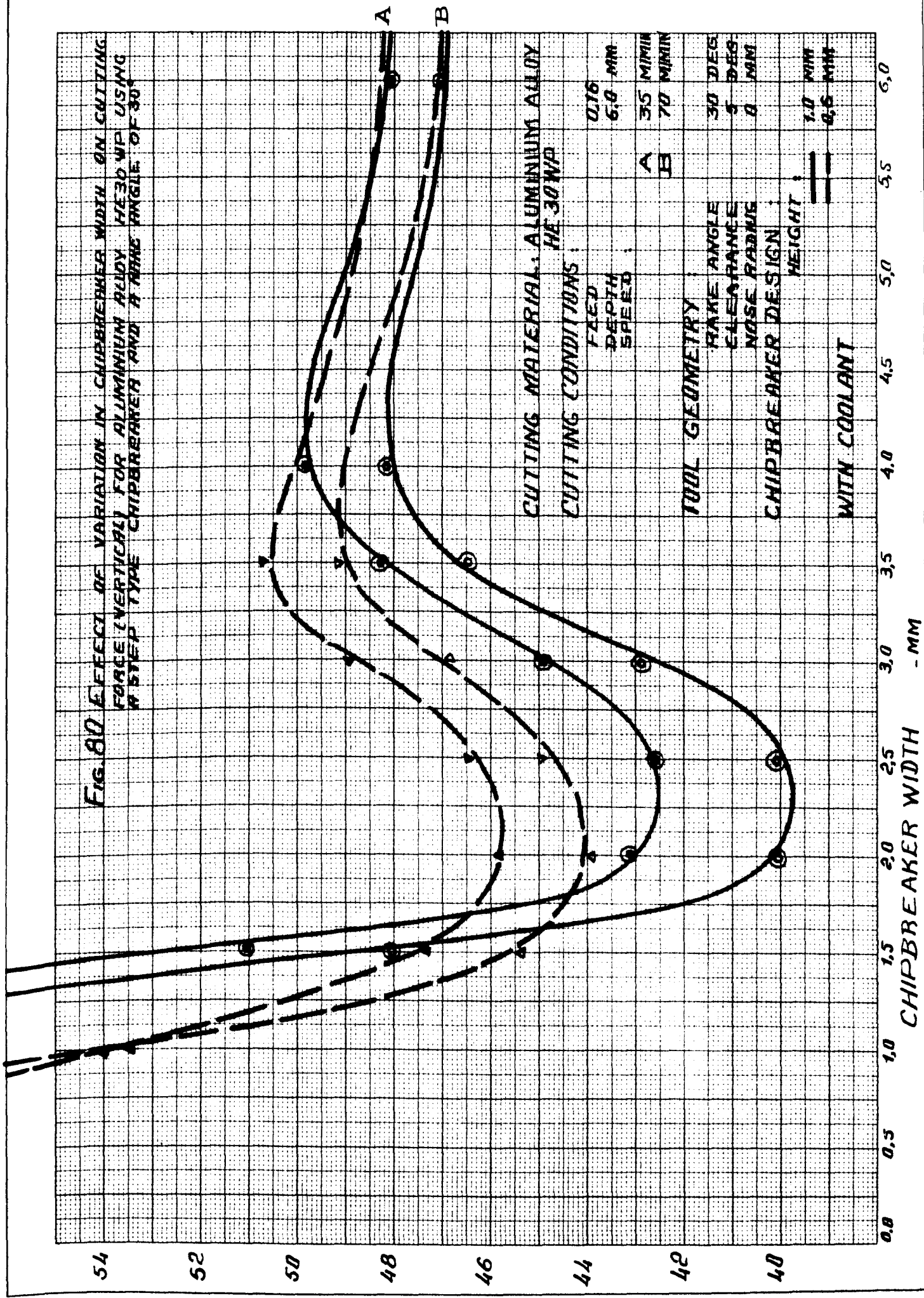


FIG. 81 EFFECT OF VARIATION IN CHIPBREAKER WIDTH ON THE CHIP THICKNESS FOR ALUMINUM ALLOY HE30 WP USING A STEP TYPE CHIPBREAKER AND A RAKE ANGLE OF 30°

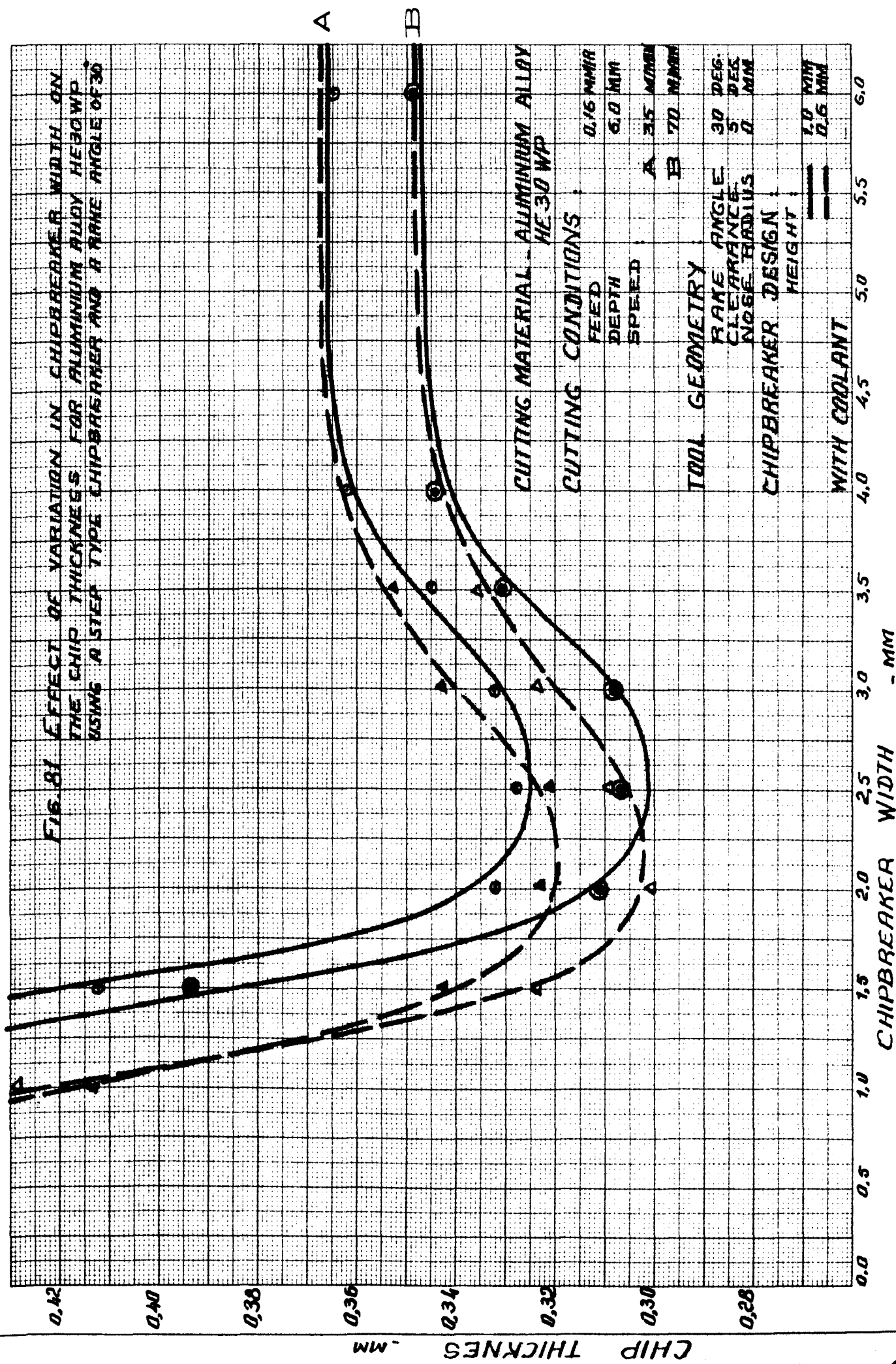


FIG. 82 EFFECT OF VARIATION IN CHIPBREAKER WIDTH ON CUTTING FORCE (VERTICAL) FOR STEEL ENIA USING A STEP TYPE CHIPBREAKER AND RAKE ANGLE OF 30°

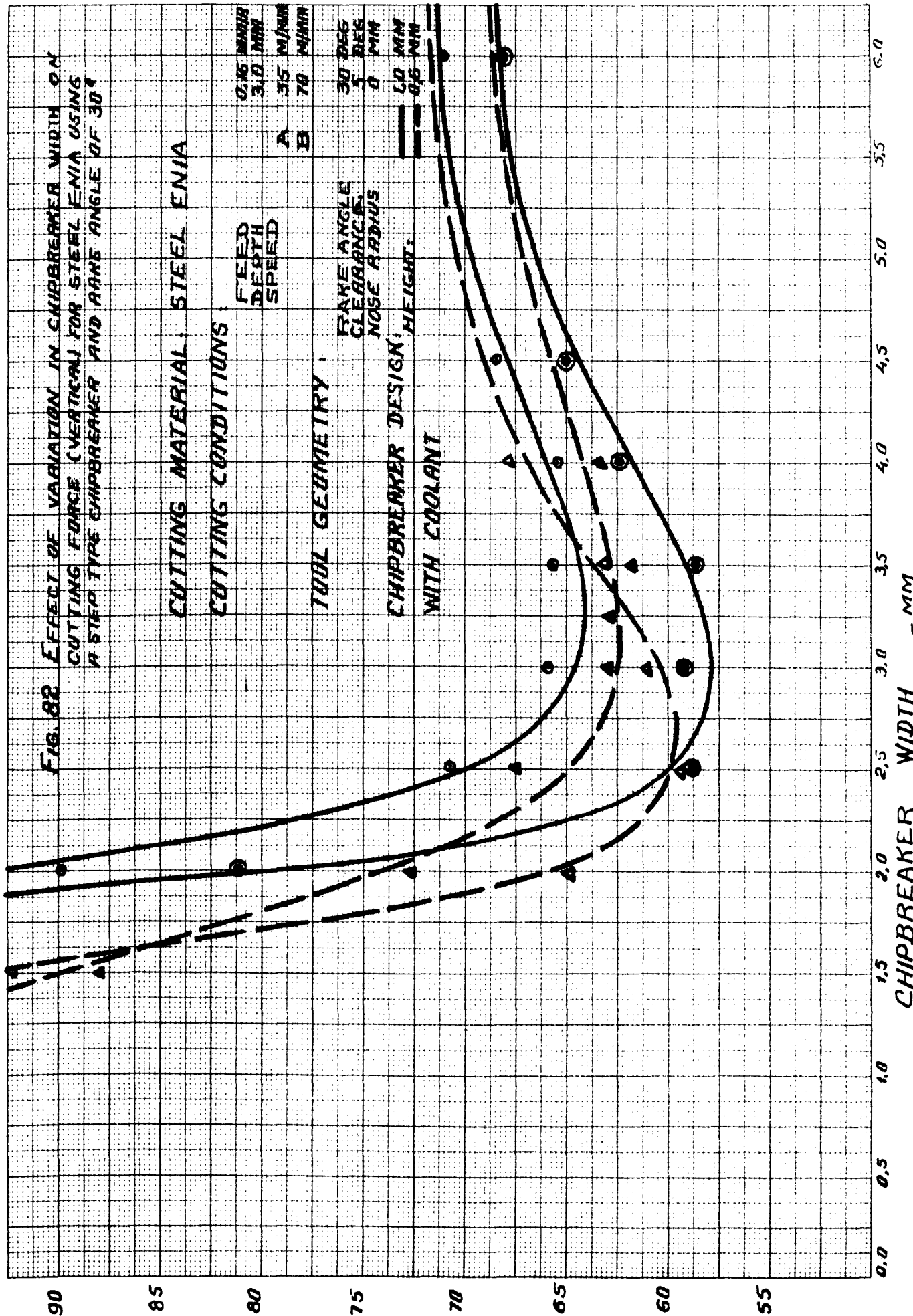
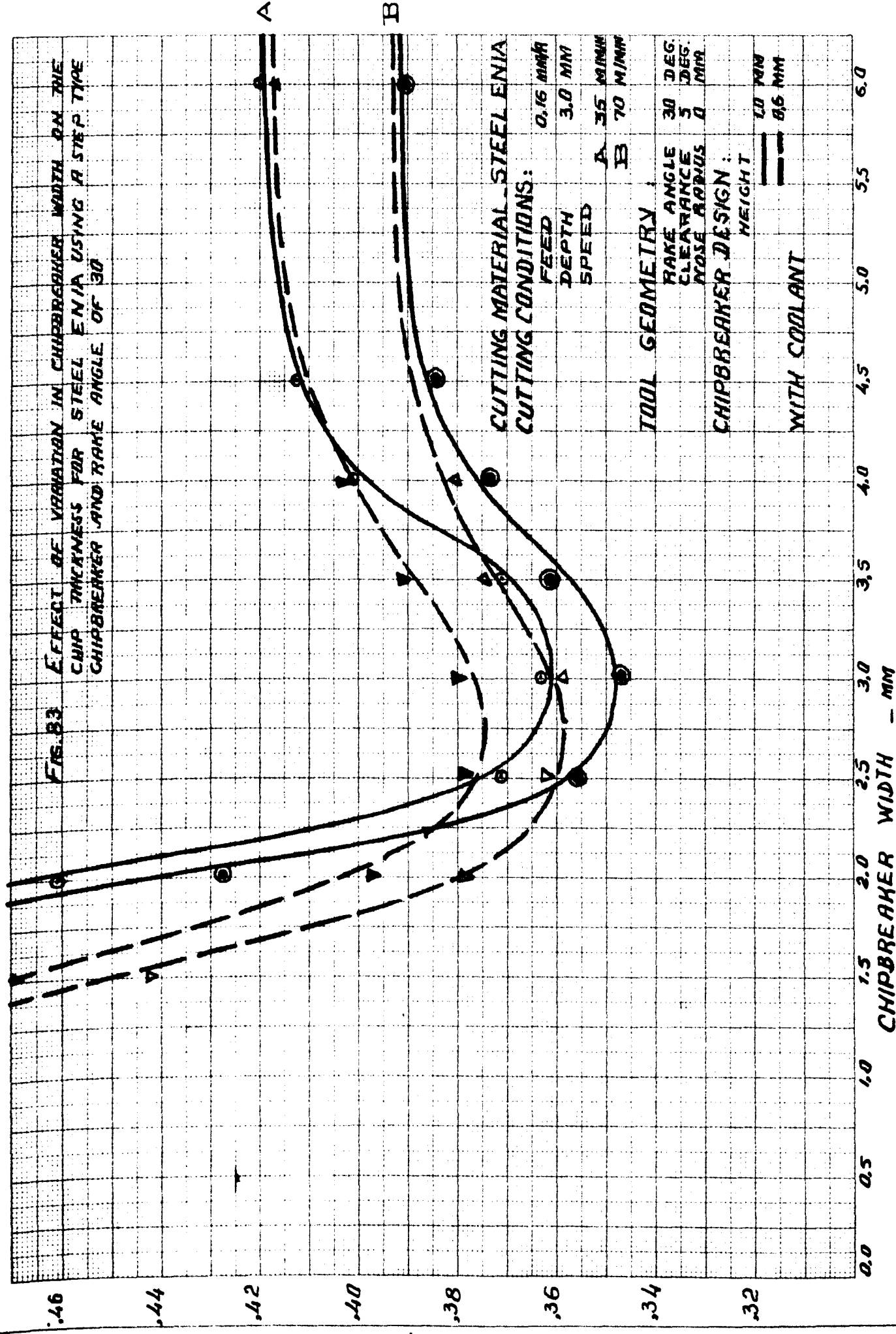


FIG. 83 EFFECT OF VARIATION IN CHIPBREAKER WIDTH ON THE CHIP THICKNESS FOR STEEL ENIA USING A STEP TYPE CHIPBREAKER AND RAKE ANGLE OF 30



CHIP THICKNESS - MM

CHIPBREAKER WIDTH - MM

CUTTING MATERIAL - STEEL ENIA
 FEED 0.16 MM/R
 DEPTH 3.0 MM
 SPEED A 35 M/MIN
 B 70 M/MIN

TOOL GEOMETRY

RAKE ANGLE 30 DEG.
 CLEARANCE 5 DEG.
 NOSE RADIUS 0 MM

CHIPBREAKER DESIGN:

HEIGHT

1.0 MM
 0.6 MM

WITH COOLANT

4.1.2 Summary of Some of the Experimental Results

It was a part of this investigation to make the task of chip control as easy as possible for the machine operator. A solution was found to the problem of chip breaking within the conventional cutting conditions. A simple method of finding the dimensions of the chipbreaker was found. Different types of chips were produced from different materials using different geometries of the chipbreaker. The chip thickness and the chip curl radius were carefully measured with a micrometer. Different regions of chip breaking were recognised such as over-broken and built-up chips (the chip length < 5 mm). (This type of chip is not recommended mainly due to the reduced tool life or some times breakage of the tool as a result of increased cutting force), effectively broken (up to 30 mm), broken (over 30 mm) and no chip breaking region. The recommended type was found to be the effectively broken chips. The chips of up to 30 mm long produced within the effectively broken region ensures satisfactory chip removal.

In order to find the optimum chipbreaker width which would give a reliable chip breaking it was necessary to have a diagram of the chip breaking effectiveness (that means the chip breaking degree in relation to the chip curl radius/feed ratio). In accordance with that a series of tests were carried out on aluminium alloy HE30WP and steel EN1A at different cutting conditions and with different tool geometries. As a result, chip breaking effectiveness was established for aluminium alloy HE30WP and steel EN1A. Figs. 53-54 show the chip breaking effectiveness for aluminium alloy HE30WP and steel EN1A respectively using a rake angle of 15° and cutting speeds of up to 100 m/min. From Figs. 53-54 it can be seen that in order to obtain effectively broken chips the chip curl radius should have a certain value which is some fixed multiple of the feed. Accordingly

the chip breaking effectiveness would best be represented by the ratio of the chip curl radius to feed (R_c/S). The reason that the ratio of R_c/S was considered to represent the chip breaking effectiveness is based on the experimental evidence derived from Figs. 53-54, and which show that all points corresponding to lines $R_c/S = 20$ for steel EN1A and $R_c/S = 25$ for aluminium alloy HE30WP, give effectively broken chips. By taking into consideration the characteristic ratios of chip curl radius and feed at which effectively chip breaking was obtained (namely $R_c/S = 25$ for aluminium alloy HE30WP and $R_c/S = 20$ for steel EN1A), charts shown in Figs. 84 and 85 were arranged for the conditions mentioned, so that to provide a speedy method of finding the dimensions of the ground step chipbreaker. An example of finding the dimensions of the chipbreaker is shown in each chart.

To use any of those charts suppose, for example, we want to obtain an effectively broken chip when cutting steel EN1A at a cutting speed of 70 m/min with a feed rate of 0.2 mm/rev. and depth of cut of 3 mm using a rake angle of 15° . According to the chart (Fig. 85) for steel EN1A we start from the point corresponding to the feed 0.2 mm/rev., and move horizontally till the intersection with the characteristic line of effectively broken chips ($R_c/S = 20$). The projection of that point will give the chip curl radius. In this example the bending radius of the chip curl is 4 mm. According to equation (3.26) this chip curl radius for a chipbreaker height of 0.7 mm corresponds to a chipbreaker width of 2.46mm. That means in order to obtain effectively broken chips for the conditions mentioned the chipbreaker step of 0.7 mm high should be grounded at a distance of 2.46mm from the cutting edge. Charts shown in Figs. 84 and 85 are of significant help to the operator and therefore it is reasonable to suggest that similar charts should be available for the conditions used in any particular work shop in order to obtain satisfactory chip breaking

FIG. 84 CHART FOR GROUND STEP
CHIPBREAKER DIMENSIONS

ALUMINIUM ALLOY HE30WP

CUTTING SPEED
100 M/MIN
RAKE ANGLE
15° DEG.
DEPTH OF CUT
6.0 MM

100 M/MIN
15° DEG.
6.0 MM

$R = 255$

$$\frac{1}{R} = C_1 \frac{H}{(d - \epsilon)^2} - C_2 \frac{1}{S}$$

($C_1 = 1.52, C_2 = 0.03$)
 $\epsilon = 0.35$

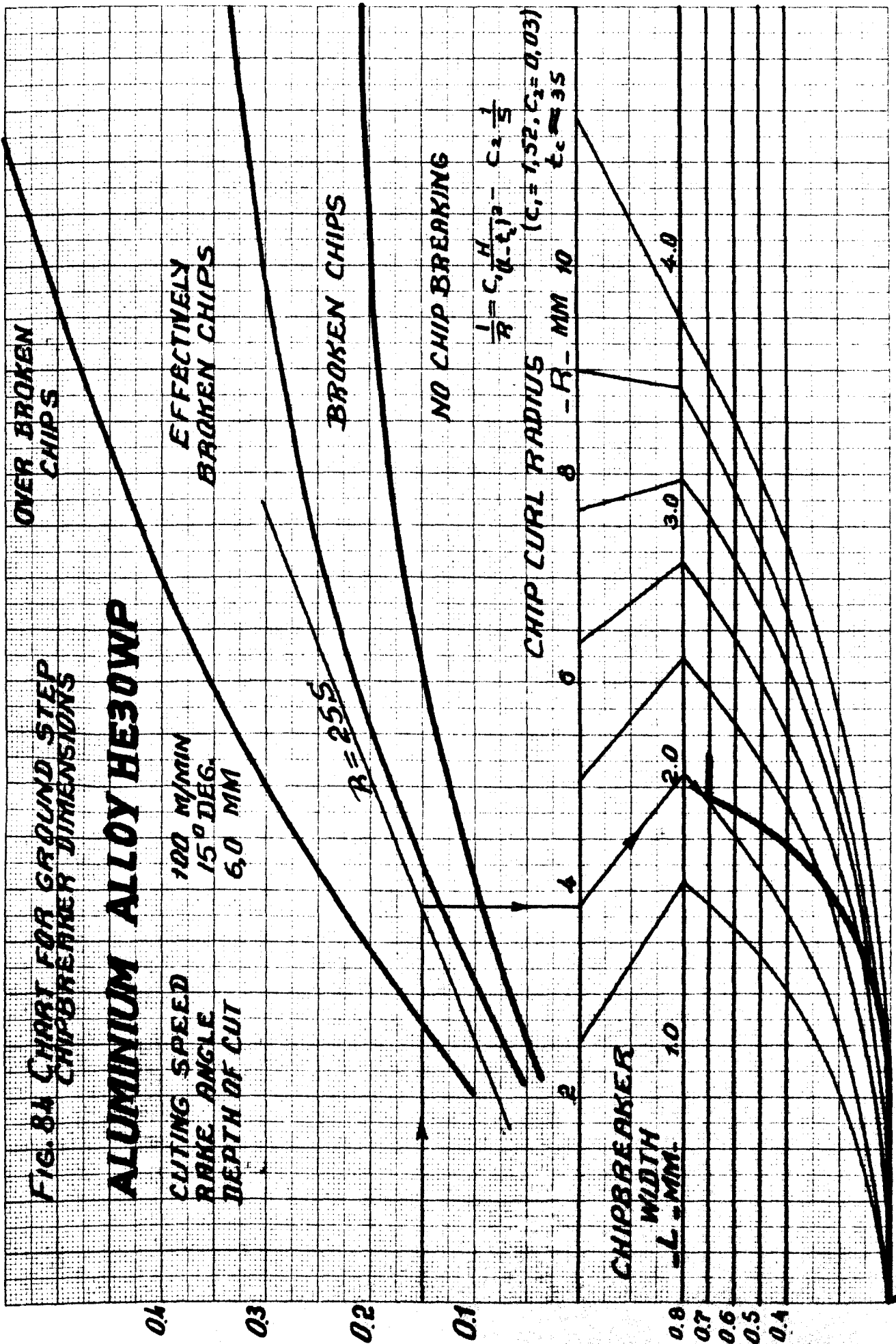


FIG. 85 CHART FOR GROUND STEP
CHIPBREAKER DIMENSIONS

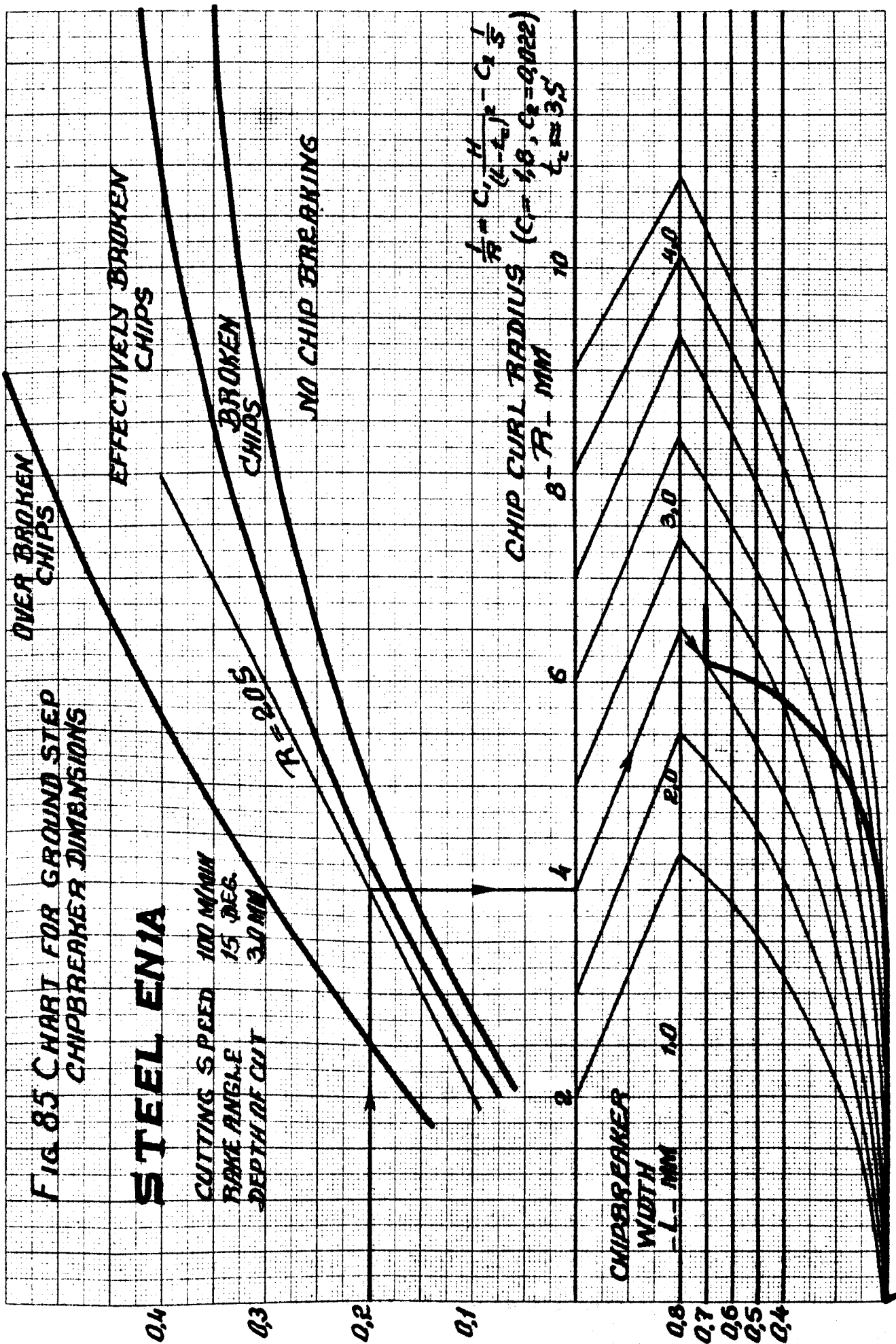
STEEL ENIA

CUTTING SPEED 100 M/MIN
 rake angle 15 DEG.
 DEPTH OF CUT 3.0 MM

R = 0.05

$$\frac{1}{R} = C_1 \frac{H}{(4 - t_c)^2} - C_2 \frac{1}{S}$$

CHIP CURL RADIUS (C₁ = 1.8, C₂ = 0.022)
 t_c = 3.5



CHIPBREAKER HEIGHT - H - MM FEED - S - MM/REV

CHIPBREAKER
WIDTH
- L - MM

2

3

4

6

8

10

0.4

0.3

0.2

0.1

0.8

0.7

0.6

0.5

0.4

results. It is important to mention that charts of this form were first developed by Henriksen⁽⁷¹⁾. However, the charts shown in Figs. 84-85 which were obtained for materials and conditions specified on them are different from those used by Henriksen, in that different approach was made for the arrangement and determination of the results.

It is significant to mention that these charts are strictly recommended for the conditions mentioned on them, and any change in any parameter affecting the cutting process (such as approach angle) will give different results.

During this work many other experimental tests were carried out such as tests on different chipbreaker wedge configuration (Fig. 86), and other shapes of the ground chipbreaker. However, it was suggested that there is no need for showing all the experimental results obtained during this investigation, and a typical example will suffice.

4.2 DEDUCTIONS FROM THE ANALYSIS OF THE EXPERIMENTAL RESULTS

4.2.1 Deductions from the Analysis of the Experimental Results Obtained at Low Cutting Speeds

1. The chip thickness as well as the cutting forces will have minimum values at a certain chipbreaker width, Figs. 55-69.
2. For ground step chipbreakers the width of the chipbreaker at which the chip thickness and the cutting force are minimum depends to a great extent on the height of the chipbreaker, Figs. 55-69.
3. The change in cutting speed up to 10 m/min has no significant effect on the optimum chipbreaker width at which chip thickness and cutting force are minimum, Fig. 55.
4. The chipbreaker width at which chip thickness and cutting force are minimum cannot be considered as the best from chip breaking point of view. However, for best chip breaking results the chipbreaker might need to be set closer to the cutting edge.

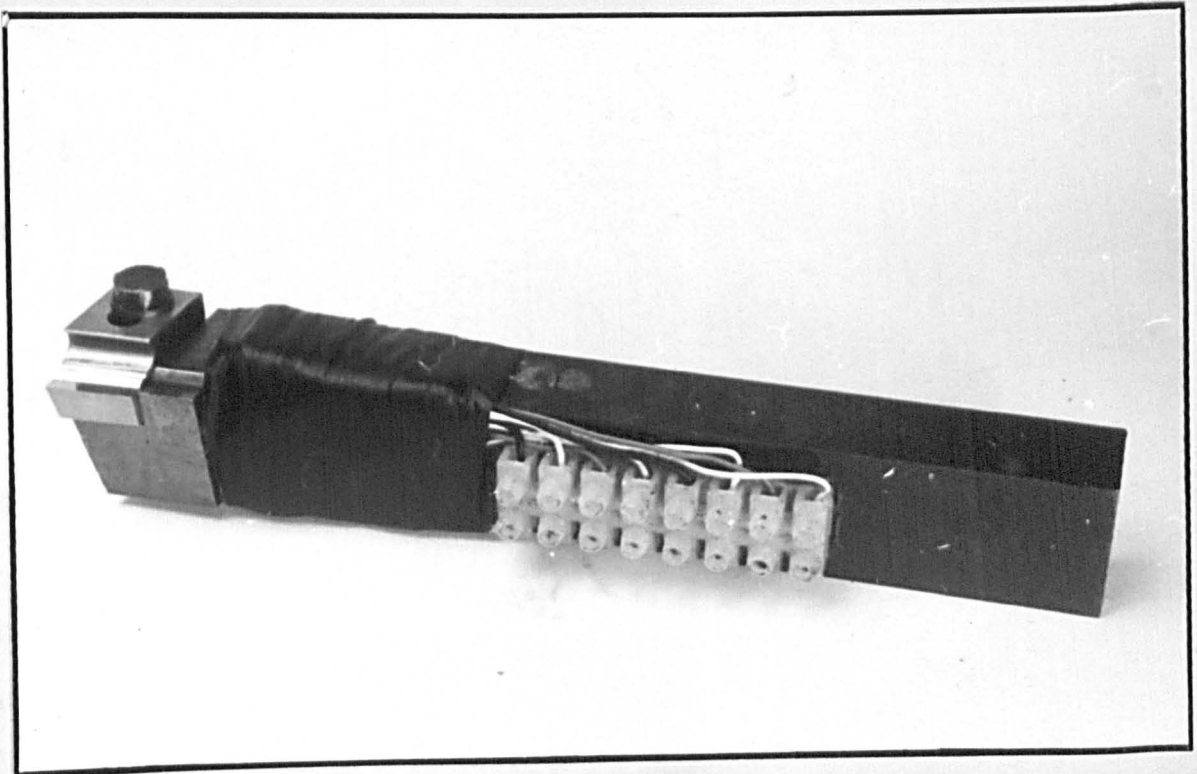
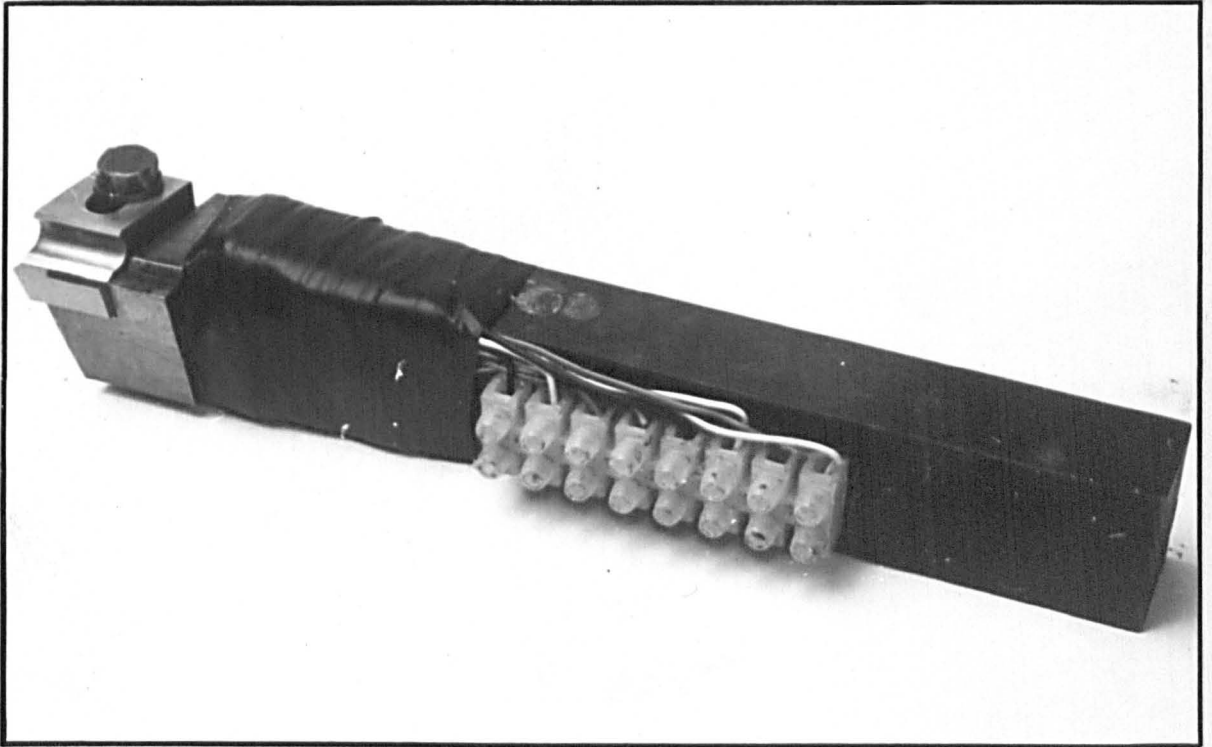


FIG. 86

5. The optimum chipbreaker width at which chip thickness and cutting force are minimum is related to the feed, Figs. 55-69. The chipbreaker width reduces with the reduction in feed.
6. Positive rake angles over 8° have no significant effect on the chip thickness. However, negative rake angles will greatly increase the chip thickness, and cutting force, Fig. 87.
7. The range of continuous chips was found to increase with increase in rake angle.
8. Negative rake angles are characterised by the production of discontinuous chips, and reduced tool life caused by the extreme conditions of high cutting force and temperature at the cutting zone.
9. The materials were found to fall in the following order in decreasing the size of the range of discontinuous chips:
Aluminium alloy HE30WP
Steel EN1A
10. The use of chipbreakers may give a reliable chip breaking with lower forces on the cutting tool.
11. The change in the cutting force and chip thickness may be explained in terms of changes in the mean coefficient of friction of the chip-tool contact.
12. The additional cutting force and change in chip thickness are to some extent affected by the amount of bending of the chip.
13. Coolant is considered to be helpful in promoting effective chip breaking, due to the elimination of the built-up edge.
14. Chip breaking is bounded by the conditions of lowest permissible chipbreaker proportions to avoid the appearance of the over-broken and built-up chips, Figs. 70-74.

ALUMINUM ALLOY HE 30 WP

CUTTING SPEED \bullet : 10 M/MIN
 FEED \bullet : 5 M/MIN
 DEPTH OF CUT \bullet : 0.13 MM/8
 CHIPBREAKER WIDTH \bullet : 6.0 MM
 CHIPBREAKER HEIGHT \bullet : 0.6 MM
 CHIPBREAKER HEIGHT \bullet : 1.5 MM

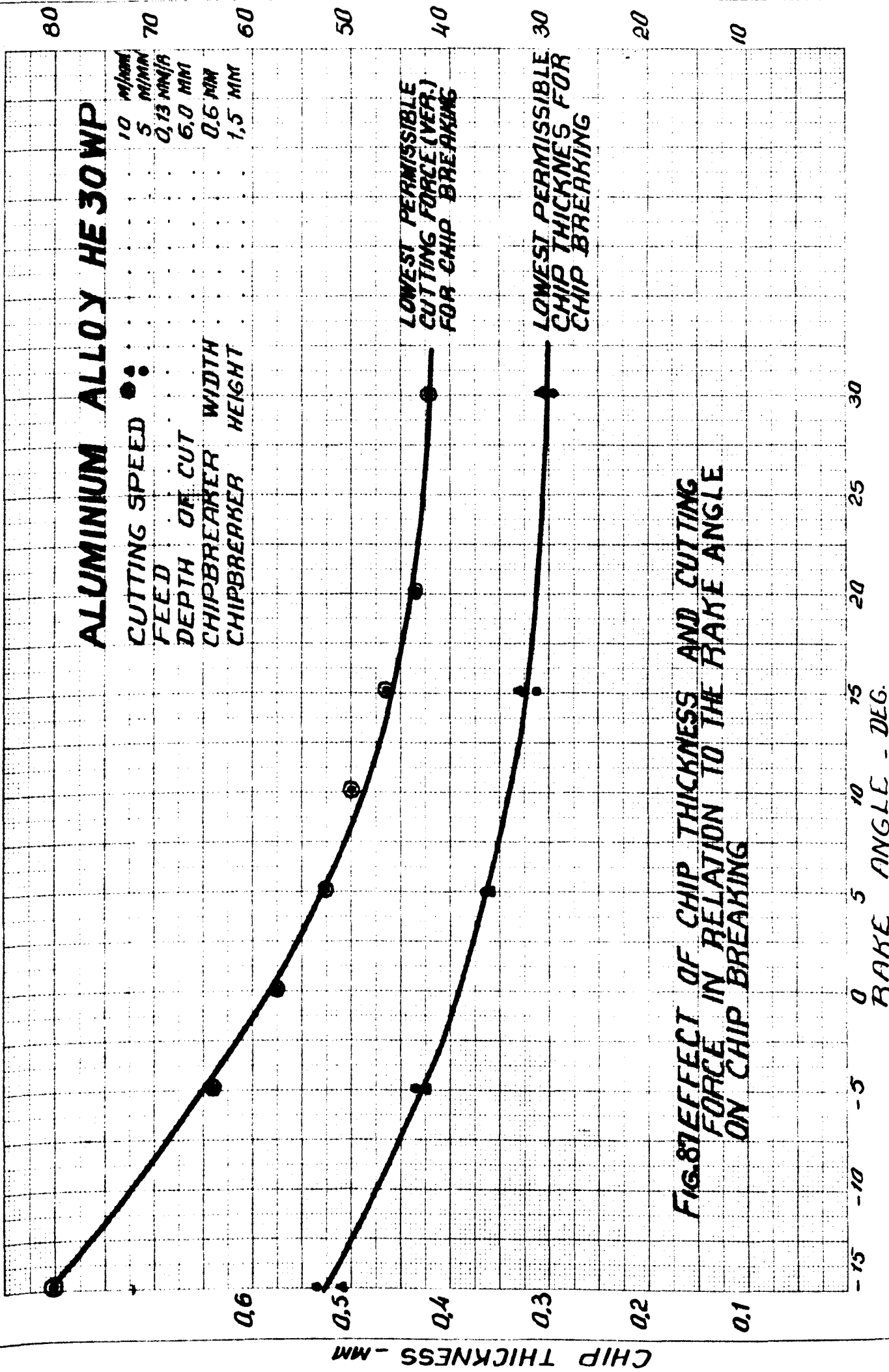


FIG. 87 EFFECT OF CHIP THICKNESS AND CUTTING FORCE IN RELATION TO THE RAKE ANGLE ON CHIP BREAKING

CUTTING FORCE (VERTICAL) - KG.

15. The lowest permissible chipbreaker proportions for steel EN1A are higher than those for aluminium alloy HE30WP, Figs. 70-74.

16. Chipbreaker proportion for satisfactory chip breaking taken within the condition of lowest permissible chipbreaker proportion and condition of minimum cutting force and chip thickness, will not lead to a significant increase in the tool wear.

17. The lathe being used was found to be satisfactory for the purpose of this work. However, some of the readings of the dial gauge dynamometer were affected by the chatter of the tool dynamometer and machine tool system.

4.2.2 Deductions From the Analysis of the Experimental Results Obtained At High Cutting Speeds

18. Similar to cutting at low cutting speeds, the vertical and horizontal components of cutting force as well as the chip thickness pass through a certain minimum value as the chipbreaker width is increased, Figs. 75-79. From this it is concluded that the use of chipbreakers for the purpose of satisfactory chip breaking will not lead to a significant increase in the cutting force and chip thickness compared with those obtained from tools without chipbreaker. However reduced cutting force and chip thickness might be observed.

19. It was concluded that if the cutting force acting on the cutting tool is not increased by more than 10% when using a chipbreaker, than those acting on the cutting tool when no chipbreaker was used, the tool wear will not be significantly increased (this is considered to be so due to the fact that during these tests it was observed that the number of regrindings required by the cutting tool at those two conditions were nearly the same).

20. The closer the chipbreaker is set to the cutting edge the more effective the chip breaking is, and the greater the danger of over-broken and built-up chips will be.

21. Conditions of minimum cutting force and 10% higher than those without chipbreaker for vertical component of the cutting force are obtained at a chipbreaker width slightly smaller than those for the horizontal component of the cutting force, Fig. 75.

22. For clamped wedge chipbreaker, in order to obtain effectively broken chips, the chipbreaker wedge must be set closer to the cutting edge as the wedge angle is reduced. In order to avoid the built-up chips, the chipbreaker wedge should not be set closer than those values corresponding to the condition of 10% increase in the cutting force.

23. The numerical values of the ratio w/s for lower cutting speeds are strictly higher than those for higher cutting speeds.

24. The cutting forces increase slightly with the reduction in the wedge angle, Figs. 75-76, due to the increase in the chip-tool contact length.

25. The ratio w/s corresponding to the conditions of minimum cutting force and chip thickness and 10% higher than those obtained without chipbreaker for both vertical and horizontal components of the cutting force for steel EN1A is higher than those for aluminium alloy HE30WP.

26. The range of effective chip breaking for aluminium alloy HE30WP is larger than steel EN1A.

27. At high cutting speeds, the use of coolant will help significantly in promoting an effective chip breaking.

28. The manner in which the height of the ground step chipbreaker, the feed, the rake angle and cutting speed affect the performance of the ground step chipbreaker is similar to those at low cutting speeds.

2.4.3 General Deductions from the Experimental Results

29. According to the length and type of chips produced, chip breaking effectiveness is classified as follows:

- (a) Over-broken and built-up chips (half turn-up to 5 mm long).
- (b) Effectively broken chips (half turn, full turn, one and a half turns - up to 30 mm long).
- (c) Broken chips (more than two turns - over 30 mm long)
- (d) Continuous chip - no chip breaking, Figs. 53-54.

30. Effective chip breaking can be obtained at considerably smaller feed when chipbreakers were used compared with the condition of discontinuous cutting with tools having no chipbreaker, Fig. 88.

31. The feed necessary to break the chip increases with the increase in the cutting speed, Fig. 88.

32. The lowest permissible chip thickness and cutting force corresponding to the condition of satisfactory chip breaking are not affected by change in the cutting speed, Fig. 89. However, increase in the cutting speed will increase the feed necessary to break the chip.

33. For each material, chip breaking effectiveness is characterised by ratios of chip curl radius to feed and of chipbreaker width to its height for ground step chipbreaker, and by the ratio of chipbreaker width to wedge angle for clamped chipbreaker.

34. The ratio of chip curl radius to feed corresponding to the condition of effective chip breaking for aluminium alloy is higher than steel.

35. The depth of cut has no significant effect on chip breaking, Fig. 90. However, at depths of cut smaller than 2 mm, the lowest permissible chip thickness for effective chip breaking is considerably affected by the change in the direction of chip flow. Decrease in depth of cut leads to a decrease in the angle between the direction

A

B

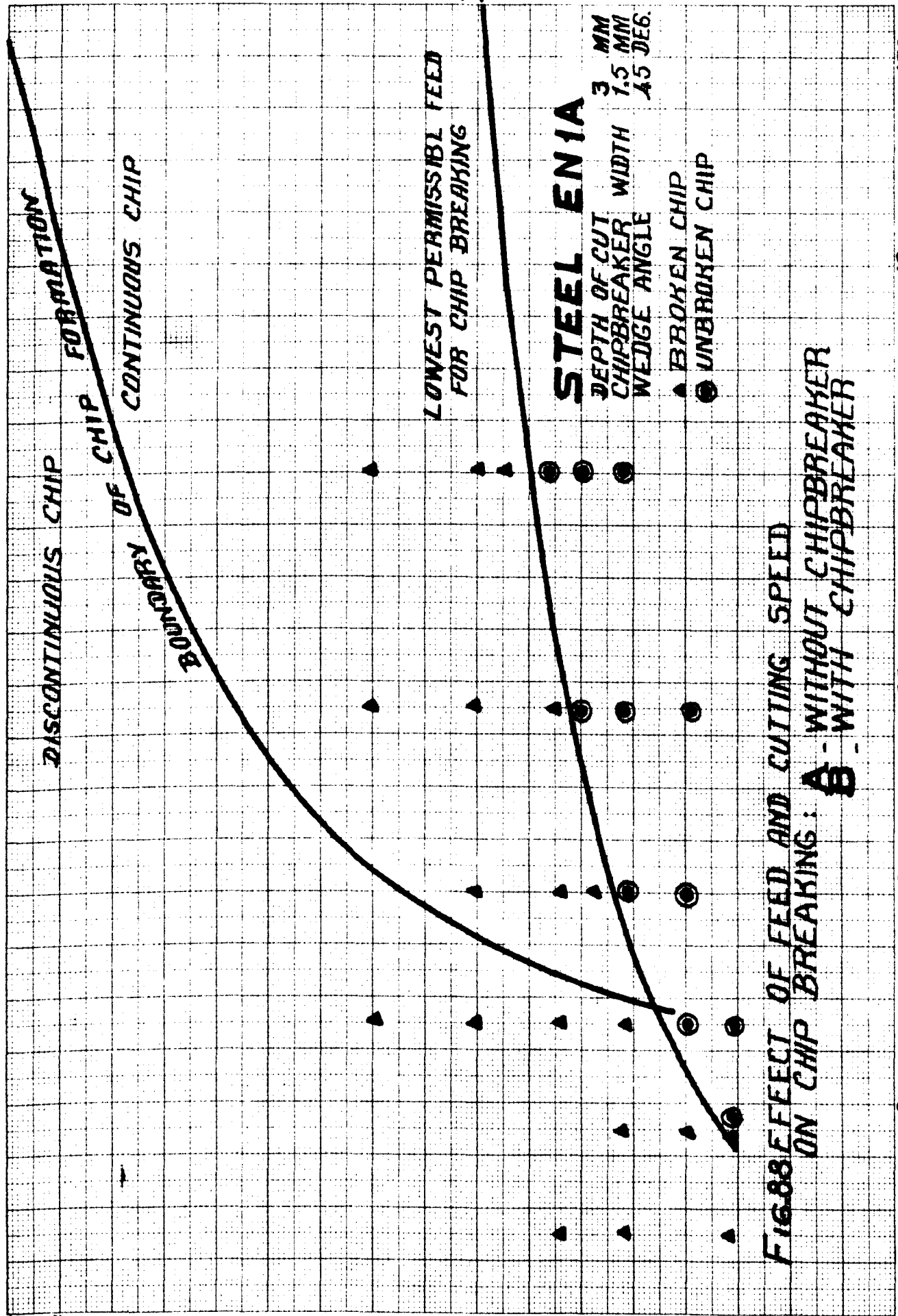


FIG. 88 EFFECT OF FEED AND CUTTING SPEED ON CHIP BREAKING: A - WITHOUT CHIPBREAKER B - WITH CHIPBREAKER

FEED - MM/REV.

CUTTING SPEED - M/MIN

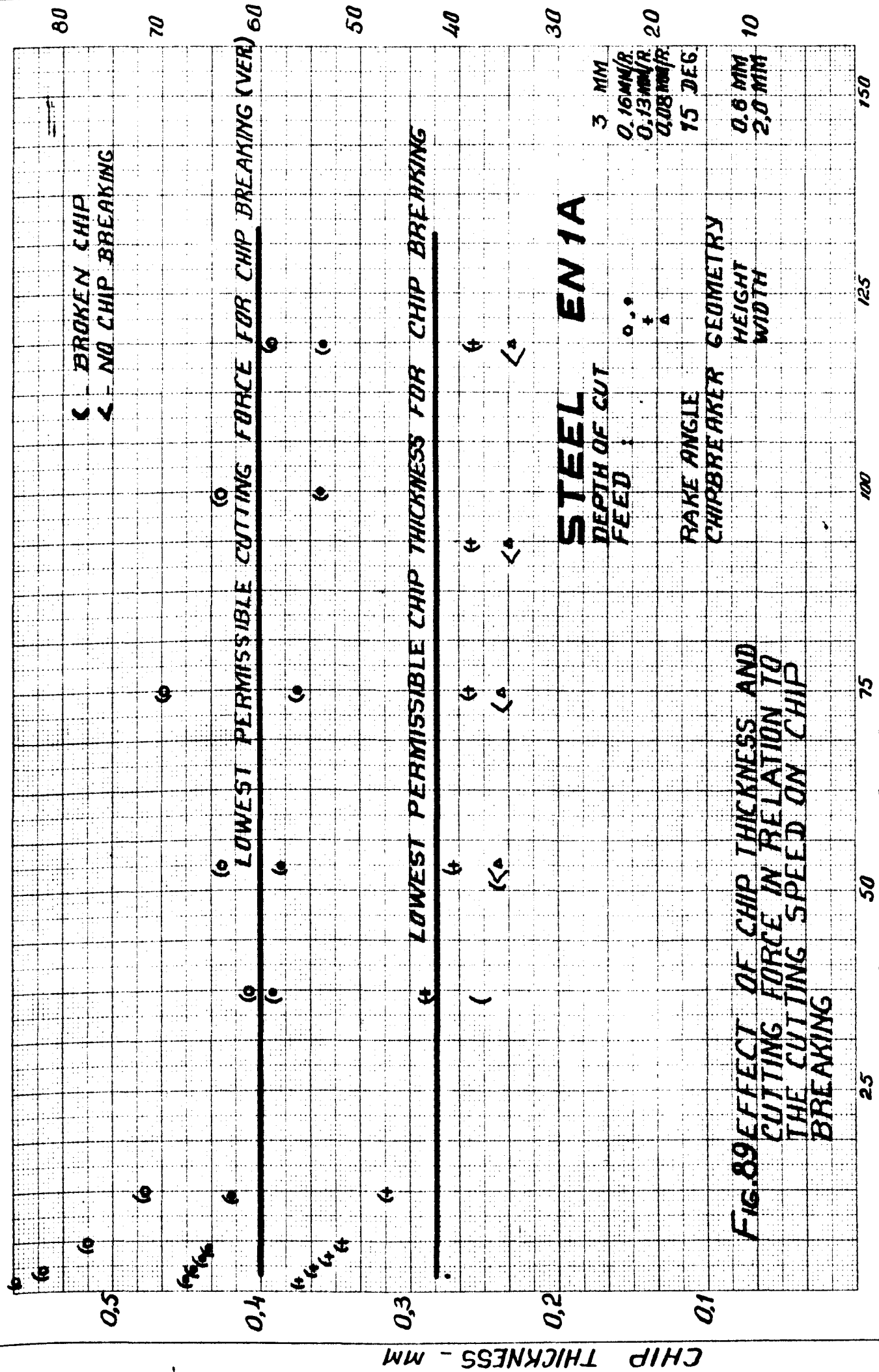


FIG.89 EFFECT OF CHIP THICKNESS AND CUTTING FORCE IN RELATION TO THE CUTTING SPEED ON CHIP BREAKING

CUTTING SPEED M/MIN

CHIP THICKNESS - MM

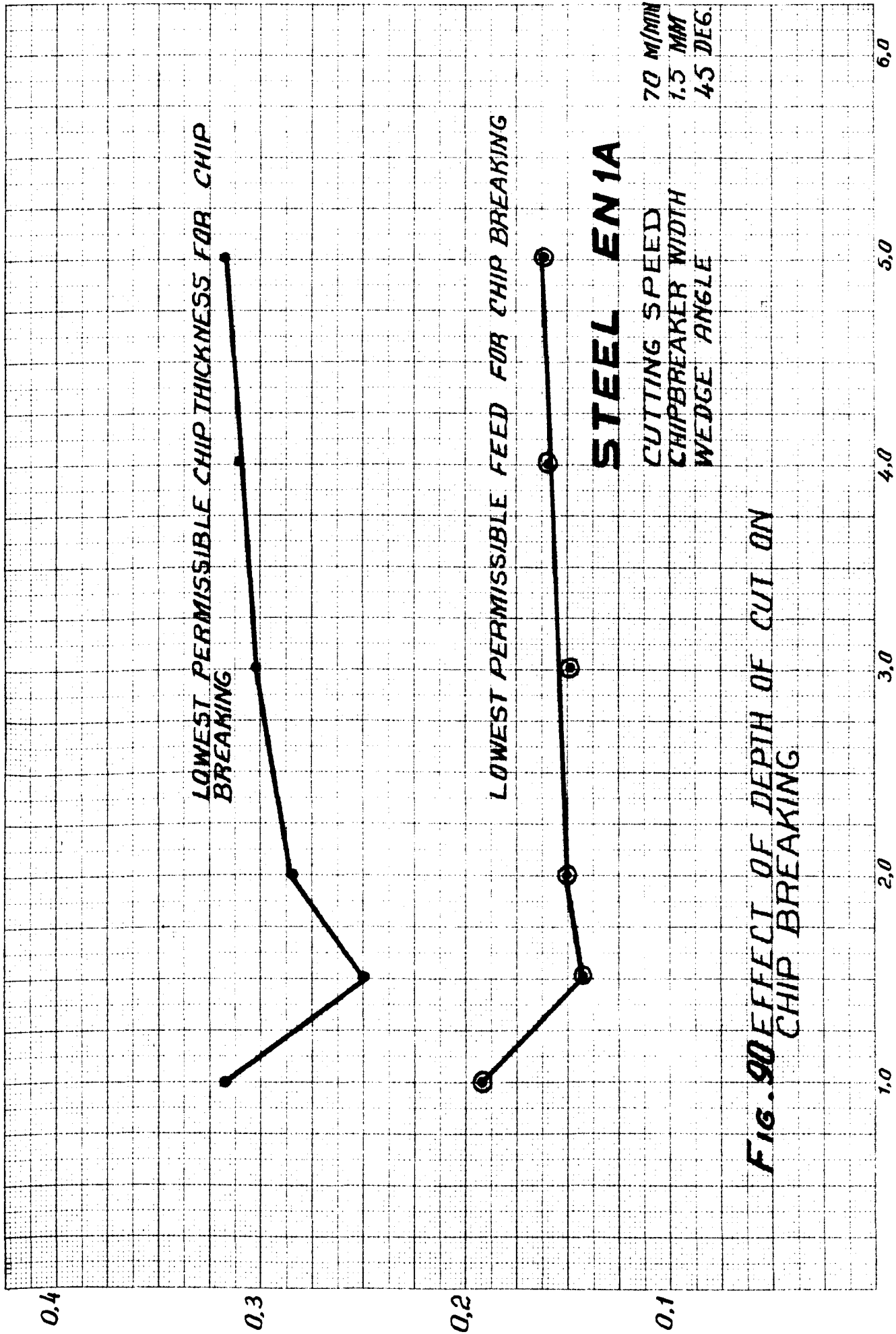


FIG. 90 EFFECT OF DEPTH OF CUT ON CHIP BREAKING

STEEL EN1A

CUTTING SPEED

CHIPBREAKER WIDTH

WEDGE ANGLE

70 M/MIN

1.5 MM

45 DEG.

LOWEST PERMISSIBLE CHIP THICKNESS FOR CHIP BREAKING

LOWEST PERMISSIBLE FEED FOR CHIP BREAKING

0.4

0.3

0.2

0.1

CHIP THICKNESS - MM
FEED - MM/REV

1.0

2.0

3.0

4.0

5.0

6.0

DEPTH OF CUT - MM

of the chip flow and side cutting edge which will direct the chip much more easily to contact with the workpiece. On the other hand, this will lead to an increase in the chip curl radius, therefore making the chip breaking much more difficult

36. Charts for finding the chipbreaker dimensions are considered to be quite reliable for the purpose of designing tools with chipbreakers which will produce effectively broken chips.

CHAPTER 5

DISCUSSION

5.1 GENERAL DISCUSSION

In the last few years much attention has been given to chip breaking without any final solution being reached. Nevertheless many manufacturing organisations are in need of satisfactory methods of chipbreaking. For the chips to be controlled at the cutting zone and effectively transported from the vicinity of the machine tool, it is essential that chipbreakers are used.

In practice, the length of coil produced in cutting operations can be controlled quite accurately by using chipbreakers, and coils up to 100 mm long are preferred. Possibly a consistent length of coil is attained because of the bending stress set up when the coil wags about, as the inertia of a certain length is sufficient to cause fracture. Cracks in the chip develop from the tightly coiled inner edge, and periodically, one of these cracks extends across the chip to cause fracture.

When the cut is continuous, curling of the chip by means of a chipbreaker step or a clamped wedge, is not always sufficient to ensure that the chip will break. It often breaks on coming into contact with some obstacle. Generally speaking, the coil must be unwound to break the chip. The lower surface of the chip is smooth and free from flaws, and the chip will stand severe bending in the direction of increasing tightness of coiling which puts this surface into tension. On the other hand, the upper surface of the chip is rough and full of cracks and fissures, so that if the chip is bent so as to put this surface into tension, i.e. bent so as to uncoil the chip, fracture occurs much sooner, than when the outer surface of the chip is compressed. For example, the chip produced by a parting tool coils back on itself. As the coil diameter grows, the chip is forced into an

increasing radius of curvature, which means that it is partially straightened, or bent to put tensile stress in upper surface. Hence when the coil reaches a certain diameter it breaks off. This can occur with cylindrical turning with zero obliquity, i.e. with the feed direction vector making a right angle with the cutting edge. In Chapter 3 chip straightening was sufficiently analysed. It is justified to say that any obstacle that arrests rotation of the coil will tend to break the chip.

As cutting speed increases, the chip tends to lose its curl. The explanation involves reduced friction at the tool face. Friction gives compressive stress on the under-side of the chip near the cutting edge, which after a short movement, is relaxed to produce curvature of the chip. It is also significant that when the chip is blued, it loses its hardening and gains ductility, and therefore will be harder to break.

During prolonged cutting, a crater is formed on the cutting (rake) face of the tool, which gives a chipbreaking effect, especially when negative rake is used. The chip must cool down before proper chipbreaking occurs. This is why better chipbreaking is obtained when coolant is used. When a high positive rake is used, the chip curvature is reduced, and the chip remains in contact with the rake face for an increased distance. Because this gives additional friction, it may nullify the reduction in power expected from the theoretically low strain in the chip. Here it may be expected that a chipbreaker would lift the chip away from the face of the tool at a short distance from the cutting edge, thus reducing friction and cutting force.

The chipbreaking problem is more acute for finishing operations than for roughing. In many roughing operations, an irregular depth of cut tends to prevent the chip from becoming too long. As the chipbreaker is brought nearer to the cutting edge, vertical and horizontal components of cutting force, chip thickness, and tool temperature will increase. Accordingly extreme conditions of high cutting force and temperature will reduce the tool life. To obtain best chipbreaking results, the chipbreaker should be set back from the cutting edge a distance equal to some fixed multiple of the feed, depending on the material being cut. For clamped chipbreakers the chipbreaker wedge should have an acute angle to avoid clogging. For this type of chipbreaker, provided the chip impinges on it, the height of the chipbreaker face is not significant. For any setting, chipbreaking performance varies with feed rate. For a very light feed there will be no chipbreaking action; at the other extreme, a feed rate will be reached when jamming-up occurs.

Apart from the ground step and clamped chipbreakers, various profiles of tool tend to promote breaking of the chip. With a normal rake angle, say $+9^\circ$, a negative rake land may be formed on the cutting edge of true width equal to $\frac{1}{2}$ to $\frac{2}{3}$ of the feed, which is usually a land width of 0.10 to 0.15 mm, but not more. This tends to promote chip curl. A radiused cutting edge may be helpful, say up to 0.1 mm. However, if this is used for low feeds, say 0.05 mm/rev. a very poor finish results.

A chipbreaker groove can often give satisfactory chipbreaking. For best chipbreaking performance the groove must approach the cutting edge to within a small distance comparable to the feed rate. The groove type chipbreaker is characterized by low cutting force. This is due to a reduced length of the chip contact path on the rake face ^(81,82,85) where friction is high.

5.2 DISCUSSION OF THE EXPERIMENTAL RESULTS

From the analysis of the experimental results obtained during this work it is well established that cutting forces acting on the tool when using a chipbreaker can be less than the cutting forces acting when no chipbreaker is used. Therefore, it is justified to suggest that the introduction of chipbreaker into the geometry of the cutting tools will not lead to an increase in the cutting forces acting on the tool, but may even give lower forces. By considering the force acting on the tool as a parameter affecting the tool wear (although they are not directly related), the reduced force obtained when chipbreakers are used can therefore be seen as an improvement in the conditions effecting the tool wear. On the other hand incorrect chipbreaker proportions may lead to an extensive increase in the force and temperature acting on the cutting face of the tool. This occurs as a result of over-breaking and building-up of the chips in the vicinity of the chipbreaker when small chipbreaker width is used. To eliminate such a possibility the chipbreaker proportion ratio should be taken larger than those corresponding to the lowest permissible chipbreaker proportion for effective chipbreaking. Physically, it is clear that on moving a chipbreaker nearer to the cutting edge, the cutting force may be first reduced due to the reduced tool-chip contact area, but ultimately the force must increase due to obstruction of the chips. The assumption made during the course of this work that if the cutting force is not increased by more than 10% the tool wear will not be excessively increased was verified by tests. However, a theoretical examination of the cutting forces would be very useful. The significance of this condition is in providing effective chip-breaking when chipbreakers were used. Therefore effective chipbreaking

may be characterized by the conditions of lowest permissible chipbreaker proportion ratio and 10% increased cutting force.

In order to design a chipbreaker which would give a satisfactory chipbreaking for any particular material it is considered to be attractively simple procedure if the material could be characterized by two experimental factors only, these factors being ratios R_c/S and L/H . The ratio of chip curl radius to feed expressing a satisfactory degree of chipbreaking while the chipbreaker proportion ratio expressing the condition for minimum cutting force. According to the experimental results obtained during this work, the ratio R_c/S was found to be the most reliable parameter in determining the degree of chipbreaking. Different chip curl radius corresponds to different degrees of chipbreaking. The effect of the feed on chip curl radius is determined by the degree of chipbreaking. For any set of cutting conditions, tool geometry and cutting material the chipbreaking effectiveness is characterized by some constant R_c/S ratio. For example, effective chipbreaking for the conditions mentioned in Figs. (53 - 54) when cutting aluminium alloy HE30WP and steel EN1A can be obtained at $R_c/S = 25$ and 20 respectively. The chipbreaker ratio expressing the force condition at the cutting face of the tool should be taken in agreement with ratio R_c/S so that to obtain effective chipbreaking without a significant increase in the cutting force.

On the basis of the experimental as well as the theoretical results it is justified to say that chipbreaking effectiveness is dependent on chip curl radius, feed and the properties of the material. In appendix I and II a simple theoretical analysis of the chip breaking is shown. Here also the chipbreaking effectiveness was found to be determined mainly by the parameters mentioned earlier. Nakayama⁽⁸⁰⁾ and Okushima, Hoshi and Fujinawa⁽¹⁰¹⁾ have concluded that limiting

condition for chip breaking is determined only by radius of the chip curl, the material to be cut and chip thickness.

The theoretical expressions shown in Chapter 3 as well as those in appendix I expressing the chipbreakers proportion in terms of chip curl radius can be used quite satisfactorily for the purpose of designing ground step and clamped chipbreakers. By substituting the value of chip curl radius corresponding to effectively broken chips together with constant C_1 and C_2 which depend on the cutting material, tool geometry and cutting conditions in equation (3.26), the chip-breaker dimensions can be calculated. However, the effects of cutting speed and depth of cut in equation (3.26) are not significant. This is due to the fact (based on the experimental results) that the cutting speed will not lead to a significant change in the chip curl radius when the feed used is not less than 0.08 mm/rev., however, at feeds smaller than 0.08 mm/rev. reduction in the cutting speed will result in a decrease in the chip curl radius in the direction of tightening the chip coil. During this work the change in depth of cut was found to have no significant effect on chip breaking. However, reduced depth of cut less than 1.5 mm will lead to a reduction in the chip flow angle (angle between the direction of chip flow and side cutting edge). Although this will lead to an easier contact of the chip with the work-piece which may give easy chip breaking, reduction in chip flow angle will lead to an increase in the actual radius of the chip flow in the direction of harder chip breaking. Similar effects of cutting speed and depth of cut on chip breaking effectiveness have been recognised by Nakayama⁽⁸⁰⁾ and Okushima⁽¹⁰¹⁾. Yoshida⁽¹⁰⁸⁾ has also confirmed that increase in depth of cut leads to an increase in the chip curl radius.

Simply speaking the chip breaking effectiveness can be controlled quite effectively by means of the chipbreaker proportion

ratio (WIDTH/HEIGHT, L/H , Fig. 37, for ground step chipbreaker and the factor of chipbreaker width to wedge angle, W/β . Fig. 38, for clamped wedge chipbreaker) by taking into consideration the ratio of the chip curl radius to feed (R_c/S).

5.3 RECOMMENDATIONS FOR FUTURE WORK ON CHIPBREAKING

In the light of this recent work the following points were recommended for the future attention:

1. The mode of action of the notch chipbreaker in the tool face is not very well understood, and exploration of the flow would be useful, though this might mean elaborate quick-stopping techniques.
2. Measurement of chip ductility, to be related to the cutting conditions and metallurgical condition of the chip.
3. Visual and photographic studies of chip formation.
4. A theoretical method of examining cutting forces as affected by the chipbreaker would be very useful.

CHAPTER 6

CONCLUSIONS

On the basis of the experimental results obtained during this investigation, the following conclusions were drawn:

1. For ground step chipbreaker, the ratio of the width of the chipbreaker (the distance from the cutting edge of the tool to the chipbreaker wedge) to its height is the most significant parameter in controlling the chipbreaking process.
2. For ground step chipbreaker, the optimum chipbreaker width corresponding to a satisfactory chipbreaking increases with the increase in the height of the chipbreaker and the feed, (Figs.55-56).
3. In roughing operations, chipbreaking can be satisfactorily achieved by changing the feed.
4. For clamped wedge chipbreaker, the wedge angle (angle of the inclination of the chipbreaker wedge from the cutting face of the tool) as well as the chipbreaker width are the most significant parameters in controlling the chip flow. The best results were obtained with wedge angle 40° to 50° .
5. For both ground step and clamped wedge chipbreaker, the cutting force as well as the chip thickness pass through a certain minimum value as the width of the chipbreaker is reduced.
6. Degree of chipbreaking can be specified in terms of the types of chips produced.

7. For any particular material, the chipbreaking effectiveness can be represented in terms of the ratio of chip curl radius to feed which expresses the degree of chipbreaking and the chipbreaker proportions which expresses the condition for minimum cutting force.
8. Chipbreaking effectiveness is affected by the feed and cutting speed only through the change in the chip thickness. However, parameters not affecting the chip thickness will have no significant effect on the chipbreaking effectiveness.
9. The chipbreaking effectiveness can be expressed in terms of theoretical relationships. Accordingly charts for designing effective chipbreakers can be drawn.
10. Chipbreaker proportions are limited on the one hand by the need to get sufficiently broken chips and on the other hand by the need to avoid an excessive increase in cutting forces, which should not increase by more than 10 % .
11. Use of chipbreakers may improve the conditions at the cutting edge (by giving reduced cutting force).

APPENDIX I

THEORETICAL ANALYSIS OF CHIP CURLING

MECHANISM FOR BOTH CLAMPED WEDGE AND

GROUND STEP CHIPBREAKERS

The mechanism of chip curling by the action of the chipbreaker has been analysed theoretically by Henriksen⁽⁷¹⁾, Okushima⁽¹⁰¹⁾, Nakayama⁽⁸⁰⁾, Dawe and Rubenstein⁽¹⁰⁵⁾, Trim and Boothroyd⁽¹⁰⁷⁾, this recent work and others. Each author has suggested a different theoretical explanation of the mechanism of chip curling by the chipbreaker. However some of these theoretical analysis were in good agreement with the experimental results. In this appendix the chip curling mechanism will be analysed from different aspect.

When the chip is straightened (as shown in Figs.91a-c and 92a-c) from its initial radius R to a radius R_c , the strains and stresses involved can simply estimated.

NOMENCLATURE

R = Initial chip curl radius or flow circle radius, Figs.91 & 92	W = Distance from the chipbreaker wedge to the cutting edge of the tool, Fig.91 _c
R_c = Final chip curl radius caused by the action of an obstacle, Figs. 91 & 92	ϵ_f = Strain corresponding to the rupture of the chip
ϵ = Strain in the outer fibre of the chip (beam)	C = Constant depending on the properties of the material being cut
t_c = Chip thickness	l = Chip-tool contact length
σ_0 = Flow stress	K = Constant for a given material
E = Modulus of elasticity	H = Height of the step of the ground step chipbreaker
β = Angle of the inclination of the chipbreaker wedge from the cutting (rake) face of the tool.	L = Distance from the cutting edge of the tool to the heel of the chipbreaker

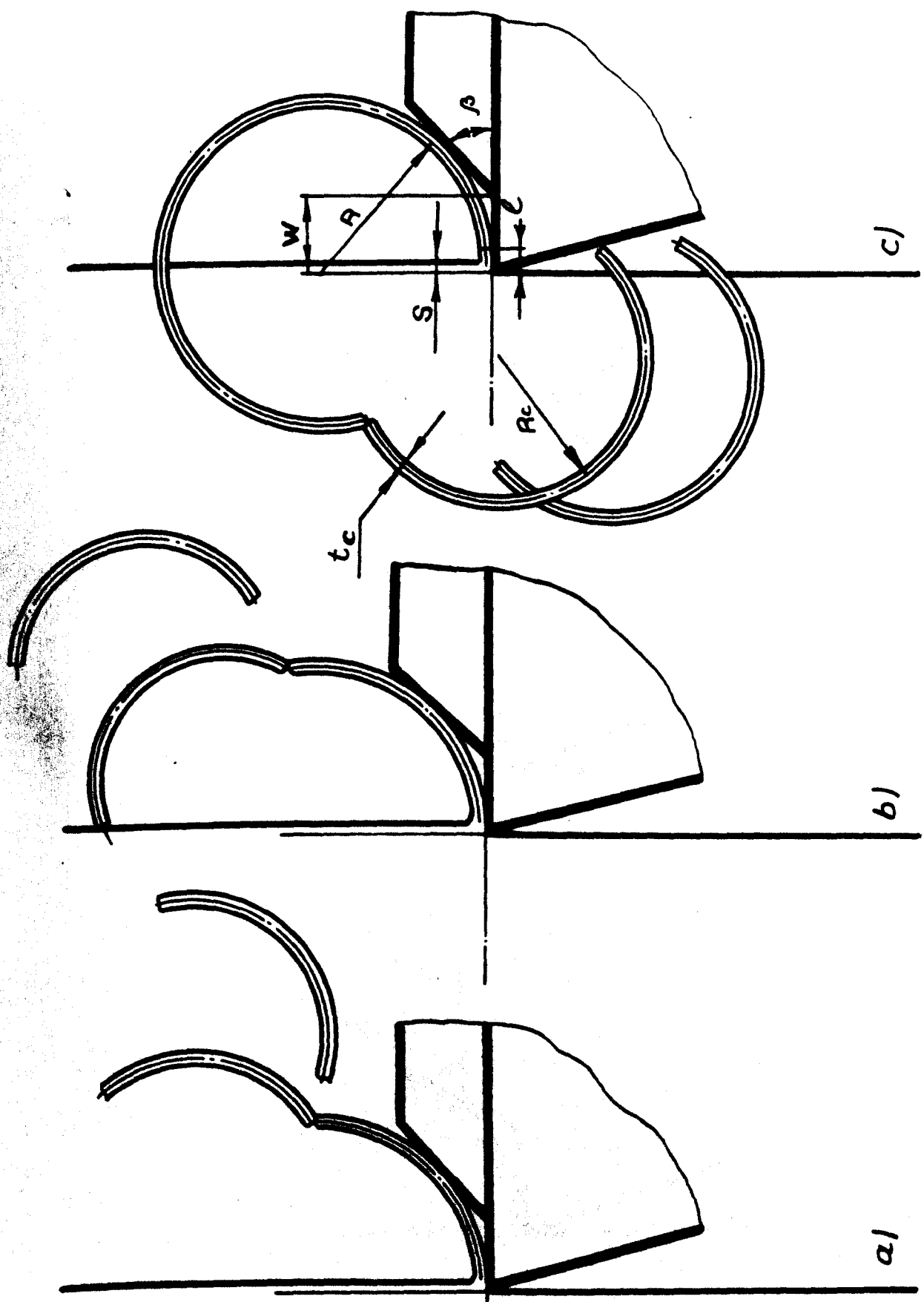


FIG.91

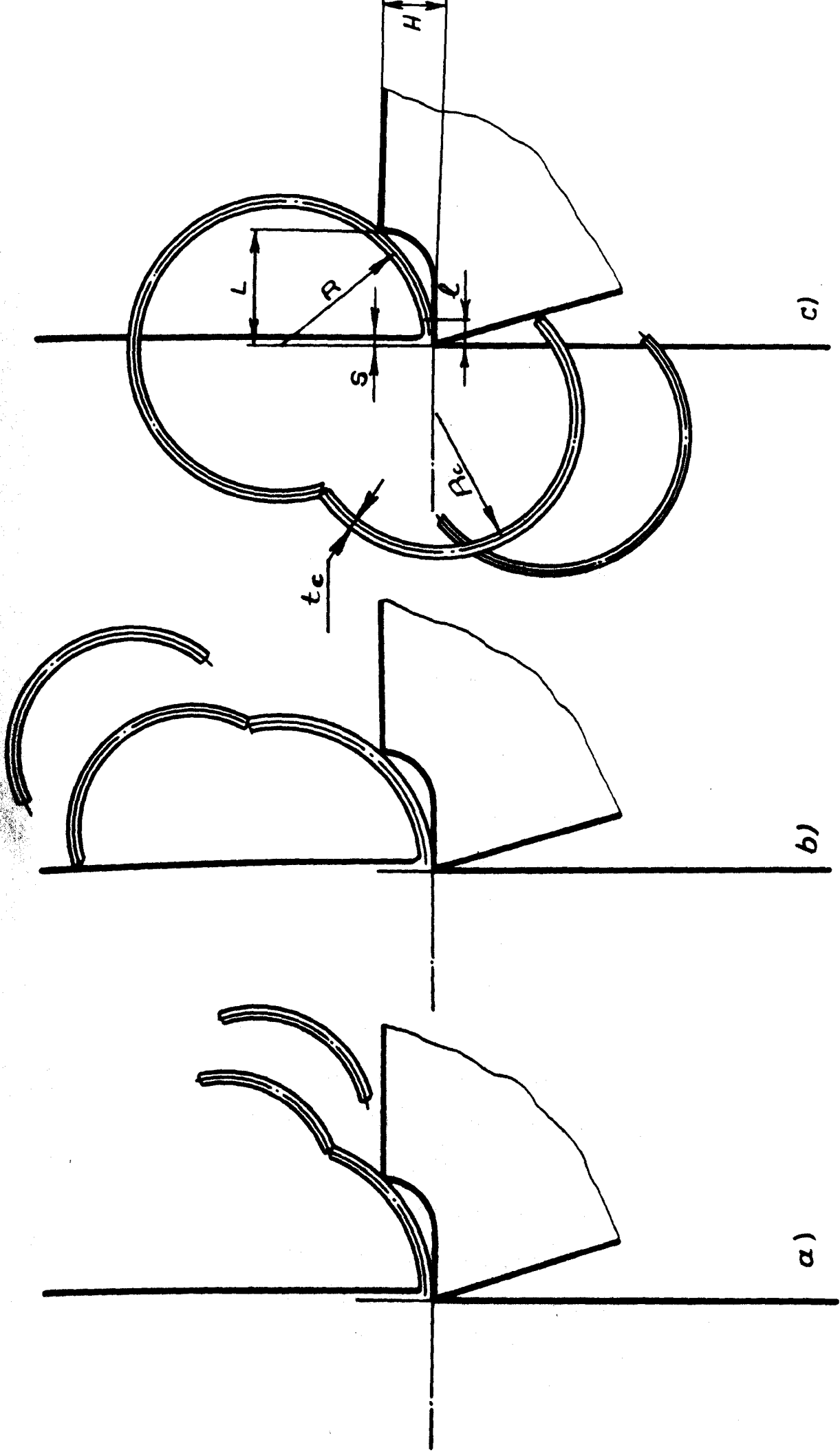


FIG.92

The strain in the outer fibres of a straight beam of thickness (t_c) bent to a radius R_c is simply⁽¹⁰⁴⁾

$$\epsilon = \pm \frac{t_c}{2R_c}$$

Hence, when a beam of radius R is bent to a new radius of R_c , the strain in the outer fibre is

$$\epsilon = \pm \frac{t_c}{2} \left(\frac{1}{R} - \frac{1}{R_c} \right) \quad (A_I.1)$$

If the straightening is elastic, the product ($E\epsilon$) cannot exceed the flow stress $\bar{\sigma}_0$. Hence the maximum change of radius is

$$\frac{1}{R} - \frac{1}{R_{\text{elastic}}} = \frac{2 \bar{\sigma}_0}{E t_c}$$

According to Cook, Jhaveri and Nayak⁽¹⁰⁴⁾ for a typical steel chip, $\bar{\sigma}_0 = 100,000 \text{ lb/in}^2$, $E = 30 \times 10^6 \text{ lb/in}^2$, $t_c = 0,005 \text{ in}$; $R = 0,020 \text{ in}$. Elastically, the initial radius of the chip curl could be increased to $R_c = 0,0205 \text{ in}$., so it can be seen that the elastic effect is insignificant and can be ignored. This means that the final chip curl radius is determined only by the plastic bending action.

As the chip comes in contact with the chipbreaker, it receives an extra bending action imposed by the chipbreaker. The final strain in the chip (as a result of its contact with any obstacle) will be calculated according to equation (A_I.1).

However, from the geometrical relationships, Figs. 91c-and 92c the initial chip curl radius (i.e. chip flow circle radius) for clamped wedge and ground step chipbreakers can be expressed as follows:

For clamped wedge chipbreaker, ⁽⁸⁰⁾ Fig. 91c.

$$R = W \cot \beta / 2 \quad (A_I.2)$$

For ground step chipbreaker ⁽⁷¹⁾, Fig. 92c

$$R = \frac{L^2 + H^2}{2H} \quad (A_I.3)$$

Hence from equations (A_I.1), (A_I.2) and (A_I.3) we obtain:

For clamped wedge chipbreaker

$$\epsilon = \frac{t_c}{2} \left(\frac{1}{W \cot \beta / 2} - \frac{1}{R_c} \right) \quad (A_I.4)$$

For ground step chipbreaker

$$\epsilon = \frac{t_c}{2} \left(\frac{2H}{L^2 + H^2} - \frac{1}{R_c} \right) \quad (A_I.5)$$

By considering

$$\frac{1}{R} - \frac{1}{R_c} \approx 0$$

Equations (A_I.4) and (A_I.5) will become

For clamped wedge chipbreaker

$$\frac{1}{R_c} = \frac{1}{W \cot \beta / 2} \quad (A_I.6)$$

For ground step chipbreaker

$$\frac{1}{R_c} = \frac{2H}{L^2 + H^2} \quad (A_I.7)$$

The chip will break away when the bending strain produced in the chip reaches a critical value corresponding to the rupture of the chip material. Therefore, equations (A_I.4) and (A_I.5) will become:

For clamped wedge chipbreaker

$$\epsilon_f = \frac{t_c}{2} (1/W \cot \beta/2 - 1/R_c)$$

or

$$\frac{1}{R_c} = \frac{1}{W \cot \beta/2} - \frac{2 \epsilon_f}{t_c} \quad (A_I.8)$$

For ground step chipbreaker

$$\epsilon_f = \frac{t_c}{2} \left(\frac{2H}{L^2 + H^2} - \frac{1}{R_c} \right)$$

or

$$\frac{1}{R_c} = \frac{2H}{L^2 + H^2} - \frac{2 \epsilon_f}{t_c} \quad (A_I.9)$$

By taking into consideration the effect of chip-tool contact length on the chip curl radius, the effective chipbreaker width will be $W - \ell$ and $L - \ell$ for both clamped wedge and ground step chipbreakers respectively. But according to Creveling, Jordan and Thomsen⁽¹⁰⁶⁾

$$\ell = K t_c \cong t_c, \quad (K \approx 1)$$

Hence equation (A_I.8) will become:

$$\frac{1}{R_c} = \frac{1}{(W-t_c) \cot \beta/2} - \frac{2 \epsilon_f}{t_c} \quad (A_I.10)$$

Putting $2 \epsilon_f = C$ in equation (A_I.10) we get

$$\frac{1}{R_c} = \frac{1}{(W-t_c) \cot \beta/2} - \frac{C}{t_c} \quad (A_I.11)$$

And similarly equation (A_I.9) will become:

$$\frac{1}{R_c} = \frac{2H}{(L-t_c)^2 + H^2} - \frac{C}{t_c} \quad (A_I.12)$$

Putting $W_{\text{effective}} = W - t_c$ and $L_{\text{effective}} = L - t_c$ in equations (A_I.6) and (A_I.7) we obtain:

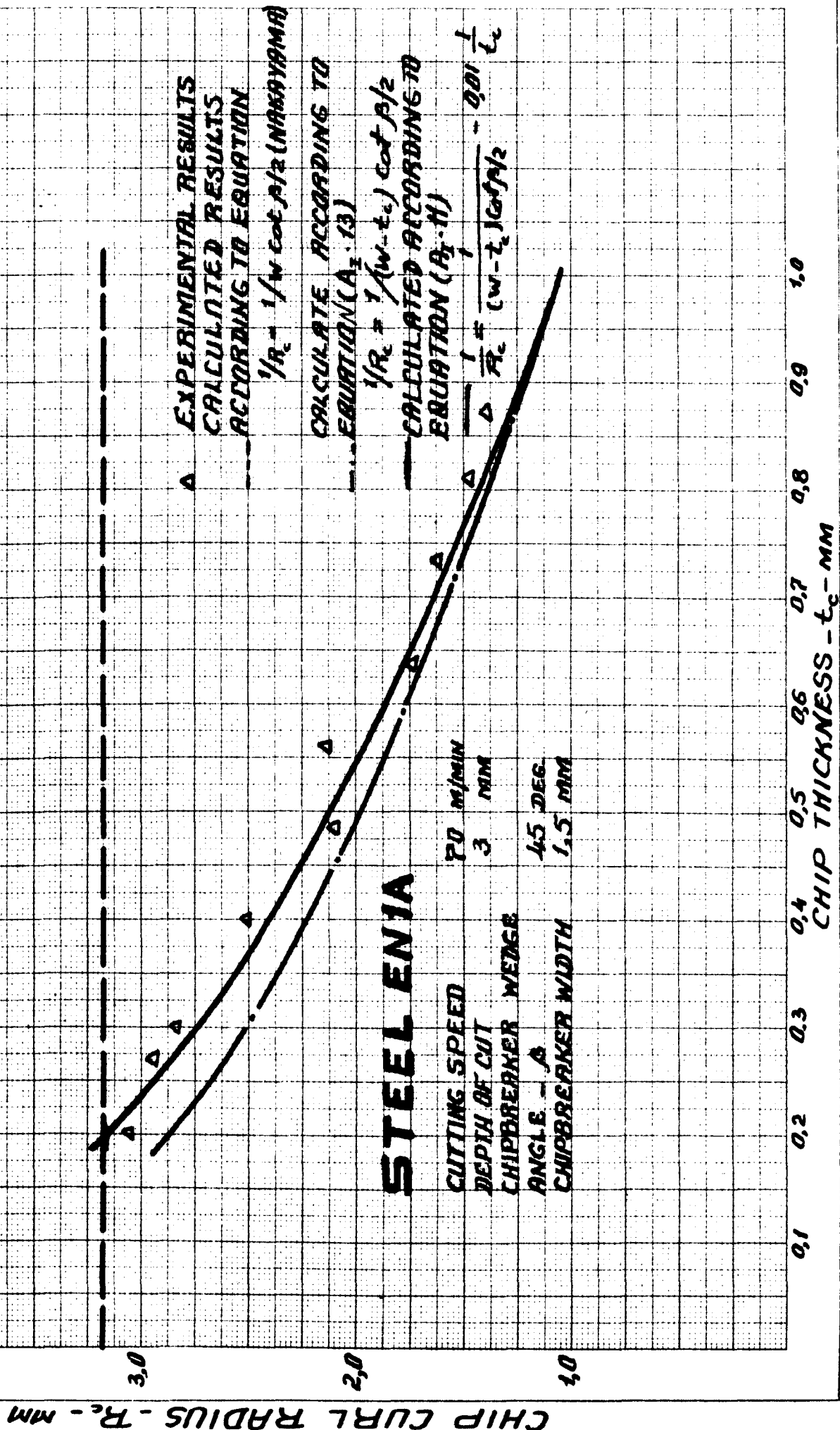
$$\frac{1}{R_c} = \frac{1}{(W-t_c) \cot \beta/2} \quad (\text{A}_{\text{I}}.13)$$

$$\frac{1}{R_c} = \frac{2H}{(L-t_c)^2 + H^2} \quad (\text{A}_{\text{I}}.14)$$

Equation (A_I.14) is similar to that of Trim and Boothroyd⁽¹⁰⁷⁾

It can be seen from equations (A_I.11) and (A_I.12) that the final chip curl radius for any particular set of cutting conditions is determined by the chipbreaker proportions, the properties of the material being cut and the chip thickness (or feed). It can also be seen that the chip curl radius decreases with an increase in the chip thickness (or feed). That explains why built-up chips occurs at large feeds. Fig.93 shows the comparison between the experimental and the theoretical (calculated according to equations A_I.2, A_I.11 and A_I.14) values of chip curl radius for a clamped chipbreaker of 45° wedge angle and with 1,5 mm chipbreaker width. The experimental results seem to be in better agreement with the results calculated according to equation A_I.11 rather than those obtained from equations A_I.2 and A_I.13.

FIG. 93 COMPARISON BETWEEN THE EXPERIMENTAL (MEASURED) CHIP CURL RADIUS AND THE THEORETICALLY CALCULATED.



APPENDIX II

FORCES ACTING ON THE CHIPBREAKER

In order to obtain satisfactory chipbreaking result with comparatively long effective life, the chipbreaker must be designed so that to minimize the force acting on its surface. The main force acting on the chipbreaker is chip curling force (force necessary to curl the chip as it leaves the cutting edge. Nevertheless the chipbreaking force (force necessary to break the chip as it comes in contact with an obstacle) has some effect on the chipbreaker. However, this force has an intermittent action and comparatively small. On the basis of this, the chip curling force will be considered as the main and only force acting on the chipbreaker.

NOMENCLATURE

M_B = bending moment at the cutting edge B	μ = coefficient of friction between the chip and the chipbreaker
F = resultant chipbreaker force	F_v = vertical component of the chipbreaker force
R = radius of the chip flow circle, Fig. 94	F_h = horizontal component of the chipbreaker force
β = chipbreaker wedge angle, Fig. 94	b = chip width
θ = angle between the resultant chipbreaker force and the vertical to the chipbreaker face, Fig. 94	t_c = chip thickness
	σ_B = yield stress of the chip

According to Nakayama⁽⁸⁰⁾, the bending moment at the cutting edge B of the tool Fig.94 caused by the chipbreaker force (chip curling force acting on the chipbreaker) is:

$$M_B = F \times \overline{BC} = F \times R \sin(\beta + \theta) - \sin \theta \quad (A_{II}.1)$$

$$\theta = \tan^{-1} \mu = 90^\circ - \beta - \tan^{-1}(F_v/F_h) \quad (A_{II}.2)$$

From the condition of the stress distribution in the chip at the cutting edge B as shown in Fig.95⁽⁸⁰⁾, we obtain,

$$M_B = b \times t_c^2 \sigma_B / 4 \quad (A_{II}.3)$$

Accordingly from equation (A_{II}.1) and (A_{II}.3) we obtain:

$$F = \frac{b t_c^2 \sigma_B}{4R \sin(\beta + \theta) - \sin \theta} \quad (A_{II}.4)$$

Equation (A_{II}.4) is the equation of the force acting on the chipbreaker.

The action of the cutting forces acting on the chipbreaker has also been investigated by Subramanian and Bhattacharyya⁽¹⁰⁹⁾.

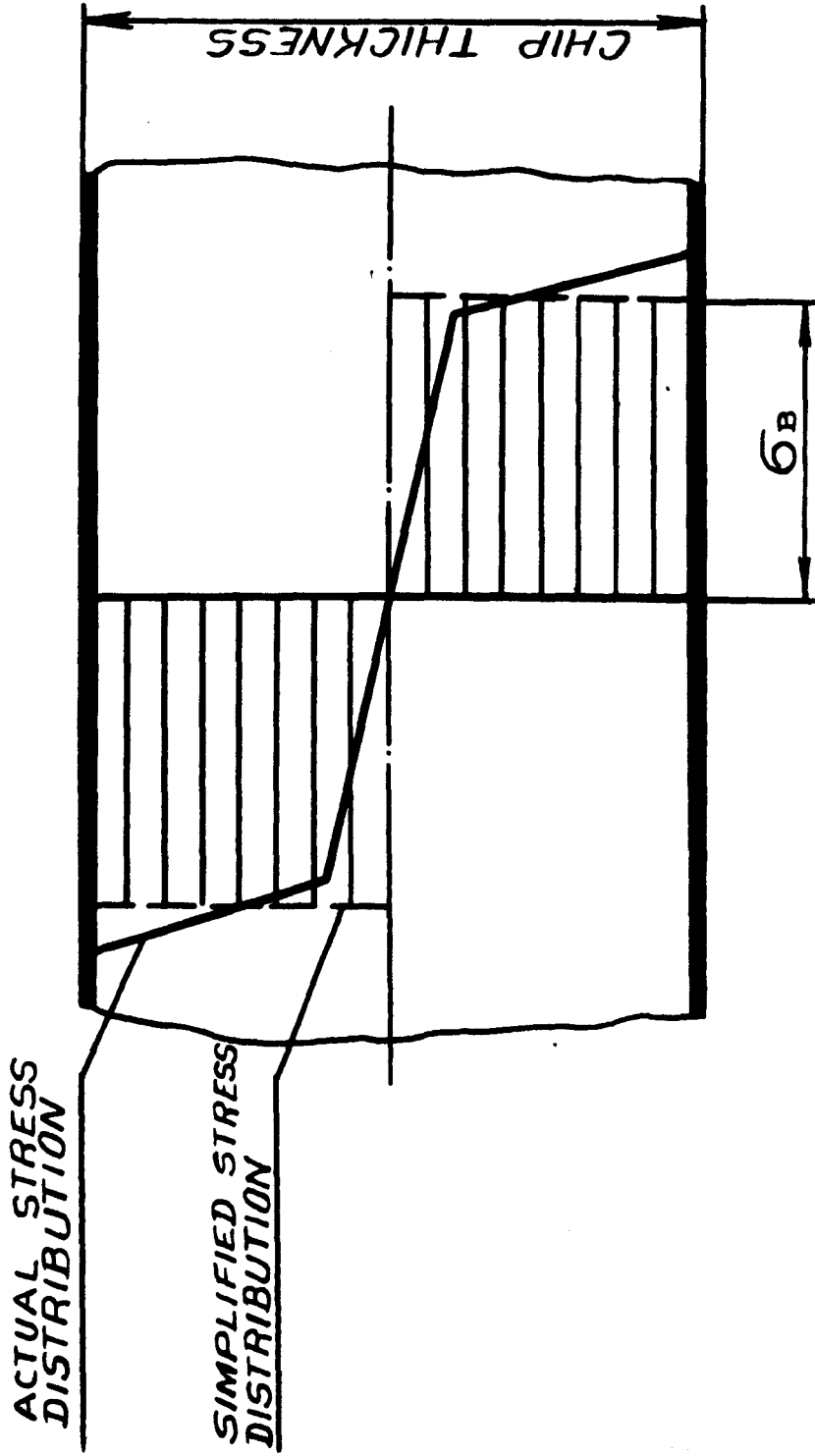


Fig. 95
STRESS DISTRIBUTION
IN CHIP

BIBLIOGRAPHY

1. K. G. Lewis "The Machinability Concept", Metal Treatment, Vol. 24, No. 142, 1957, p.p. 263-271.
2. N. E. Woldman and R. C. Gibbons "Machinability and Machining of Metals", McGraw-Hill Book Co., London, 1951, p.7.
3. C. Rubenstein "The Rule of Surface Energy in Metal Cutting", Machinability Conference, The Iron and Steel Inst., Oct. 1965, p.p. 11-15.
4. E. M. Trent "The Relationship Between Machinability and Tool Wear", Machinability Conference, The Iron and Steel Inst., Oct. 1965, p.p. 31-47.
5. P. L. B. Oxley and M. J. M. Welsh "On Machinability", Eng. Digest, Vol. 26, No. 3, 1965, p.89.
6. H. E. Enahoro and M. J. M. Welsh "The Relevance of the Mechanics of Metal Cutting to Machinability", College of Aeronautics, Cranfield, Co.A Memo, M and P No. 74, August, 1965.
7. E. M. Trent "Metallurgical Changes at the Tool/Work Interface", Machinability Conference, The Iron and Steel Inst., Oct. 1965, p.p. 45-55.
8. M. E. Hydon "Influence of Metallurgical Structure on the Machinability of Wrought Aluminium Alloys", Machinability Conference, The Iron and Steel Inst., Oct. 1965, p.p. 57-60.
9. H. Opitz and W. Konig "Basic Research on the Wear of Carbide cutting Tools", Machinability Conference, The Iron and Steel Inst., Oct. 1965, p.p. 117-123.
10. I. A. Time "Resistance of Metals and Wood to Cutting", (Soprotivleniye metalov i deriva rezaniyu) 1870.
11. K. A. Zvorkin "Work and Force Necessary for Separating a Metal Chip", (Rabota i ysiliye, neobchodimyye dlya otdeleniya metallicheskoi struzhki, Technicheskii sbornik i vestnik promyshlennosti), 1896.
12. A. A. Briks "Cutting of Metals", (Rezaniye metallov), 1896.

13. V. Piispanen "Theory of Formation of Metal Chips", Journal of Applied Physics, Vol. 19, 1948, p.876.
14. H. Ernst and M. E. Merchant "Surface Treatment of Metals - Chip Formation, Friction and High Quality Surfaces", A.S.M. Symposium, p.299.
15. M. Field and M. E. Merchant "Mechanics of Formation of Discontinuous Chip in Metal Cutting", Trans. A.S.M.E., 1949, Vol. 71, p.421.
16. N. H. Cook, I. Finnie and M. C. Shaw "Discontinuous Chip Formation", Trans. A.S.M.E., 1954, Vol. 76, p.153.
17. N. N. Zorev "Metal Cutting Mechanics", Pergamon Press, London, 1966.
18. E. H. Lee and B. W. Shapper "The Theory of Plasticity Applied to the Problem of Machining", J.Applied Mech., 1952, Vol. 19, p.238.
19. R. Hill "The Mechanics of Machining, A New Approach" J.Mech. & Phys. of Solids, Vol. 3, 1954, p.p. 47-53.
20. K. Okushima and K. Hitomi "An Analysis of the Mechanism of Orthogonal Cutting and its Application to Discontinuous Chip Formation", J.Eng. for Ind., Trans. A.S.M.E., Ser. B, Vol. 83, 1961, p.545.
21. K. Nakayama "A study on Mechanism of Metal Cutting", J. of Society for Precision Mechanics, Vol. 23, 1957, p.p. 528-532.
22. K. Okushima and K Hitomi "On the Cutting Mechanism for Soft Metals", Trans. J.S.M.E., Vol. 23, No. 134, 1957, p.p. 674-680.
23. D. Keceaoğlu "Shear Strain Rate in Metal Cutting and its Effect on Shear Flow Stress", Trans. A.S.M.E., 1958, Vol. 80, pt. 1, p.158.
24. D. G. Christopherson, P. L. Oxley and W. B. Palmer "Orthogonal Cutting of Work Hardened Material", Engineering, Vol. 186, 5th July, 1958, p.113.
25. A. A. Ilyushin "Plasticity", (Plastichnost), Gostekhizdat, 1948, U.S.S.R.
26. A. N. Malova "Handbook", (Kratki spravochnik metallica), (in Russian), Moscow, 1965.
27. N. H. Cook and M. C. Shaw "A Visual Metal Cutting Study", Mechanical Engineering, No. 11, Vol. 73, 1951.

28. A. B. Albrecht "Chip Studies Reveal What Happens",
The Machinist, No. 26, 97, 1953.
29. W. B. Palmer and "The Mechanics of Orthogonal Machining",
P. B. Oxley Proc. Inst. of Mech. Eng., Vol. 173,
1959, p.623.
30. H. E. Enahoro and "An Investigation of the Transition from
P. B. Oxley a Continuous to a Discontinuous Chip in
Orthogonal Machining", Int. J. Mech.
Sci., 1961, Vol. 3, p.p.145-156.
31. H. Banerjee and "Metal Cutting with a Discontinuous
W. B. Palmer Chip", Machine Tool Design and Research
1965, p.405.
32. P. W. Bridgman "Effects of High Shearing Stress Combined
with Hydrostatic Pressure", Phys. Review,
1953, Vol. 48, p.825.
33. C. Zener "Micromechanism of Fracture", Fracture of
Metals, p.3.
34. K. Hitomi "Fundamental Machinability Research in
Japan", J. Eng. for Ind., Trans A.S.M.E.
Ser. B, Vol. 83, 1961, p.531.
35. E. H. Lee "Plastic Flow Problem arising from the
Theory of Discontinuous Machining", Trans.
A.S.M.E., 1954, Vol. 76, p.189.
36. S. Kobayashi and "Chip Formation with Varying Undeformed
A Shabik Chip Thickness at very Low Speed", J. of
Eng. for Ind., Trans. A.S.M.E. Vol. 86,
1964, p.p. 389-394.
37. N. N. Zorev "Normal Forces and Friction Forces During
Free Cutting at an Acute Angle",
(Normalnye sily treniya pri kosougolnom
rezaniya metallov), Trudy Ts Ni mash,
book, 1948, U.S.S R.
38. K. Hoshi "On the Built-up Edge and Counterplot for
it", Trans. J.S.M.E., Vol.5, 1939, p.p.
137-148.
39. K. Nakayama and "Studies on the Built-up Edge", Journal
K. Iguchi of Society for Precision Mechanics, Vol.
22, 1956, p.p. 104-108.
40. M. Okoshi and "Formation and Disappearance of Built-up
T. Sata Edge in Machining", Journal of Scientific
Research Inst., Vol. 33, 1957, p.p. 155-164.
41. Meyer and J. D. Cumming "Handbook", Toronto, 1956, 2nd edition.
42. R. Holm "Electric Contacts", Hugo Gebers, Forlag,
Stockholm, Sweden, 1946.

43. H. Ernst and M. E. Merchant "Surface Friction of Clear Metals", Proceedings of the Special Summer Conference on Friction and Surface Finish, M.I.T., Cambridge, Mass., 1940, p.76.
44. F. P. Bowden and D. Tabor "The Friction and Lubrication of Solids", Oxford University Press, Oxford, England, 1950.
45. M. C. Shaw and E. F. Macks "Analysis and Lubrication of Bearings", McGraw Hill Book Comp., Inc., New York, N.Y., 1949.
46. S. Kobayashi and E. G. Thomsen "The Role of Friction in Metal Cutting", J. Eng. for Ind., Trans. A.S.M.E., Ser. B., Nov. 1960, p.324.
47. A. M. Rozenberg and A. N. Yeregin "Contribution to the Theory of Metal Cutting", (Kteorii protsessa rezaniya metallov), stanki i instrument, No. 10, 1949, U.S.S.R.
48. A. N. Yeregin "Physical Nature of Phenomena when Cutting Steel", (Fizicheskaya syshnost yavlenii pri rezanii stali), Mashgis, 1951, U.S.S.R.
49. A. I. Isayev "Process of Surface Layer Formation During Machining of Metals by Cutting", (Protsess obrozovaniya poverkhnostnogo sloya pri obrobotke metallov rezaniem), Mashgis, 1950, U.S.S.R.
50. M. C. Shaw, D. Piggot and Z. P. Richardson "The Effect of the Cutting Fluid Upon Chip-Tool Interface Temperature", Trans. A.S.M.E., 1951, No. 1, Vol. 73.
51. A. Nadai "Theory of Flow and Fracture of Solids", Eng. Society, Vol. 1, McGraw-Hill Book Comp., Inc., New York, N.Y., 1950, p.349.
52. M. C. Shaw "Metal Cutting Principle", 3rd Edition, The M.I.T. Press, Massachusetts Inst. of Technology, Cambridge, Mass., 1965.
53. T. Bevan "The Theory of Machines", 3rd Edition, Longman, 1956.
54. M. B. Moore "Theory and Application of Mechanical Engineering Measurements", New York, Van Nostrand, 1960.
55. A. Ansler "Some New Types of Dynamometers", Proc. Inst. Mech. Eng., 1911, p.603.
56. J. D. Hoffman "A Hydraulic Dynamometer", Trans. A.S.M.E. 1896, p.471.

57. W. F. Durand "Improved Transmission Dynamometer", Trans. A.S.M.E., 1907 (28), p.697.
58. W. H. Bird and H. P. Fairfield "A Twist Drill Dynamometer", Trans. A.S.M.E., 1905, p.355.
59. W. R. Backer and E. J. Krabacher "New Techniques in Metal Cutting Research", Trans. A.S.M.E., 1956, Vol. 78, pt. 2, p. 1497.
60. H. C. Town "Technology of the Machine Shop", London (Longman, Green & Co.), 1951.
61. H. C. Town "Cutting Tools, Jigs and Fixtures", London, Odhams Press, 1960.
62. O. W. Boston and C. J. Oxford "Power Required to Drill Cast Iron and Steel", Trans A.S.M.E., 1930.
63. F. Koenigsberger, K. D. Marwaha and A. S. P. Sabberwal "Design and Performance of Two Milling Force Dynamometers", J. Inst. Prod. Eng., Dec. 1958, p.727.
64. O. W. Boston "Research in the Elements of Metal Cutting", Trans. A.S.M.E., 1926, p.749.
65. Lomachenko "Pneumatic Lathe Dynamometer", Russian Eng. Journal, 1961, Vol. 41, Issue 2, p.p. 47-49.
66. A. Vallance and V. L. Doughtie "Design of Machine Members", New York, McGraw-Hill Book Co., 1951.
67. R. J. Roark "Handbook of Formulas for Strengths of Materials", 3rd ed., London, McGraw-Hill Book Co., 1954.
68. V. M. Faires "Design of Machine Elements", New York, (McMillan), 1955.
69. B. M. Kobana "Kratkii spravochnik mashinostroitel", Moscow, 1963.
70. C. R. Freberg and E. N. Kemler "Elements of Mechanical Vibration", 2nd ed., New York, 1952.
71. E. K. Henriksen "Chip-breaker Research", Tooling, Oct. 1955, p.p. 20-28.
72. Me. E. Muller "The Control of Chip Form in Turning", Werkstattstechnik u Maschinenbau, V. 47, No. 6, June 1957, p.p. 269-273 M.T.I.R.A. Translation.

73. E. Bickel "Control of Chip Form while Turning", Microtechnic, V. 11, No. 6, Dec. 1957.
74. K. Okushima and K. Minato "On the Behaviour of the Chip in Steel Cutting", J.S.M.E., V. 2, No. 5, 1959, p.p. 58-64.
75. E. Eugene "Experimental study of Combined Influence of Sharpening Angle of Tool and of Cutting Speed on Modalities of Chip Formation", Microtechnic, V. 11, No. 5, 1957, p.p. 223-230, No. 6, 1957, p.p. 277-284.
76. M. Kronenberg "The Inclination of the Cutting Edge and its Relation to Chip Curling", Tool Engineer, V. 14, No. 9, 1954, p.p. 12-15.
77. W. A. Carter "Economics of Broaching", Aircraft production V. 10, Nos. 111 and 112, Jan., Feb., 1948, p.p. 19-23, 62-64.
78. F. P. Malikov "Effect of Chip-breakers on Cutting Force in Broaching", Stanki i Instrument, V. 20, No. 2, Feb., 1949, p.p. 17-18.
79. V. A. Sinopalnikov "Cutting Edge Radius in Cemented Carbide, Tools", E. F. Eikhmans, Machines and Tooling To Vol. 36, No. 6, p.43, 1965.
80. K. Nakayama "A Study on Chip-Breaker", J. of the J.S.M.E., 1962, 5, 17, p.p. 142-150.
81. V. M. Lutov "Selecting the Optimum Size of Chip Breaking Grooves", Machines and Tooling Vol. 33, No. 7, p.27, 1962.
82. A. F. Kabanov "Straight Turning Tool with Chip-breaker", Machines and Tooling, Vol. XXXI, No. 9, p.42, 1960.
83. V. V. Igoshin "Tools with Chip Curling Grooves", Machines and Tooling, Vol. 36, No. 12, p.37, 1965.
84. Yu. G., Proskuryakov, V. N. Petron, and G. A. Fedordv "Chip Breaking in the Machining of Steel", Machines and Tooling, Vol. 33, No. 7, p.26, 1962.
85. I. I. Bazhenov "Chip-Breaker Grooves and Steps", Machines and Tooling, Vol. XXXIIL, No. 4, 1962, p.42.
86. M. O. Nodel Man "Cutting Tools with Fine Chip-breaker Grooves", Machines and Tooling, Vol. 33, No. 12, p.39, 1962.
87. I. I. Skuratov "New Type of Chip Breaking Step", Machines and Tooling, Vol. 33, No. 1, p.44, 1962.

88. Yu., G., Proskuryakov, "Chip Breaking in Facing the Ends of Welded Pipes", Machines and Tooling, Vol. 36, No. 6, p.46, 1965.
89. N. M. Ioffe "Dynamic Chip-breaker", Stanki i Instrument, No. 11, 1949, p.p. 18-20, M.T.I.R.A. Translation.
90. A. S. Kondratov (The Results of Tests with the Dynamic Chip-breaker", (Russian), Stanki i Instrument, V. 21, No. 4, April 1950, p.p. 21-22.
91. G. I. Kiselev "Results of a Study of the Performance of a Dynamical Chip-breaker", Stanki i Instrument, V. 22, No. 4, 28 April 1951, M.T.I.R.A. Translation.
92. P. S. Polgov "Chip-breaker with Automatically Adjustable Step", Machines and Tooling, Vol. XXXI, No. 6, p. 38-40, 1960.
93. V. N. Baranov, Yu., E. Zakharov, V. E. Moiseev "Chip Breaking Methods in Turning Ductile Metals", Machines and Tooling, Vol. 34, No. 1, p.16, 1963.
94. V. N. Poduyaev, and A. M. Bezborodov "Using Self-Excited Vibrations for Chip Breaking", Machines and Tooling, Vol. 34, No. 1, p.19, 1963.
95. I. H. M. Almandelawi and D. S. Dugdale "Chip Formation and Chip Breaking Process in Metal Cutting", Progress report, University of Sheffield, Nov., 1968.
96. J. C. Kozacka "How Tool Design Affects Cutting Forces", Amer. Machinist, V. 100, No. 14, 2 July 1956, p.p. 85-7.
97. N. N. Zakharov and B. I. Ivragimov "Hydraulic Copy Lathe Modified for Interrupted Working Traverse, Machines and Tooling, No. 5, 1964, p.p. 31-33.
98. I. D. Koponeve "Breaking a Continuous Chip by Interrupted Cutting", Machines and Tooling, V. 34, No. 6, 1963, p.p. 31-6.
99. O. Schnellmann "Chip Breaking", Aircraft Production, V. 16, No. 5, May 1954, p.p. 168-172.
100. M. Weill "The Technique of Vibrating Tools", (German), Machines Francaises, No. 48, December 1964, p.p. 51-59.
101. K. Okushima, T. Hoshi and T. Fujinawa "On Behaviour of Chip in Steel Cutting", Japan Soc. Mech. Eng. Bull., V. 3, No. 10, May 1960, p.p. 199-205.

102. G. R. Ponshe Trans. Am. Soci. Mech. Engrs., Series B. V. 89, p. 376, 1967.
103. M. M. Lamm Engineering, V. 187, p.444, 1959.
104. N. H. Cook,
P. Jhaveri
and
N. Nayak "The Mechanism of Chip Curl and Its Importance in Metal Cutting", Trans. of ASME, J. of Eng. for Ind., V. 85, Ser. B., Nov. 1963, pp. 374-380.
105. C. C. Dawe
and
C. Rubenstein "Analysis of Chip Curvature", 10th Int. M.T.D.R. Conference, University of Manchester, 17th-19th Sept. 1969.
106. J. M. Creveling,
T. F. Jordan
and
E. G. Thomsen "Some Studies of Angle Relationship in Metal Cutting", 1957, Trans. of ASME., 59, p. 127.
107. A. R. Trim
and
G. Boothroyd "Action of the Obstruction Type Chip Former", Int. J. of Prod. Res., 1968, Vol. 6, No. 3, pp. 227-240.
108. Yoshida, Serizawa
and
Toida "Report on Tool Performance", Kanagawaken Technical Institute, Japan, 1959.
109. T. L. Subramanian
and
A. Bhattacharyya "Mechanics of Chipbreakers", Int. J. Prod. Res., V.4, p. 37, 1965.

67* J. P. Den Hartog "Advanced Strength of Materials"
1st Ed., New York (McGraw-Hill), 1952.

71_A E. K. Henriksen "Chipbreaker", N.M.T.B., U.S.A.,
1953, 22 pp.